

Aims and Scope: Cell Journal (Yakhteh) is a quarterly English publication of Royan Institute of Iran. The aim of the journal is to disseminate information through publishing the most recent scientific research studies on exclusively Cellular, Molecular and other related topics. Cell J, has been certified by Ministry of Culture and Islamic Guidance since 1999 and also accredited as a scientific and research journal by HBI (Health and Biomedical Information) Journal Accreditation Commission since 2000. **This journal holds the membership of the Committee on Publication Ethics (COPE).**

1. Types of articles

The articles in the field of Fertility and Sterility can be considered for publications in Cell J. These articles are as below:

A. Original articles are scientific reports of the original research studies. The article consists of English Abstract (structured), Introduction, Materials and Methods, Results, Discussion, Conclusion, Acknowledgements, Author's Contributions, and References (**Up to 40**).

B. Review articles are the articles written by well experienced authors and those who have excellence in the related fields. The corresponding author of the review article must be one of the authors of at least three published articles appearing in the references. The review article consists of English Abstract (unstructured), Introduction, Conclusion, Author's Contributions, and References (**Up to 70**).

C. Systematic Reviews

Systematic reviews are a type of literature review that collect and critically analyzes multiple research studies or papers. The Systematic reviews consist of English Abstract (unstructured), Introduction, Materials and Methods, Results, Discussion, Conclusion, Acknowledgements, Author's Contributions, and References (**Up to 70**).

D. Short communications are the articles containing new findings. Submissions should be brief reports of ongoing researches. The short communication consists of English Abstract (unstructured), the body of the manuscript (should not hold heading or subheading), Acknowledgements, Author's Contributions, and References (**Up to 30**).

E. Case reports are short discussions of a case or case series with unique features not previously described which make an important teaching point or scientific observation. They may describe novel techniques or use equipment, or new information on diseases of importance. It consists of English Abstracts (Unstructured), Introduction, Case Report, Discussion, Acknowledgements, Author's Contributions, and References (**Up to 30**).

F. Editorial should be written by either the editor in chief or the editorial board.

G. Imaging in biology should focus on a single case with an interesting illustration such as a photograph, histological specimen or investigation. Color images are welcomed. The text should be brief and informative.

H. Letter to the editors are welcome in response to previously published Cell J articles, and may also include interesting cases that do not meet the requirement of being truly exceptional, as well as other brief technical or clinical notes of general interest.

I. Debate.

2. Submission Process

It is recommended to see the guidelines for reporting different kinds of manuscripts here. This guide explains how to prepare the manuscript for submission. Before submitting, we suggest authors familiarize themselves with Cell J format and content by reading the journal via website (www.celljournal.org). The corresponding author ensures that all authors are included in the author list and agree with its order, and they must be aware of the manuscript submission.

A. Author contributions statements

It is essential for authors to include a statement of responsibility in the manuscript that specifies the contribution of every one of them. This participation must include conception and design of the manuscript, data acquisition or data analysis and interpretation, drafting of the manuscript and/or revising it for critically important intellectual content, revision and final approval of the manuscript and statistical analysis, obtaining funding, administrative, technical, or material support, or supervision. Authors who do not meet the above criteria should be acknowledged in the **Acknowledgments Section**.

B. Cover letter

Each article should be accompanied by a cover letter, signed by all authors specifying the following statement: "The manuscript has been seen and approved by all authors and is not under active consideration for publication. It has neither been accepted for publication nor published in another journal fully or partially (except in abstract form). I hereby assign the copyright of the enclosed manuscript to Cell J. Corresponding author must confirm the proof of the manuscript before online publishing. Also, it is needed to suggest three peer reviewers in the field of their manuscript."

C. Manuscript preparation

Authors whose first language is not English encouraged to consult a native English speaker in order to confirm his manuscripts to US or British (not a mixture) English usage and grammar. The manuscript should be prepared in accordance with the "International Committee of Medical Journal Editors (ICMJE)". Please send your manuscript in two formats (word and Pdf). The abstract and text pages should have consecutive line numbers in the left margin beginning with title page and continuing through the last page of the written text. Each abbreviation must be defined in the abstract and text when they are mentioned for the first time. Avoid using abbreviation in title. Please use the

international and standard abbreviations and symbols.

It should be added that an essential step toward the integration and linking of scientific information reported in published literature is using standardized nomenclature in all fields of science and medicine. Species names must be italicized (e.g., *Homo sapiens*) and also the full genus and species written out in full, both in the title of the manuscript and at the first mention of an organism in a paper.

It is necessary to mention that genes, mutations, genotypes, and alleles must be indicated in italics. Please use the recommended name by consulting the appropriate genetic nomenclature database, e.g., HUGO for human genes. In another words; if it is a human gene, you must write all the letters in capital and italic (e.g., *OCT4*, *c-MYC*). If not, only write the first letter in capital and italic (e.g., *Oct4*, *c-Myc*). **In addition, protein designations are the same as the gene symbol but are not italicized.**

Of note, Cell J will only consider publishing genetic association study papers that are novel and statistically robust. Authors are advised to adhere to the recommendations outlined in the STREGA statement (<http://www.strega-statement.org>). The following criteria must be met for all submissions:

1. Hardy-Weinberg Equilibrium (HWE) calculations must be carried out and reported along with the P-values if applicable [see Namipashaki et al. 2015 (Cell J, Vol 17, N 2, Pages: 187-192) for a discussion].
2. Linkage disequilibrium (LD) structure between SNPs (if multiple SNPs are reported) must be presented.
3. Appropriate multiple testing correction (if multiple independent SNPs are reported) must be included.

Submissions that fail to meet the above criteria will be rejected before being sent out for review.

Each of the following manuscript components should begin in the following sequence:

Authors' names and order of them must be carefully considered (full name(s), highest awarded academic degree(s), email(s), and institutional affiliation(s) of all the authors in English. Also, you must send mobile number and full postal address of the corresponding author).

Changes to Authorship such as addition, deletion or rearrangement of author names must be made only before the manuscript has been accepted in the case of approving by the journal editor. In this case, the corresponding author must explain the reason of changing and confirm them (which has been signed by all authors of the manuscript). If the manuscript has already been published in an online issue, an erratum is needed.

Title is providing the full title of the research (do not use abbreviations in title).

Running title is providing a maximum of 7 words (no more than 50 characters).

Abstract must include Background, Materials and Methods, Results, and Conclusion (no more than **300** words).

Keywords, three to five, must be supplied by the authors at the foot of the abstract chosen from the Medical Subject Heading (MeSH). Therefore; they must be specific and relevant to the paper.

The following components should be identified after the abstract:

Introduction: The Introduction should provide a brief background to the subject of the paper, explain the importance of the study, and state a precise study question or purpose.

Materials and Methods: It includes the exact methods or observations of experiments. If an apparatus is used, its manufacturer's name and address should be stipulated in parenthesis. If the method is established, give reference but if the method is new, give enough information so that another author can perform it. If a drug is used, its generic name, dose, and route of administration must be given. Standard units of measurements and chemical symbols of elements do not need to be defined.

Statistical analysis: Type of study and statistical methods should be mentioned and specified by any general computer program used.

Ethical considerations: Please state that informed consent was obtained from all human adult participants and from the parents or legal guardians of minors and include the name of the appropriate institutional review board that approved the project. It is necessary to indicate in the text that the maintenance and care of experimental animals complies with National Institutes of Health guidelines for the humane use of laboratory animals, or those of your Institute or agency.

Clinical trial registration: All of the Clinical Trials performing in Iran must be registered in Iranian Registry of Clinical Trials (www.ircct.ir). The clinical trials performed abroad, could be considered for publication if they register in a registration site approved by WHO or www.clinicaltrials.gov. If you are reporting phase II or phase III randomized controlled trials, you must refer to the CONSORT Statement for recommendations to facilitate the complete and transparent reporting of trial findings. Reports that do not conform to the CONSORT guidelines may need to be revised before peer reviewing.

Results: They must be presented in the form of text, tables, and figures. Take care that the text does not repeat data that are presented in tables and/or figures. Only emphasize and summarize the essential features of the main results. Tables and figures must be numbered consecutively as appeared in the text and should be organized in separate pages at the end of article while their location should be mentioned in the main text.

Tables and figures: Tables should have a short descriptive heading above them and also any footnotes. Figure's legend should contain a brief title for the whole figure and continue with a short explanation of each part and also the symbols used (no more than 100 words). All figures must be prepared based on cell journal's guideline in color (no more than **6** Figures and Tables) and also in GIF or JPEG format with 300 dpi resolutions.

Supplementary materials would be published on the online version of the journal. This material is important to the understanding

and interpretation of the report and should not repeat material within the print article. The amount of supplementary material should be limited. Supplementary material should be original and not previously published and will undergo editorial and peer review with the main manuscript. Also, they must be cited in the manuscript text in parentheses, in a similar way as when citing a figure or a table. Provide a legend for each supplementary material submitted.

Discussion: It should emphasize the present findings and the variations or similarities with other researches done by other researchers. The detailed results should not be repeated in the discussion again. It must emphasize the new and important aspects of the study.

Conclusion: It emphasizes the new and important aspects of the study. All conclusions are justified by the results of the study.

Acknowledgements: This part includes a statement thanking those who contributed substantially with work relevant to the study but does not have authorship criteria. It includes those who provided technical help, writing assistance and name of departments that provided only general support. You must mention financial support in the study. Otherwise; write this sentence "There is no financial support in this study".

Conflict of Interest: Any conflict of interest (financial or otherwise) and sources of financial support must be listed in the Acknowledgements. It includes providers of supplies and services from a commercial organization. Any commercial affiliation must be disclosed, regardless of providing the funding or not.

References: The references must be written based on the Vancouver style. Thus the references are cited numerically in the text and listed in the bibliography by the order of their appearance. The titles of journals must be abbreviated according to the style used in the list of Journals Indexed in PubMed. Write surname and initials of all authors when there are six or less. In the case of seven or more authors, the names of first six authors followed by "et al." must be listed. The reference of information must be based on the following order:

Article:

Surname(s) and first letter of name & middle name(s) of author(s). Manuscript title. Journal title (abbr).publication date (year); Volume (Issue): Page number.

Example: Manicardi GC, Bianchi PG, Pantano S, Azzoni P, Bizzaro D, Bianchi U, et al. Presence of endogenous nicks in DNA of ejaculated human spermatozoa and its relationship to chromomycin A3 accessibility. *Biol Reprod.* 1995; 52(4): 864-867.

Book:

Surname(s) and first letter of name & middle name(s) of author(s). Book title. Edition. Publication place: publisher name; publication date (year); Page number.

Example: Edelman CL, Mandle CL. Health promotion throughout the life span. 2nd ed. ST Louis: Mosby; 1998; 145-163.

Chapter of book:

Surname(s) and first letter of name & middle name(s) of author(s). Chapter title. In: Surname(s) and first letter of name & middle name(s) of editor(s), editors. Book title. Edition. Publication place: publisher name; publication date (year); Page number.

Example: Phillips SJ, Whisnant JP. Hypertension and stroke. In: Laragh JH, Brenner BM, editors. Hypertension: pathophysiology, diagnosis, and management. 2nd ed. New York: Raven Press; 1995; 465-478.

Abstract book:

Example: Nabavi SM. Stem cell therapy for multiple sclerosis. *Cell J.* 2013; 5 Suppl 1: Os-13.

Thesis:

Name of author. Thesis title. Degree. City name. University. Publication date (year).

Example: Eftekhari Yazdi P. Comparison of fragment removal and co-culture with Vero cell monolayer's on development of human fragmented embryos. Presented for the Ph.D., Tehran. Tarbiyat Modarres University. 2004.

Conferences:

Name(s) of editor(s). Conference title; Holding date; Holding place. Publication place; Publisher name; Publication date (year).

Example: Harnden P, Joffe JK, Jones WG, editors. Germ cell tumors V. Proceedings of the 5th Germ Cell Tumors Conference; 2001 Sep 13-15; Leeds, UK. New York: Springer; 2002.

Internet References

Article:

Surname(s) and first letter of name & middle name(s) of author(s). Manuscript title. Journal title (abbr). Publication date (year); Volume (Issue): Page number. Available from: URL link. (Observation date).

Example: Jahanshahi A, Mirnajafi-Zadeh J, Javan M, Mohammad-Zadeh M, Rohani M. Effect of low-frequency stimulation on adenosine A1 and A2A receptors gene expression in dentate gyrus of perforant path kindled rats. *Cell J.* 2008; 10 (2): 87-92. Available from: <http://www.celljournal.org>. (20 Oct 2008).

Book:

Example: Anderson SC, Poulsen KB. Anderson's electronic atlas of hematology.[CD-ROM]. Philadelphia: Lippincott Williams & Wilkins; 2002.

Law:

Example: Embryo donation law. Iran Judicature, Official Gazette of the Islamic Republic of Iran. Available from: <http://www.dastour.ir/Brows/?lid=245069>.(20 Jul 2013).

D. Proofs are sent by email as PDF files and should be checked and returned within 72 hours of receipt. It is the authors' responsibility to check that all the text and data as contained in the page proofs are correct and suitable for publication. **We are requested to pay particular attention to author's names and affiliations as it is essential that these details be accurate when the article is published.**

E. Pay for publication: Authors do not have to pay any Manuscript Processing Charge or Open Access Publication Fee. **Before publishing author's article, it would be the author's responsibility to pay for the expenses, if the editor feels the level of English used in the manuscript requires editing.**

F. Ethics of scientific publication: Manuscripts that have been published elsewhere with the same intellectual material will refer to duplicate publication. If authors have used their own previously published work or work that is currently under review, as the basis for a submitted manuscript, they are required to cite the previous work and indicate how their submitted manuscript offers novel contributions beyond those of the previous work. Research and publication misconduct is considered a serious breach of ethics. The Journal systematically employs iThenticate, a plagiarism detection and prevention software designed to ensure the originality of written work before publication.

Plagiarism of text from a previously published manuscript by the same or another author is a serious publication offence. Some parts of text may be used, only where the source of the quoted material is clearly acknowledged.

3. General information

A. You can send your article via online submission system which is available at our website: <http://www.celljournal.org>. If the article is not prepared according to the format of **Cell J**, it will be returned to authors.

B. The order of article appearance in the Journal is not demonstrating the scientific characters of the authors.

C. **Cell J** has authority to accept or reject the articles.

D. The received articles will be evaluated by one epidemiologist. Then associate editor will determine its reviewers. If three reviewers pass their judgments on the article, it will be presented to the editorial board of **Cell J**. If the editorial board has a positive judgment about the article, reviewers' comments will be presented to the corresponding author (the identification of the reviewers will not be revealed). The executive member of journal will contact the corresponding author directly within 7-8 weeks by email. If authors do not receive any reply from journal office after the specified time, they can contact journal office. Executive manager will respond promptly to authors' message.

The Final Checklist

The authors must ensure that before submitting the manuscript for publication, they have to consider the following parts:

1. Title page should contain title, name of the author/coauthors, their academic qualifications, designation & institutions they are affiliated with, mailing address for future correspondence, email address, phone, and fax number.
2. Text of manuscript and References prepared as stated in the "guide for authors" section.
3. Tables should be in a separate page. Figures must be sent in color and also in GIF or JPEG format with 300 dpi resolutions.
4. Covering Letter.

The Editor-in-Chief: Ahmad Hosseini, Ph.D.

Cell Journal (Yakhteh),

P.O. Box: 16635-148, Iran

Tel/Fax: + 98-21-22510895

Emails: Celljournal@royaninstitute.org

info@celljournal.org



IN THE NAME OF GOD

Gone But not Forgotten

In the memory of the late Director of Royan Institute,
Founder of Stem Cells Research in Iran and Chairman of
Cell Journal (Yakhteh). May he rest in peace.

Dr. Saeed Kazemi Ashtiani

OWNED:

Royan Institute, Iranian Academic Center for Education Culture and Research (ACECR)

CHAIRMAN:

Hamid Gourabi, Ph.D., (Professor, Royan Institute, Tehran, Iran)

EDITOR IN CHIEF:

Ahmad Hosseini, Ph.D., (Professor, Shahid Beheshti Medical University, Tehran, Iran)

EDITOR ASSOCIATE:

Saeid Abroun, Ph.D., (Associate Professor, Tarbiat Modares University, Tehran, Iran)

EDITORIAL BOARD:

Saeid Abroun, Ph.D., (Associate Professor, Tarbiat Modares University, Tehran, Iran)
Kamran Alimoghadam, M.D., (Associate Professor, Tehran Medical University, Tehran, Iran)
Alireza Asgari, Ph.D., (Professor, Baghyatallah University, Tehran, Iran)
Mohammad Kazem Aghaee Mazaheri, D.D.S., (Assistant Professor, ACECR, Tehran, Iran)
Gila Behzadi, Ph.D., (Professor, Shahid Beheshti Medical University, Tehran, Iran)
Hossein Baharvand, Ph.D., (Professor, Royan Institute, Tehran, Iran)
Mary Familari, Ph.D., (Senior Lecturer, University of Melbourne, Melbourne, Australia)
Hamid Gourabi, Ph.D., (Professor, Royan Institute, Tehran, Iran)
Jurgen Hescheler, M.D., (Professor, Institute of Neurophysiology of University Zu Koln, Germany)
Ghasem Hosseini Salekdeh, Ph.D., (Assistant Professor, Agricultural Biotechnology Research Institute, Karaj, Iran)
Esmail Jabbari, Ph.D., (Associate Professor, University of South Carolina, Columbia, USA)
Suresh Jesuthasan, Ph.D., (Associate Professor, National University of Singapore, Singapore)
Bahram Kazemi, Ph.D., (Professor, Shahid Beheshti Medical University, Tehran, Iran)
Saadi Khochbin, Ph.D., (Professor, Inserm/Grenoble University, France)
Ali Khademhosseini, Ph.D., (Associate Professor, Harvard Medical School, USA)
Kun Ping Lu, M.D., Ph.D., (Professor, Harvard Medical School, Boston, USA)
Navid Manuchehrabadi, Ph.D., (Angio Dynamics, Marlborough, USA)
Hosseinali Mehrani, Ph.D., (Professor, Baghyatallah University, Tehran, Iran)
Marcos Meseguer, Ph.D., (Clinical Embryology Laboratory IVI Valencia, Valencia, Spain)
Seyed Javad Mowla, Ph.D., (Professor, Tarbiat Modares University, Tehran, Iran)
Mohammad Hossein Nasr Esfahani, Ph.D., (Professor, Royan Institute, Tehran, Iran)
Toru Nakano, M.D., Ph.D., (Professor, Osaka University, Osaka, Japan)
Donald Newgreen, Ph.D., (Professor, Murdoch Children Research Institute, Melbourne, Australia)
Mojtaba Rezazadeh Valojerdi, Ph.D., (Professor, Tarbiat Modares University, Tehran, Iran)
Mohammad Hossein Sanati, Ph.D., (Associate Professor, National Institute for Genetic Engineering and Biotechnology, Tehran, Iran)
Eimei Sato, Ph.D., (Professor, Tohoku University, Sendai, Japan)
Andreas Serra, M.D., (Professor, University of Zurich, Zurich, Switzerland)
Abdolhossein Shahverdi, Ph.D., (Professor, Royan Institute, Tehran, Iran)
Michele Catherine Studer, Ph.D., (Institute of Biology Valrose, IBV University of Nice Sophia-Antipolis, France)
Daniela Toniolo, Ph.D., (Head, Unit of Common Disorders, San Raffaele Research Institute, Milano, Italy)
Gianpaolo Zerbini, M.D., Ph.D., (San Raffaele Scientific Institute, Italy)
Shubing Zhang, Ph.D., (Associate Professor, Central South University, China)
Daniele Zink, Ph.D., (Institute of Bioengineering and Nanotechnology, Agency for Science Technology & Science, Singapore)

EXECUTIVE MANAGER:

Farideh Malekzadeh, M.Sc., (Royan Institute, Tehran, Iran)

EXECUTIVE BOARD:

Parvaneh Afsharian, Ph.D., (Royan Institute, Tehran, Iran)
Ahmad Vosough Taqi Dizaj, M.D., (Royan Institute, Tehran, Iran)
Reza Omani-Samani, M.D., (Royan Institute, Tehran, Iran)
Elham Amirchaghmaghi, M.D., Ph.D., (Royan Institute, Tehran, Iran)
Leila Daliri, M.Sc., (Royan Institute, Tehran, Iran)
Mahdi Lotfipanaah, M.Sc., (Royan Institute, Tehran, Iran)

ENGLISH EDITOR:

Naser Ansari-Pour, Ph.D., (University of Tehran, Tehran, Iran)
Saman Eghtesad, Ph.D., (Royan Institute, Tehran, Iran)
Vahid Ezzatizadeh, Ph.D., (Royan Institute, Tehran, Iran)
Jane Ferrie, Ph.D., (University College of London, London, UK)
Mojtaba Nemat, M.Sc., (Royan Institute, Tehran, Iran)
Ramin Rezaee, Pharm.D., Ph.D., (Mashhad University of Medical Sciences, Mashhad, Iran)
Kim Vagharfard, M.Sc., (Royan Institute, Tehran, Iran)
Hamid Zahednasab, M.Sc., (Royan Institute, Tehran, Iran)

GRAPHICS:

Laleh Mirza Ali Shirvani, B.Sc., (Royan Institute, Tehran, Iran)

PUBLISHED & SPONSORED BY:

Publication of Royan Institute (ACECR)

Indexed in:

1. Thomson Reuters (ISI); *Impact Factor: 2.363*
2. PubMed
3. PubMed Central (PMC)
4. National Library Medicine (NLM)
5. Biosis Preview
6. Index Medicus for the Eastern Mediterranean Region (IMEMR)
7. Index Copernicus International
8. Cambridge Scientific Abstract (CSA)
9. EMBASE
10. Scopus
11. Cinahl Database
12. Google Scholar
13. Chemical Abstract Service (CAS)
14. Proquest
15. Directory of Open Access Journals (DOAJ)
16. Open Academic Journals Index (OAJI)
17. Directory of Research Journals Indexing (DRJI)
18. Scientific Information Database (SID)
19. Iranmedex
20. Regional Information Center for Sciences and Technology (RICeST)
21. Islamic World Science Citation Center (ISC)
22. Magiran
23. Science Library Index

ACECR

All rights reserved. Any use, distribution, reproduction or abstract of this publication in any medium, with the exception of commercial purposes, is permitted provided the original work is properly cited.

Editorial Office Address (Dr. Ahmad Hosseini):

Royan Institute, P.O.Box: 16635-148,
Tehran, Iran

Tel & Fax: (+9821)22510895

Website: www.celljournal.org

Emails: info@celljournal.org

celljournal@royaninstitute.org

Printing Company:

Jurband Ghaemprint Co.
NO. 5, Jalil khoob alley, Niroo Havaei
Street, Tehran, Iran

CONTENTS

Original Articles

- **17 β -Estradiol Oxidative Stress Attenuation and Autophagy-Induced Dopaminergic Neuroprotection**
Roya Varmazyar, Ali Noori-Zadeh, Farzad Rajaei, Shahram Darabi, Salar Bakhtiyari 1
 - **Influence of Ellagic Acid and Ebselen on Sperm and Oxidative Stress Parameters during Liquid Preservation of Ram Semen**
Mustafa Numan Bucak, Mustafa Bodu, Nuri Başpınar, Şükrü Güngör, Pınar İli, Begimay Acibaeva, Tohid Rezaei Topraggaleh, Şükrü Dursun 7
 - **In Vitro Cytotoxicity of Folate-Silica-Gold Nanorods on Mouse Acute Lymphoblastic Leukemia and Spermatogonial Cells**
Neda Eslahi, Ali Shakeri-Zadeh, Khadijeh Ashtari, Vahid Pirhajati-Mahabadi, Tahereh Tohidi Moghadam, Ronak Shabani, Kamran Kamrava, Zahra Madjd, Chad Maki, Hamid Reza Asgari, Morteza Koruji 14
 - **Amentoflavone Induces Autophagy and Modulates p53**
Hye-Jung Park, Moon-Moo Kim 27
 - **Downregulation of Extracellular Matrix and Cell Adhesion Molecules in Cumulus Cells of Infertile Polycystic Ovary Syndrome Women With and Without Insulin Resistance**
Fatemeh Hassani, Shahrbanoo Oryan, Poopak Eftekhari-Yazdi, Masood Bazrgar, Ashraf Moini, Nahid Nasiri, Ali Sharifi-Zarchi 35
 - **Detection of Mycoplasma Contamination of Cell Culture by A Loop-Mediated Isothermal Amplification Method**
Zohre Soheily, Mohammad Soleimani, Keivan Majidzadeh- Ardebili 43
 - **A Simple Technique for Three-Dimensional Imaging and Segmentation of Brain Vasculature Using Fast Free-of-Acrylamide Clearing Tissue in Murine**
Arezo Khoradmehr, Fahime Mazaheri, Morteza Anvari, Amin Tamadon 49
 - **Induction Effects of *Bacteroides fragilis* Derived Outer Membrane Vesicles on Toll Like Receptor 2, Toll Like Receptor 4 Genes Expression and Cytokines Concentration in Human Intestinal Epithelial Cells**
Sara Ahmadi Badi, Shohreh Khatami, Shiva Irani, Seyed Davar Siadat 57
 - **Evaluation of Tumor Regulatory Genes and Apoptotic Pathways in The Cytotoxic Effect of Cytochalasin H on Malignant Human Glioma Cell Line (U87MG)**
Samaneh Heidarzadeh, Gholamreza Motalleb, Mohammad Jalil Zorriehzaha 62
 - **A Pathogenic Homozygous Mutation in The Pleckstrin Homology Domain of *RASA1* Is Responsible for Familial Tricuspid Atresia in An Iranian Consanguineous Family**
Ahoura Nozari, Ehsan Aghaei-Moghadam, Aliakbar Zeinaloo, Afagh Alavi, Saghar Ghasemi Firouzabdi, Shohre Minaee, Marzieh Eskandari Hesari, Farkhondeh Behjati 70
 - **Comparison of miRNA Profiles of Cord Blood Stem Cells in Identical and Fraternal Twins**
Monireh Ajami, Mohammad Hadi Sadeghian, Masoud Soleimani, Mohammad Reza Keramati, Mansoureh Ajami, Azadeh Anbarlou, Amir Atashi 78
 - **The Study of rs693 and rs515135 in *APOB* in People with Familial Hypercholesterolemia**
Fatemeh Karami, Iman Salahshourifar, Massoud Houshmand 86
 - **Comparison of The Therapeutic Effect of Syngeneic, Allogeneic, and Xenogeneic Adipose Tissue-Derived Mesenchymal Stem Cells on Abortion Rates in A Mouse Model**
Fatemeh Rezaei Kahmini, Seyed Mohammad Moazzeni 92
- Short Communication**
- **Hypothesis: A Challenge of Overexpression *Zfp521* in Neural Tendency of Derived Dental Pulp Stem Cells**
Fatemeh Behrouznezhad, Fatemeh Ejeian, Modjtaba Emadi-Baygi, Parvaneh Nikpour, Mohammad Hossein Nasr-Esfahani 99
 - **Front page of Cell Journal_(Yakhteh): Figure 2A-B, Page: 95**

17 β -Estradiol Oxidative Stress Attenuation and Autophagy-Induced Dopaminergic Neuroprotection

Roya Varmazyar, M.Sc.¹, Ali Noori-Zadeh, Ph.D.², Farzad Rajaei, Ph.D.³, Shahram Darabi, Ph.D.^{3*},
Salar Bakhtiyari, Ph.D.⁴

1. Student Research Committee, Qazvin University of Medical Sciences, Qazvin, Iran
2. Department of Clinical Biochemistry, Faculty of Allied Medical Sciences, Ilam University of Medical Sciences, Ilam, Iran
3. Cellular and Molecular Research Center, Qazvin University of Medical Sciences, Qazvin, Iran
4. Department of Clinical Biochemistry, Faculty of Medicine, Ilam University of Medical Sciences, Ilam, Iran

*Corresponding Address: P.O.Box: 59811-34197, Cellular and Molecular Research Center, Qazvin University of Medical Sciences, Qazvin, Iran
Email: shahram2005d@yahoo.com

Received: 18/Feb/2018, Accepted: 16/May/2018

Abstract

Objective: Degeneration of dopaminergic neurons in the substantia nigra of the brain stem is the main pathological aspect of Parkinson's disease (PD). 17 β -estradiol (E2) has neuroprotective effects on substantia nigra, however, the underlined mechanism is not well-known. In this study, we evaluated the neuroprotective effects of E2 in the ovariectomized 6-hydroxydopamine- (6-OHDA) rat model of PD.

Materials and Methods: In this experimental study, all animals were ovariectomized to avoid any further bias in E2 levels and then these ovariectomized rats were randomly assigned into three experimental groups (10 rats in each group): ovariectomized control group (OCG), ovariectomized degeneration group receiving 25 μ g of 6-OHDA into the left corpus striatum (ODG), and ovariectomized E2 pretreatment group pretreated with 0.1 mg/kg⁻¹ of 17 β -estradiol for three days prior to the destruction of corpus striatum with 6-OHDA (OE2PTG). The apomorphine behavioral test and Nissl staining were performed in all experimental groups. The expressions of Sequestosome-1 (*P62*), Unc-51 like autophagy activating kinase (*Ulk1*), and microtubule-associated proteins 1A/1B light chain 3B (*Lc3*) genes were evaluated using reverse transcription-polymerase chain reaction (RT-PCR).

Results: E2 administration reduced the damages to the dopaminergic neurons of the substantia nigra. The motor behavior, the number of rotations, and histological tests in the treatment group showed the cell survival improvement in comparison with the control groups indicating that E2 can inhibit the neurodegeneration. *P62* and *Lc3* were expressed in all experimental groups while *Ulk1* was not expressed in ODG group. Moreover, *Ulk1* was expressed after the treatment with E2 in OE2PTG group.

Conclusion: E2 prevents neurodegeneration in dopaminergic neurons of the midbrain by over-expression of *Ulk1* gene and augmenting the induction of autophagy.

Keywords: Autophagy, 17 β -estradiol, Parkinson's Disease, *Ulk1*

Cell Journal (Yakhteh), Vol 21, No 1, Apr-Jun (Spring) 2019, Pages: 1-6

Citation: Varmazyar R, Noori-Zadeh A, Rajaei F, Darabi S, Bakhtiyari S. 17 β -Estradiol oxidative stress attenuation and autophagy-Induced dopaminergic neuroprotection. Cell J. 2019; 21(1): 1-6. doi: 10.22074/cellj.2019.5799.

Introduction

Parkinson's disease (PD) is a neurodegenerative motor disorder that affects 50% of elderly people over 85 years old (1). Although the etiology of PD is mainly unknown, some factors such as oxidative stress-induced mitochondrial damage, which in turn, increases the protein aggregations, is the molecular and cellular characterization of the disease. Moreover, several studies have indicated the relationship between autophagy deficiency and neurodegenerative diseases such as PD. In this regard, autophagy regulation has been considered a strategy for the treatment of neurodegenerative diseases.

Autophagy is the primary cellular catabolic program in response to cellular starvation and degradation of the damaged organelles. It is well accepted that 17 β -estradiol (E2) has neuroprotective effects in many neurodegenerative diseases (2). E2 also plays a significant role in regulating the MAPK/ERK pathway (3). Epidemiological studies have demonstrated that men are more prone to PD by a ratio of 3:2 in

comparison with women and estrogen affects the disease onset and the severity of the symptoms associated with the disease (4). In addition, it acts through the antioxidant system by increasing the brain blood flow (5). Some actions of estrogen such as the regulation of neurotransmitter function are mediated through genomic and non-genomic pathways (6).

In PD, the degeneration of dopaminergic neurons results from the accumulation of aggregated proteins caused by oxidative stress in the cell. In fact, autophagy-mediated degradation of aggregated proteins and damaged organelles are disrupted, therefore, autophagy may be considered a therapeutic target. As the age increases, changes in the lysosomal activity can reduce the rate of autophagy in the neurodegenerative diseases (7, 8). However, the mechanism of its protective actions is still largely unknown, particularly in PD. In the present study, the mechanism of E2 in autophagy-mediated neuroprotection has been investigated in the rat model of PD.

Materials and Methods

Animals

In this experimental study, rats (female, Wistar) were maintained under a 12-12 hours light-dark condition at a controlled temperature of the animal laboratory. Water and food were available ad libitum for all of the animals. All ethical guidelines were followed in order to reduce the animal suffering. The study was conducted in accordance with the guidelines for working with experimental animals set by the Ethics Committee (Ethics code: IR.QUMS.REC.1395.67) of Qazvin University of Medical Sciences.

Ovariectomy of animals

In order to remove E2-producing gonads and hormonal cycle, the ovaries were both removed under sterile and aseptic conditions in all of the animals. After anesthetizing with a mixture of ketamine (100 mgkg⁻¹, Sigma-Aldrich, Germany) and xylazine (5 mgkg⁻¹, Sigma-Aldrich, Germany), the ovaries were removed after 1 cm cutting in the skin of the animal. Then, the skin of the ovariectomized rats was sutured.

Development of Parkinson's disease in ovariectomized rats

For the development of Parkinson's disease in the animal model, the ovariectomized rats were anesthetized by intraperitoneal injection of a mixture of Ketamine (100 mgkg⁻¹) and Xylazine (5 mgkg⁻¹). Their heads were then fixed in a stereotaxic device in accordance with the coordinates. The coordinates were set to 3 mm lateral to the left to cause a lesion, 4.5 mm abdominal from dura mater and +9.2 anterior-posterior to the interaural line. Incisor bar was also located 3.3 mm below the horizontal line. After fixing the animals' head on the device, the skin can be exposed by removing hairs from the head using regular razors and scissors. After disinfecting the surgical site using Betadine, an incision was created parallel to the sagittal plane from a distance between the eyes to between the ears, and the scalp was sheared from the skull. After finding the coordinates, the bone for injection was drilled at low speed in order to protect the brain tissue from an injury. In the ovariectomized control group (OCG), stereotaxic surgery was performed on the rats and 5 μ L of saline containing 0.2 % of ascorbate was injected into the left corpus striatum. In the ovariectomized degeneration group (ODG), 5 μ L saline ascorbate 0.2% contained 25 μ g of 6-OHDA was injected into the left corpus striatum of rats. The rats in ovariectomized E2 pretreatment group (OE2PTG) were pretreated with 0.1 mgkg⁻¹ of 17 β -estradiol (E8875, Sigma-Aldrich, Germany) for three days prior to the destruction of corpus striatum. After E2 pretreatment, the dura mater was exposed

and 5 μ L of saline ascorbate 0.2% contained 25 μ g of 6-OHDA was injected into the left corpus striatum of rats using a 5- μ L Hamilton syringe.

Behavioral tests

The behavioral test was performed on the rats in the three experimental groups before the surgery and four weeks afterward. Behavioral tests were carried out by intraperitoneal injection of apomorphine hydrochloride (Sigma-Aldrich, Germany) with a dose of 2.5 mgkg⁻¹. Ten minutes before the surgery (baseline) rats were kept in a cylindrical transparent chamber made of glass with the diameter of 33 cm and the height of 35 cm. After injecting medication, the total 360-degree rotation was measured manually for 60 minutes at the intervals of 10 minutes. The number of contralateral (opposite the lesion site or to the right) and the number of ipsilateral rotations (toward the lesion site or to the left side) were considered the positive and negative numbers, respectively. The net number of the rotations was calculated after subtracting rotations from two directions.

Nissl staining in experimental groups

By intraperitoneal injection of a mixture of ketamine (100 mgkg⁻¹) and xylazine (5 mgkg⁻¹), rats were anesthetized at the fourth week, i.e. after performing the behavioral tests. The rats were perfused using normal saline and formalin. After perfusion, the brain was removed from the skull. For neuronal counts, tissue blocks were provided from animals' substantia nigra. Tissue sections with the diameter of 10 μ m were made from the midbrain at intervals of 2.4 to 2.9 mm from the interaural point in accordance with the Paxinos atlas. The tissue sections were Nissl-stained with Cresyl violet solution (0.1%). The neurons in the dense part of substantia nigra were counted in sections aligned with 4 levels of Paxinos atlas (i.e., 2.96, 3.2, 3.8, and 4.2) as compared to the center of interaural line with the magnification of ($\times 200$, $\times 100$). At each level, at least two sections were counted and the neurons with the cytoplasmic domain were also counted.

Gene expression analysis

The total RNA was isolated from the striatum of each animal using Ambion kit (Invitrogen, USA) following the manufacturer's instructions. Each sample of the isolated RNA was further treated with DNase I enzyme (Invitrogen, USA). The yield and quality of the total RNA were assessed using absorbance ratio at (260 nm/280 nm) using spectrophotometry and denaturing agarose gel electrophoresis. The reverse transcription-polymerase chain reaction (RT-PCR) was performed using the RevertAid first strand

cDNA synthesis kit (Fermentas, Lithuania) according to the manufacturer's instructions. Meanwhile, glyceraldehyde-3-phosphate dehydrogenase (*Gapdh*) was used as an internal control gene. The primers have been shown in Table 1.

Table 1: The sequence of the primer pairs and corresponding amplicon sizes that have been used in this study

Gene	Primer (5'-3')	Amplicon size (bp)
<i>Ulk1</i>	F: AAGGATTGGAAGGGTGGAGG	195
	R: ATGGGAAGGATGGTGGCTG	
<i>Lc3</i>	F: TGTTAGGCTTGCTCTTTTGG	219
	R: GCAGAGGAAATGACCACAGAT	
<i>Gapdh</i>	F: ATCTGACATGCCGCTGGAG	154
	R: AAGGTGGAAGAATGGGAGTTGC	
<i>P62</i>	F: TCCTACAGACCAAGAATTATGAC	232
	R: TTCTCATGCACTTTCCTACTG	

Statistical analysis

All data were expressed as mean \pm SEM (any exception is mentioned). Moreover, one-way ANOVA was used for the results obtained from investigating apomorphine-induced rotational behavior in two periods (i.e., before and 4 weeks after surgery). One-way ANOVA was used to evaluate the mean neurons in the dense part of substantia nigra and multiple post-hoc comparisons were performed by Tukey's test between the groups. In addition, Microsoft Excel (2017) was used in order to draw the diagrams. $P < 0.05$ was considered as a significant statistical difference.

Results

Apomorphine-induced rotational behavior test

The behavioral test was performed at the 1st and 4th weeks of the surgery. The results indicated that the rotations before the surgery were 5 ± 0.36 , 3 ± 0.39 , and 4 ± 0.42 (mean \pm SEM) meanwhile at 4 weeks post-surgery the rotations were 4 ± 0.44 , 73.53 ± 1 , and 183 ± 4.78 for the OCG, OE2PTG and, ODG groups, respectively. The rotation results in the ODG group suggested the verification of substantia nigra degradation in the animal model. Moreover, E2 reduced the damage to the dopaminergic neurons of substantia nigra which was characterized by improving the

motor behavior and reducing rotations in the OE2PTG group in comparison with ODG group. There was a significant difference ($P < 0.05$) of rotations between the OCG and ODG groups (Fig.1). Before the surgery, there was no significant difference among the OCG, ODG, and OE2PTG groups in the rotations (Fig.1).

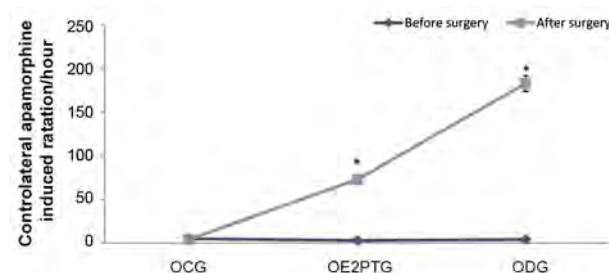


Fig.1: Before the surgery, there was no significant difference among the OCG, ODG, and OE2PTG groups in the rotations ($P < 0.05$). OCG; Ovariectomized control group, ODG; Ovariectomized degeneration group, OE2PTG; Ovariectomized E2 pretreatment group, and *; Indicates a significant difference between each experimental group with the OCG group.

Nissl staining of substantia nigra

The midbrain was separated and after preparing the tissue block, neuronal counts were done using Nissl staining. The results indicated that the means \pm SEM for the neurons in the right (normal area) substantia nigra for the OCG, OE2PTG, and ODG groups were 126 ± 3.18 , 128 ± 2.73 , and 129 ± 2.64 , respectively; suggesting that there were no significant differences among the groups. Moreover, the means \pm SEM for neurons in the left (degenerated area) substantia nigra for the OCG, OE2PTG, and ODG groups were 120 ± 2.19 , 89 ± 1.68 , and 49 ± 1.67 , respectively suggesting a significant ($P < 0.05$) reduction of neurons in the groups as compared to control group (Fig.2). Progressive degeneration of the nigral dopaminergic neurons after 6-OHDA administration was observed in ODG group (Fig.2A). In ODG group, the number of neurons was statistically less than OCG group suggesting the degeneration of neurons in substantia nigra by 6-OHDA (Fig.2). In OE2PTG group (Fig.2B), 17 β -estradiol prevented the neuronal degeneration of substantia nigra in OE2PTG group and fewer neurons degenerated in comparison with the OCG group (Fig.2C).

Gene expression analysis

The results of *P62*, *Ulk1*, and *Lc3* gene expression analyses in the three experimental groups indicated that *P62* and *Lc3* genes expressed in all groups while *Ulk1* was only expressed in ODG group. In OE2PTG group after receiving E2, *Ulk1* was overexpressed (Fig. 3). *Gapdh* was used as an internal control expressed in all groups.

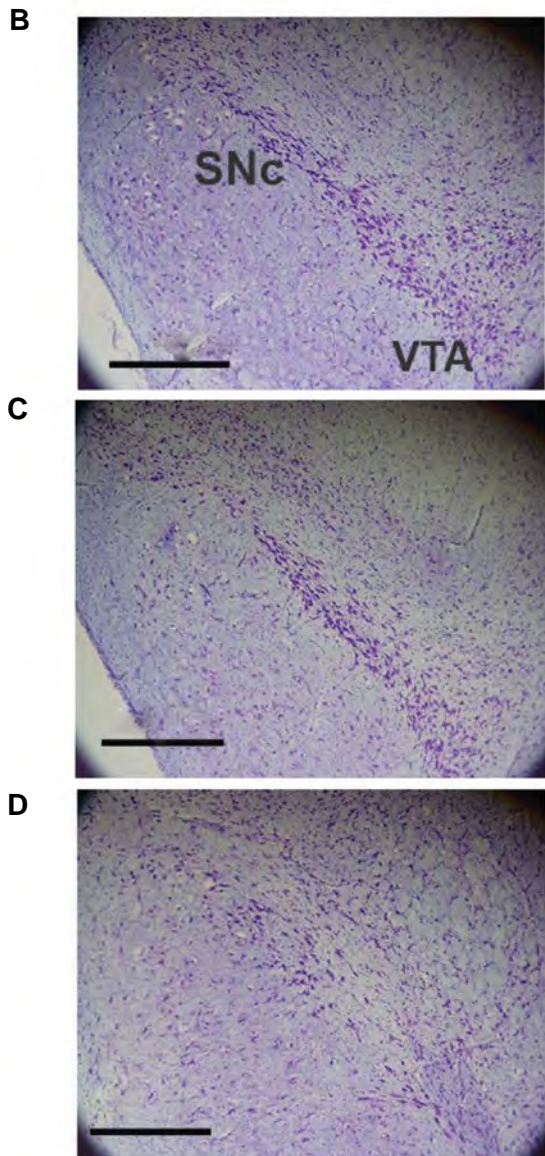
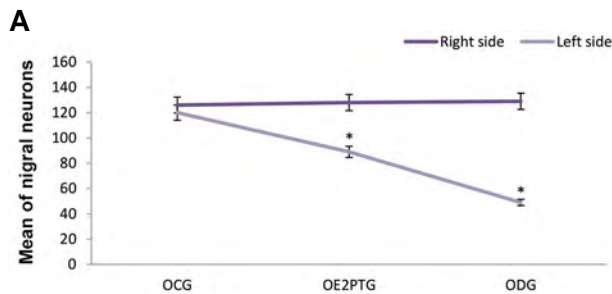


Fig.2: Neuronal counts in the substantia nigra. **A.** The means of nigral neurons in the left and right sides of the three experimental groups have been shown. On the right side, there were no significant differences among the groups. However, for the left side, a significant difference was observed for all groups ($P < 0.05$). Neurons in substantia nigra in the left side of the experimental groups with Nissl staining for **B.** OCG group, **C.** OE2PTG group, and **D.** ODG group. Abundant neurons existed in the substantia nigra and ventral tegmental area of OCG and OE2PTG groups. In contrast, the number of neurons was progressively decreased in substantia nigra ipsilateral to 6-OHDA injection in ODG group. OCG, ODG, ovariectomized E2 pretreatment group (OE2PTG), substantia nigra pars compacta (SNc), ventral tegmentum area (VTA) (scale bars: 200 μ m). OCG; Ovariectomized control group, ODG; Ovariectomized degeneration group, and *, Shows the statistically significant difference in OCG group ($P < 0.05$).

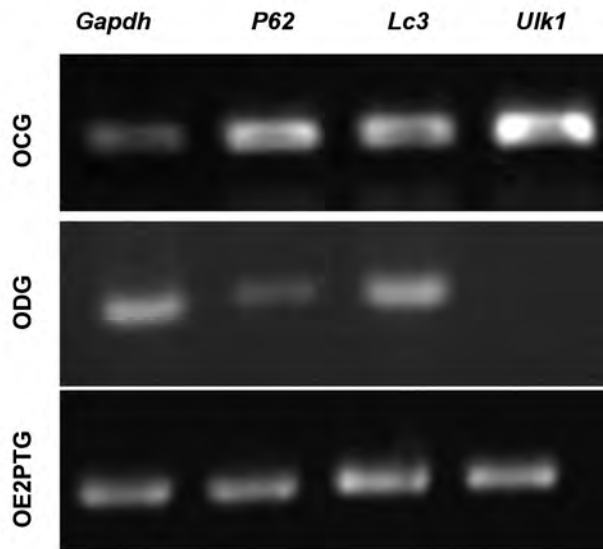


Fig.3: Gene expression results. The *P62* and *Lc3* expressed in all groups, while *Ulk1* was expressed only in ovariectomized degeneration (ODG) group. In ovariectomized rats pretreated with 17 β -estradiol before 6-hydroxydopamine injection (OE2PTG), *Ulk1* was overexpressed. *Gapdh* was used as an internal control which was expressed in all groups. OCG; Ovariectomized control group.

Discussion

In the present experimental study, 17 β -estradiol improved the motor behavior and reduced apomorphine-induced rotational behavior, ii. Reduced the degeneration of substantia nigra neurons which was induced by the neurotoxic effects of 6-OHDA, and iii. Overexpression of *ULK1* inhibited by 6-OHDA. In this study, 6-OHDA injections caused behavioral and tissue changes in accordance with PD model development. This model for PD is the most common pre-clinical model that has been well known due to its effects on the nigrostriatal dopaminergic system. 6-OHDA model caused molecular changes in the substantia nigra, which is most similar to PD characteristics in humans. The biological functions of estrogen are mediated by binding to the estrogen receptor- α and estrogen receptor- β ; by which estrogen has a slow genomic mechanism that protects the cells against apoptosis and inflammatory reactions and regulates the growth factors and neurotrophins and contributes to the formation of synapses.

Studies have also suggested that ovarian removal can cause significant behavioral changes in apomorphine-induced in animals (9). Such changes can be due to the reduced number of dopaminergic neurons in substantia nigra (10). In addition, these neurotransmitter changes following the removal of the gonads can justify the nervous system disorder in women after the menopause. Another study in ovariectomized rats indicated the ability of estrogen to increase the dopamine absorption in the nigrostriatal dopaminergic system (11). In a study conducted in monkeys, it was observed that more than 30% of dopaminergic neurons in substantia nigra were disappeared 30 days after ovariectomy and estrogen prevented the degeneration of neurons within 10 days (12),

however, they did not explore the underlying mechanism. In a study conducted *in vitro* model of PD, it was observed that estrogen is able to prevent the cell apoptosis against 6-OHDA toxicity by activating anti-apoptotic proteins and inhibiting pro-apoptotic proteins (13). Yet, they did not investigate the other estrogen pleiotropic effects. Studies have shown that 17 β -estradiol mediates its effect through the dopamine receptors (14). For the treatment of neurological diseases, cell and gene therapy along with various methods for the differentiation of mesenchymal stem cell and their differentiation into the neurons have been widely used (15-18). Moreover, epigenetic alteration and sex hormone therapy may be the other available treatment options as well. Indeed, studies have also indicated that the sex hormones are effective in the treatment of other neurodegenerative diseases (19) as we showed earlier. Consistent with our study, it has been recently shown that 17 β -estradiol can regulate autophagy (20).

Macroautophagy is a conserved protein degradation mechanism in which the cargo is surrounded by autophagosome and then fused with the lysosome. In the initiation phase of autophagy, the first step is the formation of autophagosome. ULK1 as an upstream protein starts the process of autophagy and is regulated by signals such as mTOR, AMP-activated protein kinase (AMPK), and glycogen synthase kinase 3 (GSK3) (21). Under the normal conditions, mTOR is phosphorylated and negatively regulates the complexes such as ULK1, ULK2, ATG101, ATG13, and FIP200. As mTOR is inhibited, ULK1 activation results in activation of ATG13 and FIP200 upon the initiation of autophagy. The deficiency in autophagy can cause neurodegenerative diseases such as Alzheimer's disease, Parkinson's disease, and amyotrophic lateral sclerosis (22, 23). In PD, phosphorylated α -synuclein is fibrillated and accumulated known as Lewy bodies (24). The ULK1 has been observed in Lewy bodies. Evidence suggests that the downstream protein, LC3, contributes to Lewy body formation. Phosphatidyl ethanolamine-conjugated form of LC3 (LC3II) is bound to the internal surface of autophagosome and acts as a clasp for the cargo receptors such as P62 (25). These results indicate that autophagy-lysosome system plays a significant role in the pathogenesis of PD and Lewy body formation. In the present study, 17 β -estradiol increased the expression of ULK1 in animals with PD. In another study, 17 β -estradiol prevented osteoblast cell death by activating autophagy and ER-ERK-mTOR and expressing ULK1 and Beclin-1 (20). ULK1 plays a significant role in the bingeing of the autophagy process. The deficiency in autophagy can also cause the abnormal protein accumulations and damage to the organelles in neurodegeneration. Since some PD models can impair mitochondrial functions, deficiency in controlling the mitochondrial quality plays a crucial role in the pathogenesis of PD. The studies have shown that selective degradation of damaged mitochondria is a part of an important homeostasis pathway for controlling the organelles quality and mitophagy (mitochondrial autophagy) playing a vital role in mitochondrial

decomposition and maintaining dopaminergic neurons.

On the other hand, protein accumulation as a cellular pathology has been observed in many neurodegenerative diseases including PD. In this context, autophagy is considered one of the major proteolytic systems which can maintain the homeostasis of the cellular proteins. ULK1 is required to form autophagosomes in mammalian cells. It has been proven that ULK1 and 2 are necessary for autophagy. *LC3* is one of the autophagic genes that its product accumulates in the autophagosome membrane and is considered an autophagy marker (25). ATG101 is a binding protein for ATG13 which is a part of ATG1/ULK1 serine-threonine kinase and is required for autophagy induction. The ULK1 complex contains ATG13 and FIP200 which are required for autophagy initiation. The interaction between ATG101 and ATG13 is important for the stability and phosphorylation of ATG13 and ULK1. Therefore, the lack of *ULK1* expression leads to the disturbance in the initiation of autophagy.

Conclusion

In this study, the administration of 17 β -estradiol led to *Ulk1* overexpression and regulating autophagy accompanied by the improvement in behavioral and tissue of animal model of PD.

Acknowledgments

This work was financially supported by a research grant from the Qazvin University of Medical Sciences. The authors have no conflict of interest.

Authors' Contributions

R.V.; Contributed to performing experimental procedures (creating a disease model and doing behavioral tests). A.N.-Z.; Contributed to performing experimental procedures. F.R.; Helped in tissue processing. S.D.; Involved in designing of the main idea of the current study and contributed to performing experimental procedures. S.B.; Performed the Nissl staining and edited the manuscript. All authors read and approved the final manuscript.

References

1. Collier TJ, Kanaan NM, Kordower JH. Aging and Parkinson's disease: different sides of the same coin? *Mov Disord.* 2017; 32(7): 983-990.
2. Brann DW, Dhandapani K, Wakade C, Mahesh VB, Khan MM. Neurotrophic and neuroprotective actions of estrogen: basic mechanisms and clinical implications. *Steroids.* 2007; 72(5): 381-405.
3. Sun Q, Liang Y, Zhang T, Wang K, Yang X. ER- α 36 mediates estrogen-stimulated MAPK/ERK activation and regulates migration, invasion, proliferation in cervical cancer cells. *Biochem Biophys Res Commun.* 2017; 487(3): 625-632.
4. Dluzen DE, McDermott JL. Gender differences in neurotoxicity of the nigrostriatal dopaminergic system: implications for Parkinson's disease. *J Gend Specif Med.* 2000; 3(6): 36-42.
5. Alyea RA, Laurence SE, Kim SH, Katzenellenbogen BS, Katzenellenbogen JA, Watson CS. The roles of membrane estrogen receptor subtypes in modulating dopamine transporters in PC-12 cells. *J Neurochem.* 2008; 106(4): 1525-1533.
6. Taber KH, Murphy DD, Blurton-Jones MM, Hurley RA. An update

- on estrogen: higher cognitive function, receptor mapping, neurotrophic effects. *J Neuropsychiatry Clin Neurosci*. 2001; 13(3): 313-317.
7. Filfan M, Sandu RE, Zavaleanu AD, GresiTa A, Glavan DG, Olaru DG, et al. Autophagy in aging and disease. *Rom J Morphol Embryol*. 2017; 58(1): 27-31.
 8. Lan YL, Zhao J, Li S. Update on the neuroprotective effect of estrogen receptor alpha against Alzheimer's disease. *J Alzheimers Dis*. 2015; 43(4): 1137-1148.
 9. Baraka AM, Korish AA, Soliman GA, Kamal H. The possible role of estrogen and selective estrogen receptor modulators in a rat model of Parkinson's disease. *Life Sci*. 2011; 88(19-20): 879-885.
 10. Meitzen J, Meisel RL, Mermelstein PG. Sex differences and the effects of estradiol on striatal function. *Curr Opin Behav Sci*. 2018; 23: 42-48.
 11. Morissette M, Al Sweidi S, Callier S, Di Paolo T. Estrogen and SERM neuroprotection in animal models of Parkinson's disease. *Mol Cell Endocrinol*. 2008; 290(1-2): 60-69.
 12. Leranath C, Roth RH, Elsworth JD, Naftolin F, Horvath TL, Redmond DE Jr. Estrogen is essential for maintaining nigrostriatal dopamine neurons in primates: implications for Parkinson's disease and memory. *J Neurosci*. 2000; 20(23): 8604-8609.
 13. Li XL, Cheng WD, Li J, Guo XL, Guo CJ, Meng XH, et al. Protective effect of estrogen on apoptosis in a cell culture model of Parkinson's disease. *Clin Invest Med*. 2008; 31(5): E258-E264.
 14. Bâ A, Silué S, Bamba B, Bamba L, Gahié SV. Effects of Ovariectomy and 17 β -Estradiol Replacement on dopamine D2 receptors in female rats: consequences on sucrose, alcohol, water intakes and body weight. *Behav Brain Sci*. 2018; 8(01): 1.
 15. Darabi S, Tiraihi T, Delshad A, Sadeghizadeh M, Khalil W, Taheri T. In vitro non-viral murine pro-neurotrophin 3 gene transfer into rat bone marrow stromal cells. *J Neurol Sci*. 2017; 375: 137-145.
 16. Haratizadeh S, Nazm Bojnordi M, Darabi S, Karimi N, Naghikhani M, Ghasemi Hamidabadi H, et al. Condition medium of cerebrospinal fluid and retinoic acid induces the transdifferentiation of human dental pulp stem cells into neuroglia and neural-like cells. *Anat Cell Biol*. 2017; 50(2): 107-114.
 17. Darabi S, Tiraihi T, Noori-Zadeh A, Rajaei F, Darabi L, Abbaszadeh HA. Creatine and retinoic acid effects on the induction of autophagy and differentiation of adipose tissue-derived stem cells into GABAergic-like neurons. *Journal of Babol University of Medical Sciences*. 2017; 19(8): 41-49.
 18. Kazemi H, Noori-Zadeh A, Darabi S, Rajaei F. Lithium prevents cell apoptosis through autophagy induction. *Bratisl Med J*. 2018; 119(4): 234-239.
 19. De Nicola AF, Garay LI, Meyer M, Guennoun R, Sitruk-Ware R, Schumacher M, et al. Neurosteroidogenesis and progesterone anti-inflammatory/neuroprotective effects. *J Neuroendocrinol*. 2018; 30(2).
 20. Yang YH, Chen K, Li B, Chen JW, Zheng XF, Wang YR, et al. Estradiol inhibits osteoblast apoptosis via promotion of autophagy through the ER-ERK-mTOR pathway. *Apoptosis*. 2013; 18(11): 1363-1375.
 21. Kim J, Kundu M, Viollet B, Guan KL. AMPK and mTOR regulate autophagy through direct phosphorylation of Ulk1. *Nat Cell Biol*. 2011; 13(2): 132-141.
 22. Shams Nooraei M, Noori-Zadeh A, Darabi S, Rajaei F, Golmohammadi Z, Abbaszadeh HA. Low level of autophagy-related gene 10 (ATG10) expression in the 6-hydroxydopamine rat model of parkinson's disease. *Iran Biomed J*. 2018; 22(1): 15-21.
 23. Guo F, Liu X, Cai H, Le W. Autophagy in neurodegenerative diseases: pathogenesis and therapy. *Brain Pathol*. 2018; 28(1): 3-13.
 24. Wood H. Parkinson disease: plasma alpha-synuclein-a potential marker of cognitive impairment in Parkinson disease. *Nat Rev Neurol*. 2017; 13(8): 450.
 25. Padman BS, Nguyen TN, Lazarou M. Autophagosome formation and cargo sequestration in the absence of LC3/GABARAPs. *Autophagy*. 2017; 13(4): 772-774.
-

Influence of Ellagic Acid and Ebselen on Sperm and Oxidative Stress Parameters during Liquid Preservation of Ram Semen

Mustafa Numan Bucak, Ph.D.^{1*}, Mustafa Bodu, D.V.M.¹, Nuri Başpınar, Ph.D.², Şükrü Güngör, Ph.D.³, Pınar İli, Ph.D.⁴, Begimay Acibaeva, D.V.M.⁴, Tohid Rezaei Topraggaleh, D.V.M.⁵, Şükrü Dursun, Ph.D.⁶

1. Department of Reproduction and Artificial Insemination, Faculty of Veterinary Medicine, Selcuk University, Konya, Turkey

2. Department of Biochemistry, Faculty of Veterinary Medicine, Selcuk University, Konya, Turkey

3. Department of Reproduction and Artificial Insemination, Faculty of Veterinary Medicine, Mehmet Akif Ersoy University, Burdur, Turkey

4. Pamukkale University, Denizli Health Services Vocational High School, Denizli, Turkey

5. Department of Embryology, Reproductive Biomedicine Research Center, Royan Institute for Reproductive Biomedicine, ACECR, Tehran, Iran

6. Department of Gynecology and Obstetrics, Faculty of Veterinary Medicine, Aksaray University, Aksaray, Turkey

*Corresponding Address: Department of Reproduction and Artificial Insemination, Faculty of Veterinary Medicine, Selcuk University, Konya, Turkey
Email: mnumanbucak@gmail.com

Received: 26/Oct/2017, Accepted: 10/Apr/2018

Abstract

Objective: The purpose of the present study was to assess the effects of ellagic acid and ebselen on sperm and oxidative stress parameters during liquid preservation of ram semen.

Materials and Methods: In this experimental study, sixty ejaculates from six mature Merino rams were used. In experiment 1, the ejaculates were diluted in base extender contained ellagic acid at 0 (control), 0.5, 1, and 2 mM. In experiment 2, ebselen at 0 (control), 10, 20, and 40 µM were added to the extender. Sperm motility, viability, mitochondrial membrane potential, DNA integrity, lipid peroxidation (LPO), the antioxidant potential (AOP), and total glutathione (tGSH) were evaluated at 0, 24, 48, and 72 hours of preservation.

Results: Supplementation of ellagic acid at 1 and 2 mM resulted in higher sperm motility and viability at 0 hours of storage. Ellagic acid at 2 mM led to higher motility and viability compared to controls after 0, 24, and 48 hours of preservation and increased AOP after 24 and 72 hours. Higher tGSH was at 1 mM ellagic acid, compared to control after 72 hours. Addition of ebselen at a concentration of 40 µM increased motility at 24 and 48 hours and 10 µM produced the same effect after 48 and 72 hours of storage as well as higher viability, compared to the controls after 0 hours of storage. Sperm DNA integrity was significantly improved after 24, 48, and 72 hours with the addition of ebselen at 10 µM, and after 72 hours at 40 µM. Addition of 40 mM ebselen also reduced the LPO levels after 24 hours of storage compared to the controls.

Conclusion: The results showed that supplementation of ellagic acid and ebselen in semen extender has a potential effect on sperm and oxidative stress parameters during liquid preservation of ram semen.

Keywords: Ebselen, Ellagic Acid, Preservation, Ram, Sperm Parameters

Cell Journal(Yakhteh), Vol 21, No 1, Apr-Jun (Spring) 2019, Pages: 7-13

Citation: Bucak MN, Bodu M, Başpınar N, Güngör Ş, İli P, Acibaeva B, Topraggaleh TR, Dursun Ş. Influence of ellagic acid and ebselen on sperm and oxidative stress parameters during liquid preservation of ram semen. Cell J. 2019; 21(1): 7-13. doi: 10.22074/cellj.2019.5593.

Introduction

Artificial insemination is a valuable tool that plays a critical role in the reproduction of small ruminants. It facilitates the distribution of semen from superior sires to a large number of females, allowing the improvement of desirable characteristics, e.g. milk, meat, and wool production (1, 2). Artificial insemination, which is done using fresh, liquid preserved or frozen-thawed semen, improves the lambing rate in sheep breeding (1, 3). Successful liquid preservation of ram semen is achieved by providing the necessary environmental conditions. These conditions include: i. The development of extenders that keep functional sperm parameters, ii. Minimizing the generation of reactive oxygen species (ROS), and the prevention of oxidative stress (1, 4).

Ram sperm is more susceptible to ROS than the other species due to a higher ratio of polyunsaturated/saturated fatty acids and a lower cholesterol/phospholipid molar

ratio (5). The polyunsaturated fatty acids (PUFAs) render the sperm membrane a high vulnerability to the sperm membrane to be attacked by ROS resulting in functional impairment of the sperm cells (6). The effect of ROS generated during the peroxidation of sperm membrane lipids leads to poor quality semen, decreased motility, damaged DNA, disrupted acrosome reaction, and capacitation (7). Normally, the semen contains antioxidants, including taurine, catalase, glutathione, glutathione peroxidase (GPx), and superoxide dismutase that can oppress the lipid peroxidation (LPO) and excessive ROS generation (5). However, this endogenous antioxidative capacity may be insufficient in preventing the LPO during a prolonged storage or an unfrozen state (8). Reports have indicated that the addition of antioxidants, such as methionine, dithioerythritol, taurine, lipoic acid, lycopene, cysteamine, and reduced glutathione into the sperm extenders decreased the impact of different

oxidants and protected the sperm cells from oxidative damage during liquid preservation of ram spermatozoa (9-12).

Ellagic acid is a natural phenol compound with a polyphenolic structure and a strong antioxidant. The cryoprotective and antioxidative properties of ellagic acid have been previously reported in a reduction of the LPO and increment of the total glutathione (tGSH) and GPx levels in rats (13). Also, oral administration of ellagic acid has been observed to increase epididymal sperm motility and its concentration in rats (14). Ellagic acid has also demonstrated the protective effects against adriamycin, which has the disrupting effects on epididymal sperm quality parameters and the LPO in the rat testis (15).

Ebselen (2-phenyl-1,2-benzisoselenazol-3[2H]-1) is a seleno-organic molecule which scavenges ROS by mimicking the GPx activity (16). Ebselen, with its cyto/neuroprotective effects, has been observed to reduce the DNA damage and oxidative stress caused by hydrogen peroxide generated in hamster lung fibroblasts (17). Also, ebselen was reported to reduce the LPO levels, demonstrating the protective effects in the murine cardiovascular system (18). In humans, ebselen has been reported to be a substrate for the thioreductase system and a mimetic for the GPx activity in the presence of glutathione and glutathione reductase (GR) (16).

We found that there has been no research conducted to compare the influence of the antioxidants, ellagic acid, and ebselen at different doses during liquid preservation of ram sperm. Therefore, the aim of this study is to evaluate the effects of ellagic acid and ebselen at different doses which were added to Tris extender to monitor ram sperm motility, viability, mitochondrial membrane potential, the DNA integrity as well as oxidative stress parameters (total antioxidant potential, lipid peroxidation, and total glutathione) up to 72 hours of liquid storage at 5°C.

Materials and Methods

All chemicals were obtained from Sigma Aldrich (St. Louis, MO, USA) unless otherwise indicated. In this experimental study, employed protocols were approved by the Animal Ethics Committee of the Veterinary faculty of Selcuk University, Turkey.

Animals and semen collection

The study was conducted at the Bahri Dagdaş International Agricultural Research Institute (Konya, Turkey) during the breeding season (autumn to early winter) 2016. A total number of 60 ejaculates from six mature Merino rams (2 and 3 years of age) were collected twice a week using an artificial vagina. Ejaculates meeting the following criteria were evaluated: a volume of 0.5-2 mL, a minimum sperm concentration of 2×10^9 sperm/mL, and motility of >80 %. Semen samples of six rams were pooled and ten pooled samples were used in each experiment.

Semen processing and experimental design

Semen volume was measured with a graduated conical tube and sperm concentration was determined using a hemocytometer. A Tris-based extender (Tris 297.58 mM, citric acid 96.32 mM, fructose 86.66 mM, egg yolk 15 % (v/v) at pH=6.8) was used as a base extender. This study included two experiments carried out in succession.

Experiment 1: Each pooled ejaculate was diluted in a Tris-based extender (37°C) and divided into four equal experimental groups contained ellagic acid at 0 (control), 0.5, 1, and 2 mM with a final sperm concentration of approximately 400×10^6 cells/mL.

Experiment 2: Ebselen at 0 (control), 10, 20 and, 40 µM was used as an additive to the extender and the above procedure was applied for dividing and extending the semen.

For both of experiments, diluted semen samples with antioxidants were kept in 15-mL plastic tubes and cooled down from 37 to 5°C (within one hour) and kept at 5°C during liquid preservation for up to 72 hours. The sperm quality and oxidative stress parameters were determined after 0, 24, 48, and 72 hours of liquid storage in both experiments. The procedure was repeated 10 times for each experiment.

Semen evaluation

Evaluation of sperm parameters during liquid preservation of ram semen

Motility evaluation

Sperm motility was measured using a phase-contrast microscope ($\times 200$ magnification). Five microliters of sample were dropped onto a pre-warmed microscope slide and then covered with a coverslip. For each semen sample, sperm motility was measured in three different microscopic fields. The mean of the three successive estimations was recorded as a final motility score (19).

Assessment of sperm plasma membrane integrity (viability)

Sperm plasma membrane integrity was assessed using a Sperm Viability Kit (SYBR-14/PI Molecular Probe: L 7011 Invitrogen, Carlsbad, CA) following a modified protocol from Garner et al. (20). A working solution of SYBR-14 was diluted at a ratio of 1:10 with dimethyl sulfoxide (DMSO) (Applichem A3006) and propidium iodide (PI) was dissolved in distilled water at 2 mg/mL. The semen sample was diluted at 1:3 with Tris stock solution (Tris 297.58 mM, citric acid 96.32 mM, fructose 86.66 mM) and then 30 µL of the diluted semen was mixed with 6 µL of SYBR-14 and 2.5 µL of PI. The sample was mixed and incubated at 37°C in the dark place for 20 minutes. Then, 10 µL of Hancock solution was prepared according to the protocol from Schäfer et al in order to stop the sperm motion (21). A drop of 2.5 µL sample was placed on a microscope slide and covered

with a coverslip. At least 200 spermatozoa were examined at 1000x magnification under a fluorescence microscope (Leica DM 3000 Microsystems GmbH, Ernst-Leitz-Straße, Wetzlar, Germany; excitation at 450-490 nm, emission at 520 nm) to evaluate the sperm membrane integrity. The sperms exhibiting green-red or red color were considered membrane damaged (not viable), while those displaying green color were considered intact membranes spermatozoa (viable) (22).

Evaluation of sperm mitochondrial activity

For the assessment of sperm mitochondrial activity, a stock solution contained 5, 5', 6, 6'-Tetrachloro-1, 1', 3, 3' tetraethyl-benzimidazolylcarbocyanine iodide (1.53 mM) (T3168 JC-1, Invitrogen, Carlsbad, CA) in dimethyl sulfoxide (DMSO) was prepared. The semen sample was diluted 1:3 with Tris stock solution. Subsequently, 2.5 µL of JC-1 and 2.5 µL PI were added to 300 µL of diluted samples and gently mixed and incubated at 37°C for 20 minutes in the dark place. Then, 10 µL of Hancock solution was added to stop sperm motion. A drop of (2.5 µL) the sample was placed on a microscope slide and covered with a coverslip. At least 200 sperm cells were observed at ×1000 magnification under a fluorescence microscope (Leica DM 3000 Microsystems GmbH, Ernst-Leitz-Straße, Wetzlar, Germany; excitation at 450-490 nm, emission at 520 nm) to assess the mitochondrial activity. A high level of yellow/orange and green fluorescence in sperm midpiece indicated the high and low mitochondrial activity, respectively (12).

Evaluation of sperm DNA damage

Single cell gel electrophoresis (COMET) assay was used for the evaluation of sperm DNA damage. The semen samples were centrifuged at 600x g for 10 minutes at 4°C and the remaining pellets were resuspended in phosphate buffered saline (PBS). Pre-cleaned slides were coated with a layer of 1% solution normal melting agarose in PBS and dried at room temperature. Eighteen microliters of the sperm/PBS mixture were mixed with a 0.75% solution of low melting agarose (50 µL) and placed onto first agarose layer (approximately 1×10^5 cells). The slides were kept at 4°C for 20 minutes. Then coverslips were removed and slides were immersed in lysis buffer (2.5 M NaCl, 10 mM Tris, 100 mM Na₂EDTA, 10 mM Trizma base, 1% N-lauroyl sarcosine, 1% Triton X-100, 70 mM DL Dithiothreitol, pH=10.0) contained 20 µg/mL proteinase K (Vivantis) for 2 hours at 37°C. Then slides were horizontally placed in electrophoresis buffer [1X Tris/Borate/EDTA (TBE) buffer, pH=8] and electrophoresis was performed at room temperature at 25 Volts for 20 minutes. Following the electrophoresis, slides were air-dried and stained with 50 µL of 8 µg/mL ethidium bromide and covered with a coverslip.

The images of 200 randomly selected sperm nuclei were evaluated through a visual observation (×1000 magnification) using a fluorescent microscope (Leica DM 3000 Microsystems GmbH, Ernst-Leitz-Straße, Wetzlar,

Germany). Each image was classified as damaged (sperm showing a “comet” pattern possessed a tail of fragmented DNA migrated from the sperm head) and undamaged (whole sperm heads without a comet tail). All data were expressed as the mean percentages of the undamaged sperm heads ± SEM (22).

Evaluation of oxidative stress parameters during liquid preservation of ram semen

Diluted semen samples were centrifuged at 800 xg for 10 minutes at 4°C and the spermatozoa were washed twice with saline through the procedure mentioned above. Then, the supernatant was removed, and pellets were resuspended in 500 µL of PBS, transferred into a 2-mL beaker on ice water and sonicated with a probe (Bandelin Sonopuls, Bandelin Electronic Heinrichstraße, D-12207, Gerate-Typ: UW 2070, Pro-Nr. 51900037369.004, Berlin) for 10 seconds on ice. This procedure was repeated 5 times at intervals of 30 seconds. 10 µL of Butylated Hydroxy Toluene (BHT, B-1378) was added to 120 µL of sonicated homogenate to avoid further oxidation and stored at -86°C until the LPO assay. The remaining sonicated homogenate was centrifuged at 8000 xg for 5 minutes at 4°C. The supernatant was collected and stored at -86°C until AOP and tGSH assays (22).

Determination of AOP, LPO, and tGSH levels

The AOP, LPO, and tGSH levels were measured with the use of the AOP-490™, LPO-586™ and GSH-420™ kits respectively (Oxis Research™, Bioxytech, CA, 92202, USA) according to manufacturer's instructions. Absorption was measured at 490 nm, 586 nm and 405 nm for AOP, LPO, and tGSH, respectively using a spectrophotometer (UV 2100 UV-VIS Recording Spectrophotometer Shimadzu, Japan). The results of the AOP assay were expressed as mmol (10⁹ cells/mL), LPO and tGSH were expressed as µmol (10⁹ cells/mL) (22).

Statistical analysis

The test was repeated 10 times for each experiment. The results were expressed as the mean ± SEM. The means were analyzed by analysis of variance (ANOVA) followed by Duncan's post hoc test to determine the significance in all the parameters within all groups using the SPSS/PC computer program (Version 15.0, SPSS, Chicago, IL). The differences were considered to be statistically significant when the P value was less than 0.05.

Results

Sperm motility, SYBR/PI, JC-1/PI, and the DNA integrity rate of Merino ram semen supplemented with different concentrations of ellagic acid are shown in Table 1 and oxidative stress parameters in Table 2. The sperm viability, the mitochondrial activity, and the DNA integrity are shown in Figure 1. The extender supplemented with 1 and 2 mM doses of ellagic acid resulted in a higher motility and the percentage of viable sperm in comparison to the

control groups at 0 hours of storage ($P<0.05$). Ellagic acid at 2 mM led to a higher motility and viability rates when compared to controls during 0, 24, and 48 hours of liquid storage ($P<0.05$). When ellagic acid was added, the rates of the sperm mitochondrial activity and the DNA

integrity were not statistically improved for any of the storage periods at 5°C. Ellagic acid at 2 mM concentration increased the AOP activity at 24 and 72 hours and tGSH after 72 hours at 1 mM, in comparison with the controls ($P<0.05$).

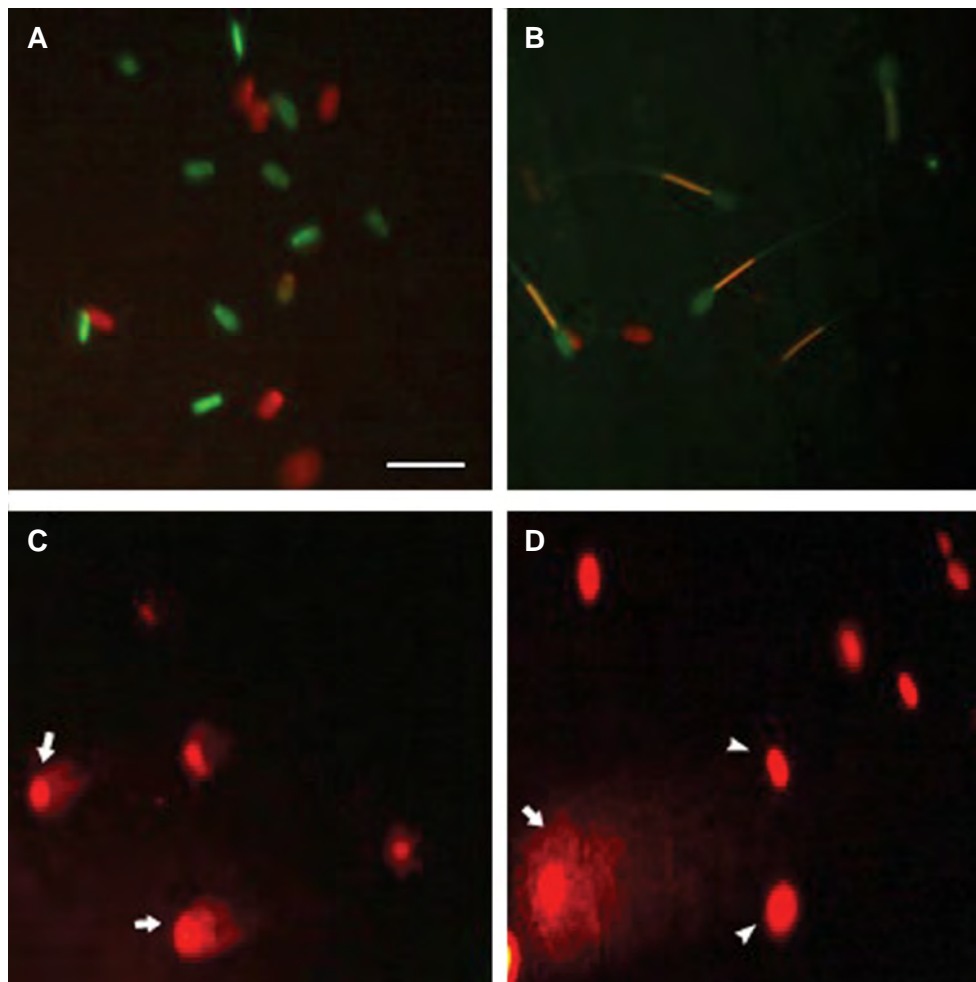


Fig.1: Viability, mitochondrial activity, and DNA integrity of ram spermatozoa. **A.** Sperm viability assessed by SYBR/PI. Sperm displaying green-red or red was considered as membrane damaged (not viable), while sperm displaying green was considered to be intact membrane (viable). **B.** JC-1/PI staining for mitochondrial activity. Yellow/orange and green fluorescence associated with midpiece of sperm indicated a high and a low mitochondrial activity, respectively. No fluorescence associated with the midpiece of sperm indicated no mitochondrial activity. **C and D.** Sperm DNA damage assessed using COMET assay. Sperm heads with undamaged (arrow) DNA and with damaged (arrowhead) DNA (scale bar: 20 μ m).

Table 1: Mean (\pm SE) sperm motility, SYBR/PI, JC-1/PI and DNA integrity (%) of Merino ram semen supplemented with different concentrations of ellagic acid for different storage times at 5°C

Groups	0 hour				24 hours				48 hours				72 hours			
	Motility	JC-1/PI	SYBR/PI	DNA Integrity	Motility	JC-1/PI	SYBR/PI	DNA Integrity	Motility	JC-1/PI	SYBR/PI	DNA Integrity	Motility	JC-1/PI	SYBR/PI	DNA Integrity
Control	79.1 (\pm 2.0 ^a)	84.0 (\pm 2.8)	71.3 (\pm 2.1 ^a)	85.5 (\pm 3.3)	70.8 (\pm 0.8 ^a)	77.8 (\pm 4.6)	64.1 (\pm 2.6 ^a)	70.0 (\pm 7.0)	63.3 (\pm 1.6 ^a)	72.5 (\pm 6.9)	54.0 (\pm 3.8 ^a)	67.6 (\pm 5.4)	54.1 (\pm 3.9)	56.7 (\pm 6.2)	58.9 (\pm 5.0)	67.3 (\pm 5.8)
0.5 mM	82.5 (\pm 1.1 ^{ab})	82.6 (\pm 4.9)	75.6 (\pm 2.5 ^{ab})	81.0 (\pm 3.6)	73.3 (\pm 1.6 ^{ab})	75.6 (\pm 5.8)	65.9 (\pm 4.1 ^{ab})	66.8 (\pm 5.8)	67.5 (\pm 1.1 ^{ab})	70.0 (\pm 5.1)	58.1 (\pm 2.6 ^a)	66.3 (\pm 4.6)	61.6 (\pm 2.1)	59.3 (\pm 6.5)	55.3 (\pm 2.2)	67.8 (\pm 3.8)
1 mM	85.8 (\pm 1.5 ^b)	85.3 (\pm 2.9)	78.9 (\pm 1.6 ^b)	82.1 (\pm 3.0)	73.3 (\pm 1.0 ^{ab})	80.6 (\pm 4.3)	63.1 (\pm 3.0 ^{ab})	73.0 (\pm 2.4)	65.8 (\pm 2.0 ^{ab})	70.9 (\pm 6.8)	58.4 (\pm 2.6 ^a)	69.0 (\pm 2.6)	57.5 (\pm 2.5)	64.1 (\pm 7.3)	57.0 (\pm 4.1)	70.3 (\pm 3.5)
2 mM	85.0 (\pm 1.2 ^b)	85.2 (\pm 4.9)	78.7 (\pm 2.0 ^b)	85.0 (\pm 2.4)	75.0 (\pm 0 ^b)	78.1 (\pm 5.8)	73.0 (\pm 1.9 ^b)	76.5 (\pm 2.9)	69.1 (\pm 2.0 ^b)	71.7 (\pm 5.4)	69.4 (\pm 2.6 ^b)	78.0 (\pm 3.0)	63.3 (\pm 1.6)	69.2 (\pm 6.2)	64.0 (\pm 1.8)	70.5 (\pm 2.9)

Means with different letters (a, b) in the same column demonstrate significant differences ($P<0.05$).

The sperm motility, SYBR/PI, JC-1/PI, and the sperm DNA integrity in Merino ram semen supplemented with different concentrations of ebselen are shown in Table 3 and oxidative stress parameters in Table 4. The extender supplemented with 40 μM ebselen led to higher motility rates in comparison with the control groups at 24 and 48 hours and at 48 and 72 hours time points with 10 μM . Ebselen at a concentration of 10 μM resulted in a higher

viability rate compared to control group at 0 hours of storage. The DNA integrity analysis revealed that ebselen provided a better protective effect on the DNA integrity compared to other groups at 10 μM after 24, 48 and 72 hours, and after 72 hours at 40 μM ($P < 0.05$). Regarding the biochemical parameters, only a dose of 40 mM ebselen reduced the LPO levels during 24 hours of liquid storage compared to controls ($P < 0.05$).

Table 2: Mean (\pm SE) LPO (μmol , 10^9 Cells/ml), tGSH (μmol , 10^9 Cells/ml) and AOP ($\text{mM} \times 10^9$) levels of Merino ram semen diluted with different doses of ellagic acid at different storage times at 5°C

Groups	0 hour			24 hours			48 hours			72 hours		
	AOP	LPO	tGSH	AOP	LPO	tGSH	AOP	LPO	tGSH	AOP	LPO	tGSH
Control	36.0 (\pm 5.0)	70.5 (\pm 32.9)	2142.5 (\pm 802.7)	28.4 (\pm 3.1 ^a)	57.7 (\pm 8.6)	1808.4 (\pm 320.6)	29.89 (\pm 4.6)	55.0 (\pm 11.5)	1644.0 (\pm 184.2)	28.9 (\pm 4.1 ^a)	41.4 (\pm 5.3)	1024.4 (\pm 187.2 ^a)
0.5 mM	66.5 (\pm 11.0)	100.8 (\pm 84.9)	2087.2 (\pm 1135.0)	58.5 (\pm 12.4 ^{ab})	74.7 (\pm 14.5)	1661.7 (\pm 276.8)	62.19 (\pm 12.1)	67.0 (\pm 14.0)	1445.4 (\pm 167.0)	63.5 (\pm 12.5 ^{ab})	84.1 (\pm 16.0)	1655.4 (\pm 240.1 ^{ab})
1 mM	55.1 (\pm 10.1)	58.9 (\pm 19.7)	2483.0 (\pm 978.5)	82.8 (\pm 18.8 ^{ab})	71.3 (\pm 7.5)	2392.0 (\pm 479.0)	65.24 (\pm 10.6)	53.3 (\pm 10.0)	2515.6 (\pm 725.0)	65.9 (\pm 12.9 ^{ab})	78.9 (\pm 17.0)	2630.9 (\pm 615.3 ^b)
2 mM	83.5 (\pm 18.3)	89.5 (\pm 31.6)	2494.7 (\pm 2203.0)	91.4 (\pm 18.2 ^b)	70.6 (\pm 17.3)	2197.8 (\pm 588.9)	56.75 (\pm 12.4)	68.8 (\pm 12.0)	1402.9 (\pm 131.3)	71.7 (\pm 9.7 ^b)	64.2 (\pm 15.2)	1718.2 (\pm 335.9 ^{ab})

Means with different letters (a, b) in the same column demonstrate significant differences ($P < 0.05$). LPO; Lipid peroxidation, tGSH; Total glutathione, and AOP; Total antioxidant potential.

Table 3: Mean (\pm SE) sperm motility, SYBR/PI, JC-1/PI and DNA integrity (%) of Merino ram semen supplemented with different concentrations of ebselen for different storage times at 5°C

Groups	0 hour				24 hours				48 hours				72 hours			
	Motility	JC-1/PI	SYBR/PI	DNA Integrity	Motility	JC-1/PI	SYBR/PI	DNA Integrity	Motility	JC-1/PI	SYBR/PI	DNA Integrity	Motility	JC-1/PI	SYBR/PI	DNA Integrity
Control	89.1 (\pm 0.8)	64.6 (\pm 2.4)	85.5 (\pm 1.3 ^a)	72.0 (\pm 1.3)	78.3 (\pm 1.0 ^a)	63.0 (\pm 1.1)	81.2 (\pm 1.8)	58.5 (\pm 3.1 ^a)	69.1 (\pm 0.8 ^a)	62.8 (\pm 1.5)	79.6 (\pm 2.3)	51.5 (\pm 1.6 ^a)	63.3 (\pm 1.0 ^a)	59.8 (\pm 2.2 ^{ab})	72.4 (\pm 1.9)	44.0 (\pm 2.6 ^a)
10 μM	90.0 (\pm 0)	71.5 (\pm 1.3)	93.3 (\pm 1.8 ^b)	68.2 (\pm 1.5)	80.8 (\pm 0.8 ^{ab})	64.7 (\pm 1.7)	83.9 (\pm 2.1)	65.3 (\pm 1.1 ^b)	73.3 (\pm 1.0 ^b)	62.7 (\pm 2.2)	80.0 (\pm 1.1)	58.0 (\pm 0.4 ^b)	69.1 (\pm 1.0 ^b)	63.4 (\pm 2.7 ^{ab})	73.0 (\pm 1.5)	54.3 (\pm 0.8 ^b)
20 μM	90.0 (\pm 0)	65.5 (\pm 1.9)	88.3 (\pm 0.9 ^{ab})	70.3 (\pm 2.9)	81.6 (\pm 1.0 ^{ab})	60.7 (\pm 0.6)	81.0 (\pm 3.3)	63.0 (\pm 0.8 ^{ab})	72.5 (\pm 1.1 ^{ab})	65.1 (\pm 1.6)	73.7 (\pm 2.7)	54.1 (\pm 1.2 ^a)	65.8 (\pm 1.1 ^a)	53.7 (\pm 1.5 ^a)	70.9 (\pm 3.3)	51.1 (\pm 1.3 ^{ab})
40 μM	90.0 (\pm 0)	67.6 (\pm 2.6)	88.6 (\pm 2.7 ^{abc})	71.5 (\pm 2.9)	82.6 (\pm 1.2 ^b)	61.2 (\pm 2.8)	79.3 (\pm 1.4)	62.6 (\pm 1.7 ^{ab})	73.3 (\pm 1.0 ^b)	62.7 (\pm 1.5)	79.8 (\pm 1.4)	53.1 (\pm 1.0 ^a)	65.0 (\pm 1.1 ^a)	59.0 (\pm 0.9 ^b)	70.0 (\pm 2.4)	53.3 (\pm 4.2 ^b)

Means with different letters (a, b) in the same column demonstrate significant differences ($P < 0.05$).

Table 4: Mean (\pm SE) LPO (μmol , 10^9 Cells/ml), tGSH (μmol , 10^9 Cells/ml) and AOP ($\text{mM} \times 10^9$) levels of Merino ram semen diluted with different doses of ebselen at different storage times at 5°C

Groups	0 hour			24 hours			48 hours			72 hours		
	AOP	LPO	tGSH	AOP	LPO	tGSH	AOP	LPO	tGSH	AOP	LPO	tGSH
Control	43.0 (\pm 7.2)	114.9 (\pm 25.3)	8088.6 (\pm 1784.5)	39.5 (\pm 4.3)	310.2 (\pm 52.4 ^b)	4860.2 (\pm 1063.2)	33.9 (\pm 5.4)	204.3 (\pm 32.3)	5627.3 (\pm 1362.1)	29.9 (\pm 4.2)	101.8 (\pm 11.9)	5214.2 (\pm 1376.6)
10 μM	45.2 (\pm 4.5)	156.8 (\pm 25.1)	10700.5 (\pm 4287.1)	38.5 (\pm 8.7)	186.1 (\pm 31.2 ^{ab})	4276.1 (\pm 952.6)	33.8 (\pm 5.1)	194.5 (\pm 41.5)	6468.4 (\pm 1120.8)	24.3 (\pm 6.5)	86.5 (\pm 9.2)	5626.2 (\pm 854.7)
20 μM	28.9 (\pm 2.2)	122.3 (\pm 67.1)	5411.9 (\pm 989.1)	35.6 (\pm 3.1)	313.8 (\pm 39.1 ^b)	4947.1 (\pm 865.5)	24.3 (\pm 3.8)	153.0 (\pm 21.3)	4790.2 (\pm 989.5)	35.7 (\pm 6.9)	104.9 (\pm 19.9)	4688.7 (\pm 1391.9)
40 μM	38.1 (\pm 2.0)	171.6 (\pm 45.9)	8220.4 (\pm 2761.6)	47.7 (\pm 6.7)	153.0 (\pm 22.9 ^a)	4277.7 (\pm 605.6)	37.9 (\pm 6.6)	157.4 (\pm 17.0)	6198.4 (\pm 1804.5)	26.1 (\pm 4.8)	92.1 (\pm 9.9)	4174.3 (\pm 727.7)

Means with different letters (a, b) in the same column demonstrate significant differences ($P < 0.05$). AOP; Total antioxidant potential, LPO; Lipid peroxidation, and tGSH; Total glutathione.

Discussion

Ram spermatozoa are more susceptible to ROS induced damages (decreased membrane integrity, motility, DNA intactness, and consequently low fertility) due to the high amounts of PUFAs in membrane structure (23, 24). Supplementation of appropriate antioxidants in semen extender prior to liquid storage prevents these damages (10, 25). The following study was conducted to find out which antioxidants demonstrate the highest effective protection against the sperm damage during liquid preservation. Our results demonstrate an improvement of sperm motility owing to the addition of ellagic acid to the extender at 1 and 2 mM doses. However, at a concentration of 2 mM higher effectiveness was shown in extending the duration of effective liquid storage.

It is assumed that ellagic acid with its phenolic structure may increase the antioxidative capacity by protecting against the harmful effects of free radicals. Sperm motility is linked to three main factors: regulation, structural integrity, and continuity of the energy. While the flagellar part is responsible for motility, the principal portion of the spermatozoa is in charge of hyperactivation (26, 27). However, PUFAs in the middle portion render this structure a sensitivity to free radical attacks (27). Ellagic acid (at 2 mM dose) is thought to protect this functional structure of the middle part of the spermatozoa, which consists of highly vulnerable PUFAs and improve the sperm motility during liquid storage and increase the total AOP levels during 24 and 72 hours of storage.

These results are in accordance with Türk et al. (14), who reported the effect of ellagic acid on increase in the epididymal sperm motility in rats. In another study, Çeribaşı et al. (15) displayed the effects of ellagic acid on the ameliorating adriamycin- induced high LPO levels and apoptosis in rats. Also, Ömür and Cayan reported improving effects of ellagic acid on ram semen after freezing/thawing (28). With all the results obtained from these studies, it can be postulated that ellagic acid may be a powerful antioxidative agent, protecting the cell membranes from cryoinjury.

A seleno-organic molecule, ebselen has cyto/neuroprotective effects through reducing the DNA damage and oxidative stress caused by the generation of hydrogen peroxide in hamster lung fibroblasts (17). In the current study, ebselen (40 μ M dose) reduced the LPO levels at 24 hours of liquid storage in ram semen. In humans, ebselen has been reported to be a substrate for the thioreductase system and mimics the GPx activity in the presence of GSH and GR (16, 29). The different effects of ebselen may be due to cell metabolism since ebselen increases the LPO levels in human multiple myeloma cells at a dose of 10 mM (30). In the same study, ebselen decreased the mitochondrial activity and induced apoptosis. In the current study, however, ebselen did not affect the mitochondrial activity. As spermatozoa have 22-75 mitochondria, we speculated that the different effects

of ebselen on the spermatozoa may stem from variations in the metabolism.

During liquid storage, with the extension of time, the motility, viability, and the DNA integrity rates were decreased. It was observed that ebselen improved the motility and the DNA integrity rates. It can be argued that a positive effect of ebselen on sperm motility is mediated via the retention of the DNA integrity, rather than the reduction of the LPO levels. Furthermore, the LPO may not be a major factor influencing the sperm motility during the cooled storage. This is in contrast to the findings of Baumber et al. (31) who demonstrated a markedly decline in equine sperm motility associated with ROS. This study was contradicted to those that indicate supplementation of boar and canine semen with antioxidants increases the sperm motility through the prevention of ROS generation (32, 33). The different observations in the susceptibility of sperm to oxidative stress may be due to the differences in experimental methodology and animal species.

Conclusion

Ellagic acid at 2 mM led to a higher motility and viability rates compared to the controls during 0, 24 and, 48 hours of liquid preservation. Ebselen led to a higher motility rate in comparison to the control groups at 24 and 48 hours at a dose of 40 μ M and after 48 and 72 hours at 10 μ M. The DNA integrity analysis showed that ebselen provided a protective effect on DNA integrity in comparison to the other groups for 24, 48, and 72 hours at 10 μ M, and for 72 hours at 40 μ M. Only a dose of 40 μ M ebselen reduced the LPO levels during 24 hours of liquid preservation, compared to the control group. Ellagic acid led to increasing in the AOP activity in comparison to the control groups after 24 and 72 hours at 2 mM and increased tGSH after 72 hours at a concentration of 1 mM. Addition of these antioxidants prior to the freezing process is suggested to enhance the sperm liquid storage techniques in the sheep breeding industry. Furthermore, future research should focus on a better understanding of the molecular and biochemical mechanisms of the cryoprotective effects of antioxidants, such as ellagic acid and ebselen in a cooled storage of ram semen.

Acknowledgements

This study was financially supported by Scientific and Technological Research Council of Turkey (TUBITAK) (Project No: 112 O 845). There is no conflict of interest in this study.

Authors' Contributions

M.N.B.; Semen collection and semen processing, semen parameters evaluating, statistical analysis. N.B.; Biochemical parameters analysis. P.İ.; DNA damage analysis. T.R.T.; Statistical analysis and manuscript editing. Ş.D.; Semen processing, farm organization, ram

management and feeding. M.B., Ş.G.; Semen processing, semen parameters evaluating. B.A.; Semen parameters evaluating, DNA integrity. All authors read and approved the final manuscript.

References

- Maxwell WM, Salamon S. Liquid storage of ram semen: a review. *Reprod Fertil Dev.* 1993; 5(6): 613-638.
- Unal N, Akcapinar H, Atasoy F, Aytac M. Some reproductive and growth traits of crossbred genotypes produced by crossing local sheep breeds of Kivircik x White Karaman and Chios x White Karaman in steppe conditions. *Arch Tierz.* 2006; 49(1): 55-63.
- O'Hara L, Hanrahan JP, Richardson L, Donovan A, Fair S, Evans AC, et al. Effect of storage duration, storage temperature, and diluent on the viability and fertility of fresh ram sperm. *Theriogenology.* 2010; 73(4): 541-549.
- Paulenz H, Söderquist L, Ådnøy T, Fossen OH, Berg KA. Effect of milk-and TRIS-based extenders on the fertility of sheep inseminated vaginally once or twice with liquid semen. *Theriogenology.* 2003; 60(4): 759-766.
- Holt WV. Fundamental aspects of sperm cryobiology: the importance of species and individual differences. *Theriogenology.* 2000; 53(1): 47-58.
- Sanocka D, Kurpisz M. Reactive oxygen species and sperm cells. *Reprod Biol Endocrinol.* 2004; 2(1): 12-19.
- Agarwal A, Virk G, Ong C, du Plessis SS. Effect of oxidative stress on male reproduction. *World J Mens Health.* 2014; 32(1): 1-17.
- AKALIN PP, BAŞPINAR N, COYAN K, BUCAK MN, GÜNGÖR Ş, ÖZTÜRK C. Effects of ultrasonication on damaged spermatozoa and mitochondrial activity rate. *Turk J Vet Anim Sci.* 2016; 40(2): 195-199.
- Bucak MN, Tekin N. Protective effect of taurine, glutathione and trehalose on the liquid storage of ram semen. *Small Ruminant Res.* 2007; 73(1): 103-108.
- Çoyan K, Başpınar N, Bucak MN, Akalin PP, Ataman MB, Ömür AD, et al. Influence of methionine and dithioerythritol on sperm motility, lipid peroxidation and antioxidant capacities during liquid storage of ram semen. *Res Vet Sci.* 2010; 89(3): 426-431.
- Câmara DR, Mello-Pinto MMC, Pinto LC, Brasil OO, Nunes JF, Guerra MMP. Effects of reduced glutathione and catalase on the kinematics and membrane functionality of sperm during liquid storage of ram semen. *Small Ruminant Res.* 2011; 100(1): 44-49.
- Bucak MN, Ataman MB, Başpınar N, Uysal O, Taşpınar M, Bilgili A, et al. Lycopene and resveratrol improve post-thaw bull sperm parameters: sperm motility, mitochondrial activity and DNA integrity. *Andrologia.* 2015; 47(5): 545-552.
- Hassoun EA, Vodhanel J, Holden B, Abushaban A. The effects of ellagic acid and vitamin E succinate on antioxidant enzymes activities and glutathione levels in different brain regions of rats after subchronic exposure to TCDD. *J Toxicol Environ Health A.* 2006; 69(5): 381-393.
- Türk G, Ateşşahin A, Sönmez M, Çeribaşı AO, Yüce A. Improvement of cisplatin-induced injuries to sperm quality, the oxidant-antioxidant system, and the histologic structure of the rat testis by ellagic acid. *Fertil Steril.* 2008; 89(5 Suppl): 1474-1481.
- Çeribaşı AO, Sakin F, Türk G, Sönmez M, Ateşşahin A. Impact of ellagic acid on adriamycin-induced testicular histopathological lesions, apoptosis, lipid peroxidation and sperm damages. *Exp Toxicol Pathol.* 2012; 64(7-8): 717-724.
- Müller A, Gabriel H, Sies H, Terlinden R, Fischer H, Römer A. A novel biologically active selenoorganic compound--VII: Biotransformation of ebselen in perfused rat liver. *Biochem Pharmacol.* 1988; 37(6): 1103-1109.
- Yang CF, Shen HM, Ong CN. Protective effect of ebselen against hydrogen peroxide-induced cytotoxicity and DNA damage in HepG2 cells. *Biochem Pharmacol.* 1999; 57(3): 273-279.
- Chew P, Yuen DY, Stefanovic N, Pete J, Coughlan MT, Jandeleit-Dahm KA, et al. Antiatherosclerotic and renoprotective effects of ebselen in the diabetic apolipoprotein E/GPx1-double knockout mouse. *Diabetes.* 2010; 59(12): 3198-3207.
- Bucak MN, Tuncer PB, Sarıözkan S, Ulutaş PA, Çoyan K, Başpınar N, et al. Effects of hypotaurine, cysteamine and aminoacids solution on post-thaw microscopic and oxidative stress parameters of Angora goat semen. *Res Vet Sci.* 2009; 87(3): 468-472.
- Garner DL, Thomas CA, Joerg HW, DeJarnette JM, Marshall CE. Fluorometric assessments of mitochondrial function and viability in cryopreserved bovine spermatozoa. *Biol Reprod.* 1997; 57(6): 1401-1406.
- Schäfer S, Holzmann A. The use of transmigration and Spermac stain to evaluate epididymal cat spermatozoa. *Anim Reprod Sci.* 2000; 59(3-4): 201-211.
- Akalin PP, Bucak MN, Gungur Ş, Baspınar N, Coyan K, Dursun Ş, et al. Influence of lycopene and cysteamine on sperm and oxidative stress parameters during liquid storage of ram semen at 5° C. *Small Ruminant Res.* 2016; 137: 117-123.
- Alvarez JG, Storey BT. Differential incorporation of fatty acids into and peroxidative loss of fatty acids from phospholipids of human spermatozoa. *Mol Reprod Dev.* 1995; 42(3): 334-346.
- Griveau JF, Dumont E, Renard P, Callegari JP, Le Lannou D. Reactive oxygen species, lipid peroxidation and enzymatic defence systems in human spermatozoa. *J Reprod Fertil.* 1995; 103(1): 17-26.
- Maxwell W, Stojanov T. Liquid storage of ram semen in the absence or presence of some antioxidants. *Reprod Fertil Dev.* 1996; 8(6): 1013-1020.
- Turner RM. Moving to the beat: a review of mammalian sperm motility regulation. *Reprod Fertil Dev.* 2006; 18(1-2): 25-38.
- Suarez SS, Marquez B, Harris TP, Schimenti JC. Different regulatory systems operate in the midpiece and principal piece of the mammalian sperm flagellum. *Soc Reprod Fertil Suppl.* 2007; 65: 331-334.
- Omur AD, Coyan K. Protective effects of the antioxidants curcumin, ellagic acid and methionine on motility, mitochondrial transmembrane potential, plasma membrane and acrosome integrity in freeze-thawed Merino ram sperm. *Vet Med.* 2016; 61(1): 10-16.
- Zhao R, Holmgren A. A novel antioxidant mechanism of ebselen involving ebselen diselenide, a substrate of mammalian thioredoxin and thioredoxin reductase. *J Biol Chem.* 2002; 277(42): 39456-39462.
- Zhang L, Zhou L, Du J, Li M, Qian C, Cheng Y, et al. Induction of apoptosis in human multiple myeloma cell lines by ebselen via enhancing the endogenous reactive oxygen species production. *Biomed Res Int.* 2014; 2014: 696107.
- Baumber J, Ball BA, Gravance CG, Medina V, Davies-Morel MC. The effect of reactive oxygen species on equine sperm motility, viability, acrosomal integrity, mitochondrial membrane potential, and membrane lipid peroxidation. *J Androl.* 2000; 21(6): 895-902.
- Cerolini S, Maldjian A, Surai P, Noble R. Viability, susceptibility to peroxidation and fatty acid composition of boar semen during liquid storage. *Anim Reprod Sci.* 2000; 58(1-2): 99-111.
- Michael AJ, Alexopoulos C, Pontiki EA, Hadjipavlou-Litina DJ, Saratsis P, Ververidis HN, et al. Effect of antioxidant supplementation in semen extenders on semen quality and reactive oxygen species of chilled canine spermatozoa. *Anim Reprod Sci.* 2009; 112(1-2): 119-135.

In Vitro Cytotoxicity of Folate-Silica-Gold Nanorods on Mouse Acute Lymphoblastic Leukemia and Spermatogonial Cells

Neda Eslahi, Ph.D.¹, Ali Shakeri-Zadeh, Ph.D.², Khadijeh Ashtari, Ph.D.^{3,4}, Vahid Pirhajati-Mahabadi, Ph.D.⁵, Tahereh Tohidi Moghadam, Ph.D.⁶, Ronak Shabani, Ph.D.^{1,3}, Kamran Kamrava, M.D.⁷, Zahra Madjd, Ph.D.⁸, Chad Maki, D.V.M.⁹, Hamid Reza Asgari, Ph.D.¹, Morteza Koruji, Ph.D.^{1,3*}

1. Department of Anatomical Sciences, School of Medicine, Iran University of Medical Sciences, Tehran, Iran
2. Department of Medical Physics, School of Medicine, Iran University of Medical Sciences, Tehran, Iran
3. Cellular and Molecular Research Center, Iran University of Medical Sciences, Tehran, Iran
4. Department of Medical Nanotechnology, Faculty of Advanced Technologies in Medicine, Iran University of Medical Sciences, Tehran, Iran
5. Neuroscience Research Center, Iran University of Medical Sciences, Tehran, Iran
6. Department of Nanobiotechnology, Faculty of Biological Sciences, Tarbiat Modares University, Tehran, Iran
7. Clinical Nanomedicine Laboratory, ENT-Head and Neck Research Center, Hazrat Rasoul Akram Hospital, Iran University of Medical Sciences, Tehran, Iran
8. Oncopathology Research Center and Dep Pathology, Faculty of Medicine Iran University of Medical Sciences, Tehran, Iran
9. VetCell Therapeutics, Daimler St, Santa Ana CA, USA

*Corresponding Addresses: P.O.Box: 354-14665, Cellular and Molecular Research Center, Iran University of Medical Sciences, Tehran, Iran
Department of Anatomical Sciences, School of Medicine, Iran University of Medical Sciences, Tehran, Iran
Email: koruji.m@iums.ac.ir

Received: 4/Jan/2018, Accepted: 27/May/2018

Abstract

Objective: The purpose of this study was to evaluate *in vitro* cytotoxicity of gold nanorods (GNRs) on the viability of spermatogonial cells (SSCs) and mouse acute lymphoblastic leukemia cells (EL4s).

Materials and Methods: In this experimental study, SSCs were isolated from the neonate mice, following enzymatic digestion and differential plating. GNRs were synthesized, then modified by silica and finally conjugated with folic acid to form F-Si-GNRs. Different doses of F-Si-GNRs (25, 50, 75, 100, 125 and 140 μ M) were used on SSCs and EL4s. MTT (3-(4,5-dimethylthiazol-2-yl)-2,5-diphenyltetrazolium bromide) proliferation assay was performed to examine the GNRs toxicity. Flow cytometry was used to confirm the identity of the EL4s and SSCs. Also, the identity and functionality of SSCs were determined by the expression of specific spermatogonial genes and transplantation into recipient testes. Apoptosis was determined by flow cytometry using an annexin V/propidium iodide (PI) kit.

Results: Flow cytometry showed that SSCs and EL4s were positive for *Plzf* and *H-2kb*, respectively. The viability percentage of SSCs and EL4s that were treated with 25, 50, 75, 100, 125 and 140 μ M of F-Si-GNRs was $65.33 \pm 3.51\%$, $60 \pm 3.6\%$, $51.33 \pm 3.51\%$, $49 \pm 3\%$, $30.66 \pm 2.08\%$ and $16.33 \pm 2.51\%$ for SSCs and $57.66 \pm 0.57\%$, $54.66 \pm 1.5\%$, $39.66 \pm 1.52\%$, $12.33 \pm 2.51\%$, $10 \pm 1\%$ and $5.66 \pm 1.15\%$ for EL4s respectively. The results of the MTT assay indicated that 100 μ M is the optimal dose to reach the highest and lowest level of cell death in EL4s and in SSCs, respectively.

Conclusion: Cell death increased with increasing concentrations of F-Si-GNRs. Following utilization of F-Si-GNRs, there was a significant difference in the extent of apoptosis between cancer cells and SSCs.

Keywords: Acute Lymphoblastic Leukemia Cells, Cytotoxicity, Folic Acid, Gold Nanorods, Spermatogonial Cells

Cell Journal (Yakhteh), Vol 21, No 1, Apr-Jun (Spring) 2019, Pages: 14-26

Citation: Eslahi N, Shakeri-Zadeh A, Ashtari K, Pirhajati-Mahabadi V, Tohidi Moghadam T, Shabani R, Kamrava K, Madjd Z, Maki C, Asgari HR, Koruji M. *in vitro* cytotoxicity of folate-silica-gold nanorods on mouse acute lymphoblastic leukemia and spermatogonial cells. Cell J. 2019; 21(1): 14-26. doi: 10.22074/cellj.2019.5691.

Introduction

Cancer is a disease that grows fast and out of control which is capable of spreading and growing anywhere in the body. The incidence of childhood cancer is annually 141 per million in the USA. In Iran, Cancer is the third cause of death (1). Childhood cancer is a treatable disease due to the development of chemo- and radiation therapies, but long-term survivors may be suffering from infertility.

Cytotoxic factors and radiation impair spermatogenesis cause oligospermia or azoospermia as well as genetic damage in sperm. An approach to overcome this problem in a child with leukemia or other metastatic cancers is the use of fresh or cryopreserved testicular cells that are not infected with cancer cells (2). After treating cancer in these patients, spermatogonial stem cell (SCC) transplantation

into the testes can potentially restart spermatogenesis (3).

The number of transplanted stem cells is critical for the effectiveness of the transplantation technique (4) and stem cell enrichment for transplantation may be necessary (5, 6). On the other hand, with leukemia or any kind of childhood metastatic cancer, there is a risk of contamination of SSCs with cancer cells. In addition to SSC manipulation (enrichment, purification and cryopreservation), decontamination of cancer cells from testicular suspension may be necessary and unavoidable for patients at risk before autotransplantation (7, 8).

Cell sorting is a good method to decontaminate cancer cells from normal cells. These approaches include immunomagnetic (MACS) and immunofluorescent

(FACS)-based strategies, but sorting does not properly remove contaminated cells in all cases (9, 10). Shabani et al. (7, 11) applied cisplatin before cell sorting to eliminate contaminated malignant cells from germ cells. They discovered that treatment with effective doses of cisplatin was useful in the isolation of SSCs from tumour cells. As a suggestion, applying gold nanoparticles (NPs) may be beneficial to remove malignant cells before cell sorting.

Gold NPs play a great role in cancer treatment because their exposure to UV and infrared radiation destroys cancer cells through the production of heat. They also increase the lifetime and delivery of drugs such as anticancer drugs that are very insoluble or unstable in the biological environment (12). Therefore, gold NPs may be used in chemotherapy, photothermal therapy (PTT), radiation therapy (RT) and photodynamic therapy (PDT) (13, 14).

Examples of GNPs are gold nano cages (GNCs), gold nanorods (GNRs), and gold nanospheres (GNSs). Among them, GNRs have been shown to be the most efficient NPs at absorbing near-infrared (NIR) light and converting that energy to heat (15) which could be at least 6X more effective than gold nanospheres or nanoshells (16). Nowadays, for selectively targeting cancer cells, a specific binding site on the surface of the cell, such as a receptor, is used (17). A more effective and active targeting system is needed to increase intracellular uptake of NPs containing drugs by cancer cells in the tumor site. Different ligands such as vitamins, hormones and monoclonal antibodies against tumor cell-specific receptors have been loaded on the surface of NPs to deliver them into cells via receptor-mediated endocytosis (18). Among them, the vitamin folic acid (folate) has been extensively used as the best target for different anti-cancer drugs (17, 19). In order to enhance stability of gold NPs thermodynamically and chemically, silica coating has been used (20, 21).

Xia et al. (22) used F-Si-GNRs on A549 cells and HeLa cells. They show that uptake of NPs into HeLa cells via receptor-mediated endocytosis was more efficient than folate receptor-deficient A549 cells. Huang et al. (23) used F-Si-GNRs on MGC803 gastric cancer cells. Also, Gao et al. (24) showed high uptaking occurred for F-Si-GNRs by HepG2.

In this study, we performed the MTT (3-(4,5-dimethylthiazol-2-yl)-2,5-diphenyltetrazolium bromide) proliferation assay to evaluate the cytotoxicity of F-Si-GNRs on SSC and EL4 cells. To achieve an effective dose and incubation time with F-Si-GNRs, we examined different doses of F-Si-GNRs at different times on cancer cells and germ cells.

Materials and Methods

Materials for synthesis and surface modification of gold nanorods

In this experimental study, $\text{HAuCl}_4 \cdot 3\text{H}_2\text{O}$, NaBH_4 , Ascorbic acid, Hexadecyl trimethyl ammonium bromide

(CTAB), AgNO_3 , Tetraethylorthosilicate (TEOS) and Folate were purchased from Sigma (Germany). Phosphate buffered saline tablet (PBS) and also Sodium acetate was obtained from Merck (USA). Glassware was thoroughly cleansed with a dilute sulfochromic acid solution and detergent, followed by rinsing with de-ionized (DI) water.

Preparation of Au seeds and nanorods

GNRs were synthesized via sequential seed-mediated growth method, as described elsewhere (23). In summary, small spherical gold NPs (seeds) were prepared by mixing aqueous solutions of $\text{HAuCl}_4 \cdot 3\text{H}_2\text{O}$ (250 μL , 0.01 M) and CTAB (7.5 mL, 0.095 M), followed by immediate addition of an ice-cold NaBH_4 solution (600 μL , 0.01M). The reactants were mixed by rapid inversion for two minutes and kept undisturbed at room temperature for a minimum of 2 hours. Then the growth solution was accumulated by sequential addition of CTAB (9.5 mL, 0.095 M), $\text{HAuCl}_4 \cdot 3\text{H}_2\text{O}$ (400 μL , 0.01 M), AgNO_3 (60 μL , 0.01 M) and ascorbic acid (64 μL 0.10 M) solutions, followed by mixing with seed particles (40 μL). It takes several hours for termination of the reaction and formation of rod-shaped nanostructures.

Purification of gold nanorods

The unreacted gold ions and excess cationic surfactant (CTAB) were removed by centrifugation (14,000 rpm, 7 minutes). The sediment was diluted with distilled water, then the purified sample sonicated for several minutes to redisperse the nanorods. Prior to surface modification with silica, absorbance intensity of the stock GNRs was adjusted to optical density (OD).

Surface modification of gold nanorods

Ten milliliters of purified GNRs were redispersed in ethanol, and the pH was adjusted to 10 using ammonia. The suspension was sonicated in a water bath for several minutes. 20 μL of TEOS was diluted to 1 mL with ethanol which was sequentially added to GNRs (20 μL each time) at 30 min intervals. The solution was vigorously stirred overnight. Silica-coated GNRs (Si-GNRs) were purified by centrifugation at 3,500 rpm for 30 minutes followed by several rounds of washing with water and ethanol. 1.5 mg folate was dissolved in 2 mL dimethyl sulfoxide (DMSO). For each 10 mL suspension of GNRs in ethanol, 250 μL of folate solution was used. Samples were further purified and used for characterizations.

Equipment for characterization

Characteristic surface plasmon resonances of GNRs were recorded in the wavelength region of 400 to 900 nm, using a Perkin Elmer spectrophotometer (Lambda 25). For Fourier-transform infrared spectroscopy (FTIR) analysis, samples of bare GNRs, silica, and folic acid modified GNRs were made into a dry powder by a lyophilizer (LYSFME-Snijders scientific). Spectra were recorded on a NICOLET IR 100 (FT-IR) and reported in the range of 500-3,800 cm^{-1} .

For transmission electron microscopy (TEM) characterization, purified and surface modified GNRs were deposited on carbon-coated copper grids and imaged utilizing TEM (LEO 906, Zeiss).

The dynamic light scattering (DLS) was performed by Brookhaven 90Plus Nanoparticle Size Analyzer to identify the effective diameter and size distribution of GNRs. The surface charge of F-Si-GNR was measured with Zeta potential measurements in water (NICOMP 380ZLS Zeta potential/Particle sizer).

Animals

In this study, 120 neonatal mice between 3-6 days old were used. These animals were obtained from the Experimental and Comparative Studies Center of Iran University of Medical Sciences (IUMS). The animals were housed in cages at 22-25°C with a 12 hours: 12 hours cycle and given free access to food and water at all times. All studies were performed in accordance with the Ethical guidelines set by the “animal care and use committee (ACUC), Iran University of Medical Sciences” (code: IR.IUMS.rec.1394-01-1172-5884).

Isolation and culture of spermatogonial stem cells

Testes were collected aseptically from 3-6-day-old mice. First of all, testes were decapsulated, then minced and suspended in Dulbecco's Modified Eagle Medium (DMEM, Life Technologies, Carlsbad, CA, USA) supplemented with 1.37 g/L NaHCO₃ (Sigma-Aldrich, St Louis, MO, USA), penicillin (100 IU/mL), streptomycin (100 µg/mL), gentamycin (40 µg/mL) and single-strength nonessential amino acids, (all from Life Technologies).

Testicular cells were isolated according to our previous study (25). In summary, testes fragments were digested in DMEM containing 0.5 mg/mL collagenase/dispase, 0.5 mg/mL Trypsin, and 0.05 mg/mL DNase (all from Sigma-Aldrich), for 30 minutes at 37°C. The interstitial cells were removed by washing in DMEM medium. The second step of digestion was performed by adding the same fresh enzyme solution in DMEM media as described above. After cell separation and filtration through 70-µm nylon filters, cell viability was determined and the harvested cells were used for cell culture. Myoid and Sertoli cells were also separated by overnight differential plating in DMEM containing 5% fetal calf serum (FCS). Then the harvested spermatogonia were cultured in DMEM containing 5% FCS and 10 ng/mL GDNF for 2 weeks. The cells were incubated at 32°C, 5% CO₂, approximately 85% humidity, and the medium was refreshed every 2-3 days.

Reverse transcription polymerase chain reaction

This study was performed in following groups: cells obtained from enzyme digestion, cells derived from cultured colonies after two weeks, and mouse testis tissue as a positive control. The expression of spermatogonial genes was determined based on previous animal studies. RNA was extracted using a standard RNA extraction kit (Qiagen, Germany) per the manufacturer's instructions.

The RNA was examined for purity and integrity by a 260/280 nm ratio measurement. In the reverse transcription reaction, 1 µg of total RNA was used with QuantiTect® Reverse Transcription Kit (Qiagen) per the manufacturer's instructions.

The primers specific for GDNF family co-receptor $\alpha 1$ (*Gfra-1*), promyelocytic leukemia zinc-finger (*Plzf*), *Itgb1* ($\beta 1$ -integrin), *Itga6* ($\alpha 6$ -integrin), VASA homologue (*Mvh*), octamer-binding transcription factor 4 (*Oct4*) and *Gapdh* genes were designed using mouse sequences (Gene Bank) and Gene Runner software (version 3.02, Hastings Software Inc, USA) as shown in Table 1. *Gapdh* was a housekeeping gene. Reverse-transcription polymerase chain reaction (RT-PCR) was performed using the primers, the prepared complementary deoxyribonucleic acid (cDNA) and PCR Master Mix 2X kit (Fermentas, Germany), under the following conditions: 95°C for 3 minutes, followed by 35 cycles at 95°C for 30 seconds, under specific annealing temperature for each primer (*Plzf*, 55°C; *Oct4*, 60°C; *Gfra-1*, 52°C; *Vasa*, 62°C; *Itga6*, 52°C; *Itgb1*, 55°C and *Gapdh*, 60°C) for 45 seconds, 72°C for 60 seconds, and a final extension of 72°C for 10 minutes.

PCR products were separated by resolving 1 µL of each sample on a 1.2% agarose gel, and electrophoresis was performed with Tris-Borate-EDTA (TBE) 1x loading buffer (Sigma-Aldrich, Germany) at a voltage of 95 for 45 minutes. The gels were stained with 0.1 µg/mL Gel Red™ (Biotium Inc, USA) and we used Gel Logic for visualization of bands (Carestream Health Inc., Rochester, NY, USA).

Confirmation of the spermatogonial stem cells

For functional confirmation, spermatogonial stem cells were labeled with DiI (Invitrogen, Carlsbad, CA, USA) and DAPI (Sigma, Germany), then injected into the seminiferous tubules of busulfan-treated mice. 5 mg/ml DMSO was used as a solvent for preparation of the busulfan dosage. Also an equal volume of warm (40°C) distilled water was added to above solution to prevent precipitation of DMSO. A single dose of busulfan (40 mg/kg) was injected intraperitoneally in the NMRI mice (25).

Mice weighing 25 g were treated with 400 µl of the final busulfan solution. 4 weeks after treatment with busulfan, mice were devoid of most endogenous germ cells. The mice (n=5) were anesthetized with intraperitoneal (i.p.) injection of ketamine hydrochloride 10% (Rotexmedica, Germany) (100 mg/kg) and xylazine 2% (Alfasan, Holland, 10 mg/kg). Then spermatogonial cells (SSCs, 10⁶/ml) were resuspended in 10 µl DMEM/F12 and injected directly through the efferent ductus and into the seminiferous tubules of the busulfan-treated mice. Seminiferous tubules were visualized by addition of trypan blue in the injection media. 8 weeks after transplantation, survival and proliferation rates of cells were estimated by fluorescent microscopy (type CH₂, 4009 magnifications; Olympus, Japan).

Table 1: The sequence of the designed primers used for reverse transcriptase polymerase chain reaction

Genes	Primer sequences (5'-3')	Annealing temperature (°C)	Size (bp)
<i>Iga6</i>	F: CTC AGA ATA TCA AGC TCC CT R: AAA CAC TAA TAG AGC CAG CA	60	148
<i>Gfra1</i>	F: AAT TGT CTG CGT ATC TAC TGG R: ACA TCT GAT ATG AAC GGG AC	60	130
<i>Igβ1</i>	F: GAC ATT ACT CAG ATC CAA CCA R: AGG TAG TAG AGA TCA ATA GGG T	60	115
<i>Oct4</i>	F: GAA CTA GCA TTG AGA ACC GT R: CAT ACT CGA ACC ACA TCC TTC	60	115
<i>Plzf</i>	F: CCC GTT GGG GGT CAG CTA GAA R: CTG CAA GGT GGG GCG GTG TAG	61	137
<i>Mvh(Vasa)</i>	F: GAT AAT CAT TTA GCA CAG CCT C R: GTC AAC AGA TGC AAA CAC AG	59-61	149
<i>Gapdh</i>	F: CAA CTC CCA CTC TTC CAC TT R: GCA GCG AAC TTT ATT GAT GGT A	60	125

Culture and tumorigenicity confirmation of EL-4 cell line

We commercially obtained the mouse acute lymphoblastic leukemia cell line EL4 from Pasteur Institute (Tehran, Iran). The EL4 cells were cultured in HEPES DMEM/F12 (Gibco, USA), 2% fetal bovine serum (Gibco, USA), 1% penicillin (Invitrogen, UK), and 1% streptomycin (Invitrogen, UK). For Confirmation of tumorigenicity and induction of the xenograft tumor model, 5×10^4 EL4s in 10 μ l medium were transplanted through the efferent ductus and into the seminiferous tubules of azoospermia busulfan-treated male NMRI mice (20-30 g) (26). The shape and thickness of each tumour was evaluated eight weeks after EL4 cell injection. Both testes were surgically removed and processed for histological examination. 5 μ m thickness sections were stained with hematoxylin and eosin (H&E). The volume of tumors (Vt) was estimated in the formula: $Vt = \pi (b^2 \times a) / 6$ (b and a are the minimum and maximum diameters in millimeters respectively).

Flow cytometry

We used flow cytometry to confirm the identity of the EL4s and SSCs. Isolated SSCs (10^6 per 100 μ l PBS) were incubated in the dark for 30 minutes at 4°C with PLZF monoclonal antibody (ebiosciences, 53-9320-82, 1: 50). Then, the cells were washed with PBS (three times). Also, the EL4 cells (10^6 per 100 μ l PBS) were incubated with a FITC-conjugated mouse anti-*H-2kb* monoclonal antibody (ebiosciences; 553569, 1: 50).

Experimental groups and MTT assay

In this study, EL4s and SSCs were divided into five groups: control (medium without F-Si-GNRs) and experimental groups, with cells distributed in a 96-well plate at a cell density of 15×10^3 cells per well in the different concentrations of F-Si-GNRs (25, 50, 75, 100, 125, and 140 μ M) for different incubation periods (6, 12 hours). We performed the MTT (3-(4,5-dimethylthiazol-2-yl)-2,5-diphenyltetrazolium bromide proliferation assay to determine the toxicity of F-Si-GNRs. After centrifuging the cells, washing was done with PBS. Then 100 μ l of MTT solution [MTT tetrazolium salt (5 mg/ml)] was added to each well and incubated for 3-4 hours, followed by centrifugation of the solution and removal of the supernatant. Next, 100 μ l of DMSO was added to the wells, and plates were shaken for 10 minutes in a microplate shaker before observation with the ELISA reader at 570 nm.

Transmission electron microscopy

For TEM technique, SSCs and FL4 cells were washed with PBS, then 2.5% glutaraldehyde was used as a primary fixation for 2 hours. For removal of free glutaraldehyde, the cells were rinsed 2-3 times with PBS. Then, 1% osmium tetroxide was used as a secondary fixation for 1.5 hours. The cells were dehydrated in acetone (50, 70, 90, 100%), infiltrated by resin and finally embedded in pure resin (Epon 812, TAAB, UK). Semi-thin (500 nm) and thin (50 nm) sections were performed for light and electron microscopy respectively. Thin sections were

transferred on the 200-mesh uncoated grids and stained with uranyl acetate and lead citrate before imaging with TEM (LEO 906; Zeiss). It should be noted that for GNR imaging, NPs were deposited on carbon-coated copper grids directly.

Apoptosis evaluation in SSCs and EL4 cells after treatment with F-Si-GNRs

In this study, we used an optimal mean dose of F-Si-GNRs (100 μ M) for 6 hours. The apoptosis was measured using annexin V-fluorescein isothiocyanate (FITC) apoptosis detection. At first, the cells were plated at a density of 200,000 cells/well in 24-well plates. The cells were washed with PBS and then resuspended in annexin binding buffer. Then cells were incubated with annexin-FITC/PI in the dark for 15 minutes. In the next step, reasonable results were obtained by flow cytometric counting of viable cells. Viable cells were negative for both PI and annexin V-FITC; necrotic cells were positive for PI and negative for annexin-V-FITC. early apoptotic cells were positive for annexin-V-FITC and negative for PI, whereas late apoptotic cells were positive for both annexin-V-FITC and PI.

Statistical analysis

Data have been presented as the mean \pm SD with at least three biological independent repeats. Differences between groups were assessed by One-way ANOVA using the SPSS version 25 software (SPSS Inc., Chicago, IL, USA). The difference between groups was considered statistically reliable if $P \leq 0.05$.

Results

Expansion and characterization of spermatogonial cells

Following the enzymatic digestion of the testicular tissue, the SSCs were isolated and cultured in DMEM/F12 medium containing 5% FBS for 2 weeks. In order to increase the proliferation of the cells, GDNF (10 ng/ml) was added to the culture medium. After 24 hours (Fig.1A), the SSCs formed colonies, and after 72 hours the platform was covered with cluster colonies. About 2-3 days after the primary culture, the cluster of germ cells appeared on a feeder layer. These were clumpy and had individually recognizable cells. They were then enzymatically dispersed and subcultured. During 2 weeks of culture, SSCs could start the formation of new clusters. The addition of GDNF in culture resulted in a significant improvement in SCC proliferation. In transmission electron microscope, the heterochromatin nucleus (N), eccentric small compact and highly reticulated nucleoli (Nu) and very high mitochondria (M) were observed in SSCs clusters (Fig.1B).

In order to confirm the identity of spermatogonial stem cells, the expression of specific SCC markers was analyzed in the fresh tissue (without enzymatic digestion), isolated testicular cells (after first day of culture) and cultured

cells (after 2 weeks of culture) by RT-PCR. As shown in Figure 1C-E, specific genes of SSCs are expressed in all samples (*Oct4*, *Itga6*, *Plzf*, *Gfra1*, *Mvh*, *Itgb1*, and *Gapdh* as a housekeeping gene).

The results of flow cytometry show that the average amount of *Plzf* expression in SSCs at the end of the first and second weeks of culture were $45.63 \pm 5.71\%$ and $84.68 \pm 4.02\%$, respectively (Fig.1F-H).

Culture of the EL-4 cells and characterization

Tumor cells were purchased from the Pasteur Institute (Tehran, Iran) after the fourth passage and cultured in DMEM/F12 medium containing 2% FBS. The cells were cultured in suspension and passaged every 48 hours. The margins of these cells were irregular. It should be noted that these cells don't form colonies and have a high proliferation rate (Fig.2A, B). The ultrastructural characteristics of EL4s were examined via TEM. The nucleus and cytoplasm had an irregular shape. The cytoplasm was characterized by organelles, eg, mitochondria, rough endoplasmic reticulum. A large number of spherical mitochondria were found (Fig.2C, D). EL4s cells were confirmed by *H-2kb* monoclonal antibodies, respectively. The results of flow cytometry show that about $96.25 \pm 2.81\%$ of EL-4 cells expressed *H-2kb* (Fig.2E, F).

Tumorigenicity confirmation of EL-4 cells

In order to confirm tumorigenicity, 5×10^4 EL4 cells were transplanted through the efferent ductus and into the seminiferous tubules of azoospermia mice. After 8 weeks, the shape and thickness of any tumours were evaluated. Histological evaluations showed that after 8 weeks, a tumor had formed in 70% of the mice. The volume of tumours (V_t) was estimated in the formula: $V_t = \pi (b^2 \times a) / 6$ where b and a are the minimum and maximum diameters in millimeters, respectively. The average tumor size was 142 mm^3 (Fig.2G). After 8 weeks, we observed that leukemic cells had infiltrated the interstitial tissue. These cells were polygonal with spherical nuclei (Fig.2H). The results showed that tumorigenicity of EL4 cells was restricted to testicular tissue.

Synthesis and characterization of F-Si-GNR

Surface plasmon resonance bands of GNR were monitored in the visible and NIR region, representing oscillation of the conduction band electrons along the short and long axis of GNRs. The appearance of a strong longitudinal surface plasmon resonance (LSPR) band around 798 nm, along with a transverse SPR band of weaker intensity around 512 nm is characteristic of formation of nanostructures with rod morphology. Changes in the SPR bands were also monitored upon formation of a silica layer around nanostructures. Stability of GNRs was checked in ammonia and ethanol, prior to interaction with tetraethyl orthosilicate (data not shown). Upon addition of TEOS, the longitudinal

surface plasmon absorption band experienced a decrease in intensity; whereas the transverse surface plasmon absorption band did not undergo any remarkable changes. Due to the sensitivity of SPR bands to trace changes in the local environment, alterations in the intensity or wavelength position of the bands could be attributed to the interaction of the nanostructures with molecules. Hence, a decrease of longitudinal LSPR band intensity of GNRs upon interaction with TEOS represents the formation of a silica layer around the nanostructures. Such a type of coating is considered

to be a useful strategy in replacement/coating of the cationic surfactant (i. e. CTAB), enabling application of GNRs as biocompatible platforms in a variety of biomedical approaches. Coating of GNRs with a very thin silica film (2.56 ± 0.62 nm in this study) improves the colloidal stability of the nanorods by reducing aggregation and allows for shape stability as well as surface modification. Furthermore, silica is porous and can be feasibly loaded with molecules of interest such as chemicals, drugs, dyes, or imaging agents either via physical adsorption or covalent attachment.

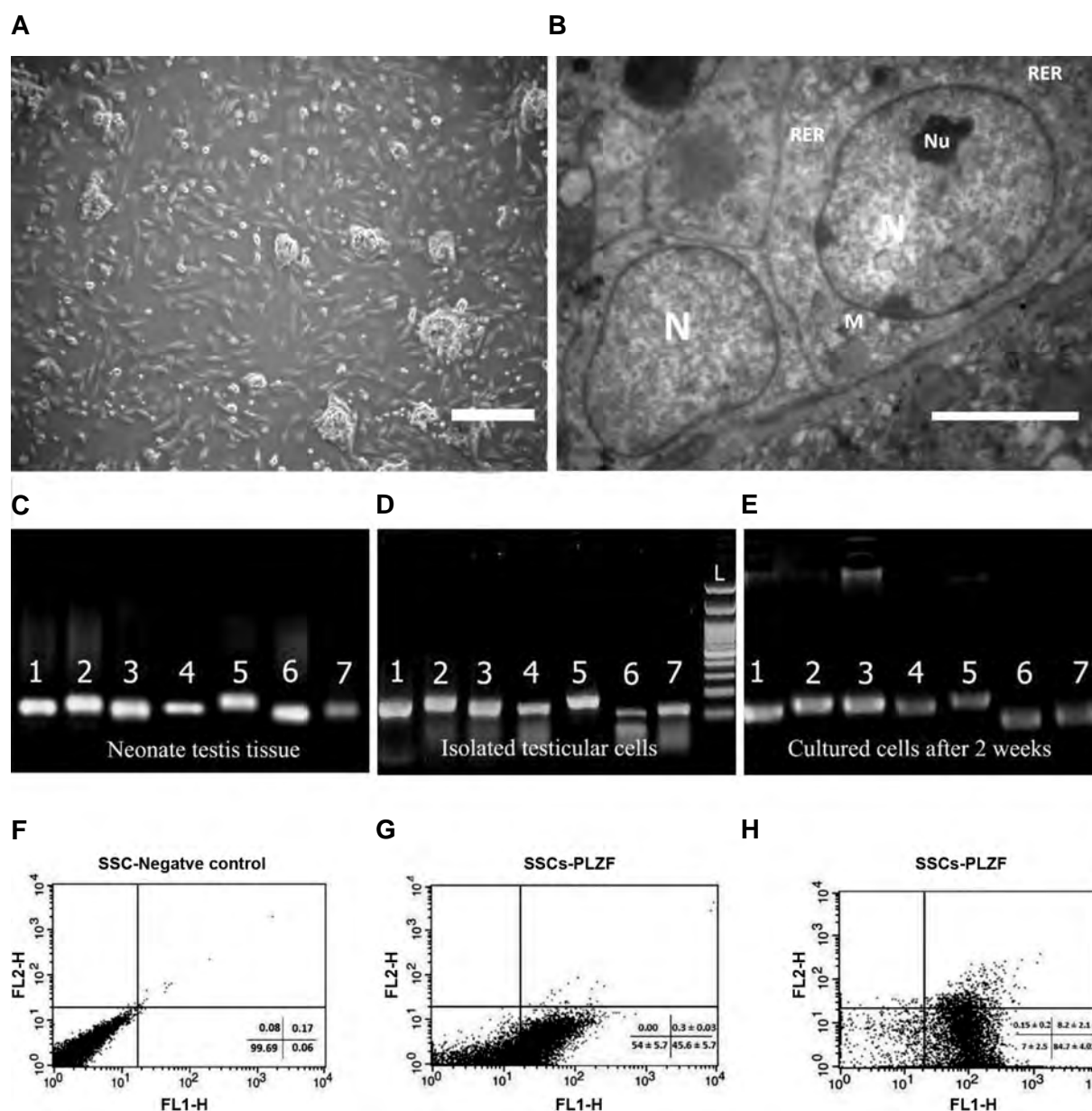


Fig.1: Spermatogonial cells characterization. **A.** The morphology of a spermatogonial-derived cluster formed from the culturing of spermatogonial cells after 24 hours (scale bar: 200 μ m), **B.** Representative transmission electron micrographs from spermatogonial cells (SSCs) clusters (scale bar: 5 μ m). The heterochromatin nucleus (N), eccentric small compact and highly reticulated nucleoli (Nu), Rough endoplasmic reticulum (RER) and very high mitochondria (M) were observed in cells. Reverse transcription polymerase chain reaction (RT-PCR) was used to determine the expression of specific spermatogonia and germ cell markers in **C.** Neonate testis tissue (fresh tissue without enzymatic digestion), **D.** Cultured cells after the first day and **E.** Two weeks of culture. 1; *Oct4* (129 bp), 2; *Itga6* (148 bp), 3; *Plzf* (137 bp), 4; *Gfra1* (130 bp), 5; *Mvh* (*Vasa*, 149 bp), 6; *Itgb1* (115 bp), 7; *Gapdh* (125 bp). Flow cytometric analysis of spermatogonial cells: **F.** Spermatogonial negative control, **G.** The PLZF positive spermatogonial cells at the end of the first week were $45.63 \pm 5.71\%$, and **H.** At the end of the second week was $84.68 \pm 4.02\%$.

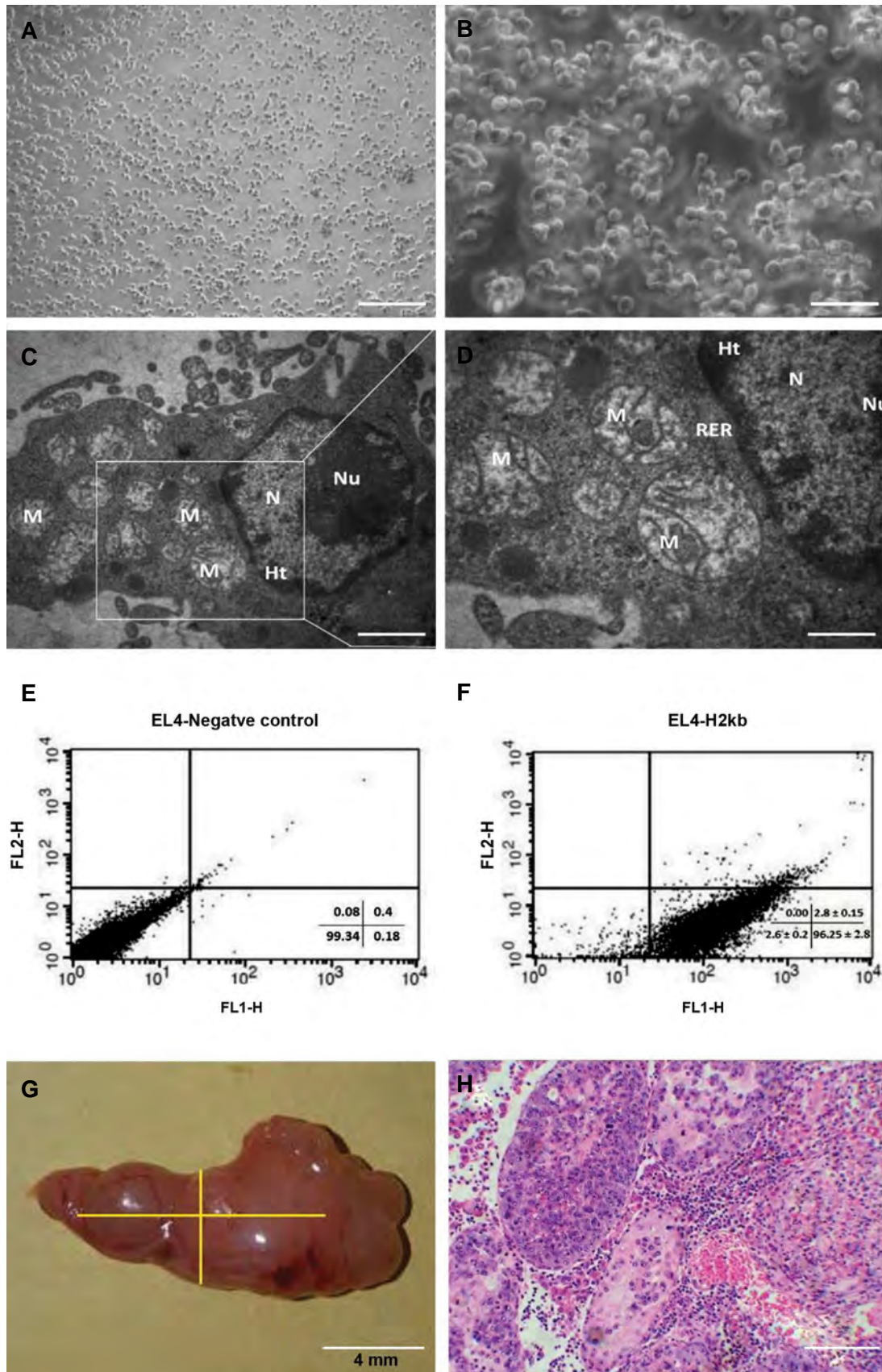


Fig.2: EL-4 cells characterization. **A, B.** Representative phase contrast images (scale bar, A: 200 μ m, B: 50 μ m), **C, D.** Transmission electron micrographs from EL4s (scale bar, C: 2 μ m, D: 1 μ m). These cells formed irregular margins. Spherical mitochondria were found in relatively high numbers. In addition, the nucleus of some cells had marginal heterochromatin. Nucleus (N), Nucleolus (Nu), Mitochondria (M), Rough endoplasmic reticulum (RER) and Heterochromatin (Ht), **E, F.** Flowcytometry analysis of EL-4 cells labeled for H-2Kb. The H-2Kb positive EL4s were $96.25 \pm 2.81\%$, and **G, H.** tumor formation of EL-4 cells in azoospermic recipient mouse model. In this model, 50,000 EL4s were transplanted, **G.** A testicular tumor formed 8 weeks after transplantation of EL4s (tumor size: 142 mm³) in recipient testis, **H.** Histological section of tumour formed from EL4 cells stained with H&E (scale bar: 50 μ m).

Comparison of both of the characteristic SPR bands of GNRs after 30 minutes and 11 hours showed that within a typical range of concentration of TEOS, there is no change in the thickness of the silica layer over the nanostructures. Furthermore, the interaction of silica coated GNRs with folate shows a decreased intensity of both transverse and LSPR absorption bands, representing physisorption of folate onto the matrix of silica coated GNRs.

We analysed TEM images of the GNRs with a size distribution histogram (an average of 562 NPs) (Fig.3A). An average diameter of 5.55 ± 1.56 nm was determined from the statistical analysis of the TEM images (Fig.3B). The images clearly show the formation of the rod morphology as well as a coating of the silica layer around GNRs (Fig.3C). Based on TEM images, the size of the nanostructures was 20.43 ± 2.18 nm in length and 5.55 ± 1.56 nm in width. The thickness of the silica layer coating

around the nanostructures was 2.56 ± 0.62 nm.

Analysis of FTIR spectra for silica coated GNRs before and after physisorption of folic acid is shown in Figure 3D. A glance at the figure shows that upon modification of silica coated GNRs with folic acid, the spectral features have been changed. Folic acid is composed of p-aminobenzoic acid, glutamic acid, and a hetero-bicyclic pteridine that band between 1475 and 1500 cm^{-1} . This is attributed to the characteristic absorption band of the phenyl and PT ring. Apart from the displacement in vibrations related to carbonyl group (1712 cm^{-1}) and $\text{C}=\text{C}$ (1388.49 cm^{-1}), the characteristic vibrational bands of folic acid for the phenyl and pterin ring (around 1478 cm^{-1}), the OH carboxylic of glutamic acid moiety and the NH group of the pterin ring, (stretching in the range of 3500 - 3700 cm^{-1}), depicts adsorption of folic acid molecules onto the matrix of silica-coated GNRs (Fig.3E).

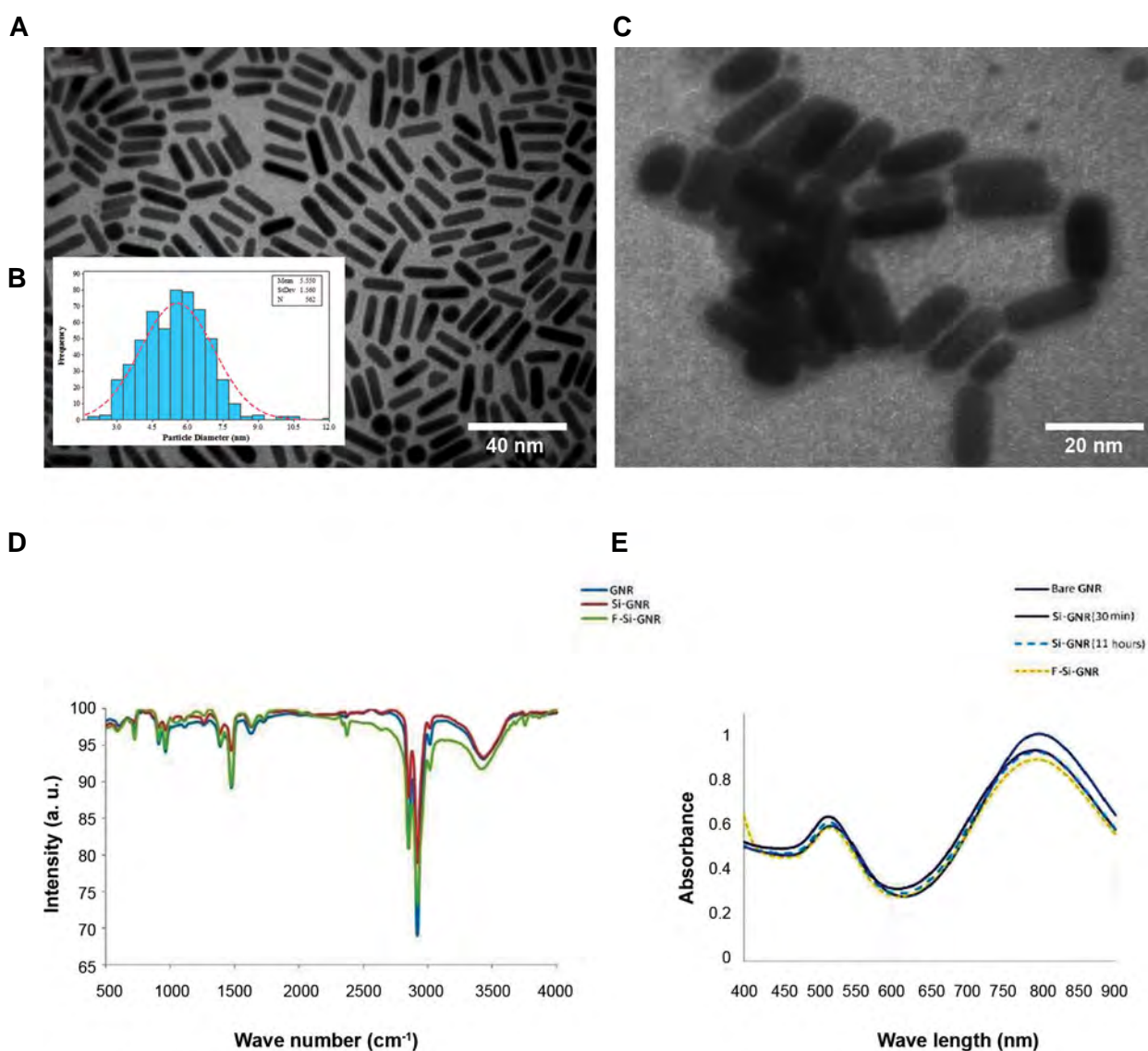


Fig.3: Analysis of the gold nanoparticles (GNRs). **A.** Transmission electron microscopy images of purified GNRs, **B.** Inset size distribution histogram (an average of 562 nanoparticles), **C.** Silica-coated GNRs. The thickness of silica layer was 2.56 ± 0.62 nm, **D.** Characteristic SPR bands of GNRs, before and after surface modification with silica and folate, and **E.** FTIR spectra of GNRs, silica coated GNRs (Si-GNR) and folic acid modified Si-GNR (F-Si-GNR).

Optimal dosages and duration of F-Si-GNR for EL4s and spermatogonial stem cells was assessed. The survival of EL4s and SSCs after treatment with F-Si-GNR was assessed using the MTT test. The concentrations of F-Si-GNR tested ranged from 25, 50, 75, 100, 125 and 140 μM for different incubation periods (6, 12 hours). The percent viability of SSCs and EL4s that were treated with 25, 50, 75, 100, 125 and 140 μM of GNRs was $65.33 \pm 3.51\%$, $60 \pm 3.6\%$, $51.33 \pm 3.51\%$, $49 \pm 3\%$, $30.66 \pm 2.08\%$ and $16.33 \pm 2.51\%$ for SSCs and $57.66 \pm 0.57\%$, $54.66 \pm 1.5\%$, $39.66 \pm 1.52\%$, $12.33 \pm 2.51\%$, $10 \pm 1\%$ and $5.66 \pm 1.15\%$ for EL4s respectively. Given that there were not significant differences between 6 and 12 hour incubation periods, we chose 6 hours for incubation. It means that cell death increased with an increase in the quantity of GNRs. The results show that the optimal mean dose for the highest cell death in EL4s and lowest in SSCs is 100 μM of GNRs (Fig.4).

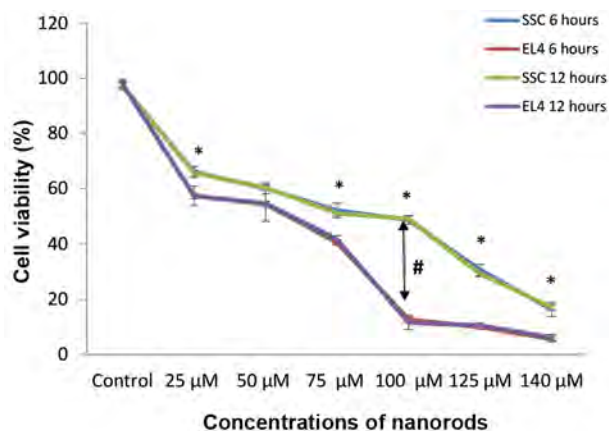


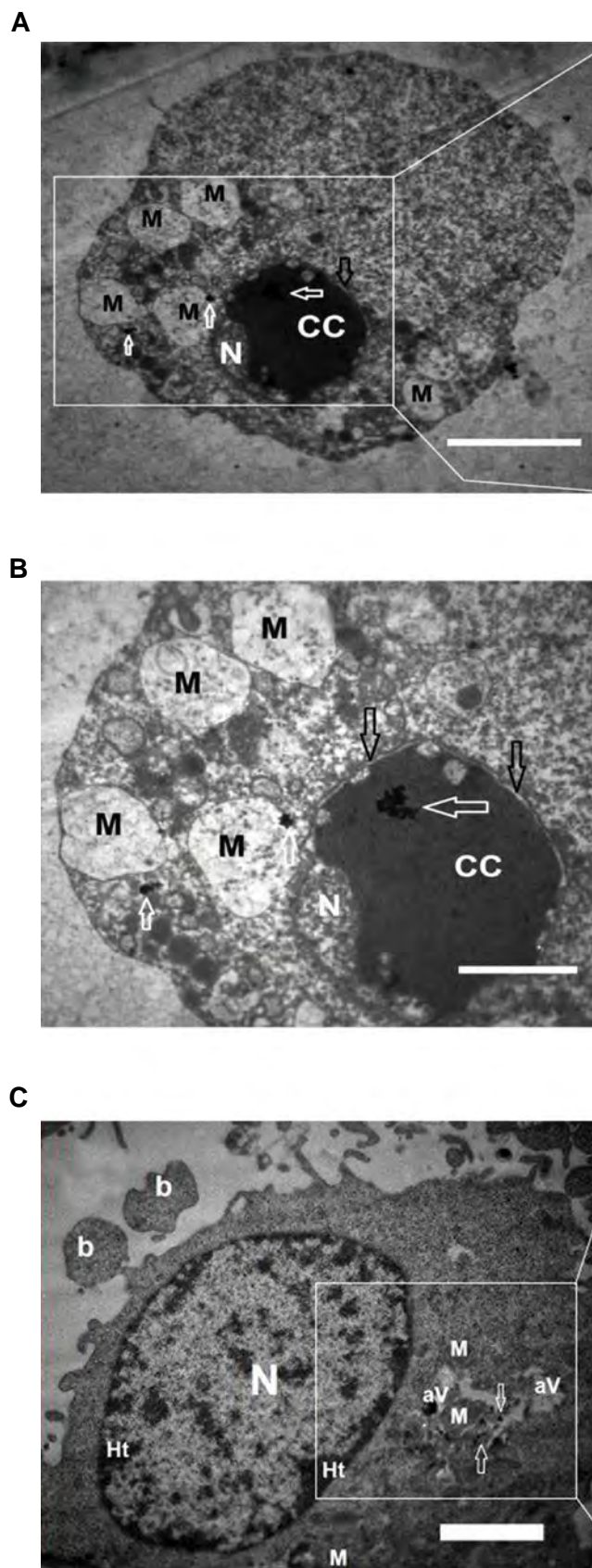
Fig.4: EL-4 and spermatogonial stem cells viability at varying concentrations of nanorods (6, 12 hours). Cell death rates in EL4 cells were higher than SSCs, especially in 100 μM of GNRs, but there weren't significant differences between 6 and 12 hours incubation periods. In each dosage category, there aren't significant differences between groups 6 and 12 hours. The diagram shows that the optimal mean dose for highest cell death in EL4s and lowest in SSCs is 100 μM of GNRs. In each dosage category. *; There are significant differences between EL4s and SSCs groups.

Ultrastructure and apoptosis evaluation in SSCs and EL4 cells after treatment with F-Si-GNR

The ultrastructural characteristics of EL4s and SSCs after treatment with F-Si-GNR were examined via TEM. The chromatin condensation was observed in the EL4s cells and the nucleus membrane was swollen. Swelling of the nuclear membrane is the first manifestation of injury to cells. Spherical mitochondria were also damaged (Fig.5A, B). The heterochromatin nucleus, plasma membrane blebbing and rough endoplasmic reticulum were observed in SSCs. The mitochondria were found in relatively high numbers in the SSCs clusters whereas a few they were with damaged cristas. Gold nanorods were observed in the mitochondria and cytoplasm, and also the autophagic vacuoles were consist of nanoparticles (Fig.5C-E).

The apoptosis was measured using annexin V-FITC

apoptosis detection kit. The apoptotic rates of the EL4s (51.1 ± 6) were significantly higher than SSCs (Fig.5F, G) (32.9 ± 2 , $P < 0.001$). Also, after incubation with F-Si-GNR, necrotic SSCs and EL4s weren't observed. Necrotic cells were positive for PI and negative for annexin V-FITC.



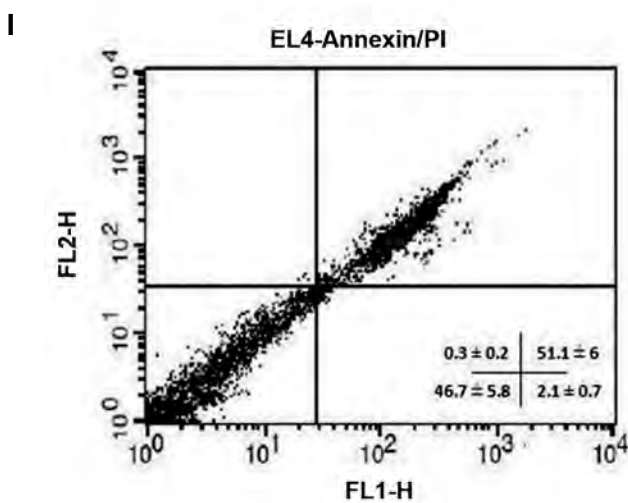
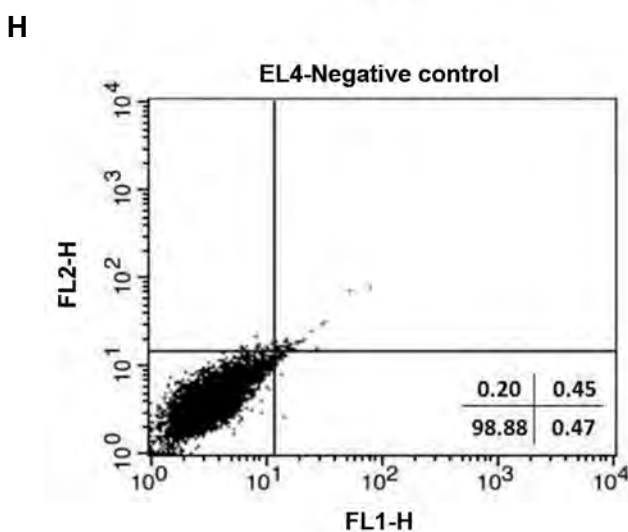
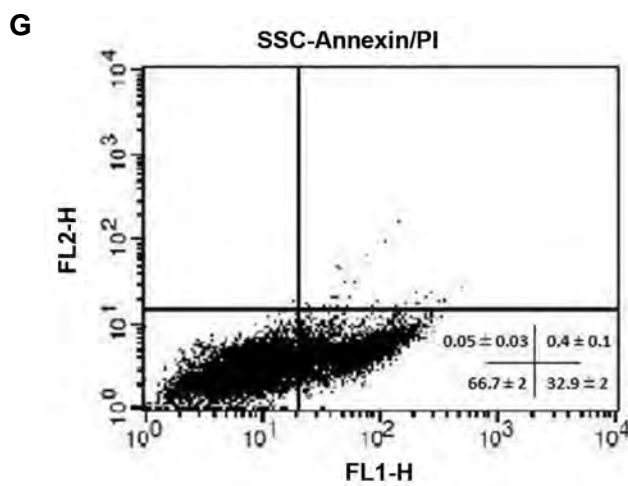
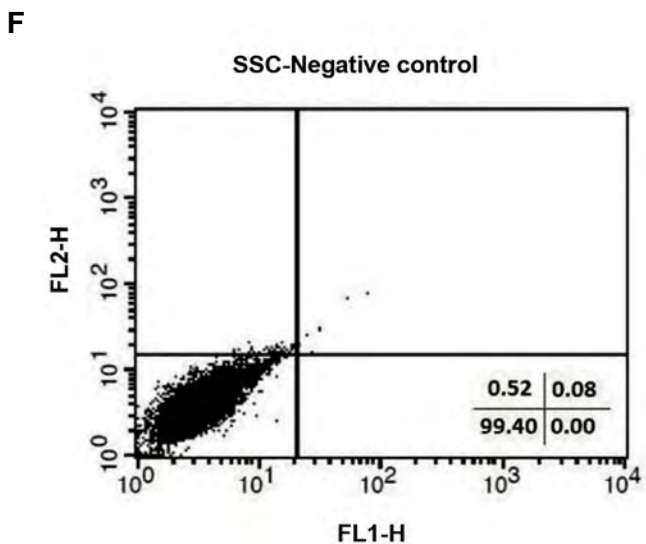
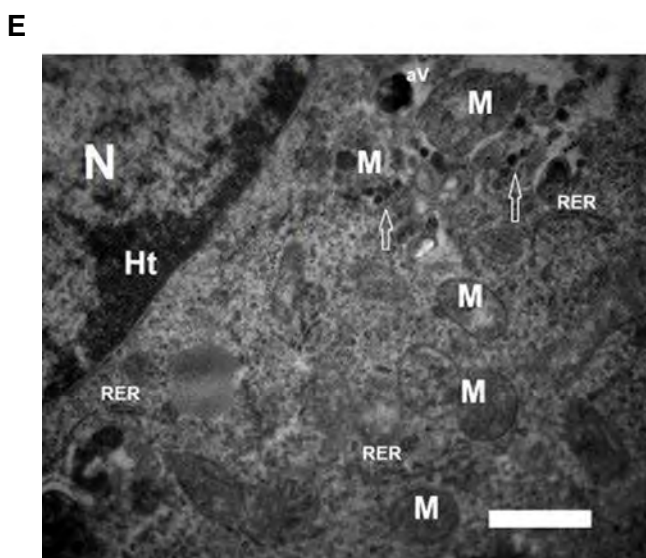
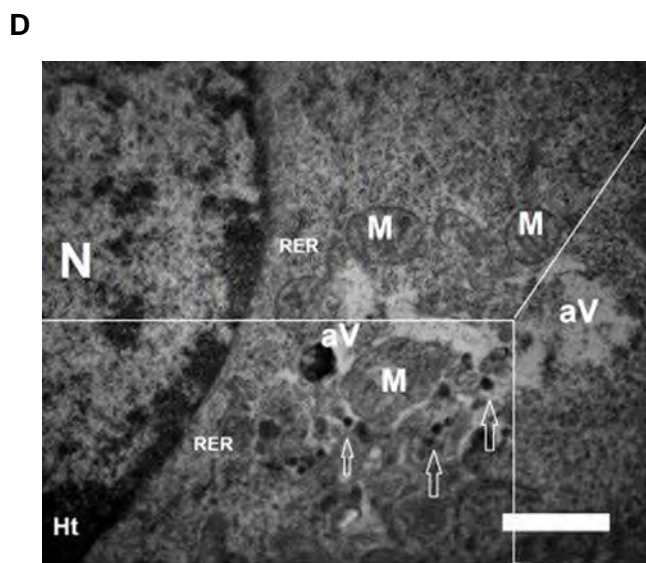


Fig.5: Ultrastructure and apoptosis in SSCs and EL4s after treatment with F-Si-GNR. Transmission electron micrographs from **A, B.** EL4s and **C-E.** SSCs after treatment with F-Si-GNR. Mitochondria were damaged and chromatin condensation was observed in EL4s also swelling of the nucleus membrane was observed in EL4s. The Rough endoplasmic reticulum (RER), autophagic vacuoles (aV) and very high mitochondria (M) were observed in SSCs. Swollen membrane (black arrows), F-Si-GNR (white arrows), nucleus (N), chromatin condensation (CC), Mitochondria (M), plasma membrane blebbing (b), (scale bar: A: 4 μm, B: 2 μm, C: 2 μm, D, E: 1 μm). Effects of F-Si-GNR administration on the apoptosis in **F, G.** SSCs, and **H, I.** EL4s determined by flow cytometry analysis. The diagram shows that after incubation with F-Si-GNR, necrotic SSCs and EL4 cells weren't observed. F-Si-GNR; Folic acid-conjugated silica-coated gold nanorods.

Discussion

Since cancers, and especially testicular cancer, affects male fertility in many ways, an increase in the survival of male cancer patients of the fertile age has become a new challenge to male fertility. Cancer treatment, including radiation therapy, chemotherapy, and surgery, can be temporary and also have permanent harmful effects on male fertility (27). The isolation of cancer cells from healthy cells (germ cells) is a great challenge. Nowadays, the process of isolating testicular germ cells from malignant cells while avoiding contamination is in progress (26). So far, there are several techniques used to separate tumor cells from normal cells, including MACS and FACS-based sorting strategies and additional sorting techniques that avoid contamination of harmful cancer cells (9, 10).

Nanotechnology has made a major stride in selective cancer targeting. They can be designed for targeting the favorable cells by changing various modifications of NPs such as their shape, size, physical and chemical properties (28). Gold NPs have a very high potential for cancer therapy based on their light absorption and scattering properties. NPs cause intracellular oxidative stress by disrupting the balance between antioxidative and oxidative processes. Research shows that some NPs can produce reactive oxygen species (ROS) which cause inflammation and even cell death (29). GNRs can be observed in many various shapes but most notably they are seen as nanorods and spherical clusters. Wang et al. (30) determined that nanorods are more cytotoxic than spherical gold nanomaterials to human HeCaT keratinocytes. GNRs support longitudinal plasmon resonances at NIR modulation with better quality factors than those of spherical gold NPs in the same resonance modulation (31), and they are extremely effectual at converting light energy into heat, especially if embedded in media of low thermal conductance (32). However, by themselves, the gold NPs desire to aggregate in solution and can smelt under laser irradiation. Silica coating is one of the golden functionalization tools that has been proven to increase the consistency of gold NPs, both thermodynamically and chemically (20, 21). The superior consistency with silica coating makes it the best choice for many applications.

Gold NPs can bind to antibodies and molecular ligands and they are suitable for medical applications (14, 18). According to Mehdizadeh et al. (19) studies, we used folate as a targeting ligand for gold NPs. Folate is transmitted in healthy cells and cancer cells by folate receptors on the cell membrane. Folate synthesizes thymine by dihydrofolate reductase in the cytoplasm of cells, so these cells regulate the presence of folate receptors on their surface. Because DNA synthesis and cell division are dependent on the presence of folate, a cancer cell needs a lot more folate than a healthy cell (22). Receptors of folate are located in caveolae on the cell membrane. After folate attachment to their receptors, it is internalized into the cytoplasm through the endocytic pathway (33). Previous studies have

confirmed that folate-receptors are highly overexpressed on the surface of tumor cell types (17).

Li et al. (34) found that gold NPs functionalized with folate are selectively internalized into cells expressing folate receptor. Other studies showed that the increase of cytotoxicity for FR-targeted gold NPs loaded with doxorubicin in FR-expressing cells related to FR-mediated endocytosis (35). The benefits of synthesis of folate-functionalized gold NPs loaded with curmin (35) or cisplatin (36) as a chemotherapeutic cargo and resultant increase in cellular uptake of FR-targeted gold NPs has been reported. Zhang et al. (37) showed that superparamagnetic NPs conjugated with folate have better uptake in tumor cells. Mansoori et al. (38) investigated cell death in HeLa (high level of folate receptor expression) and MCF-7 (low level of folate receptor expression) cells. Their results also showed that uptake of folate-conjugated gold NPs in HeLa cells were more than for MCF-7 cells and that this difference was related to the number of folate receptors on the surface of the cell. Also, in another study, Xia et al. (22) used F-Si-GNRs on HeLa cells and A549 cells. The results indicated that more F-Si-GNRs were uptaken into HeLa cells via receptor-mediated endocytosis as compared to A549 cells.

Here, in this study, we described a novel approach for elimination of cancerous cells from SSCs with treatment by F-Si-GNRs. We isolated SSCs from 3-6-day-old mice. To confirm the identity of these cells, RT-PCR using spermatogonial and germ cell markers was performed. SSCs expressed *Itga6*, *Gfra1*, *Itgb1*, *Oct4*, *Plzf* and *Mvh* markers and our findings are in line with results of previous research (25). SSCs demonstrated colonies by their morphology and they had a regular round nuclei that are similar to those found in other research (11, 25). EL4 cells were non-adherent and maintain their homogeneity. The margins of these cells were irregular. It should be noted that these cells don't form colonies and have a high proliferation rate. Also, evaluation by flow cytometry showed that *Plzf* and *H-2kb* markers are expressed in SSCs and EL-4 cells, respectively.

In order to confirm tumorigenicity, EL4 cells were transplanted through the efferent ductus and into the seminiferous tubules of azoospermia mice. After transplantation, histological evaluations confirmed that EL4s can produce a tumor *in vivo*. Our findings are consistent with other studies (11).

In the present research, the survival of EL4s and SSCs after treatment with F-Si-GNRs was assessed using the MTT proliferation test. For dose response, we used multiple doses of F-Si-GNRs that consisted of 25, 50, 75, 100, 125 and 140 μ M for 6 hours. Our study identified that cell death increased with an increase in the quantity of GNRs. In this study, we tried to find an effective dose of F-Si-GNRs for the elimination of EL4s, while maintaining SSC health and viability. The results of MTT assay showed that the optimal mean dose for the highest cell death in EL4s and lowest in SSCs is 100 μ M of F-Si-

GNRs for a 6 hour incubation period.

Our results demonstrated that cytotoxicity of F-Si-GNRs increased in EL4 cells in comparison to SSCs. Similar to other studies, the increase in cytotoxicity is related to FR-mediated endocytosis and following uptake of F-Si-GNRs in tumor cells (22, 38). Moreover, the present study shows that different doses of F-Si-GNRs have concentration-dependent cytotoxic effects on EL4s and germ cells. The size of the NPs was found to play a crucial role in both the rate and extent of cellular uptake. Pan et al. (29) showed that toxicity of gold NPs are size-dependent. In our study, the size of the F-Si-GNRs was 20.43 ± 2.18 nm in length and 5.55 ± 1.56 nm in width. The thickness of the silica layer coating around the GNRs was 2.56 ± 0.62 nm, and this resulted in more toxicity compared to other studies (23, 24).

After incubation of SSCs and EL4s with F-Si-GNRs, apoptosis evaluation was performed using an annexin V-FITC apoptosis detection kit. The results showed that apoptotic rates of the EL4s were significantly higher than SSCs and this finding is similar to other research (11). This means that the numbers of folate receptors on the surface of EL4 cells are more abundant than for SSCs. After internalization, F-Si-GNRs were taken up by lysosomes. The lysosomal membrane is protected from acidic hydrolases by specific expression of lysosomal membrane proteins (39). The lysosomes were heavily disrupted and further damaged the mitochondrial membranes. Mitochondrial damage further activated the apoptosis-associated signaling pathways. In this research, electron microscopy studies showed F-Si-GNRs after cellular internalization and illustrated how these cause damage to the mitochondria, which is consistent with other studies (40).

Conclusion

Here, we report the synthesis and characterization of folate conjugated silica modified GNRs and their *in vitro* effects on the viability of SSCs and EL4s. In addition, our results indicated that EL4s had a greater amount of uptake of F-Si-GNRs as compared to SSCs, and this was related to the amount of folate receptor that was present on the cells. The obtained results support the use of the optimal dose of F-Si-GNRs as a useful approach for treating testicular cancer. We anticipate that this NPs will have great potential for the development of therapies for clinical patients with cancer in near future.

Acknowledgments

This study was funded by a grant from Iran University of Medical Sciences (IUMS) (Number: 94-01-117-25884). All experiments have been performed in the Cellular and Molecular Research Center (IUMS, Tehran, Iran). The authors declare that they have no conflict of interest.

Authors' Contributions

N.E., K.A., A.S.-Z., K.K., Z.M., M.K.; Contributed

to conception and design. N.E., A.S.-Z., V.P.-M., R.S., T.T.M.; Contributed to experimental work, data and statistical analysis, and interpretation of data. V.P.-M.; Performed transmission electronic microscopy process. T.T.M.; Prepared gold nanorods and their modifications. C.M., H.R.A., N.E.; Wrote the manuscript. M.K.; Was responsible for overall supervision. C.M., H.R.A.; Performed advising to cell culture and molecular experiments. All authors performed editing and approving the final version of this paper for submission.

References

- Rouhollahi MR, Mohagheghi MA, Mohammadrezai N, Ghiasvand R, Ghanbari Mottagh A, Harirchi I, et al. Situation analysis of the national comprehensive cancer control program (2013) in the I. R. of Iran; assessment and recommendations based on the IAEA IMPACT mission. *Arch Iran Med.* 2014; 17(4): 222-231.
- Aliakbari F, Sedighi Gilani MA, Yazdekhashti H, Koruji M, Asgari HR, Baazm M, et al. Effects of antioxidants, catalase and α -tocopherol on cell viability and oxidative stress variables in frozen-thawed mice spermatogonial stem cells. *Artif Cells Nanomed Biotechnol.* 2017; 45(1): 63-68.
- Azizollahi S, Aflatoonian R, Sedighi-Gilani MA, Jafarabadi MA, Behnam B, Azizollahi G, et al. Recruiting testicular torsion introduces an azoospermic mouse model for spermatogonial stem cell transplantation. *Urol J.* 2014; 11(3): 1648-1655.
- Koruji M, Movahedin M, Mowla SJ, Gourabi H, Pour-Beiranvand S, Jabbari Arfaee AJ. Autologous transplantation of adult mice spermatogonial stem cells into gamma irradiated testes. *Cell J.* 2012; 14(2): 82-89.
- Koruji M, Shahverdi A, Janan A, Piryaei A, Lakpour MR, Gilani Sedighi MA. Proliferation of small number of human spermatogonial stem cells obtained from azoospermic patients. *J Assist Reprod Genet.* 2012; 29(9): 957-967.
- Shams A, Eslahi N, Movahedin M, Izadyar F, Asgari H, Koruji M. Future of spermatogonial stem cell culture: application of nanofiber scaffolds. *Curr Stem Cell Res Ther.* 2017; 12(7): 544-553.
- Shabani R, Ashjari M, Ashtari K, Izadyar F, Behnam B, Khoei S, et al. Elimination of mouse tumor cells from neonate spermatogonial cells utilizing cisplatin-entrapped folic acid-conjugated poly(lactic-co-glycolic acid) nanoparticles *in vitro*. *Int J Nanomedicine.* 2018; 13: 2943-2954.
- Aliakbari F, Gilani MA, Amidi F, Baazm M, Koruji M, Izadyar F, et al. Improving the Efficacy of Cryopreservation of Spermatogonia Stem Cells by Antioxidant Supplements. *Cell Reprogram.* 2016; 18(2): 87-95.
- Geens M, Van de Velde H, De Block G, Goossens E, Van Steirteghem A, Tournaye H. The efficiency of magnetic-activated cell sorting and fluorescence-activated cell sorting in the decontamination of testicular cell suspensions in cancer patients. *Hum Reprod.* 2007; 22(3): 733-742.
- Hou M, Andersson M, Zheng C, Sundblad A, Söder O, Jahnukainen K. Immunomagnetic separation of normal rat testicular cells from Roser's T-cell leukaemia cells is ineffective. *Int J Androl.* 2009; 32(1): 66-73.
- Shabani R, Ashtari K, Behnam B, Izadyar F, Asgari H, Asghari Jafarabadi M, et al. *In vitro* toxicity assay of cisplatin on mouse acute lymphoblastic leukaemia and spermatogonial stem cells. *Andrologia.* 2016; 48(5): 584-594.
- Brown SD, Nativo P, Smith J-A, Stirling D, Edwards PR, Venugopal B, et al. Gold nanoparticles for the improved anticancer drug delivery of the active component of oxaliplatin. *J Am Chem Soc.* 2010; 132(13): 4678-4684.
- Jelveh S, Chithrani DB. Gold nanostructures as a platform for combinational therapy in future cancer therapeutics. *Cancers (Basel).* 2011; 3(1): 1081-1110.
- Ashjari M, Dehfuly S, Fatehi D, Shabani R, Koruji M. Efficient functionalization of gold nanoparticles using cysteine conjugated protoporphyrin IX for singlet oxygen production *in vitro*. *RSC Advances.* 2015; 5(127): 104621-104628.
- Tong L, Wei Q, Wei A, Cheng JX. Gold nanorods as contrast agents for biological imaging: optical properties, surface conjugation and photothermal effects. *Photochem Photobiol.* 2009; 85(1): 21-32.
- Cole JR, Mirin NA, Knight MW, Goodrich GP, Halas NJ. Photother-

- mal efficiencies of nanoshells and nanorods for clinical therapeutic applications. *J Phys Chem C*. 2009; 113(28): 12090-12094.
17. Shakeri-Zadeh A, Mansoori GA, Hashemian AR, Eshghi H, Sazgarinia A, Montazerabadi AR. Cancerous cells targeting and destruction using folate conjugated gold nanoparticles. *Dyn Biochem Process Biotechnol Mol Biol*. 2010; 4(1): 6-12.
 18. Li W, Liu Z, Li C, Li N, Fang L, Chang J, et al. Radionuclide therapy using ¹³¹I-labeled anti-epidermal growth factor receptor-targeted nanoparticles suppresses cancer cell growth caused by EGFR overexpression. *J Cancer Res Clin Oncol*. 2016; 142(3): 619-632.
 19. Mehdizadeh A, Pandesh S, Shakeri-Zadeh A, Kamrava SK, Habib-Agahi M, Farhadi M, et al. The effects of folate-conjugated gold nanorods in combination with plasmonic photothermal therapy on mouth epidermal carcinoma cells. *Lasers Med Sci*. 2014; 29(3): 939-948.
 20. Chen YS, Frey W, Kim S, Homan K, Kruizinga P, Sokolov K, et al. Enhanced thermal stability of silica-coated gold nanorods for photoacoustic imaging and image-guided therapy. *Opt Express*. 2010; 18(9): 8867-8878.
 21. Luke GP, Bashyam A, Homan KA, Makhija S, Chen Y-S, Emelianov SY. Silica-coated gold nanoplates as stable photoacoustic contrast agents for sentinel lymph node imaging. *Nanotechnology*. 2013; 24(45): 455101.
 22. Xia HX, Yang XQ, Song JT, Chen J, Zhang MZ, Yan DM, et al. Folic acid-conjugated silica-coated gold nanorods and quantum dots for dual-modality CT and fluorescence imaging and photothermal therapy. *J Mater Chem B*. 2014; 2(14): 1945-1953.
 23. Huang P, Bao L, Zhang C, Lin J, Luo T, Yang D, et al. Folic acid-conjugated silica-modified gold nanorods for X-ray/CT imaging-guided dual-mode radiation and photo-thermal therapy. *Biomaterials*. 2011; 32(36): 9796-9809.
 24. Gao B, Shen L, He KW, Xiao WH. GNRs@ SiO₂-FA in combination with radiotherapy induces the apoptosis of HepG2 cells by modulating the expression of apoptosis-related proteins. *Int J Mol Med*. 2015; 36(5): 1282-1290.
 25. Eslahi N, Hadjighassem MR, Joghataei MT, Mirzapour T, Bakhtiyari M, Shakeri M, et al. The effects of poly L-lactic acid nanofiber scaffold on mouse spermatogonial stem cell culture. *Int J Nanomedicine*. 2013; 8: 4563-4576.
 26. Fujita K, Tsujimura A, Miyagawa Y, Kiuchi H, Matsuoka Y, Takao T, et al. Isolation of germ cells from leukemia and lymphoma cells in a human in vitro model: potential clinical application for restoring human fertility after anticancer therapy. *Cancer Res*. 2006; 66(23): 11166-11171.
 27. Ginsberg JP, Carlson CA, Lin K, Hobbie WL, Wigo E, Wu X, et al. An experimental protocol for fertility preservation in prepubertal boys recently diagnosed with cancer: a report of acceptability and safety. *Hum Reprod*. 2010; 25(1): 37-41.
 28. Sutradhar KB, Amin ML. Nanotechnology in cancer drug delivery and selective targeting. *ISRN Nanotechnology*. 2014; 2014: 1-12.
 29. Pan Y, Leifert A, Ruau D, Neuss S, Bornemann J, Schmid G, et al. Gold nanoparticles of diameter 1.4 nm trigger necrosis by oxidative stress and mitochondrial damage. *Small*. 2009; 5(18): 2067-2076.
 30. Wang S, Lu W, Tovmachenko O, Rai US, Yu H, Ray PC. Challenge in understanding size and shape dependent toxicity of gold nanomaterials in human skin keratinocytes. *Chem Phys Lett*. 2008; 463(1-3): 145-149.
 31. Wu K, Chen J, McBride JR, Lian T. CHARGE TRANSFER. Efficient hot-electron transfer by a plasmon-induced interfacial charge-transfer transition. *Science*. 2015; 349(6248): 632-635.
 32. Harris-Birtill D, Singh M, Zhou Y, Shah A, Ruenaroengsak P, Gallina ME, et al. Gold nanorod reshaping in vitro and in vivo using a continuous wave laser. *PLoS One*. 2017; 12(10): e0185990.
 33. Hashemian A, Mansoori GA. Cancer nanodiagnostics and nanotherapeutics through the folate-conjugated nanoparticles. *J Biomed Biomed*. 2013; 5(3): 61-64.
 34. Li G, Li D, Zhang L, Zhai J, Wang E. One-Step Synthesis of Folic Acid Protected Gold Nanoparticles and Their Receptor-Mediated Intracellular Uptake. *Chemistry*. 2009; 15(38): 9868-9873.
 35. Manju S, Sreenivasan K. Gold nanoparticles generated and stabilized by water soluble curcumin-polymer conjugate: blood compatibility evaluation and targeted drug delivery onto cancer cells. *J Colloid Interface Sci*. 2012; 368(1): 144-151.
 36. Patra CR, Bhattacharya R, Mukherjee P. Fabrication and functional characterization of gold nanoconjugates for potential application in ovarian cancer. *J Mater Chem*. 2010; 20(3): 547-554.
 37. Zhang Y, Kohler N, Zhang M. Surface modification of superparamagnetic magnetite nanoparticles and their intracellular uptake. *Biomaterials*. 2002; 23(7): 1553-1561.
 38. Mansoori GA, Brandenburg KS, Shakeri-Zadeh A. A comparative study of two folate-conjugated gold nanoparticles for cancer nanotechnology applications. *Cancers (Basel)*. 2010; 2(4): 1911-1928.
 39. Boya P, Kroemer G. Lysosomal membrane permeabilization in cell death. *Oncogene*. 2008; 27(50): 6434-6451.
 40. Zhang F, Zhu X, Gong J, Sun Y, Chen D, Wang J, et al. Lysosome-mitochondria-mediated apoptosis specifically evoked in cancer cells induced by gold nanorods. *Nanomedicine (Lond)*. 2016; 11(15): 1993-2006.

Amentoflavone Induces Autophagy and Modulates p53

Hye-Jung Park, M.Sc.¹, Moon-Moo Kim, Ph.D.^{2*}

1. Department of Chemistry and Biology, Dong-Eui University, Busan, Republic of Korea
2. Department of Applied Chemistry, Dong-Eui University, Busan, Republic of Korea

*Corresponding Address: Department of Applied Chemistry, Dong-Eui University, Gaya-3-dong, Jin-gu, Busan 614-714, Republic of Korea
Email: mmkim@deu.ac.kr

Received: 22/Jan/2018, Accepted: 10/Apr/2018

Abstract

Objective: Amentoflavone is the main component of *Selaginella tamariscina* widely known as an oriental traditional medicinal stuff that has been known to have a variety of medicinal effects such as the induction of apoptosis, anti-metastasis, and anti-inflammation. However, the effect of amentoflavone on autophagy has not been reported until now. The aim of this study was to investigate whether amentoflavone has a positive effect on the induction of autophagy related to cell aging.

Materials and Methods: In this experimental study, the aging of young cells was induced by the treatment with insulin-like growth factor-1 (IGF-1) at 50 ng/mL three times every two days. The effect of amentoflavone on the cell viability was evaluated in A549 and WI-38 cells using 3-(4,5-dimethyl-2-yl)-2,5-diphenyl tetrazolium bromide (MTT) assay. The induction of autophagy was detected using autophagy detection kit. The expression of proteins related to autophagy and IGF-1 signaling pathway was examined by western blot analysis and immunofluorescence assay.

Results: First of all, it was found that amentoflavone induces the formation of autophagosome. In addition, it enhanced the expression level of Atg7 and increased the expression levels of Beclin1, Atg3, and LC3 associated with the induction of autophagy in immunofluorescence staining and western blot analyses. Moreover, amentoflavone inhibited the cell aging induced by IGF-1 and hydrogen peroxide. In particular, the levels of p53 and p-p21 proteins were increased in the presence of amentoflavone. Furthermore, amentoflavone increased the level of SIRT1 deacetylating p53.

Conclusion: Our results suggest that amentoflavone could play a positive role in the inhibition of various diseases associated with autophagy and the modulation of p53.

Keywords: Aging, Amentoflavone, Autophagy, p53, SIRT1

Cell Journal (Yakhteh), Vol 21, No 1, Apr-Jun (Spring) 2019, Pages: 27-34

Citation: Park HJ, Kim MM. Amentoflavone Induces Autophagy and Modulates p53. Cell J. 2019; 21(1): 27-34. doi: 10.22074/cellj.2019.5717.

Introduction

Amentoflavone used in the study is mainly contained in *Selaginella tamariscina* to have a hemostatic effect, anti-inflammatory and anti-cancer effect (1). *Selaginella tamariscina* has been used as an anti-cancer agent and contains many different compounds such as biflavonoids (2) which are widely present in vascular plants and have a variety of physiological activities (3, 4). Amentoflavone is a dimer composed of apigenin that has the capability to promote the cell cycle arrest and induction of apoptosis through the p53-related pathway as well as the induction of autophagy in several human cancer cell lines (5). However, the role of amentoflavone in the mechanism of the induction of autophagy remains unclear.

Anti-aging studies have focused on manipulation of genes involved in histone acetylation, Insulin-like growth factor-1 (IGF-1) pathway, and p53 system to suppress the senescence as a mean to extend the lifespan of the mammalian model (6, 7). However, the efforts increasing longevity in complex animal models do not have a sufficient understanding of the life mechanism. On the other hand, p53, a tumor suppressor protein, is closely related to aging as well as the induction of autophagy and apoptosis. In particular, the activated IGF-1 signaling is involved in the senescence and cell growth via p53

protein dependently. The short-term of IGF-1 treatment promotes the cell growth by up-regulating PI3K/AKT pathway through IGF1R against p53 protein. In contrast, the long-term IGF-1 treatment induces the senescence and is also very closely related to the development of cancer, depending on the concentration of the p53 protein that is as a substrate for SIRT1, a histone deacetylase, resulting in the inhibition of cell aging caused by long-term IGF-1 treatment (8, 9).

In recent years, resveratrol or spermidine, calorie restriction, and rapamycin have been reported to induce autophagy associated with longevity (10). Therefore, it is important to study the relationship and the mechanism of senescence related to IGF-1, p53, and HAT/SIRT1 pathway associated with the induction of autophagy to remove the cellular wastes such as organelles and macromolecules damaged by internal and external stimuli. In addition, the previous study reported that there is substantial evidence supporting the roles of autophagy in megakaryopoiesis. The engagement of transcription factors, cytokines, and extracellular stress synergically promotes the maturation of megakaryocytes (11). Transcription factors, such as SCL, GATA1, GATA2, and NF-E2 allow the development of megakaryocyte/erythroid

progenitor cells (12). The abrogation of autophagy from stem cell stage by hematopoietic knockout of ATG7 leads to impaired megakaryopoiesis, the loss of autophagy caused mitochondrial and cell cycle dysfunction, impeding megakaryopoiesis, and megakaryocyte differentiation (13).

While the active autophagy process prolongs the cell survival and lifespan, the over-activated autophagy leads to autophagic cell death (14). In the autophagic process, Beclin1 (Atg6) in the initial formation of autophagosome acts as a partner of Bcl-2 as an anti-apoptosis factor that exerts an anti-autophagic effect as well as anti-apoptosis (15). Recently, some studies in breast cancer cell line confirmed that the expression level of Beclin1 is remarkably low and induces the tumor activity of cells (16).

Accordingly, in this study, we investigated whether amentoflavone could modulate autophagy related to cell aging through the modulation of p53 and SIRT1.

Materials and Methods

This experimental study was conducted at the Department of Applied Chemistry at Dong-Eui University (Republic of Korea). In this study, Amentoflavone was obtained from Sigma-Aldrich (St. Louis, MO, USA). Dulbecco's modified Eagle's medium (DMEM), trypsin-EDTA, penicillin/streptomycin/ amphotericin (10000 U/ml, 10000 g/ml, and 2500 g/ml, respectively), and fetal bovine serum (FBS) were obtained from Gibco BRL, Life Technologies (NY, USA). A549 (ATCC # CRL-6323) and WI38 (ATCC # CRL-75) cells were purchased from ATCC. 3-(4,5-dimethyl-2-yl)-2,5-diphenyl tetrazolium bromide (MTT) reagent, agarose, and other materials were purchased from Sigma Chemical Co. (St. Louis, MO, USA).

Cell line and culture

This project was approved by the Ethics Committee of Dong-Eui University of Applied Chemistry, Busan, Republic of Korea. Cell lines were separately grown as monolayers at 5% CO₂ at 37°C in the humidified atmosphere using appropriate media supplemented with 5% FBS, 2 mM glutamine, and 100 g/ml penicillin-streptomycin. DMEM was used as the culture medium for A549 cells. Cells were passaged 3 times a week by treating with trypsin-EDTA.

MTT assay

Cytotoxic levels of amentoflavone were measured using MTT method as described previously by Hansen et al. (17). The viability of cells was quantified as a percentage compared to the control (optical density of treated cells/optical density of blank×100) and dose-response curves were developed. The data were expressed as the mean from at least three independent

experiments and P<0.05 was considered significant.

Autophagosome detection assay

Autophagy activity was detected using a commercially available autophagy/cytotoxicity dual staining kit from Cayman Chemical Company (Item No. 600140). Autophagy assay was performed according to the manufacturer's protocol. In brief, A549 cells were seeded in a 96-well plate at a density of 5×10⁴ cells/well in DMEM culture medium and incubated overnight at 37°C. Then, cells were treated with different concentrations of amentoflavone and tamoxifen as a positive control and incubated overnight. On the third day, cells were stained with propidium iodide (PI) and monodansylcadaverine (MDC) according to the manufacturer's protocol. Autophagic vacuole staining intensity can be detected using an excitation wavelength of 335 nm and an emission wavelength of 512 nm using microplate reader (Tecan Austria GmbH, Austria). The cells were also analyzed by fluorescent microscopy according to the manufacturer's protocol. Dead cells are stained by propidium iodide and can be detected with a rhodamine filter (excitation/emission=540/570 nm).

Analyses of proteins expression using western blot

Western blotting was performed according to the standard procedures. Cells treated with different concentrations of amentoflavone were lysed with RIPA lysis buffer (Sigma Chemical Co., St. Louis, MO, USA). The cell lysates were resolved on a 4-20% Novex®gradient gel (Invitrogen, USA), electrotransferred onto a nitrocellulose membrane and blocked with 10% skim milk. The primary antibodies (1:1,000) including p-p21(sc-12902, Santa Cruz Biotechnology, CA, USA), p53(sc-126X), p-p53(9286S, Sell Signaling Technology, MA, USA), ac-p53(06-758, Upstate Biotechnology Inc., NY 12946 USA), Atg3 (sc-393623), Atg7 (2631S, Sell Signaling), Beclin1 (3738, Sell Signaling), LC-3 (sc-292354), Bcl-2 (sc-492-G), β-actin (sc-1616), and their secondary antibodies (1:5,000) (sc-1616, sc-2354, sc-2005, Santa Cruz Biotechnology, CA, USA) were used to detect the respective proteins using a chemiluminescent ECL assay kit (Amersham Pharmacia Biosciences, NJ, USA) according to the manufacturer's instructions. Protein bands were visualized using AlphaEase®gel image analysis software (Alpha Innotech, CA, USA) and protein expression was quantified by Multi Gauge V3.0 software (Fujifilm Life Science, Japan).

Analysis of protein expression using immunofluorescence staining

Cells were seeded onto a slide chamber and were incubated overnight at 37°C. Then, the cells were treated with different concentrations of amentoflavone. After 24 hours of incubation, cells were fixed with 10% formalin for 15 minutes at room temperature followed

by the permeabilization with phosphate buffer solution (PBS) containing 0.5% tween 20 (0.5% PBS T-20) and washed three times by 0.1% PBS T-20. The cells had preconditioning process with 5% Donkey normal serum and immunofluorescence staining with primary antibodies (anti-Atg7, anti-p53, anti-p-p21, anti-p-mTOR) (1:500) for 24 hours at room temperature. After, the cells were then washed with 0.1% PBS T-20 three times for 5 minutes, respectively and treated with the secondary antibodies (donkey anti-rabbit conjugated CY3, donkey anti-goat conjugated CY3, donkey anti-goat conjugated FITC, donkey anti-rabbit conjugated CY3, donkey anti-goat conjugated FITC, donkey anti-mouse conjugated FITC, donkey anti-rabbit conjugated CY3) (CY3 1:400, FITC 1:200) at room temperature for 1 hour. The cells were then washed with 0.1% PBS T-20 three times and PB once for 5 minutes, respectively. Finally, the slide was spread using DAPI solution and examined using iRiS™ Digital Cell Imaging System (Logos Biosystems, Annandale, US).

SA- β -galactosidase staining

According to the method of Tran (8), WI38 and A549 cells were incubated in a 24-well plate format under a serum starvation state for 4 days, then exposed to 5 ng/mL of IGF-1 treatment for 6 days as a long-term treatment or 10 μ M H₂O₂ treatment for 24 hours. After the treatment for 24 hours with a proper concentration of amentoflavone, the cell culture medium was aspirated and the cells were twice washed with PBS. After the last rinse, PBS was replaced with 250 μ l of 4% paraformaldehyde (PFA) for the fixation. The cells were incubated for 5 minutes at room temperature. The 4% PFA was aspirated and the cells were washed two times for 5 minutes each at room temperature with gentle shaking with 500 μ l of PBS. Each well was exposed to 250 μ l of SA- β -gal staining solution. The cells were incubated in the dark in a 37°C incubator. The reaction was terminated when the cells were stained as blue-green. To terminate the reaction, the staining solution was aspirated and replaced with distilled water. The cells were washed for the second time with distilled water. After the last wash, 500 μ l of distilled water was added to each well and the plate was observed under the microscope.

Statistical analysis

Data were analyzed using Student's t test for paired data (comparison with the control group) and MEGFL. Data are represented as the mean of values \pm S.D and obtained from three independent experiments (*P<0.05, **P<0.01, ***P<0.001).

Results

Effect of amentoflavone on the cytotoxicity

The cytotoxic effect of amentoflavone was investigated using MTT assay. Amentoflavone above 8 μ M exhibited

the cytotoxicity in cancerous human lung fibroblasts (A549 cells) as shown in Figure 1A. In addition, amentoflavone above 1 μ M showed the cytotoxicity in normal human lung fibroblasts (WI38 cells) as shown in Figure 1B.

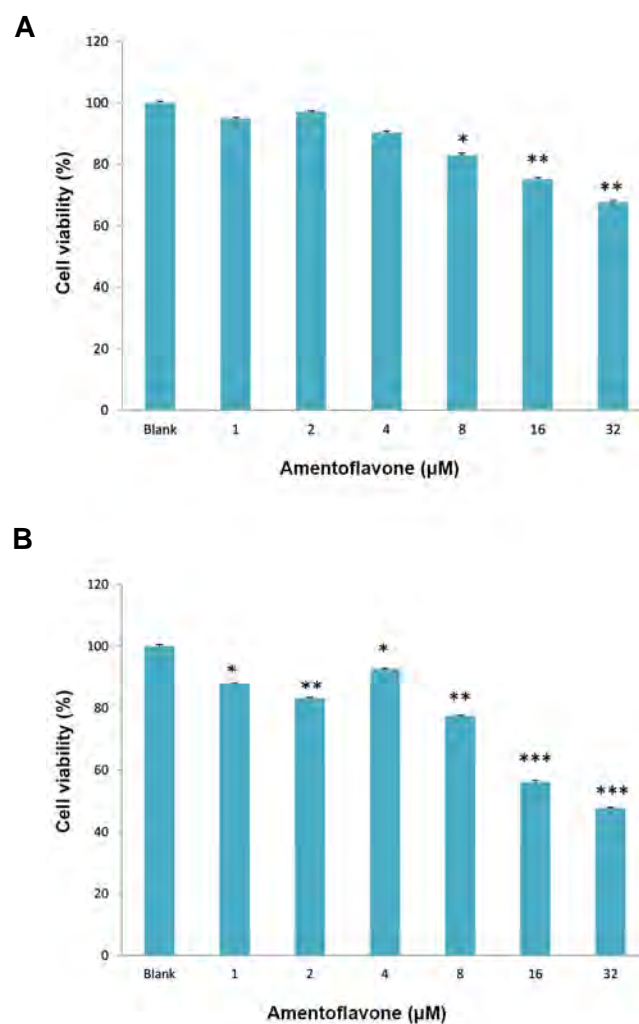


Fig.1: Effect of amentoflavone on cell viability. **A.** Amentoflavone was treated to A549 cells and **B.** Amentoflavone was treated to WI38 cells. The cells were treated with amentoflavone at the indicated concentration and the cell viability was determined by MTT assay after 48 hours. Data are presented as the mean of values \pm SD obtained from three independent experiments. The level of significance was identified statistically (*; P<0.05, **; P<0.01, ***; P<0.001) using Student's t test.

Effect of amentoflavone on the formation of autophagosome

The effect of amentoflavone on the formation of autophagosome was investigated by the degree of MDC absorbed into autophagosome by the action of autophagy. Amentoflavone above 2 μ M displayed a remarkable fluorescence image in A549 cells as shown in Figure 2A. It was observed that it induced autophagy by 1.7-fold increase compared with tamoxifen treatment group used as a positive control in Figure 2B. In order to examine its cytotoxicity at the same time, the cells were stained with PI. Amentoflavone above 2 μ M showed PI staining that means the cell death as shown in Figure 2C.

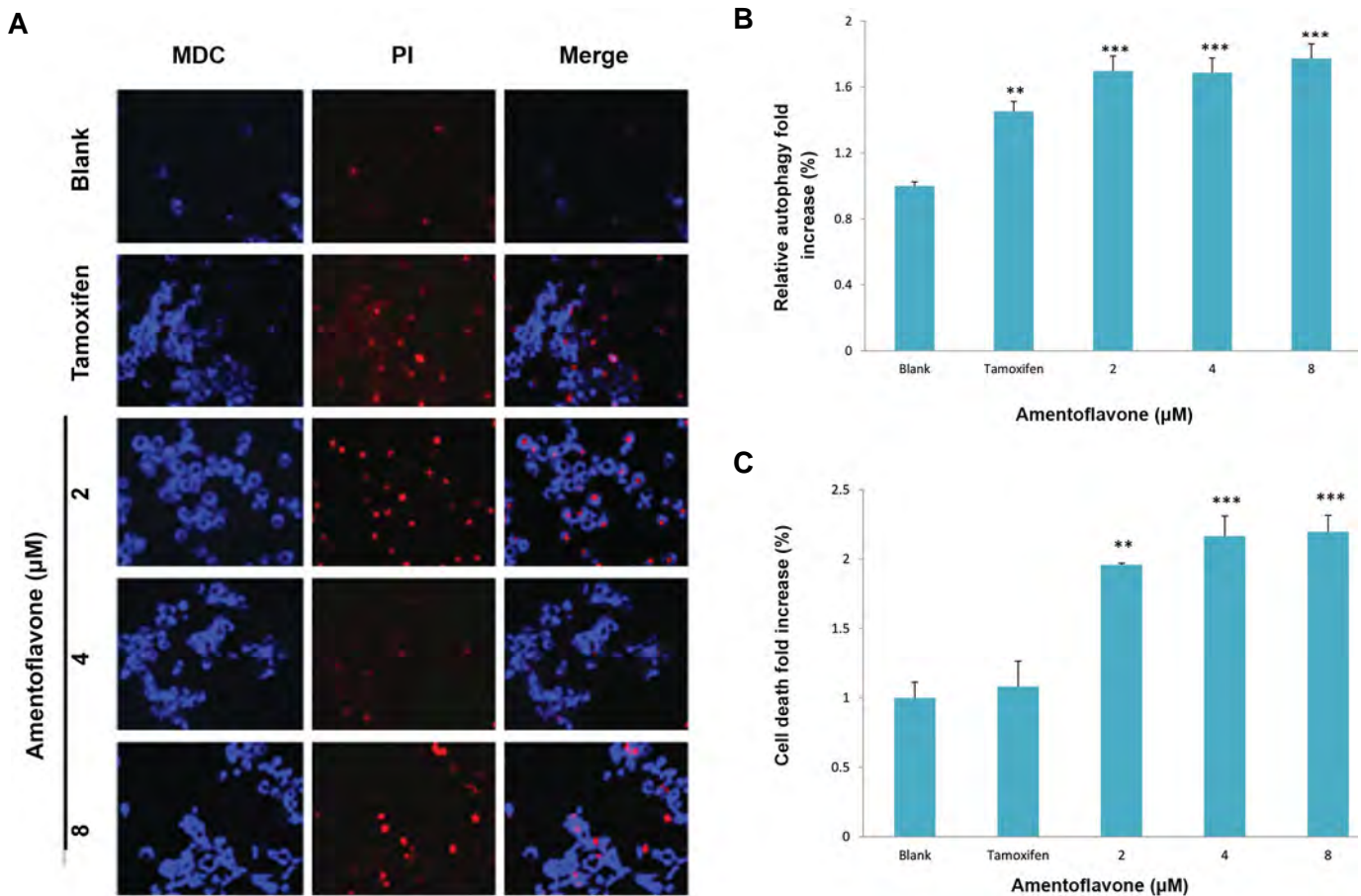


Fig.2: Effect of amentoflavone on formation of autophagosome in A549 cells. The cells (1×10^5 cells) were treated with amentoflavone at the indicated concentration. The level of autophagosome formation was evaluated in the presence of amentoflavone or tamoxifen. **A.** The autophagosome was stained by MDC and the damaged cells or dying cells were stained by PI, **B.** The effect of amentoflavone on autophagy was analyzed by the fluorescence measurement of autophagic vacuole. The cells showing autophagic vacuoles were quantified by fold increase in green detection reagent signal, and **C.** The effect of amentoflavone on the cell viability was analyzed by the fluorescence measurement of dead cells stained by propidium iodide. Data are shown as the mean of values \pm SD obtained from three independent experiments. The level of significance was identified statistically (**; $P < 0.01$, ***; $P < 0.001$) using Student's t test. MDC; Monodansylcadaverine and PI; propidium iodide.

Effect of amentoflavone on the expression of Atg7 and autophagy-related proteins

In order to confirm the effect of amentoflavone on the induction of autophagy, the expression of Atg7, an autophagic marker, was examined in A549 cells using immunofluorescence analysis. Cell nuclei were labeled with blue DAPI fluorescence dye and the target protein Atg7 was stained with a red CY3 fluorescence dye as shown in Figure 3A. It was confirmed that amentoflavone at 4 μ M exhibited a higher red image than tamoxifen at 20 μ M used as a positive control, indicating that amentoflavone could induce a higher expression of Atg7 protein related to induction of autophagy. Western blotting was also carried out to examine the level of autophagy-related proteins by amentoflavone. Amentoflavone at 8 μ M remarkably increased the levels of LC3, Becline1, and Atg7 involved in the formation of autophagosome in A549 cells as shown in Figure 3B and 3C. Moreover, it was found that it can increase the levels of above-mentioned proteins at a higher level than the tamoxifen group. However, amentoflavone decreased the level of Bcl-2

protein, an anti-autophagy marker, and did not affect the level of Atg3.

Effect of amentoflavone on the expression of proteins related to p53 signaling pathway

In order to investigate the effect of amentoflavone on p53 signaling pathway involved in the senescence mechanism, immunofluorescence for p53 and p21 proteins were performed in this study. The nucleus of A549 cells was stained with DAPI, and the p-p21 and p53 proteins were labeled with green FITC and red CY3 fluorescence dyes, respectively. Amentoflavone treatment above 2 μ M or 4 μ M remarkably increased the levels of p53 protein and p-p21 proteins, respectively, as shown in Figure 4A. The effect on the level of proteins related to p53 signaling pathway was examined using western blot analysis. Amentoflavone above 2 μ M increased the level of p53 as shown in Figure 4B and C. Similarly, the level of p-p21 protein was enhanced in the presence of amentoflavone above 2 μ M. However, amentoflavone above 2 μ M decreased the level of acetyl-p53.

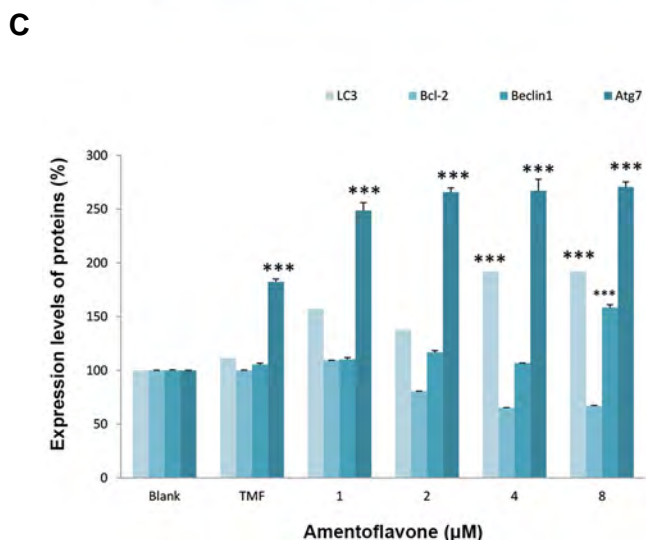
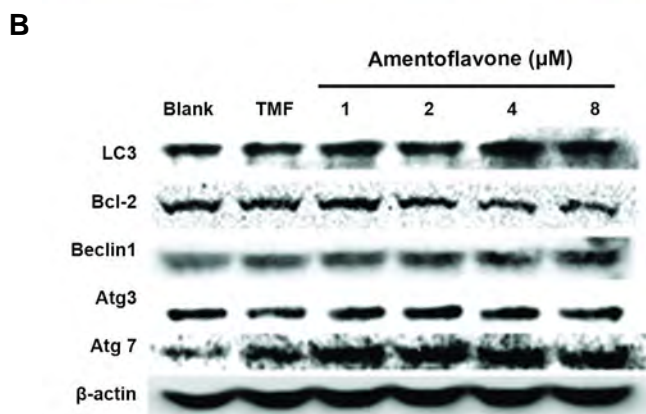
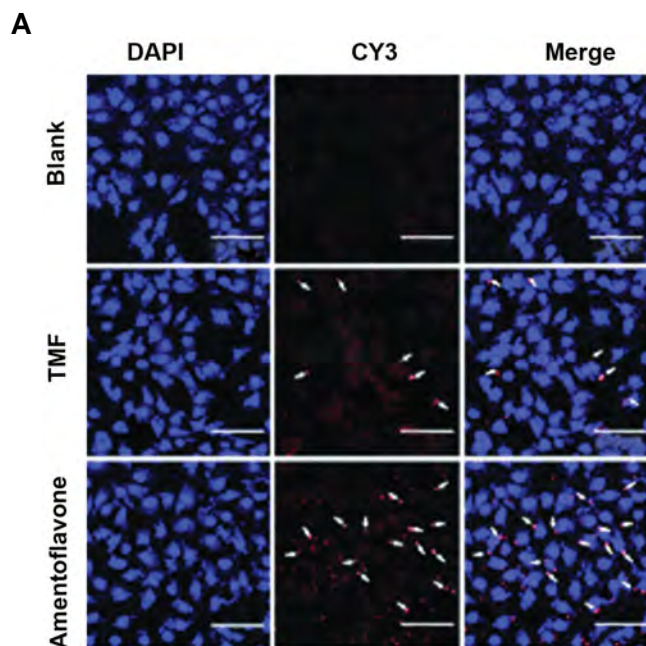


Fig.3: Effect of amentoflavone on the expression of Atg7 and autophagy-related proteins. **A.** The images of Atg7 immunofluorescence-stained A549 cells were shown by the red color. The arrows show Atg7 has been localized to the cell cytosol (scale bar: 100 μm). **B.** The effect of amentoflavone on protein expressions of LC3, Bcl-2, Beclin1, Atg3, Atg7, and β-actin was analyzed by western blot, and **C.** The level of proteins expression was quantified by Multi Gauge V3.0 software. Data are presented as the mean of values ± SD from three independent experiments. The level of significance was identified statistically (***) using Student's t test.

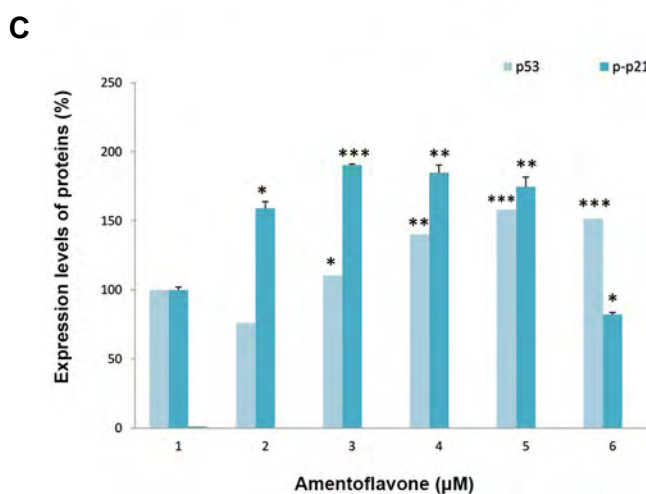
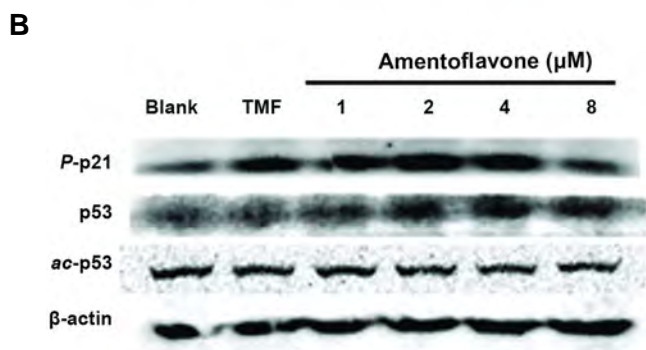
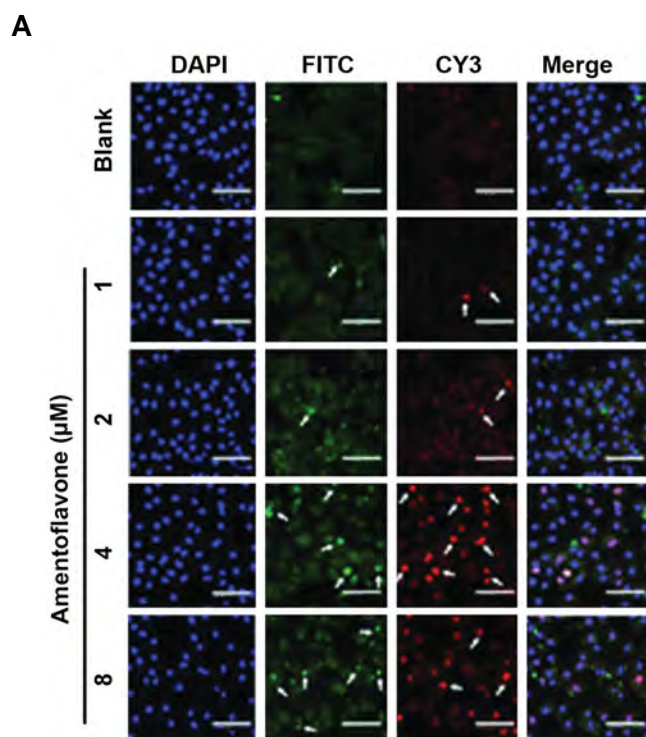


Fig.4: Effect of amentoflavone on the expression of proteins related to p53 signaling pathway. **A.** The images of p53 (FITC) and p-p21 (CY3) immunofluorescence-stained A549 cells were shown by the green and red color, respectively. Arrows show p53 and p-p21 have been localized to the cell cytosol or nuclear (scale bar: 100 μm). **B.** The effect of amentoflavone on protein expressions of p-p21, p53, ac-p53, and p-p53 was analyzed by western blot, and **C.** The level of protein expressions was quantified by Multi Gauge V3.0 software.

Immunofluorescence analysis for the effect of amentoflavone on expression of SIRT1

The anti-aging effect of amentoflavone was investigated by the analysis of SIRT1 protein expression involved in the senescence mechanism using immunofluorescence staining. The nucleus of the cell was stained with DAPI, and the SIRT1 protein was labeled with a red CY3 fluorescence dye, respectively. Resveratrol treatment used as a positive control showed the highest level of SIRT1 protein in the treatment groups as shown in Figure 5. Although the effect of amentoflavone on the level of SIRT1 was lower than that of the resveratrol treatment group, it remarkably increased the level of SIRT1 compared with the blank group.

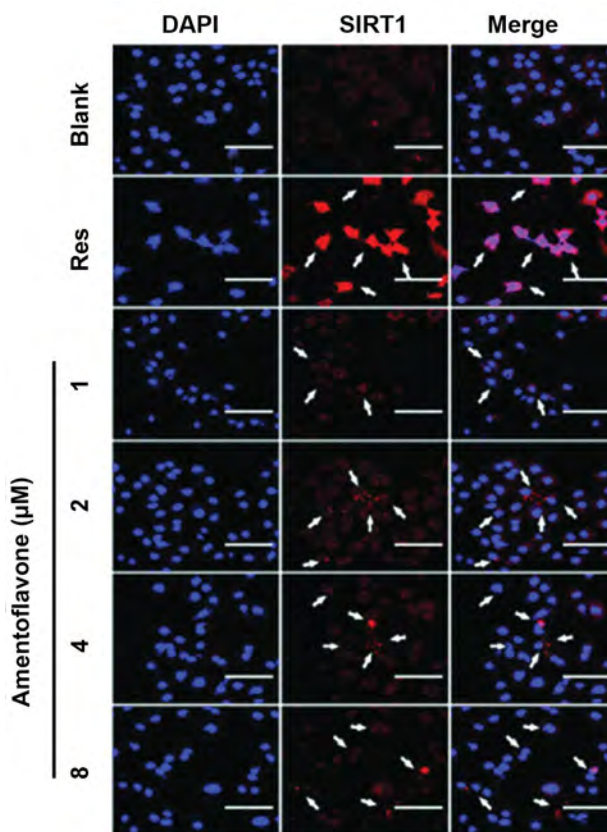


Fig.5: Immunofluorescence analysis of the effect of amentoflavone on expression of SIRT1. The images of SIRT1 (CY3) immunofluorescence-stained A549 cells were shown by the red color. The cells were cultured in the presence of amentoflavone and detected with a rabbit polyclonal antibody against SIRT1. Arrows show SIRT1 has been localized to the cell cytosol. Res stands for resveratrol used as a positive control in this study (scale bar: 100 µm).

Effect of amentoflavone on cell aging in A549 cells and WI38 cells

The effect of amentoflavone on aging of A549 cells was investigated using SA-β-galactosidase staining assay as a senescence marker. In this study, the aging of cells was induced by the short-term of treatment with H₂O₂ at 10 µM. H₂O₂ treatment showed a higher blue staining image than the blank group, indicating that H₂O₂ can induce the cell

aging as shown in Figure 6A. However, amentoflavone treatment remarkably decreased the blue staining image induced by H₂O₂, indicating that the cell aging induced by H₂O₂ is inhibited by amentoflavone. The effect of amentoflavone on senescence was also examined using SA-β-galactosidase staining assay normal lung fibroblasts (WI38 cells). The senescence of WI38 cells was induced by the long-term treatment of 5 ng/mL of IGF-1 or the treatment with H₂O₂ at 10 µM. The IGF-1 treated group exhibited a good phenotype of the cellular senescence showing a strong blue staining with a wide flattened shape, a typical shape of the aged cell as shown in Figure 6B. H₂O₂ treated group showed the phenotype of the cellular senescence but the shape of the aged cell was slightly less than the IGF-1 treated group. It was observed that the amentoflavone treatment group above 2 µM reduced the degree of blue staining and increased the cell size into the wide flattened shape, indicating that amentoflavone reduces the senescence.

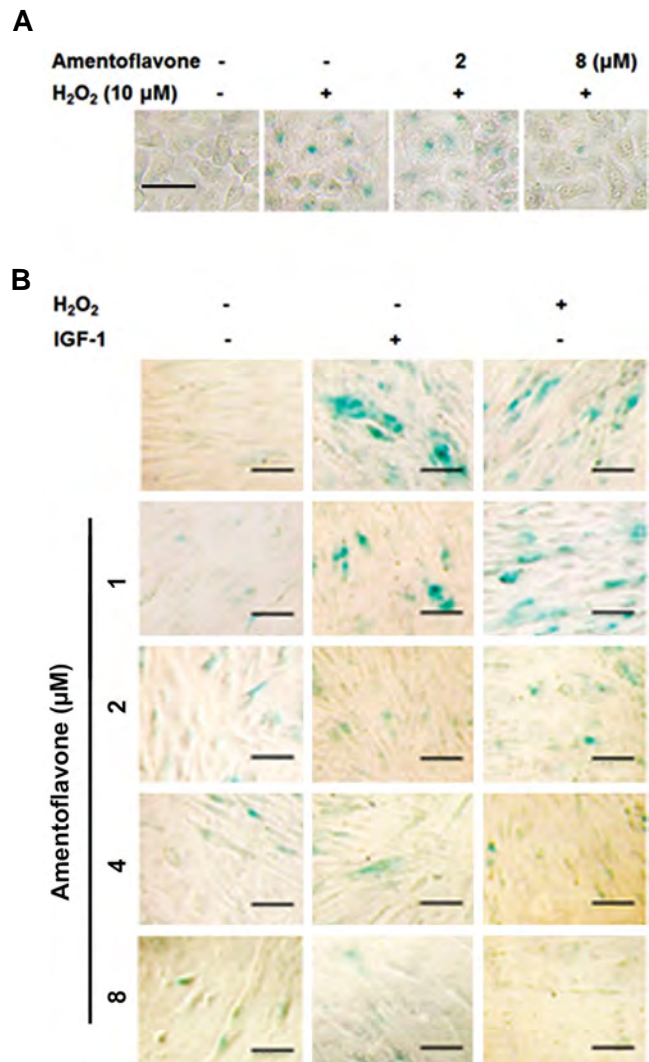


Fig.6: Effect of amentoflavone on senescence-associated (SA)-β-galactosidase staining in A549 cells and in human lung fibroblast cells (WI38). **A.** After the cells were treated with amentoflavone and H₂O₂ (10 µM) for 24 hours, SA-β-gal staining was carried out (scale bar: 100 µm). The senescent cells were stained by the blue color and **B.** After the cells were treated with amentoflavone and IGF-1 (5 ng/mL) for 6 days or H₂O₂ (10 µM) for 24 hours, SA-β-gal staining assay was carried out (scale bar: 100 µm).

Discussion

As various studies on longevity have progressed, a variety of pathways associated with aging have been found and some gene manipulations succeed the life extension of the simple model such as the nematode (18). In recent years, autophagy is closely related to the aging. Fasting related to IGF-1 pathway and rapamycin associated with mTOR mechanism necessarily require autophagy process for the life extension (19). Therefore, this study focused on the investigation whether the inductive effect of amentoflavone, a biflavonoid compound contained in *Selaginella tamariscina*, on autophagy could modulate the senescence induced by the long-term of IGF-1 treatment via p53 and SIRT1 signaling pathway.

In the first place, the effect of amentoflavone on the induction of autophagy was determined by the formation of autophagosome that is the first step in autophagy process. Beclin1 (Atg6) and class III phosphatidylinositol 3-kinase (PI3 kinase) form a complex with Vps34, creating inactive form of the autophagosome (20). Amentoflavone increased the formation of such autophagosome and, remarkably, also enhanced the level of Beclin1 in A549 cells. Amentoflavone exhibited a higher effect than tamoxifen used as a positive control in forming autophagosome. Amentoflavone is believed to promote the formation of the initial autophagosome by increasing not only the extension of the phagophore and the expression of LC3 (Atg8) protein promoting the formation of autophagosome but also the expression of Atg7 activating its ubiquitination. Ubiquitin-like protein of Atg8 exists in a complex form (Atg8-PE) with phosphatidylethanolamine (PE) in autophagic membranes (or phagophore) and mediates the fusion portion of liposomes containing Atg8-PE and tethering in *in vitro* system (21). Therefore, the positive effect of amentoflavone on the expression of LC3 and Atg7 proteins could affect even after the formation of autophagosome, and the effect of amentoflavone on a later stage of autophagy should be further studied.

These findings confirm that amentoflavone strongly promotes the autophagy process in the early stage, in particular by increasing the formation of autophagosome than tamoxifen by increasing the level of the Beclin1, Atg7, and LC3 proteins. Moreover, a previous study reported that the crosstalk between autophagy and apoptosis can be modulated by the interaction between Bcl-2 family proteins and Beclin1, a Bcl-2 interacting protein that promotes autophagy (22).

On the other hand, it was previously reported that apigenin. The monomer of amentoflavone, inhibits mTOR, an autophagy repressor, and its downstream target p70S6K, but does not alter the level of Beclin1, (23). In addition, it was found that the induction of autophagy by apigenin-mediated AMPK activation is accompanied by the inhibition of the mTOR signaling pathway as a potent chemopreventive agent (24).

In this study, amentoflavone inhibited the protein expression of Bcl-2, which is consistent with the previous

report that Bcl-2 not only acts as an anti-apoptosis factor but also functions as an anti-autophagy factor (25), indicating that amentoflavone could induce apoptosis. Amentoflavone decreased the level of Bcl-2 protein which inhibits the formation of Bcl-2-Beclin1, complex and promotes the dissociation of Beclin1, leading to the induction of autophagy as well as apoptosis which is promoted by the inhibition of Bcl-2 protein (26). At this point, the action mechanism of amentoflavone on the induction of autophagy is distinct from that of apigenin.

The previous studies have suggested that amentoflavone has a great development potential as an anti-cancer drug on apoptosis in this inductive effect (25, 27). Our findings also suggest that amentoflavone could be developed as a potential anti-cancer drug. Although p53 induces apoptosis, it is a tumor suppressor protein which is closely involved in the development of cancer (28). Moreover, p53 protein is closely related to the aging mechanism (29). SIRT1 and p53 proteins have been reported to play a key role in the senescence induced by the insulin-like growth factor-1 (8). The activity of SIRT1, suppressed by the treatment of IGF-1 in the long-term, reduces the deacetylation of p53, resulting in the induction of senescence. In another report, SIRT1 suppresses the senescence in normal cells such as HDF, but it induces the senescence in some cancer cells such as MCF-7 and H1299 by inhibiting their growth and proliferation (30, 31). Thus, SIRT1 is an important factor in determining the activity of p53 (8). The activation of p53 protein is made by the SIRT1, as a histone deacetylase, that directly deacetylates p53 protein (32). In this study, amentoflavone increased the level of p53 protein, matching the increase of p-p21 expression activated by the p53 transcription factor. However, the level of acetyl-p53 protein was decreased by amentoflavone.

Although the expression of p53 is increased by amentoflavone, the activation of the p53 protein by the increased SIRT1 is believed to be offset. Therefore, this result is explained to be caused by the increased expression of SIRT1. The previous studies on the interaction of SIRT1 with p53 protein support that amentoflavone increases the level of p53 protein, but rather its increase in SIRT1 level explains very well our result that it could induce autophagy higher than apoptosis (8, 33). Moreover, most of aging studies have reported that the accumulation of p53 protein causes the aging of cells, but the explanation on the aging of an organism is not sufficient yet by the accumulation of p53 protein alone. In fact, p53 protein inhibits the aging of cells, and the inhibitory effect of the cell aging by p53 protein disappears by nutrin3a, a p53 inhibitor (34). Finally, the study on the premature aging of WI38 cells induced by H₂O₂ and the long-term of IGF-1 confirmed that amentoflavone could inhibit the aging of these cells. In this study, we investigated to observe the effect of amentoflavone on the induction of autophagy at the protein level, and how the induction of autophagy affects the aging of the cell.

Conclusion

Amentoflavone increases the expression of Beclin1, Atg7, Atg8, and LC3 proteins but decreases the expression of Bcl-2, leading to the promotion of initial autophagy by contributing to the formation of autophagosome. Furthermore, the inductive effect of autophagy by amentoflavone reduced the senescence. In addition, the levels of p53 and SIRT1 proteins were increased in the presence of amentoflavone. Therefore, these results suggest that amentoflavone increases the survival rate of cells by the induction of autophagy, which is expected as a potential candidate inhibiting various diseases related to autophagy and cell aging.

Acknowledgments

We wish to thank Professor Yunghee Oh for the kind advice and help on the experiment of this study. We don't have any financial support and conflicts of interest in this study.

Authors' Contributions

M.-M.K.; Contributed to the conception and design, all experimental work, data, and statistical analysis interpretation of the data and overall supervision. H.-J.P.; Contributed to experimental work and the interpretation of data. All authors read and approved the final manuscript.

References

- Di Carlo G, Mascolo N, Izzo AA, Capasso F. Flavonoids: old and new aspects of a class of natural therapeutic drugs. *Life Sci.* 1999; 65(4): 337-353.
- Zhang YX, Li QY, Yan LL, Shi Y. Structural characterization and identification of biflavones in *Selaginella tamariscina* by liquid chromatography-diode-array detection/electrospray ionization tandem mass spectrometry. *Rapid Commun Mass Spectrom.* 2011; 25(15): 2173-2186.
- Banerjee T, Valacchi G, Ziboh VA, van der Vliet A. Inhibition of TNF- α -induced cyclooxygenase-2 expression by amentoflavone through suppression of NF- κ B activation in A549 cells. *Mol Cell Biochem.* 2002; 238(1-2): 105-110.
- Kim HP, Son KH, Chang HW, Kang SS. Anti-inflammatory plant flavonoids and cellular action mechanisms. *J Pharmacol Sci.* 2004; 96(3): 229-245.
- Sung B, Chung HY, Kim ND. Role of apigenin in cancer prevention via the induction of apoptosis and autophagy. *J Cancer Prev.* 2016; 21(4): 216-226.
- Peleg S, Feller C, Ladurner AG, and Imhof A. The metabolic impact on histone acetylation and transcription in ageing. *Trends Biochem Sci.* 2016; 41(8): 700-711.
- Rai P, Troen BR. Cellular and molecular aging. In: Gordon DA, Katlic MR, editors. *Pelvic floor dysfunction and pelvic surgery in the elderly.* New York: Springer; 2017; 39-52.
- Tran D, Bergholz J, Zhang H, He H, Wang Y, Zhang Y, et al. Insulin-like growth factor-1 regulates the SIRT1-p53 pathway in cellular senescence. *Aging Cell.* 2014; 13(4): 669-678.
- Korotchikina LG, Leontieva OV, Bukreeva EI, Demidenko ZN, Gudkov AV, Blagosklonny MV, et al. The choice between p53-induced senescence and quiescence is determined in part by the mTOR pathway. *Aging (Albany NY).* 2010; 2(6): 344-352.
- Jain P, Sharma P, Shrivastava A, Saran S. *Dictyostelium discoideum*: A model system to study autophagy mediated life extension. *Topics in biomedical gerontology.* Singapore: 2017; Springer; 35-55.
- Deutsch VR, Tomer A. Megakaryocyte development and platelet production. *Br J Haematol.* 2006; 134(5): 453-466.
- McDonald TP, Sullivan PS. Megakaryocytic and erythrocytic cell lines share a common precursor cell. *Exp Hematol.* 1993; 21(10): 1316-1320.
- Cao Y, Cai J, Zhang S, Yuan N, Li X, Fang Y, et al. Loss of autophagy leads to failure in megakaryopoiesis, megakaryocyte differentiation, and thrombopoiesis in mice. *Exp Hematol.* 2015; 43(6): 488-494.
- Gomes LC, Odedra D, Dikic I, Pohl C. Autophagy and modular restructuring of metabolism control germline tumor differentiation and proliferation in *C. elegans*. *Autophagy.* 2016; 12(3): 529-546.
- Cao Y, Klionsky DJ. Physiological functions of Atg6/Beclin 1: a unique autophagy-related protein. *Cell Res.* 2007; 17(10): 839-849.
- Levine B, Kroemer G. Autophagy in the pathogenesis of disease. *Cell.* 2008; 132(1): 27-42.
- Hansen MB, Nielsen SE, Berg K. Re-examination and further development of a precise and rapid dye method for measuring cell growth/cell kill. *J Immunol Methods.* 1989; 119(2): 203-210.
- Metheerairut C, Suthammarak W. *Caenorhabditis elegans*, an invertebrate model organism for biomedical research. *Siriraj Med J.* 2016; 67(3): 149-154.
- Jung CH, Ro SH, Cao J, Otto NM, Kim DH. mTOR regulation of autophagy. *FEBS Lett.* 2010; 584(7): 1287-1295.
- Juhász G, Hill JH, Yan Y, Sass M, Baehrecke EH, Backer JM, et al. The class III PI (3) K Vps34 promotes autophagy and endocytosis but not TOR signaling in *Drosophila*. *J Cell Biol.* 2008; 181(4): 655-666.
- Nakatogawa H, Ichimura Y, Ohsumi Y. Atg8, a ubiquitin-like protein required for autophagosome formation, mediates membrane tethering and hemifusion. *Cell.* 2007; 130(1): 165-178.
- Erllich S, Mizrachy L, Segev O, Lindenboim L, Zmira O, Adi-Harel S, et al. Differential interactions between Beclin 1 and Bcl-2 family members. *Autophagy.* 2007; 3(6): 561-568.
- Ruela-de-Sousa RR, Fuhler GM, Blom N, Ferreira CV, Aoyama H, Peppelenbosch MP. Cytotoxicity of apigenin on leukemia cell lines: implications for prevention and therapy. *Cell Death Dis.* 2010; 1: e19.
- Tong X, Smith KA, and Pelling JC. Apigenin, a chemopreventive bioflavonoid, induces AMP-activated protein kinase activation in human keratinocytes. *Mol Carcinog.* 2012; 51(3): 268-279.
- Hwang IS, Lee J, Jin HG, Woo ER, Lee DG. Amentoflavone stimulates mitochondrial dysfunction and induces apoptotic cell death in *Candida albicans*. *Mycopathologia.* 2012; 173(4): 207-218.
- Guruvayoorappan C, Kuttan G. Amentoflavone stimulates apoptosis in B16F-10 melanoma cells by regulating bcl-2, p53 as well as caspase-3 genes and regulates the nitric oxide as well as proinflammatory cytokine production in B16F-10 melanoma cells, tumor associated macrophages and peritoneal macrophages. *J Exp Ther Oncol.* 2008; 7(3): 207-218.
- Pei JS, Liu CC, Hsu YN, Lin LL, Wang SC, Chung JG, et al. Amentoflavone induces cell-cycle arrest and apoptosis in MCF-7 human breast cancer cells via mitochondria-dependent pathway. *In Vivo.* 2012; 26(6): 963-970.
- Brown JM, Wouters BG. Apoptosis, p53, and tumor cell sensitivity to anticancer agents. *Cancer Res.* 1999; 59(7): 1391-1399.
- Chen Z, Trotman LC, Shaffer D, Lin HK, Dotan ZA, Niki M, et al. Crucial role of p53-dependent cellular senescence in suppression of Pten-deficient tumorigenesis. *Nature.* 2005; 436(7051): 725-730.
- Ota H, Tokunaga E, Chang K, Hikasa M, Iijima K, Eto M, et al. Sirt1 inhibitor, Sirtinol, induces senescence-like growth arrest with attenuated Ras-MAPK signaling in human cancer cells. *Oncogene.* 2005; 25(2): 176-185.
- Huang J, Gan Q, Han L, Li J, Zhang H, Sun Y, et al. SIRT1 overexpression antagonizes cellular senescence with activated ERK/S6k1 signaling in human diploid fibroblasts. *PLoS One.* 2008; 3(3): e1710.
- Solomon JM, et al. Inhibition of SIRT1 catalytic activity increases p53 acetylation but does not alter cell survival following DNA damage. *Mol Cell Biol.* 2006; 26(1): 28-38.
- Kamel C, Abrol M, Jardine K, He X, McBurney MW. SirT1 fails to affect p53-mediated biological functions. *Aging Cell.* 2006; 5(1): 81-88.
- Efeyan A, Ortega-Molina A, Velasco-Miguel S, Herranz D, Vassilev LT, Serrano M. Induction of p53-dependent senescence by the MDM2 antagonist nutlin-3a in mouse cells of fibroblast origin. *Cancer Res.* 2007; 67(15): 7350-7357.

Downregulation of Extracellular Matrix and Cell Adhesion Molecules in Cumulus Cells of Infertile Polycystic Ovary Syndrome Women With and Without Insulin Resistance

Fatemeh Hassani, Ph.D.^{1*}, Shahrbanoo Oryan, Ph.D.¹, Poopak Eftekhari-Yazdi, Ph.D.^{2*}, Masood Bazrgar, Ph.D.³, Ashraf Moini, M.D.^{4,5}, Nahid Nasiri, M.Sc.², Ali Sharifi-Zarchi, Ph.D.⁶

1. Department of Animal Biology, Faculty of Biological Sciences, Kharazmi University, Tehran, Iran

2. Department of Embryology, Reproductive Biomedicine Research Center, Royan Institute for Reproductive Biomedicine, ACECR, Tehran, Iran

3. Department of Genetics, Reproductive Biomedicine Research Center, Royan Institute for Reproductive Biomedicine, ACECR, Tehran, Iran

4. Department of Endocrinology and Female Infertility, Reproductive Biomedicine Research Center, Royan Institute for Reproductive Biomedicine, ACECR, Tehran, Iran

5. Department of Obstetrics and Gynecology, Arash Women's Hospital, Tehran University of Medical Sciences, Tehran, Iran

6. Department of Stem Cells and Developmental Biology, Cell Science Research Center, Royan Institute for Stem Cell Biology and Technology, ACECR, Tehran, Iran

*Corresponding Addresses: P.O.Box: 15719-14911, Department of Animal Biology, Faculty of Biological Sciences, Kharazmi University, Tehran, Iran

P.O.Box: 16635-148, Department of Embryology, Reproductive Biomedicine Research Center, Royan Institute for Reproductive Biomedicine, ACECR, Tehran, Iran

Emails: fateme.hassani@gmail.com, eftekhari@royaninstitute.org

Received: 16/Oct/2017, Accepted: 27/Mar/2018

Abstract

Objective: The extracellular matrix (ECM) of the cumulus oocyte complex (COC) is composed of several molecules that have different roles during follicle development. This study aims to explore gene expression profiles for ECM and cell adhesion molecules in the cumulus cells of polycystic ovary syndrome (PCOS) patients based on their insulin sensitivity following controlled ovarian stimulation (COS).

Materials and Methods: In this prospective case-control study enrolled 23 women less than 36 years of age who participated in an intracytoplasmic sperm injection (ICSI) program. Patients were subdivided into 3 groups: control (n=8, fertile women with male infertility history), insulin resistant (IR) PCOS (n=7), and insulin sensitive (IS) PCOS (n=8). We compared 84 ECM component and adhesion molecule gene expressions by quantitative real-time polymerase chain reaction array (qPCR-array) among the groups.

Results: We noted that 21 of the 84 studied genes differentially expressed among the groups, from which 18 of these genes downregulated. Overall, comparison of PCOS cases with controls showed downregulation of extracellular matrix protein 1 (*ECM1*); catenin (cadherin-associated protein), alpha 1 (*CTNNA1*); integrin, alpha 5 (*ITGA5*); laminin, alpha 3 (*LAMA3*); laminin, beta 1 (*LAMB1*); fibronectin 1 (*FN1*); and integrin, alpha 7 (*ITGA7*). In the IS group, there was upregulation of ADAM metalloproteinase with thrombospondin type 1 motif, 8 (*ADAMTS8*) and neural cell adhesion molecule 1 (*NCAM1*) compared with the controls ($P < 0.05$).

Conclusion: Downregulation of ECM and cell adhesion molecules seem to be related to PCOS. Gene expression profile alterations in cumulus cells from both the IS and IR groups of PCOS patients seems to be involved in the composition and regulation of ECM during the ovulation process. This study highlights the association of ECM gene alteration as a viewpoint for additional understanding of the etiology of PCOS.

Keywords: Cumulus Cells, Extracellular Matrix, Gene Expression, Insulin Resistance, Polycystic Ovary Syndrome

Cell Journal (Yakhteh), Vol 21, No 1, Apr-Jun (Spring) 2019, Pages: 35-42

Citation: Hassani F, Oryan S, Eftekhari-Yazdi P, Bazrgar M, Moini A, Nasiri N, Sharifi-Zarchi A. Downregulation of extracellular matrix and cell adhesion molecules in cumulus cells of infertile polycystic ovary syndrome women with and without insulin resistance. Cell J. 2019; 21(1): 35-42. doi: 10.22074/cellj.2019.5576.

Introduction

Polycystic ovary syndrome (PCOS) is a frequent endocrinopathic condition among reproductive aged women with a prevalence of 8-12% (1). According to the Rotterdam ESHRE/ASRM Consensus, diagnostic criteria for PCOS include oligo/anovulation, hyperandrogenism, and polycystic ovaries (detected by sonography) (2). Although the etiology of PCOS is uncertain, there is a confirmed familial and genetic basis for PCOS (3). The consequential complications of PCOS are follicular maturation arrest and insulin resistance (4, 5). Insulin resistance is defined as the impaired insulin ability to

maintain glucose homeostasis, which leads to an increase in insulin levels in the bloodstream (6). The role of insulin resistance in the pathogenesis of PCOS is uncertain, but studies lend support to the hypothesis that insulin plays an important role in regulating the response of human granulosa cells to gonadotropins (7). Hyperinsulinemia is a condition that damages oocyte developmental competence, resulting in reduced rates of fertilization, embryonic development, and implantation in obese PCOS patients (8).

Folliculogenesis needs communication between the oocyte and surrounding somatic cells (9, 10). These

somatic cells comprise two populations, specialized layers of flattened granulosa cells which line the antrum of follicles and a specified type of granulosa cells called cumulus cells which surround the oocyte in the preovulatory follicle. Cumulus cells undergo “cumulus expansion”, a process that requires these cells to form new ECM that binds the oocyte and cumulus cells together (5, 11). This process enables the oocyte to resume maturation. A surge of luteinizing hormone (LH) is necessary to initiate ovulation (5).

The extracellular matrix (ECM) of the cumulus oocyte complex (COC) is composed of several molecules with varying roles such as differentiation, division, cell death, and migration. Interestingly, all of these roles are associated with follicle development. Appropriate formation of the expanded cumulus matrix is critical for ovulation. Successful follicular rupture and fertilization is sensitive to perturbations in the composition and functional capacity of the cumulus matrix (11). The backbone of the expanded cumulus matrix is hyaluronic acid (HA), a large disaccharide chain common to numerous ECM. Synthesis of HA requires glucose. Glucose uptake and glycolytic activity in cumulus cells are markedly stimulated by the LH surge in rodents, cows, and humans. During oocyte maturation, there is an increase in glucose flux in the COC. The basement membrane that surrounds the granulosa layers of all follicles is composed of type I collagen, fibronectin, and laminin (12).

Proteoglycans such as versican (VCAN) are produced primarily by mural granulosa cells and rapidly incorporate into developing cumulus matrix. This suggests that VCAN binds to HA through its link module and is another organizer of the COC matrix structure. Deregulation of ECM matrix compartment genes during follicular development is important in the pathogenesis of PCOS (13).

Follicular growth and rupture, as well as early luteal formation, partially occur through the action of matrix metalloproteinase (MMPs) and their inhibitors. The MMP system is involved in connective tissue remodeling processes throughout the body. This system comprises both proteolytic enzymes and their associated inhibitors. MMPs have a potent ability to bind and cleave gelatin and act to degrade major constituents of basement membranes that include type IV collagen, laminin, and fibronectin. In the ovary, MMPs and their inhibitors are hypothesized to play a critical role in ECM remodeling associated with ovulation, luteal formation, and regression (14).

Follicular development and ovulation are dynamic processes that need broad tissue remodeling. Previous studies have reported the abnormal turnover of ovarian ECM components that lead to development of PCOS (15).

In the present study, we assessed the gene expression profiles for ECM and adhesion molecules in the cumulus cells of infertile PCOS patients based on their insulin sensitivity following ovarian stimulation with a gonadotropin-releasing hormone (GnRH) antagonist protocol. We reported downregulation of ECM and cell adhesion molecules as a probable etiology of PCOS infertility.

Materials and Methods

Patient selection

The Ethics Committee at Royan Institute approved this prospective case-control study (No. EC/93/1078). All participants gave informed consent prior to inclusion in the study. We ensured the confidentiality of patients' identities this research by data anonymization during analysis. This research did not incur any additional costs to the patients, nor did it affect their treatment in any way. Study participants comprised 23 women, less than 36 years of age, who underwent intracytoplasmic sperm injection (ICSI) and were not affected by thyroid disorders, diabetes, or ovarian hyperstimulation syndrome (OHSS). We allocated 15 PCOS patients previously diagnosed by the Rotterdam 2004 criteria whose partners had normal spermogram results (2) to one of two groups, insulin resistant (IR) or insulin sensitive (IS), based on fasting insulin (FI, cutoff: 12 mU/L) levels and the homeostasis model assessment of insulin resistance (HOMA-IR, cutoff: 2.57). We calculated HOMA-IR as follows: $[(\text{fasting serum insulin [mU/L]} \times \text{fasting serum glucose [mmol/L]}) / 22.5]$ (16).

The IR group consisted of 7 PCOS patients ($\text{FI} \geq 12$ mU/L, $\text{HOMA-IR} \geq 2.57$). The IS group consisted of 8 patients ($\text{FI} < 12$ mU/L; $\text{HOMA-IR} < 2.57$). The control group consisted of 8 healthy, normal ovulatory fertile women with male infertility history.

Stimulation protocol

Controlled ovarian stimulation (COS) was initiated from the third day of the cycle. Patients received regular, daily subcutaneous (SC) injections of recombinant follicle-stimulating hormone (rFSH, Gonal-F, Serono, Switzerland). We adjusted the starting dose of rFSH according to each patient's response as measured by transvaginal ultrasonography, antral follicle count (AFC), estradiol (E_2) level, and anti-Müllerian hormone (AMH). Once the ovarian follicles reached 12 mm in diameter, patients received SC injections of a GnRH antagonist, cetrorelix (Cetrotide®, Merck Serono, Germany). The protocol consisted of daily Cetrotide® SC injections until the criteria for human chorionic gonadotropin (hCG) administration was met. When more than 3 follicles reached diameters of at least 18 mm and E_2 levels of 1000-4000 pg/mL, each patient received an intramuscular (IM) injection of 10000 IU of hCG (Pregnyl®, Organon, Netherlands) or SC injection of 250 µg Ovidrel (Merck Serono, Germany).

Isolation of cumulus cells

Following oocyte pick-up, the COCs were washed 3-5 times in G-IVF™ medium (Vitrolife, Sweden) to remove blood and excess cells. After washing, the COCs were placed in a CO₂ incubator at 37°C for 2 hours in G-IVF™ (Vitrolife, Sweden). Oocyte denudation was performed with 80 IU of hyaluronidase, (Sigma, USA) (17). Immediately after oocyte denudation, cumulus cells were washed with phosphate-buffered saline (PBS) and we added RNA protect, after which the cells were snap frozen in liquid nitrogen and

stored at -80°C until RNA extraction. Cumulus cells were collected from metaphase II oocytes (MII). MII oocytes were fertilized by ICSI within 10 minutes after denudation, and then incubated until transfer. The regular fertilization rate was controlled (16-20 hours after ICSI). Based on our laboratory standards, embryos were graded at the pronuclear (16-20 hours) and cleavage (48-72 hours) stages (18, 19). We selected 1-2 embryos for transfer based on the embryos' grades, patient age, and previous assisted reproductive technology (ART) cycles.

Purification and preparation of RNA

Total RNA was extracted by a Pico Pure RNA Isolation Kit (Arcturus, USA) and treated with RNase-free DNase I according to the manufacturer's instructions. RNA concentration and purity were quantified using a Nanodrop 2000 Spectrophotometer (Thermo, USA).

Quantitative real-time PCR array

We preamplified 50 ng of total RNA using the RT² PreAMP cDNA Synthesis Kit (Qiagen, USA) in a 12-cycle multiplex PCR for all genes of interest. We examined the same set of genes in the 3 study groups. Quantitative real-time PCR array (qPCR-array) was performed using the Human Extracellular Matrix & Adhesion Molecules RT² Profiler PCR Array (Qiagen, USA). These SYBR Green-based arrays were designed as one sample/one 96-well plate using primers for a preset list of genes that included 84 ECM and adhesion molecule genes in addition to 12 control wells. Only experiments that passed the PCR array run quality control were included in the data analyses. Briefly, cDNA volumes were adjusted to 2.5 ml with RT² Real-Time SYBR Green/ROX PCR Master Mix (Qiagen, USA). A total of 25 μL cDNA mix was added to all wells. Real-time PCR was performed in a StepOnePlus™ instrument (Applied Biosystems, USA).

Bioinformatics and statistical analysis

Relative gene expressions were calculated by the $2^{-\Delta\Delta\text{Ct}}$ method. Ct indicated the cycle threshold, the fractional cycle number where the fluorescent signal reached the detection threshold. The normalized ΔCt value of each sample was calculated using reference genes with a Ct variation less than one among all experiments. Reference genes included beta-2 microglobulin (*B2M*); ribosomal protein, large, P0 (*RPLP0*); hypoxanthine phosphoribosyltransferase 1 (*HPRT1*); actin, beta (*ACTB*); and glyceraldehyde 3-phosphate dehydrogenase (*GAPDH*). The statistical significance of differentially expressed genes (DEG) was measured by the two-tailed t test. Two-sided $P < 0.05$ were considered significant.

Visualization of the biological function network of DEG was performed using a search tool for the retrieval of interacting genes/proteins (STRING; <http://string-db.org/>), an online functional protein interaction network.

Web-based RT² Profiler PCR Array data analysis software was used for gene expression. Also, clinical parameters were analyzed generalized linear model (GLM) procedure.

Multiple comparisons were implemented using LSMEANS statement. All analyses were conducted in SAS version 9.4 (SAS Institute Inc., Cary, NC, USA). Differences at $P \leq 0.05$ and $0.05 < P < 0.10$ were considered statistically significant and tended to be statistically significant, respectively.

Results

Clinical parameters including age, LH/FSH ratio, body mass index (BMI), and concentration of fasting blood glucose did not significantly differ among the three groups ($P > 0.05$). Duration of infertility tended to be longer in IR patients as compared with the control group ($P = 0.097$); however, it was not different considering other comparisons ($P > 0.05$). LH concentration tended to be higher in IS patients than the control group ($P = 0.079$), but it did not differ between other groups ($P > 0.05$).

The number of follicles and oocytes collected per patient did not significantly differ between groups ($P > 0.05$). Number of MII oocytes was greater in the control group compared with IS ($P = 0.015$) and IR ($P = 0.048$) groups. However, number of MII oocytes was not different between IS and IR groups ($P > 0.05$). There was no difference in the fertilization rate of oocytes among the three groups. Both the IR and IS groups had significantly lower numbers of good quality cleavage stage embryos compared to the control group ($P < 0.01$). The number of transferred embryos did not differ between groups ($P > 0.05$, Tables 1, 2).

We analyzed the expression profiles of 84 genes related to the ECM protein and adhesion molecule pathway. Of the five reference genes, *B2M*, *RPLP0* and *HPRT1*, with a Ct variation less than one among all experiments, were chosen for normalization. Table 3 shows the fold differences for DEG among the groups ($P < 0.05$). In the IS group, ADAM metalloproteinase with thrombospondin type 1 motif, 8 (*ADAMTS8*) and neural cell adhesion molecule 1 (*NCAM1*) upregulated whereas integrin, alpha 2 (*ITGA2*); collagen, type I, alpha 1 (*COL1A1*); fibronectin 1 (*FNI*); integrin, alpha 7 (*ITGA7*); and matrix metalloproteinase 2 (*MMP2*) downregulated compared to the control group. Extracellular matrix protein 1 (*ECM1*) and integrin, alpha 5 (*ITGA5*) downregulated in the IR group compared to the control group ($P = 0.030$ and $P = 0.052$, respectively). A comparison of the IR group with the IS group showed downregulation of catenin (cadherin-associated protein), beta 1 (*CTNNB1*); catenin (cadherin-associated protein), delta 1 (*CTNND1*); intercellular adhesion molecule 1 (*ICAM1*); Kallmann syndrome 1 sequence (*KALI*); laminin, alpha 1 (*LAMA1*); laminin, alpha 2 (*LAMA2*); *VCAN*, and vitronectin (*VTN*) along with upregulation of *ITGA2*. Comparison between all PCOS patients to controls showed downregulation of *ECM1*; catenin (cadherin-associated protein), alpha 1 (*CTNNA1*); *ITGA5*; laminin, alpha 3 (*LAMA3*); laminin, beta 1 (*LAMB1*); *FNI*; and *ITGA7*. Figure 1 shows the network of the respective proteins of DEG. Although this figure does not show a mechanism behind our observation, it shows interactions among these genes. Hence, they are not isolated, independent genes; rather, their produced proteins might cooperate as a cluster.

Table 1: Clinical parameters for control and PCOS patients

Patients (n)	Control group	IR group	IS group	P value
	n=8	n=7	n=8	
Age (Y)	30.29 ± 2.15	27.75 ± 1.37	26.25 ± 1.13	NS
Duration of infertility (Y)	3.14 ± 1.23	6.75 ± 1.25	5.31 ± 0.96	NS
BMI (kg/m ²)	23.60 ± 1.47	27.61 ± 1.04	27.18 ± 1.98	NS
FSH (U/L)	5.37 ± 0.59	7.55 ± 1.56	6.51 ± 0.75	NS
LH (U/L)	5.10 ± 0.59	6.19 ± 0.7	8.12 ± 1.24	NS
LH/FSH	1.14 ± 0.32	1.07 ± 0.26	1.27 ± 0.17	NS
Fasting glucose (mg/dl)	93.14 ± 2.87	91.75 ± 1.42	93.38 ± 3.56	NS

Variables are presented as Mean ± SE. P values determined by analyzed generalized linear model (GLM) procedure with significance level of P<0.05. PCOS; Polycystic ovary syndrome, BMI; Body mass index, FSH; Follicle-stimulating hormone, LH; Luteinizing hormone, IS; Insulin sensitive, IR; Insulin resistant, and NS; Not significant.

Table 2: Cycle characteristics and IVF/ICSI outcomes in controls compared to PCOS patients

Variables	Control group	IR group	IS group	P value
	n=8	n=7	n=8	
Number of follicles	14.14 ± 1.55	18.25 ± 1.67	14.75 ± 2.30	NS
Number of oocytes retrieved	16.43 ± 1.45	13.00 ± 1.68	12.38 ± 1.92	NS
Number of MII oocytes	15.43 ± 1.23 ^a	10.88 ± 1.27 ^b	9.88 ± 1.22 ^c	a, b=0.048 a, c=0.015
Regular fertilization rate, % (# of 2PN/# MII oocytes)	72 (78/108)	69 (54/78)	68 (54/79)	NS
Total embryos	10.14 ± 0.86	7.25 ± 1.25	8.00 ± 1.18	NS
Number of good quality embryos	5.14 ± 0.83 ^a	2.00 ± 0.78 ^b	1.62 ± 0.60 ^c	a, b=0.016 a, c=0.005
Number of ET	1.00 ± 0.49	1.75 ± 0.53	1.13 ± 0.44	NS

Variables are presented as Mean ± SE. P values determined with significance level of P<0.05. PCOS; Polycystic ovary syndrome, IVF; *In vitro* fertilization, ICSI; Intracytoplasmic sperm injection, IS; Insulin sensitive, IR; Insulin resistant, MII; Metaphase II oocytes, NS; Not significant, 2PN; Two pronuclei, ET; Embryos transferred, ^{a, b, c}; Statistically significant differences between IR patients vs. controls, and ^{a, c}; Statistically significant differences between IS patients vs. controls.

Table 3: Differentially expressed gene fold differences among groups

Gene symbols	IS vs. control	IR vs. control	IR vs. IS	PCOS vs. control	P value
<i>ADAMTS8</i>	3.32 ^a	0.63	2.26	2.77	a=0.031*
<i>COL1A1</i>	0.43 ^a	2.21	0.94	0.62	a=0.020*
<i>CTNNA1</i>	0.60	0.98	0.58	0.59 ^d	d=0.022*
<i>CTNNB1</i>	3.78	1.18	0.31 ^c	2.19	c=0.013*
<i>CTNND1</i>	1.78	0.73	0.41 ^c	1.18	c=0.028*
<i>ECM1</i>	0.66 ^a	0.49 ^b	0.73	0.57 ^d	a=0.052 [†] b=0.030* d=0.011*
<i>FNI</i>	0.51 ^a	0.65	1.27	0.57 ^d	a=0.004** d=0.012*
<i>ICAM1</i>	1.94	0.78	0.4 ^c	1.27	c=0.011*
<i>ITGA2</i>	0.54 ^a	0.88	1.64 ^c	0.68	a=0.020* c=0.042*
<i>ITGA5</i>	0.63	0.58 ^b	0.92	0.61 ^d	b=0.052 [†] d=0.033*
<i>ITGA7</i>	0.45 ^a	0.51	1.14	0.47 ^d	a=0.046* d=0.017*
<i>KALI</i>	2.09	1.21	0.58 ^c	1.62	c=0.002**
<i>LAMA1</i>	3.96	1.13	0.28 ^c	2.20	c=0.028*
<i>LAMA2</i>	2.19	0.86	0.39 ^c	1.42	c=0.018*
<i>LAMA3</i>	0.68	0.52 ^b	0.76	0.6 ^d	b=0.059 [†] d=0.022*
<i>LAMB1</i>	0.67	0.60	0.90	0.64 ^d	d=0.020*
<i>MMP2</i>	0.40 ^a	1.69	4.21	0.79	a=0.037*
<i>NCAM1</i>	2.72 ^a	1.64	0.60	2.15	a=0.049*
<i>THBS3</i>	0.48 ^a	0.77	1.60	0.60	a=0.039*
<i>VCAN</i>	3.50	1.01	0.29 ^c	1.96	c=0.030*
<i>VTN</i>	2.29	1.26	0.55 ^c	1.73	c=0.037*

The statistical significance of differentially expressed genes (DEG) was measured by the two-tailed t test.

IS; Insulin sensitive, IR; Insulin resistant, PCOS; Polycystic ovary syndrome, *; P<0.05, **; P<0.01, †; statistically marginal difference 0.05<P<0.06. Last column represents P value of comparison between groups, ^a; IS vs. control, ^b; IR vs. control, ^c; IR vs. IS, and ^d; PCOS vs. control.

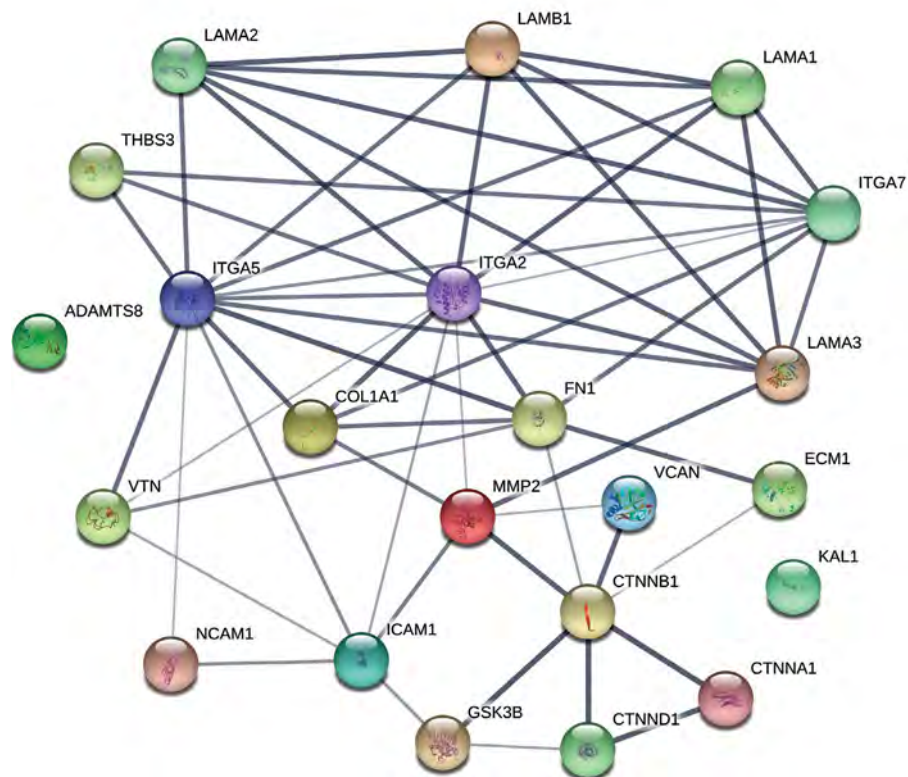


Fig.1: Protein-protein interaction network of respective proteins to differentially expressed genes (DEG) in cumulus cells from among the groups. Thicknesses of interactions show confidence levels according to the STRING database.

Discussion

In terms of *in vitro* fertilization (IVF)/ICSI outcome, the present study showed that IR might be associated with low oocyte maturity in infertile PCOS women, but this did not affect the regular fertilization rate of oocytes between the 3 groups. According to our data, both the IR and IS groups had significantly lower numbers of good quality embryos compared to the control group.

The expression pattern of cumulus cells of infertile PCOS patients in an IVF program was studied and compared based on their insulin sensitivity. Differences arise in the expression of genes involved in the composition and regulation of COC ECM. We highlighted the association of ECM and cell adhesion molecule gene alterations in order to understand the etiology of PCOS as a genetically complex disorder. The importance of cumulus cells in the control of oocyte metabolism has been reported (20). Malfunction of these cells might have a role in PCOS pathogenesis (21).

Since the report on insulin hypersecretion by Burghen et al. (22), this disorder has been reported consistently in women with PCOS. There are molecular mechanisms that can elucidate insulin resistance in PCOS patients. It seems that a major contributor to insulin resistance in PCOS patients is a reduction in insulin sensitivity secondary to a defect in insulin signaling (23). Recent *in vitro* studies have revealed differential insulin signaling in human luteinized granulosa cells of PCOS patients with

and without insulin resistance (24). According to recent studies, comparison of PCOS patients with controls has shown differential expression of ECM related genes. The studied DEGs associated with O- and N-glycosylation, which is important in ECM components gathering; these mechanisms highlight the key role of ECM components during folliculogenesis (25). Differential expression of ECM and cell adhesion molecules genes were identified in IR versus IS PCOS patients. It seemed that dysregulation of ECM components could associate with defective oocyte maturation, as well as a decrease in embryo quality, even after IVF treatment.

Among DEG detected in this study, an association with some genes had previously been reported with PCOS, such as *ADAMTS8*; integrin, beta 2 (*ITGB2*); *CTNNB1*; and cadherin 1 (*CDH1*) (26, 27).

In the present study, we have observed downregulation of *CTNNB1* and *CTNND1* in IR PCOS patients compared to IS PCOS patients. *CTNNB1*, is a key effector of the canonical Wnt/frizzled (FZD) pathway. *CTNNB1* not only mediates cell-cell adhesion, but also acts as a transcription factor. In the latter context, *CTNNB1* protein is phosphorylated and subsequently degraded by a large multi-protein complex that includes glycogen synthase kinase 3 beta (*GSK3 β*) (28). Microarray analysis of PCOS ovaries compared to normal ovaries have shown downregulation of genes

that encode for components of Wnt signaling (27). In animal studies, disruption of *CTNNB1* expression in granulosa cells is predictive of major changes in granulosa cell performance (29).

We observed downregulation of *VCAN* in IR versus IS patients, which agreed with a recent study that has highlighted a possible role for *VCAN* in ovulatory dysfunction of PCOS patients (30). *VCAN* is one of the markers of oocyte developmental competence. According to Gebhardt et al. (31), cumulus cells separated from oocytes that led to live birth had significantly elevated *VCAN* expression.

Expression of the *KALI* gene decreased significantly in IR versus IS patients. A recent study highlighted the role of *KALI* as one of the ECM components in oocyte maturation (32). In our study, downregulation of *KALI* in IR versus IS patients interfered with normal oocyte maturation.

We observed downregulation of *MMP2* in the IS group compared to the control group. Curry and Osteen (33) proposed that the MMP system might regulate normal follicular maturation and atresia in order to attain the appropriate number of ovulatory follicles. Recent studies showed that *MMP2* highly expressed during ovulation (34); therefore, downregulation of this gene in PCOS patients could affect normal ovulation.

Insulin resistance can lead to structural alterations in the basal lamina of the insulin-responsive organs. Under the influence of insulin resistance, ovulation mechanisms in the ovaries are impaired and hyperinsulinemia is present prior to anovulation (6, 24). Cumulus cells organize the ECM structure prior to ovulation and provide a microenvironment essential for normal fertilization. In this regard, ECM components play a critical role in reproductive performance (15). An abnormal turnover of ovarian ECM components has been considered in PCOS patients in a previous report (35). Of the altered genes, downregulation of *COL1A1* and *FNI* in IS patients in addition to *LAMA1* and *LAMA2* in IR versus IS patients was not previously reported. To the best of our knowledge, the current study was the first real time based simultaneous analysis of more than 80 ECM and cell adhesion genes as a more reliable technique compared to microarrays.

ECMI is a secretory glycoprotein which regulates cell proliferation and invasion by an increase in glucose transporter (GLUT) expression (36). In this study, we found that the *ECMI* gene downregulated in the IR group. Since glucose is necessary for oocyte maturation, *ECMI* downregulation could reflect the role of IR in antral follicle arrest in PCOS patients.

Integrin (ITG) families are heterodimeric integral membrane proteins composed of an alpha subunit and a beta subunit that function in cell surface adhesion and signaling (37). According to the results by Liu et al. (38), the ITG gene family downregulated in PCOS cumulus

cells compared with a control group. Due to the importance of ITG genes in cell adhesion, they suggested that the communication of oocyte and its neighboring cumulus cells in PCOS patients might be disrupted. According to our data, *ITGA5* and *ITGA7* downregulated in PCOS patients compared to the control group. *ITGA7* functions as receptor for the basement membrane protein laminin-1. *ITGA5* is known as a fibronectin receptor. Recent studies have shown that alterations of some genes are associated with oocyte nuclear maturation in PCOS (39). Cell-matrix adhesion molecules such as ITG family are important in this process.

Conclusion

Downregulation of ECM and cell adhesion molecule genes in cumulus cells of infertile PCOS women with and without insulin resistance can have an association with decreased numbers of mature oocytes and good quality embryos.

Acknowledgments

This study was funded by Royan Institute (code number: 91000396). The authors wish to thank Forough Azam Sayahpour, Kim Vagharfard, and Dr. Gopal Lakshmi and Dr. Vahid Akbarinejad for their assistance and editing the manuscript. We express our appreciation to the staff of the Embryology Laboratory at Royan Institute for their assistance in isolating cumulus cell samples. The author(s) declared no potential conflicts of interest with respect to the research, authorship, and publication of this article.

Authors' Contributions

F.H., S.O., P.E.-Y., M.B., A.M.; Contributed to manuscript drafting and revising. F.H., S.O., P.E.-Y., M.B., A.M.; Collected the data. F.H., P.E.-Y., N.N.; Assisted in the study design. M.B., A.S.-Z.; Performed the statistical analyses. All authors read and approved the final version of the manuscript.

References

1. Wiser A, Shehata F, Holzer H, Hyman JH, Shalom-Paz E, Son WY, et al. Effect of high LH/FSH ratio on women with polycystic ovary syndrome undergoing in vitro maturation treatment. *J Reprod Med*. 2013; 58(5-6): 219-223.
2. Rotterdam ESHRE/ASRM-Sponsored PCOS Consensus Workshop Group. Revised 2003 consensus on diagnostic criteria and long-term health risks related to polycystic ovary syndrome. *Fertil Steril*. 2004; 81(1): 19-25.
3. Qiao J, Feng HL. Extra- and intra-ovarian factors in polycystic ovary syndrome: impact on oocyte maturation and embryo developmental competence. *Hum Reprod Update*. 2011; 17(1): 17-33.
4. Franks S, Mason H, Willis D. Follicular dynamics in the polycystic ovary syndrome. *Mol Cell Endocrinol*. 2000; 163(1-2): 49-52.
5. Dunaif A. Insulin resistance in women with polycystic ovary syndrome. *Fertil Steril*. 2006; 86 Suppl 1: S13-S14.
6. Holte J. Disturbances in insulin secretion and sensitivity in women with the polycystic ovary syndrome. *Baillieres Clin Endocrinol Metab*. 1996; 10(2): 221-247.
7. Niu Z, Lin N, Gu R, Sun Y, Feng Y. Associations between insulin resistance, free fatty acids, and oocyte quality in polycystic ovary syndrome during in vitro fertilization. *J Clin Endocrinol Metab*. 2014; 99(11): E2269-E2276.
8. Vlaisavljević V, Kovac V, Sajko MC. Impact of insulin resistance on

- the developmental potential of immature oocytes retrieved from human chorionic gonadotropin-primed women with polycystic ovary syndrome undergoing in vitro maturation. *Fertil Steril*. 2009; 91(3): 957-959.
9. Knight PG, Glister C. Local roles of TGF-beta superfamily members in the control of ovarian follicle development. *Anim Reprod Sci*. 2003; 78(3-4): 165-183.
 10. Cecconi S, Ciccarelli C, Barberi M, Macchiarelli G, Canipari R. Granulosa cell-oocyte interactions. *Eur J Obstet Gynecol Reprod Biol*. 2004; 115 Suppl 1: S19-S22.
 11. Christensen AP, Patel SH, Grasa P, Christian HC, Williams SA. Oocyte glycoproteins regulate the form and function of the follicle basal lamina and theca cells. *Dev Biol*. 2015; 401(2): 287-298.
 12. Rodgers RJ, Irving-Rodgers HF, Russell DL. Extracellular matrix of the developing ovarian follicle. *Reproduction*. 2003; 126(4): 415-424.
 13. Heeren AM, van Iperen L, Klootwijk DB, de Melo Bernardo A, Roost MS, Gomes Fernandes MM, et al. Development of the follicular basement membrane during human gametogenesis and early folliculogenesis. *BMC Dev Biol*. 2015; 15: 4.
 14. Uyar A, Torrealday S, Seli E. Cumulus and granulosa cell markers of oocyte and embryo quality. *Fertil Steril*. 2013; 99(4): 979-997.
 15. Russell DL, Robker RL. Molecular mechanisms of ovulation: coordination through the cumulus complex. *Hum Reprod Update*. 2007; 13(3): 289-312.
 16. Ma F, Qiao L, Yue H, Xie S, Zhou X, Jiang M, Zhang W, Qi J, Wang L, Xu K. Homeostasis model assessment-insulin resistance (HOMA-IR), a key role for assessing the ovulation function in polycystic ovary syndrome (PCOS) patients with insulin resistance. *Endocr J*. 2008; 55(5): 943-945.
 17. Wissing ML, Sonne SB, Westergaard D, Nguyen KD, Belling K, Høst T, et al. The transcriptome of corona radiata cells from individual MII oocytes that after ICSI developed to embryos selected for transfer: PCOS women compared to healthy women. *J Ovarian Res*. 2014; 7: 110.
 18. Eftekhari-Yazdi P, Valojerdi MR, Ashtiani SK, Eslamnejad MB, Karimian L. Effect of fragment removal on blastocyst formation and quality of human embryos. *Reprod Biomed Online*. 2006; 13(6): 823-832.
 19. Valojerdi MR, Karimian L, Yazdi PE, Gilani MA, Madani T, Baghestani AR. Efficacy of a human embryo transfer medium: a prospective, randomized clinical trial study. *J Assist Reprod Genet*. 2006; 23(5): 207-212.
 20. Downs SM. The influence of glucose, cumulus cells, and metabolic coupling on ATP levels and meiotic control in isolated mouse oocyte. *Dev Biol*. 1995; 167(2): 502-512.
 21. Haouzi D, Assou S, Monzo C, Vincens C, Dechaud H, Hamamah S. Altered gene expression profile in cumulus cells of mature MII oocytes from patients with polycystic ovary syndrome. *Hum Reprod*. 2012; 27(12): 3523-3530.
 22. Burghen GA, Givens JR, Kitabchi AE. Correlation of hyperandrogenism with hyperinsulinism in polycystic ovarian disease. *J Clin Endocrinol Metab*. 1980; 50(1): 113-116.
 23. Dunaif A, Segal KR, Shelley DR, Green G, Dobrjansky A, Licholai T. Evidence for distinctive and intrinsic defects in insulin action in polycystic ovary syndrome. *Diabetes*. 1992; 41(10): 1257-1266.
 24. Belani M, Deo A, Shah P, Banker M, Singal P, Gupta S. Differential insulin and steroidogenic signaling in insulin resistant and non-insulin resistant human luteinized granulosa cells—a study in PCOS patients. *J Steroid Biochem Mol Biol*. 2018; 178: 283-292.
 25. Kenigsberg S, Bentov Y, Chalifa-Caspi V, Potashnik G, Ofir R, Birk OS. Gene expression microarray profiles of cumulus cells in lean and overweight obese polycystic ovary syndrome patients. *Mol Hum Reprod*. 2009; 15(2): 89-103.
 26. Lan CW, Chen MJ, Tai KY, Yu DC, Yang YC, Jan PS, et al. Functional microarray analysis of differentially expressed genes in granulosa cells from women with polycystic ovary syndrome related to MAPK/ERK signaling. *Sci Rep*. 2015; 5: 14994.
 27. Kaur S, Archer KJ, Devi MG, Kriplani A, Strauss JF 3rd, Singh R. Differential gene expression in granulosa cells from polycystic ovary syndrome patients with and without insulin resistance: identification of susceptibility gene sets through network analysis. *J Clin Endocrinol Metab*. 2012; 97(10): E2016-E2021.
 28. Jansen E, Laven JS, Dommerholt HB, Polman J, van Rijt C, van den Hurk C, et al. Abnormal gene expression profiles in human ovaries from polycystic ovary syndrome patients. *Mol Endocrinol*. 2004; 18(12): 3050-3063.
 29. Fan HY, O'Connor A, Shitanaka M, Shimada M, Liu Z, Richards JS. Beta-catenin (CTNNB1) promotes preovulatory follicular development but represses LH-mediated ovulation and luteinization. *Mol Endocrinol*. 2010; 24(8): 1529-1542.
 30. Özler S, Öztaş E, Tokmak A, Ergin M, Kuru Pekcan M, Gümüş Güler B, et al. Role of Versican and ADAMTS-1 in polycystic ovary syndrome. *J Clin Res Pediatr Endocrinol*. 2017; 9(1): 24-30.
 31. Gebhardt KM, Feil DK, Dunning KR, Lane M, Russell DL. Human cumulus cell gene expression as a biomarker of pregnancy outcome after single embryo transfer. *Fertil Steril*. 2011; 96(1): 47-52. e2.
 32. Virant-Klun I, Leicht S, Hughes C, Krijgsveld J. Identification of maturation-specific proteins by single-cell proteomics of human oocytes. *Mol Cell Proteomics*. 2016; 15(8): 2616-2627.
 33. Curry TE Jr, Osteen KG. Cyclic changes in the matrix metalloproteinase system in the ovary and uterus. *Biol Reprod*. 2001; 64(5): 1285-1296.
 34. Vos MC, van der Wurff AA, Last JT, de Boed EA, Smeenk JM, van Kuppevelt TH, et al. Immunohistochemical expression of MMP-14 and MMP-2, and MMP-2 activity during human ovarian follicular development. *Reprod Biol Endocrinol*. 2014; 12: 12.
 35. Oksjoki S, Söderström M, Inki P, Vuorio E, Anttila L. Molecular profiling of polycystic ovaries for markers of cell invasion and matrix turnover. *Fertil Steril*. 2005; 83(4): 937-944.
 36. Lee KM, Nam K, Oh S, Lim J, Lee T, Shin I. ECM1 promotes the Warburg effect through EGF-mediated activation of PKM2. *Cell Signal*. 2015; 27(2): 228-235.
 37. Skubitz AP. Adhesion molecules. *Cancer Treat Res*. 2002; 107: 305-329.
 38. Liu Q, Li Y, Feng Y, Liu C, Ma J, Li Y, et al. Single-cell analysis of differences in transcriptomic profiles of oocytes and cumulus cells at GV, MI, MII stages from PCOS patients. *Sci Rep*. 2016; 6: 39638.
 39. Huang X, Hao C, Shen X, Zhang Y, Liu X. RUNX2, GPX3 and PTX3 gene expression profiling in cumulus cells are reflective oocyte/embryo competence and potentially reliable predictors of embryo developmental competence in PCOS patients. *Reprod Biol Endocrinol*. 2013; 11: 109.

Detection of Mycoplasma Contamination of Cell Culture by A Loop-Mediated Isothermal Amplification Method

Zohre Soheily, M.Sc.¹, Mohammad Soleimani, Ph.D.^{1,2*}, Keivan Majidzadeh-Ardebili, M.D., M.PH., Ph.D.^{3,4}

1. Department of Microbiology, Qom Branch, Islamic Azad University, Qom, Iran

2. Department of Microbiology, Faculty of Medicine, AJA University of Medical Sciences, Tehran, Iran

3. Tasnim Biotechnology Research Center (TBRC), Faculty of Medicine, AJA University of Medical Sciences, Tehran, Iran

4. Motamed Cancer Institute, ACECR, Tehran, Iran

*Corresponding Address: P.O.Box: 14185611, Department of Microbiology, Faculty of Medicine, AJA University of Medical Sciences, Tehran, Iran

Email: soleimanidor@yahoo.com

Received: 27/Nov/2017, Accepted: 12/May/2018

Abstract

Objective: Mycoplasmas are major contaminants of cell culture and affect *in vitro* biological and diagnostic tests. Mycoplasma detection is conducted using culture and molecular methods. These methods vary in terms of accuracy, reliability and sensitivity. Loop-mediated isothermal amplification (LAMP) is used to amplify target DNA in a highly specific and rapid manner. This study aimed to develop a LAMP method for rapid detection of Mycoplasma in culture samples.

Materials and Methods: In this descriptive laboratory study, for LAMP detection of Mycoplasma contaminations in cell culture, we used primers specifically designed for targeting the 16S rRNA conserved gene of *Mycoplasma* spp. For a positive control structure, 16S rRNA amplified based on PCR, was cloned in a plasmid vector and sequenced. The assay specificity was evaluated using Mycoplasma genomic DNA and a panel containing genomes of gram-positive and gram-negative organisms.

Results: In this study, the method developed for detection of Mycoplasma contamination of cell cultures was a rapid, sensitive and cost-effective LAMP approach. The results demonstrated that this method benefits from high specificity (100%) for amplification of Mycoplasma strains and high speed (multiplication within 60 minutes), while it does not require expensive laboratory equipment compared to those needed for polymerase chain reaction (PCR)-based detection.

Conclusion: Our study is the first report about application of LAMP assay based on 16S rRNA gene for detection of Mycoplasma strains; this technique could be considered a useful tool for rapid detection of contamination of cell culture.

Keywords: Cell Culture, Loop-Mediated Isothermal Amplification, Mycoplasma, Polymerase Chain Reaction

Cell Journal (Yakhteh), Vol 21, No 1, Apr-Jun (Spring) 2019, Pages: 43-48

Citation: Soheily Z, Soleimani M, Majidzadeh-Ardebili K. Detection of mycoplasma contamination of cell culture by a loop-mediated isothermal amplification method. Cell J. 2019; 21(1): 43-48. doi: 10.22074/cellj.2019.5624.

Introduction

Over the last decades, cell culture has been frequently used as a main research tool in medical and biological experiments (1). Cell culture contaminants can be categorized into chemical and biological contaminants. Impurities in media, and sera, endotoxins, and detergents are major chemical contaminants, and bacteria, molds, yeasts, viruses, mycoplasma, and cross contamination of other cell lines, are regarded as biological contaminants (2). Mycoplasma contamination is a serious concern that exists when using cell culture (3, 4). The primary starting material, glassware or apparatus, culture reagents (mainly fetal bovine serum), laboratory staff and cross-contamination of infected cultures are examples of Mycoplasma contamination sources (5, 6). The prevalence of Mycoplasma contamination of cell cultures has been estimated to range from 5 to 35% (7, 8) while prevalence of cell culture infections with two or more *Mycoplasma* species are between 7 and 60% (1). Mycoplasma infection affects different aspects of the infected cell culture, resulting in obtaining spurious experimental data (5, 9). Mycoplasmas are the smallest free-living microorganisms which are characterized by their round or filamentous shape, absence of a rigid cell wall and a DNA genome in

the Mb range (4, 7, 10). Most of *Mycoplasma* species are not pathogenic (7); however, *Mycoplasma pneumoniae* is a human pathogen (11). The species that are frequently found in cell culture are *Acholeplasma laidlawii*, *Mycoplasma arginini*, *Mycoplasma fermentans*, *Mycoplasma hominis*, *Mycoplasma hyorhinis*, and *Mycoplasma orale* (12).

Several methods have been developed for detection of *Mycoplasma* spp. (13) including microbiological cultivation, biochemical assays, ELISA, direct or indirect fluorescent staining, immunofluorescence and nucleic acid amplification techniques [direct or nested polymerase chain reaction (PCR)] (7, 9). Isolation on selective microbiological growth media has been regarded as the reference method as well the 'gold standard' assay, for a long period of time (14). Unfortunately, routine diagnosis procedures are usually time-consuming (i.e. several weeks are required to achieve results) and need high-level technical skills and expert personnel. Thus, fast and sensitive detection methods are needed to evaluate putative contaminated cell cultures. In this regard, newer test systems developed based on molecular biological methods, in particular PCR, which give results within 4.5-24 hours are commonly used by cell culture laboratories

(15). However, complicated procedures and relatively costly machinery required for PCR and electrophoresis processes have restricted its use (16, 17). Therefore, development of simple, sensitive, specific, rapid and low-cost detection methods is of crucial importance (11).

Loop-mediated isothermal amplification (LAMP) assay is a novel gene amplification technique which uses 4-6 primers that recognize specific regions on the target DNA. The LAMP reaction is carried out under isothermal conditions (60-65°C), thereby obviating the need for a thermal cycler (18, 19). This method amplifies specific sequences of DNA in a shorter period of time compared to PCR with high specificity and efficiency but no need for a special reagent (17). Moreover, the LAMP reaction's product can be detected in real time by turbidity monitoring, which the turbidity is correlated with the production of magnesium pyrophosphate (20), or optical monitoring of a fluorescent intercalating dye by naked eyes (21). Therefore, it can be used for a rapid detection of various infectious diseases (18, 22).

The aim of this study was to design and develop a reliable, rapid and specific LAMP assay based on the conserved section of 16S rRNA gene for detection of Mycoplasma contamination of cell cultures. To the best of our knowledge, this is the first report on application of this method for detection of *Mycoplasma* contamination in cell cultures based on 16S rRNA gene.

Materials and Methods

Primer design

Initially, 16S rRNA sequences of *Mycoplasma* spp. were retrieved from GenBank (<http://www.ncbi.nlm.nih.gov/genbank/>). These sequences were selected from 12 *Mycoplasma hominis*, 8 *Mycoplasma hyorhinitis*, 3 *Mycoplasma salivarium*, 3 *Mycoplasma orale*, 3 *Acholeplasma laidlawii*, 1 *Mycoplasma arginine*, 5 *Mycoplasma fermentans*, and 5 *Spiroplasma*. The sequences were aligned using CLC Sequence Viewer 6.4 (CLC bio, Aarhus, Denmark). Then, a set of six Mycoplasma-specific LAMP primers containing outer primers (F3-Myco and B3-Myco primers), inner primers (FIP-Myco and BIP-Myco) and a loop primer (loop-Myco) were designed based on the consensus sequence of the target gene by an online software program (Primer

Explorer V4) from Eiken chemical (<http://primerexplorer.jp/e/>). The theoretical specificity of the designed primers was checked by an in-silico analysis using BLAST and Primer-BLAST on NCBI Server (<http://www.blast.ncbi.nlm.nih.gov/>). The LAMP primers were synthesized commercially (Bioneer, Korea) (Table 1).

Cell culture and bacteria and DNA extraction

To perform this descriptive laboratory study, ten cell cultures contaminated with mycoplasmas, some non-contaminated cell culture and a DNA reference standard Mycoplasma were obtained from the Academic Center for Education, Culture and Research of Tehran, Iran. The standard bacteria including *Shigella sonnei* ATCC 9290, enteropathogenic *Escherichia coli* (EPEC) ATCC 43887, *Klebsiella pneumoniae* ATCC 7881, *Bacillus subtilis* ATCC 6051, *Pseudomonas aeruginosa* ATCC 9027, *Staphylococcus aureus* ATCC 25923, *Enterococcus faecalis* ATCC 29212, and *Yersinia enterocolitica* ATCC 23715, were used as negative control in specificity testing. DNA of all cell cultures and standard bacterial species were extracted using the EZ-10 Spin Column Genomic DNA kit (Bio Basic Inc., Ontario, CA) according to the manufacturer's instructions. DNA was quantified spectrophotometrically and then stored at -20°C till used as PCR template DNA and in LAMP assay and specificity tests.

Polymerase chain reaction reactions

Amplification reaction was performed for DNA of contaminated cell cultures, non-contaminated cell cultures, *Mycoplasma* DNA reference and negative control strains in 25 µl volume containing 6 µl of purified DNA, 12.5 µl of 2X reaction mix, 0.5 µM of each F3-Myco and B3-Myco outer primers (Table 1), 1 U of Taq DNA polymerase and 4.5 µl double distilled water. The PCR conditions were as follows: After an initial denaturing step at 94°C for 4 minutes, 35 cycles of the following steps were carried out: denaturation at 94°C for 45 seconds; annealing at 48.1°C for 45 seconds, and extension at 72°C for 45 seconds. Thermal cycling was carried out using an ABI 2720 thermocycler (Applied Biosystems, Warrington, UK). PCR products were separated on 2% agarose gels and compared against 100 bp DNA ladder (Fermentas, Lithuania) as a size marker, under UV gel documentation.

Table 1: Primers for 16S rRNA gene of *Mycoplasma* spp. used in the loop-mediated isothermal amplification and polymerase chain reaction

Primer	Sequence (5'-3')
F3-Myco	GCG ATG GCT AAC TAT GTC CC
B3-Myco	TCG CCT TTG GTG TTC TTC C
FIP-Myco	AGC CTA CGA ACG CTT TAC GCC CAG CCG TAA TAC ATA GG
BIP-Myco	AAC CCT GGC TCG CTT TGG ATA CGC ATT TCA CCG CTT CA
LOOP-Myco	CAA TAA TTC CGG ATA ACG CTT GC

Cloning and preparation of standard plasmid

After PCR amplification of the 16S rRNA gene of *Mycoplasma* using the outer primers, TA cloning of the product was performed. For this purpose, the PCR product was purified using the PCR Purification Kit (Bioneer, Korea). The purified 16S rRNA gene fragment with the length of 219 bp was ligated into pTZ57R/T vector by 1 U of T4 DNA ligase, according to instructions of InsTAclone™ PCR Cloning Kit (Fermentas, Lithuania). Competent cells of *E. coli* Top10 F' were transformed with the ligation reaction product. The transformed cells were incubated at 37°C for 24 hours on Luria-Bertani (Merck, Germany) medium containing 38.4 µg/ml IPTG (isopropyl-beta-D-thiogalactopyranoside, Sigma, St. Louis, MO, USA), 40 µl/ml X-gal (5-bromo-4-chloro-3-indolyl beta D-galactoside, Sigma, Germany), 50 µg/ml nalidixic acid and 100 µg/ml ampicillin (Merck, Germany). Recombinant clones on the medium were identified by blue/white screening and some white colonies containing recombinant vector were chosen for extra evaluation. Then, plasmids of the selected clones were extracted by AccuPrep Plasmid Mini Extraction kit (Bioneer, Korea) and 16S rRNA gene containing recombinant plasmids, were confirmed by PCR with the outer primers and sequencing. The confirmed plasmid was named pTZ57R/T-16S rRNA and quantified using UV absorbance measurement at 260 and 280 nm and further used as positive control in the LAMP assay.

The loop-mediated isothermal amplification assay

The LAMP reaction was conducted for all *Mycoplasma* DNA extracted from cell culture samples in 25 µl reaction mixture containing 12.5 µl 2X reaction mix, 1.5 µl the primer mix (40 pmol of each inner primer and 5 pmol of each outer primer) (Table 1), 8 U of Bst DNA polymerase large fragment (New England Biolabs, Ipswich, MA, USA), 6 µl of template genomic DNA and 5 µl molecular grade water. The mixture was incubated at 63°C for 60 minutes in a Loopamp real-time turbidimeter (LA-320C, Teramecs, Japan), and turbidity of the reaction mix was determined at 650 nm every 6 seconds. Finally, the reaction was terminated by heating to 80°C for 5 minutes in order to denature the Bst DNA polymerase large fragment. The LAMP reactions were examined by Loopamp real-time turbidimeter, electrophoresis of products on 2% agarose gel and direct visual observation to judge turbidity. Cycle sequencing method using F3-Myco and B3-Myco primers, was performed for final confirmation of the amplified products. The sequencing results were checked by BLAST (<http://blast.ncbi.nlm.nih.gov/Blast.cgi>). To determine the optimum temperature that

should be considered for LAMP reactions, the LAMP reactions were also performed at temperatures 60 and 65°C for 60 minutes. In order to assess the effect of the loop primer on amplification speed, 20 pmol of the loop primer (LOOP-Myco) was added to the reaction mixture and LAMP reaction was conducted after 30, 45 and 60 minutes. The negative control tubes (without template DNA) were included in each run.

Specificity and sensitivity of the loop-mediated isothermal amplification assay

For evaluation of the specificity of the test, the LAMP reactions were performed (based on the above-noted protocol) using genomic DNA of *Mycoplasma* spp. and also genomic DNA of non-*Mycoplasma* organisms (negative control bacteria). The reactions were assessed with naked eye inspection and the Loopamp real-time turbidimeter. In addition, electrophoresis on 2% agarose gel was carried out to confirm the results.

Moreover, 10-fold serial dilutions of pTZ57R/T-16S rRNA plasmid (135 ng to 0.135 fg equal 4×10^{10} to ~4 copies) were applied in LAMP experiment to examine the sensitivity of the assay. The results of amplified target sequence were analyzed by using Loopamp real-time turbidimeter, visual observation of turbidity by naked eye and electrophoresis on 2% agarose gel. Finally, sensitivity or detection limit (LOD) of the assay was determined.

Results

Analysis of the polymerase chain reaction products and cloning

The PCR reaction was carried out using F3-Myco and B3-Myco primers on DNA of contaminated cell cultures, non-contaminated cell cultures, *Mycoplasma* DNA reference and negative control strains. PCR products of the tubes containing *Mycoplasma* DNA showed about 219 bp bands on 2% agarose gel. Based on comparison made against 100 bp DNA ladder, no significant difference found in banding pattern compared to the reference *Mycoplasma* strains (Fig.1A). The PCR reaction was specific as it showed exclusive amplification for *Mycoplasma* spp. while this result for 8 non-*Mycoplasma* bacteria species was negative (Fig.1B). Confirmatory test based on the cloning process was conducted by PCR assay with the outer primers (F3 and B3) on the extracted recombinant 16S rRNA-plasmids from white colonies and as expected, a clear and sharp 219 bp band on agarose gel was observed. In addition, the sequence of the amplified 16S rRNA gene was confirmed through direct sequencing, in which the obtained sequences perfectly matched the expected DNA sequences (data not shown).

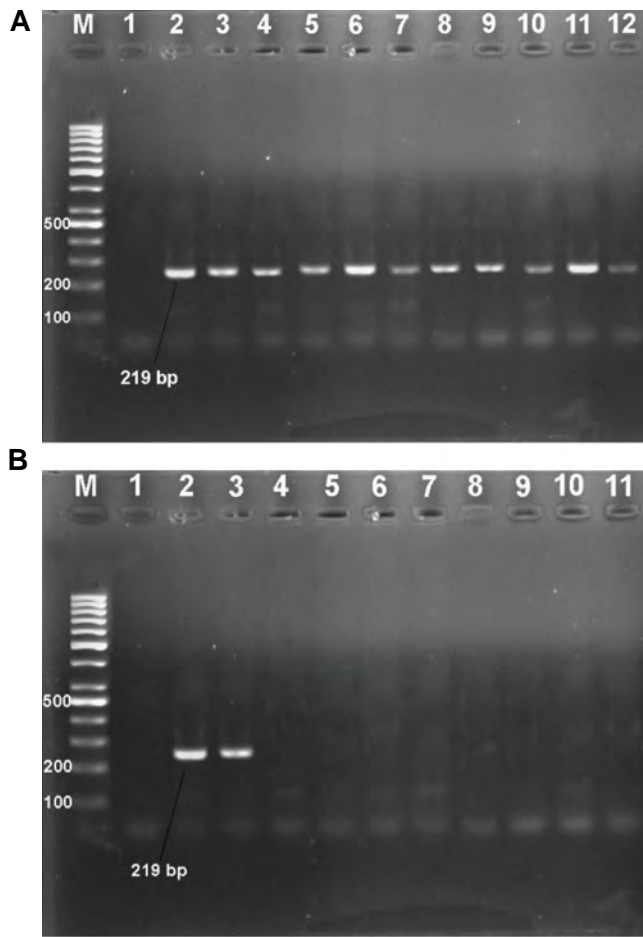


Fig.1: Polymerase chain reaction (PCR) experiments on contaminated cell cultures and negative control samples. **A.** Agarose gel electrophoresis of 16S rRNA PCR products (~ 219 bp) of *Mycoplasma* by using F3-Myco and B3-Myco primers. Lane M; 100 bp DNA ladder, Lane 1; Negative control, Lane 2; Standard Mycoplasma, Lanes 3-12; Positive amplification of contaminated cell cultures and **B.** Specificity of the 16S rRNA Mycoplasma PCR. Lane M; 100 bp DNA ladder, Lane 1; Negative control, Lane 2; Standard Mycoplasma, Lane 3; Contaminated cell culture, Lane 4; *Shigella sonnei* ATCC 9290, Lane 5; *Escherichia coli* ATCC 43887, Lane 6; *Klebsiella pneumoniae* ATCC 7881, Lane 7; *Bacillus subtilis* ATCC 6051, Lane 8; *Pseudomonas aeruginosa* ATCC 9027, Lane 9; *Staphylococcus aureus* ATCC 25923, Lane 10; *Enterococcus faecalis* ATCC 29212, and Lane 11; *Yersinia enterocolitica* ATCC 23715.

Analysis of the loop-mediated isothermal amplification reaction

In the tubes with positive reaction for isothermal amplification, the turbidity (caused by white magnesium pyrophosphate precipitation) was observed with naked eye (Fig.2A). Electrophoresis of the LAMP products on 2% agarose gel showed clear ladder-like DNA amplification (Fig.2B). Amplification graph of the real-time turbidimeter confirmed amplification of the 16s rRNA gene (Fig.2C). The specificity of the LAMP products was verified by cycle sequencing. Comparison of the sequencing results with the 16S rRNA sequences of *Mycoplasma* spp. in Gene bank database confirmed the validity of the products. Amplification was detected at 60, 63, and 65°C, and showed higher levels of amplified DNA at 60°C when compared to other temperatures. Also, effect of the loop primer (LOOP-Myco) on diminution of incubation time was explored. In the reactions without

the loop primer, ideal time for isothermal amplification was 60 minutes while in the reaction containing the loop primer, it was 30 minutes.

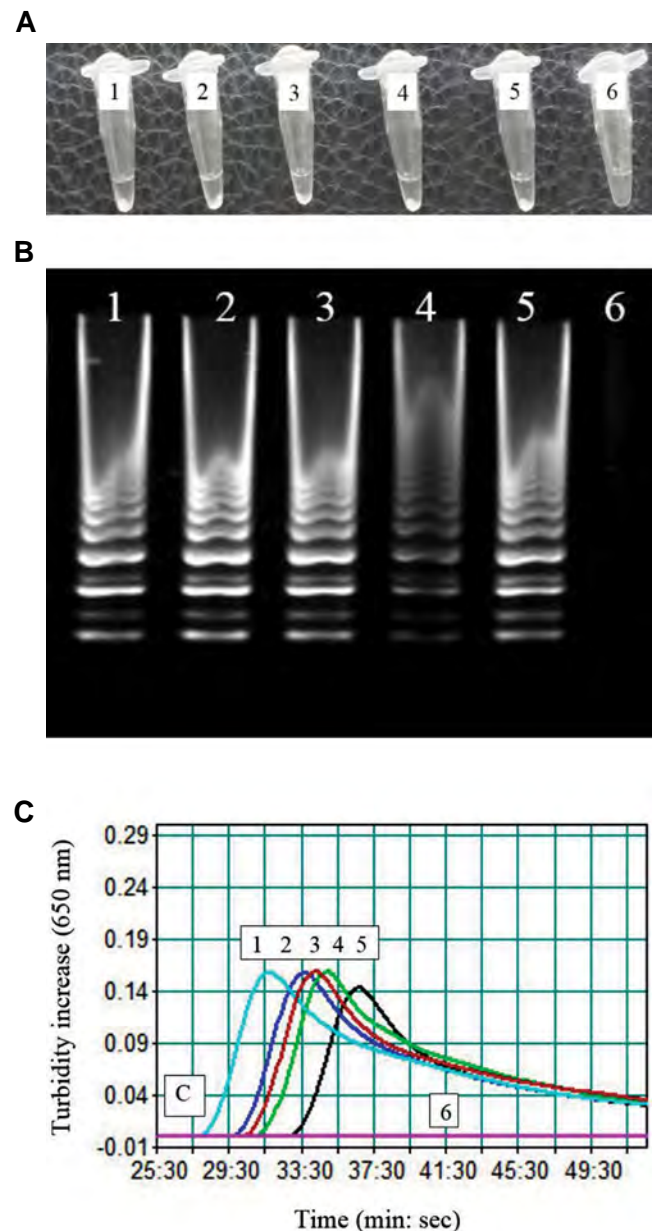


Fig.2: Loop-mediated isothermal amplification (LAMP) experiments on contaminated cell cultures. **A.** Visual appearance of the LAMP reactions. Showing white turbidity, the tubes 1-5 (contaminated cell culture samples) were positive, while the tube 6 was negative, **B.** Electrophoretic analysis of the LAMP products. In lanes 1-5, contaminated cell culture samples showed ladder-like pattern, lane 6 was negative control and had no ladder-like pattern, and **C.** A representative turbidity amplification graph of the LAMP reaction. Curves 1-5 represent contaminated cell cultures and curve 6 is for negative control.

Specificity and sensitivity of the loop-mediated isothermal amplification assay

The LAMP assay was specific because judgment graph of the real-time turbidimeter showed exclusive amplification for *Mycoplasma* spp. while 8 non-*Mycoplasma* bacteria species had negative results. Consistently, *in silico*

analysis using BLAST, indicated that there were no false-positive nor false-negative amplification. In addition, gel agarose electrophoresis of the LAMP products showed the characteristic ladder-like multiple bands only in the tubes containing *Mycoplasma* spp. genome DNA. Inspecting the judgment plot, agarose gel electrophoresis and visual detection of turbidity, the LOD of the assay was found ~4000 copy per reaction tube.

Discussion

Contamination of cell cultures by *Mycoplasma* spp. is a main problem in cell culture for which an accurate diagnostic method is highly required. There are several conventional and molecular diagnostic techniques available for detection of *Mycoplasma* spp. (9, 14). In the last decade, in Iran, several studies established PCR assays using 16S rRNA gene for detection of different species of mycoplasmas such as *M. orale* (23), *Mycoplasma* and *Ureaplasma* species (24), *Mycoplasma* spp. (25-27), in cell culture. The results of these papers demonstrated that 16S rRNA-based PCR could detect all common *Mycoplasma* that contaminate cell cultures. The findings of the current study are in agreement with those reported by Tang et al. (9) which confirmed that 16S rRNA is a suitable target for *Mycoplasma* detection using PCR; however, few cross-reactions were observed with closely related Gram-positive organisms. In addition, Molla Kazemiha et al. (28) showed that real-time PCR and PCR assays developed based on the public sequences in the 16S rRNA, are suitable methods with high sensitivity, specificity and accuracy for detection of mycoplasma contamination of cell cultures. However, these molecular methods are complex and time-consuming and they pose a risk of contamination with ethidium bromide that requires expensive apparatus and qualified laboratory technicians.

As LAMP method has several advantages benefits including no need for a special process, completion of the reaction in a single tube and approval by naked eye contrary to electrophoresis, it can be a suitable alternative for techniques used for *Mycoplasma* detection (29). Another advantage of the LAMP method is the high stability of Bst polymerase enzyme compared to a number of inhibitory factors such as EDTA, bile salts, and NaCl in the amplification reaction (30, 31). These characteristics show that utilization of the LAMP assay in laboratories with limited equipment and in large scale, is valuable. Yoshino et al. (32) showed the same sensitivity and specificity when comparing LAMP assay with a PCR assay, for rapid detection of *M. pneumoniae*. Also, a good global agreement between the LAMP assay and serological results for *M. pneumoniae* detection in pediatric patients, was revealed by Gotoh et al. (11).

Our study defines a rapid, sensitive and cost-effective LAMP method which is comparable to other DNA amplification procedures that are extensively used for identification of various microorganisms in laboratory. Previously, various sequences in the genome of human pathogenic species of *Mycoplasma* were used in the

LAMP assay for detection of different species belonging to this genus, such as *pdhD* gene of *M. genitalium* (21), *mhp165* gene of *M. hyopneumoniae* (17), *uvrC* gene of *Mycoplasma bovis* (33), *p36* gene of *Mycoplasma hyopneumoniae* (34), the SDC1 sequence (M35024) of *Mycoplasma pneumoniae* (11, 32, 35), and P1 adhesin gene of *M. pneumoniae* (36). We used the 16S rRNA gene which is highly conserved in all *Mycoplasma* species and is the best target for genus-level detection of *Mycoplasma* spp. (37). Our finding demonstrated that ideal time and temperature for isothermal amplification was at 60°C in 60 minutes while Davudi-Asl optimized the LAMP test using the large Bst enzyme fragment at 66°C for 1 hour (36).

The primers designed in this study were theoretically completely specific for the 16S rRNA gene of *Mycoplasma*. Therefore, amplification was carried out only with DNA of *Mycoplasma*; also, neither false-positive and false-negative results in the LAMP assay nor any cross-reactivity with other species was observed. In addition, the sequencing results were in accordance with deposited sequence of 16S rRNA in NCBI. These results demonstrated that this technique has high specificity (100%) for the amplification of *Mycoplasma* strains and detected it with high efficiency. It seems that the extremely high specificity of the LAMP method is a result of using four primers that recognize distinct regions on the target sequences (38). Furthermore, using the designed loop primers in the mixture could increase rapidity and efficiency of amplification by attaching to the stem loops formed during reaction process (39). In our study, the LAMP assay was able to detect *Mycoplasma* DNA extracted from culture medium which approves this assay for detection of *Mycoplasma* strains in cell culture samples; with the help of such assays, *Mycoplasma* infection can be discovered at an early stage.

Conclusion

Our study is the first report about designing and developing a LAMP assay based on 16S rRNA gene for determination of *Mycoplasma* strains contaminating cell culture. Based on our findings, LAMP assay developed based on 16S rRNA gene is highly suggested as a useful tool for rapid diagnosis of common *Mycoplasma* which contaminate cell culture.

Acknowledgements

The authors wish to thank the Faculty of Medicine, Islamic Republic of Iran Army University of Medical Sciences for their support and contribution to this study. Also, the authors gratefully acknowledge the financial support provided by of Qom Branch, Islamic Azad University, Iran. There is no conflict of interest in this study.

Authors' Contributions

Z.S.; Participated in all experiments, performed data collection and, statistical analysis, and wrote the

manuscript. M.S.; Is responsible for overall supervision, extensively contributed to data interpretation, drawing conclusions and revised the final version of the manuscript. K.M.-A.; Extensively contributed to data interpretation and drawing conclusions. All authors participated in the finalization of the manuscript and approved the final draft.

References

- Nikfarjam L, Farzaneh P. Prevention and detection of Mycoplasma contamination in cell culture. *Cell J*. 2012; 13(4): 203-212.
- Stacey GN. Cell culture contamination. *Methods Mol Biol*. 2011; 731: 79-91.
- Geraghty RJ, Capes-Davis A, Davis JM, Downward J, Freshney RI, Knezevic I, et al. Guidelines for the use of cell lines in biomedical research. *Br J Cancer*. 2014; 111(6): 1021-1046.
- Razin S, Hayflick L. Highlights of mycoplasma research-an historical perspective. *Biologicals*. 2010; 38(2): 183-190.
- Drexler HG, Uphoff CC. Mycoplasma contamination of cell cultures: Incidence, sources, effects, detection, elimination, prevention. *Cytotechnology*. 2002; 39(2): 75-90.
- Mirjalili A, Parmoor E, Moradi Bidhendi S, Sarkari B. Microbial contamination of cell cultures: a 2 years study. *Biologicals*. 2005; 33(2): 81-85.
- Young L, Sung J, Stacey G, Masters JR. Detection of Mycoplasma in cell cultures. *Nat Protoc*. 2010; 5(5): 929-934.
- Uphoff CC, Denkmann S-A, Drexler HG. Treatment of mycoplasma contamination in cell cultures with Plasmocin. *J Biomed Biotechnol*. 2012; 2012: 267678.
- Tang J, Hu M, Lee S, Roblin R. A polymerase chain reaction based method for detecting Mycoplasma/Acholeplasma contaminants in cell culture. *J Microbiol Methods*. 2000; 39(2): 121-126.
- Degeling MH, Maguire CA, Bovenberg MS, Tannous BA. Sensitive assay for mycoplasma detection in mammalian cell culture. *Anal Chem*. 2012; 84(9): 4227-4232.
- Gotoh K, Nishimura N, Ohshima Y, Arakawa Y, Hosono H, Yamamoto Y, et al. Detection of Mycoplasma pneumoniae by loop-mediated isothermal amplification (LAMP) assay and serology in pediatric community-acquired pneumonia. *J Infect Chemother*. 2012; 18(5): 662-667.
- Clyde Jr W, Senterfit L. Laboratory diagnosis of mycoplasma infections. *Mycoplasma pathogenicity*. 2013: 391.
- Baczynska A, Svenstrup HF, Fedder J, Birkelund S, Christiansen G. Development of real-time PCR for detection of Mycoplasma hominis. *BMC Microbiol*. 2004; 4: 35.
- Jean A, Tardy F, Allatif O, Grosjean I, Blanquier B, Gerlier D. Assessing mycoplasma contamination of cell cultures by qPCR using a set of universal primer pairs targeting a 1.5 kb fragment of 16S rRNA genes. *PLoS One*. 2017; 12(2): e0172358.
- Mariotti E, Mirabelli P, Di Noto R, Fortunato G, Salvatore F. Rapid detection of mycoplasma in continuous cell lines using a selective biochemical test. *Leuk Res*. 2008; 32(2): 323-326.
- Song Q, Wang L, Fang R, Khan MK, Zhou Y, Zhao J. Detection of Mycoplasma wenyonii in cattle and transmission vectors by the loop-mediated isothermal amplification (LAMP) assay. *Trop Anim Health Prod*. 2013; 45(1): 247-250.
- Li J, Minion FC, Petersen AC, Jiang F, Yang S, Guo P, et al. Loop-mediated isothermal amplification for rapid and convenient detection of Mycoplasma hyopneumoniae. *World J Microbiol Biotechnol*. 2013; 29(4): 607-616.
- Notomi T, Mori Y, Tomita N, Kanda H. Loop-mediated isothermal amplification (LAMP): principle, features, and future prospects. *J Microbiol*. 2015; 53(1): 1-5.
- Notomi T, Okayama H, Masubuchi H, Yonekawa T, Watanabe K, Amino N, et al. Loop-mediated isothermal amplification of DNA. *Nucleic Acids Res*. 2000; 28(12): E63.
- Zhang X, Lowe SB, Gooding JJ. Brief review of monitoring methods for loop-mediated isothermal amplification (LAMP). *Biosens Bioelectron*. 2014; 61: 491-499.
- Edwards T, Burke P, Smalley HB, Gillies L, Longhurst D, Vipond B, et al. Loop-mediated isothermal amplification (LAMP) for the rapid detection of Mycoplasma genitalium. *Diagn Microbiol Infect Dis*. 2015; 83(1): 13-17.
- Fu S, Qu G, Guo S, Ma L, Zhang N, Zhang S, et al. Applications of Loop-Mediated Isothermal DNA Amplification. *Appl Biochem Biotechnol*. 2011; 163(7): 845-850.
- Fazli A, Pournakhsh SA, Asli E, Hadadi A. Detection of Mycoplasma orale contamination in cell culture by PCR method. *Iran J Med Microbiol*. 2013; 7(1): 7-14.
- Salari MH, Hafezi R, Khosravipoor H. Study of Mycoplasma and Ureaplasma Species as Contaminants of Cell Cultures. *Iranian J Publ Health*. 2002; 31(3-4): 126-128.
- Ghiasi MS, Shah HMM, Mohajerani HR. The development of a PCR method for mycoplasma testing in cell culture. *New Cellular & Molecular Biotechnology Journal*. 2014; 4(14):41-46 .
- Arabestani MR, Fazeli H, Jedi Tehrani M, Shokri F. The comparison of microbial culture and PCR methods in detection of cell line to mycoplasma. *Journal of Isfahan Medical School*. 2011;28(121): 1676-1683.
- Shahhosseiny MH, Hosseiny Z, Tabarraei B, Akhlaghi F, Shokrgozar MA, Moslemi E. PCR detection of Mycoplasma spp. contamination in cell culture. *Iran J Med Microbiol*. 2008; 2(2): 15-25.
- Molla Kazemiha V, Bonakdar S, Amanzadeh A, Azari S, Memarnejadian A, Shahbazi S, et al. Real-time PCR assay is superior to other methods for the detection of mycoplasma contamination in the cell lines of the National Cell Bank of Iran. *Cytotechnology*. 2016; 68(4): 1063-1080.
- Sidoti F, Bergallo M, Costa C, Cavallo R. Alternative molecular tests for virological diagnosis. *Mol Biotechnol*. 2013; 53(3): 352-362.
- Francois P, Tangomo M, Hibbs J, Bonetti E-J, Boehme CC, Notomi T, et al. Robustness of a loop-mediated isothermal amplification reaction for diagnostic applications. *FEMS Immunol Med Microbiol*. 2011; 62(1): 41-48.
- Liang SY, Chan YH, Hsia KT, Lee JL, Kuo MC, Hwa KY, et al. Development of loop-mediated isothermal amplification assay for detection of Entamoeba histolytica. *J Clin Microbiol*. 2009; 47(6): 1892-1895.
- Yoshino M, Annaka T, Kojima T, Ikedo M. Sensitive and rapid detection of Mycoplasma pneumoniae by loop-mediated isothermal amplification. *Kansenshogaku Zasshi*. 2008; 82(3): 168-176.
- Bai Z, Shi L, Hu C, Chen X, Qi J, Ba X, et al. Development of a loop-mediated isothermal amplification assay for sensitive and rapid detection of Mycoplasma bovis. *Afr J Biotech*. 2011; 10(57): 12333-12338.
- Liu MJ, Du GM, Bai FF, Wu YZ, Xiong QY, Feng ZX, et al. A rapid and sensitive loop-mediated isothermal amplification procedure (LAMP) for Mycoplasma hyopneumoniae detection based on the p36 gene. *Genet Mol Res*. 2015; 14(2): 4677-4686.
- Aizawa Y, Oishi T, Tsukano S, Taguchi T, Saitoh A. Clinical utility of loop-mediated isothermal amplification for rapid diagnosis of Mycoplasma pneumoniae in children. *J Med Microbiol*. 2014; 63(Pt 2): 248-251.
- Davudi-Asl F, Shahhosseiny M, Keshavarz F. Rapid detection of Mycoplasma pneumonia by loop mediated isothermal amplification (LAMP). *J Gorgan Univ Med Sci*. 2015; 17(3): 127-133.
- Daxboeck F, Krause R, Wenisch C. Laboratory diagnosis of Mycoplasma pneumoniae infection. *Clin Microbiol Infect*. 2003; 9(4): 263-273.
- Saito R, Misawa Y, Moriya K, Koike K, Ubukata K, Okamura N. Development and evaluation of a loop-mediated isothermal amplification assay for rapid detection of Mycoplasma pneumoniae. *J Med Microbiol*. 2005; 54(Pt 11): 1037-1041.
- Yoshikawa T, Ihira M, Akimoto S, Usui C, Miyake F, Suga S, et al. Detection of human herpesvirus 7 DNA by loop-mediated isothermal amplification. *J Clin Microbiol*. 2004; 42(3): 1348-1352.

A Simple Technique for Three-Dimensional Imaging and Segmentation of Brain Vasculature Using Fast Free-of-Acrylamide Clearing Tissue in Murine

Arezoo Khoradmehr, M.Sc.^{1#}, Fahime Mazaheri, M.Sc.^{1#}, Morteza Anvari, Ph.D.^{1,2*}, Amin Tamadon, Ph.D.^{3*}

1. Research and Clinical Center for Infertility, Yazd Reproduction Sciences Institute, Shahid Sadoughi University of Medical Sciences, Yazd, Iran
2. Department of Biology and Anatomical Sciences, Shahid Sadoughi University of Medical Sciences, Yazd, Iran
3. The Persian Gulf Marine Biotechnology Research Center, The Persian Gulf Biomedical Sciences Research Institute, Bushehr University of Medical Sciences, Bushehr, Iran

The first two authors equally contributed to this work.

*Corresponding Addresses: P.O.Box: 89195-999, Department of Biology and Anatomical Sciences, Shahid Sadoughi University of Medical Sciences, Yazd, Iran

P.O.Box: 3537, The Persian Gulf Marine Biotechnology Research Center, The Persian Gulf Biomedical Sciences Research Institute, Bushehr University of Medical Sciences, Bushehr, Iran
Emails: moanvari@gmail.com, amintamaddon@yahoo.com

Received: 30/Dec/2017, Accepted: 30/Apr/2018

Abstract

Objective: Fast Free-of-Acrylamide Clearing Tissue (FACT) is a recently developed protocol for the whole tissue three-dimensional (3D) imaging. The FACT protocol clears lipids using sodium dodecyl sulfate (SDS) to increase the penetration of light and reflection of fluorescent signals from the depth of cleared tissue. The aim of the present study was using FACT protocol in combination with imaging of auto-fluorescence of red blood cells in vessels to image the vasculature of a translucent mouse tissues.

Materials and Methods: In this experimental study, brain and other tissues of adult female mice or rats were dissected out without the perfusion. Mice brains were sliced for vasculature imaging before the clearing. Brain slices and other whole tissues of rodent were cleared by the FACT protocol and their clearing times were measured. After 1 mm of the brain slice clearing, the blood vessels containing auto-fluorescent red blood cells were imaged by a z-stack motorized epifluorescent microscope. The 3D structures of the brain vessels were reconstructed by Imaris software.

Results: Auto-fluorescent blood vessels were 3D imaged by the FACT in mouse brain cortex. Clearing tissues of mice and rats were carried out by the FACT on the brain slices, spinal cord, heart, lung, adrenal gland, pancreas, liver, esophagus, duodenum, jejunum, ileum, skeletal muscle, bladder, ovary, and uterus.

Conclusion: The FACT protocol can be used for the murine whole tissue clearing. We highlighted that the 3D imaging of cortex vasculature can be done without antibody staining of non-perfused brain tissue, rather by a simple auto-fluorescence.

Keywords: FACT, Rodent, Three-Dimensional Imaging, Tissue, Vasculature

Cell Journal (Yakhteh), Vol 21, No 1, Apr-Jun (Spring) 2019, Pages: 49-56

Citation: Khoradmehr A, Mazaheri F, Anvari M, Tamadon A. A simple technique for three-dimensional imaging and segmentation of brain vasculature using fast free-of-acrylamide clearing tissue in murine. Cell J. 2019; 21(1): 49-56. doi: 10.22074/cellj.2019.5684.

Introduction

Three-dimensional (3D) imaging has enabled the study of systems from various cellular and extracellular structures, such as vasculature structure or neuronal networks in the brain (1, 2). Such studies require an extremely transparent tissue for the detection. Different protocols have been developed for the whole tissue clearing and 3D imaging. Benzyl alcohol and benzyl benzoate (BABB) were the first to make fixed tissues as thick as 2 cm transparent for the deep microscopic imaging compared to <50 μm using conventional immunohistochemical techniques (3). Several advances have been made for a high-resolution and a large-scale imaging of cleared tissue, including Scale (4), dibenzyl ether (DBE) (5), three-dimensional imaging of solvent-cleared organs (3DISCO) (6), See Deep Brain (seeDB) (7), ClearT (8), Clear Unobstructed Brain/Body Imaging Cocktails (CUBIC) (9), System-Wide control of Interaction Time and kinetics of Chemical (SWITCH) (10), and ultimate DISCO (uDISCO) (11).

Considering the limitations of the mentioned techniques including, fluorescence quenching of samples, incomplete clearing specimens, and lack of feasibility for antibody labeling, a series of other techniques have been developed. The fact that the cell membrane phospholipids are the main source of light scatter in tissues and the lipid removal is a potential approach for increasing the tissue transparency. Several techniques of the lipid removing transparency have been developed for the 3D imaging of tissues, including using acrylamide protocols such as CLARITY (12), passive CLARITY (2), PACT, PARS (13), and also without applying acrylamide methods including FASTClear (14) and Fast Free-of-Acrylamide Clearing Tissue (FACT) (15).

Some of these techniques use hydrogel embedding such as CLARITY and PACT. Not only are they costly, but they change the tissue volume even after using the refractive index matching solutions (RIMs). The complete tissue clearing needs several days to weeks to disrupt the

fluorescent signal of chemically labeled proteins and it cannot finally prevent the quenching of fluorescent protein signals for a long time. These hydrogel-based techniques also need further toxic chemicals, labor work and the equipment. Therefore, a simple technique is appropriate for laboratories in developing countries. One of these newly-developed simple techniques is the FACT (15) requiring the lower labor work, and the use of toxic and environmentally hazardous chemicals in comparison to acrylamide-based protocols. Another limitation in the developing countries is the lack of advanced microscopes, i.e. confocal, 2-photon and light sheet microscopes. To date, all of the introduced protocols for the 3D imaging of tissues have used the advanced microscopes. Adopting FACT approach with a conventional epifluorescent microscope was another goal of this study.

Hopefully, this methodology may help in studying the brain vascular architecture for fundamental evaluation of pathological alterations in cerebral disorders including the vessels such as ischemia (16), Alzheimer's disease (17), and cancer (18). Therefore, the aims of the present study were to evaluate the ability of the FACT protocol for clearing different whole tissue of mice and rats and 3D imaging of the brain cortex vasculature with FACT method in mice using a simple epifluorescent microscope in a non-developed imaging lab.

Materials and methods

Animals

The present experimental study has been performed according to Shahid Sadoughi University of Medical Sciences Guidelines for Animal Handling and the Ethics Committee of Research and Clinical Center for Infertility (No: 91/8/2/2168). Adult female mice (n=3) and rats (n=3) were used and kept in Laboratory Animal Center of the Center of Infertility, Shahid Sadoughi University of Medical Sciences, Yazd, Iran.

FACT protocol

The rats and mice were euthanized by ether inhalation and then cervical dislocation. The experiment protocol has been summarized in Figure 1. Then, tissues including the brain, spinal cord, heart, lung, adrenal gland, pancreas, liver, esophagus, duodenum, jejunum, ileum, skeletal muscle, bladder, ovary, and uterus were dissected out. They were separately transferred into 4% paraformaldehyde (PFA, Merck KCaA, Germany) diluted in phosphate-buffered saline (PBS, Gibco, UK) solution (0.01 M) as a fixative solution (pH=7.5, room temperature). Tissues were fixed in the fixative solution at 4°C for 3 days. Then, the brain was coronally 1 mm-sliced, coronally.

The whole and sliced tissues were cleared according to the FACT protocol (15). In details, the tissues were cleared with clearing solution containing 8% (wt/vol) sodium dodecyl sulfate (SDS) in 0.01 M PBS (pH=7.5) with 0.02% sodium azide at 37°C with mild rotational horizontal shaking (100 r/minutes) in a shaker incubator (Jaltajhiz, Iran). The clearing solution was refreshed daily for 3 days and then was replaced weekly until the visual confirmation of 80% tissue transparency by an observation through the tissue of clear black grid lines printed on a white paper. Transparency of the tissue during the clearing procedure was imaged using a DP71 camera (Olympus, Japan) on a stage of a loop microscope (SZX16, Olympus, Japan) for background illumination. The start and end date of clearing were recorded for all tissues.

Imaging of auto-fluorescent vessels in brain cortex

The brain slices were washed once in PBS with 0.02% sodium azide, and then were shaken gently 12 hours in the same solution at 37°C in horizontally fixed falcon tubes. For complete transparency and refractive index (RI) matching, samples were placed in 80% glycerol in double distilled water for 3 to 12 hours in room temperature prior to imaging.

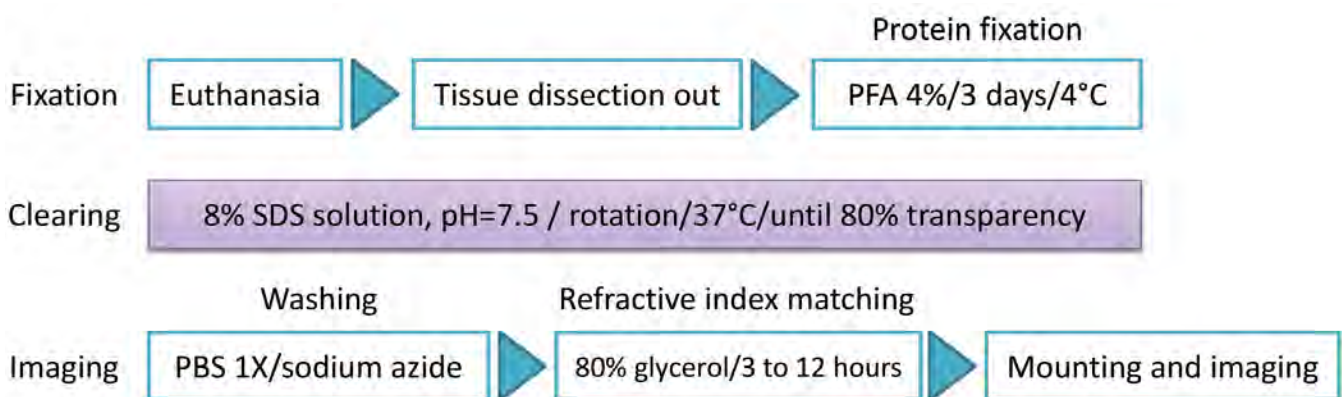


Fig.1: Protocol of clearing and imaging of brain cortex vasculature by Fast Free-of-Acrylamide Clearing Tissue (FACT) based on the presence of red blood cells and their auto-fluorescent signal. PFA; Paraformaldehyde, PBS; Phosphate buffer saline, and SDS; Sodium dodecyl sulfate.

3D epifluorescent microscopy

For 3D imaging, brain slices were individually mounted between two glass slides which were surrounded by same thickness non-colorful putty that formed a horse-shoe-like chamber (1-mm thickness wall) to protect the tissues' thickness from pressing between the slides and provides a chamber for the RI matching solution. This chamber between two slides was filled with fresh 80% glycerol. The auto-fluorescent vessels were imaged by an epifluorescence microscope (BX51 with a DP72 camera, Olympus, Japan), and CellSens imaging software (Version 1.4.1, Olympus, Japan). After the apparatus was fixed on the microscope stage, the specimen was imaged by an air/dry objective lens 10× (UPlanSApo, Olympus Co. Ltd.; numerical aperture : 0.4 and working distance: 3.1 mm) which was water immersed to increase working distance. The EPI illumination mode and red excitation (650 nanometers) and deep red emission (690 nanometers) were applied for imaging. For this purpose, selected area was imaged on a z-stack manner (each 10- μ m step) for the depth of 150 μ m from the tissue surface, automatically.

3D image preparation

The TIFF image sequences were obtained from the microscope and transferred to Imaris software (version 7.4.2, ImarisX64, Bitplane AG) for the 3D reconstruction (19). In details, after importing TIFF files, in the "Display Adjustment" tabs, the color and name of the channels were changed. Then, in the drop-down list under the "Edit" button and "Image Properties" panel, the thickness of the tissue was corrected according to the z-stack imaging information of an epifluorescent microscope. To 3D crop, the final images and removing the excess parts, in the drop-down list under the "Edit" button and "Crop 3D" option were used. The size of the field was adjusted by dragging the borders.

In the "Surpass" panel, vessels of brain cortex were 3D reconstructed using the filaments algorithm and based on the detected signals. In detail, a new Filament was created in the "Filaments" button. In the "Slice" panel, the thinnest and the largest diameter of the imaged vessels were defined. On the "Measure" panel, the distance automatically was shown after selecting two points at the maximum width of the thinnest and thickest vessels. After defining the largest and thinnest thickness, data were entered in the "Surpass" panel. Then, the thresholds of starting and seed points were adjusted. Tracing the length of vessels, using "Select" tab in the "Camera" panel, some of the automatically produced seed points were manually removed by pressing shift on the keyboard and left clicking on the point. The 3D image rotation was done by selecting "Navigate" and moving the pointer of the mouse device, to ensure that the correct seed points have been retained.

Then, the highest threshold for the local contrast was

selected. At the last step, without the selection of "Detect Spines", the blood vessel reconstruction was finalized. The excess parts of the vessels which were not matched on the signals were removed in the "Edit" panel. The color of reconstructed cylinders was edited by clicking the "Color" tab.

Comparing antibody stained and auto-fluorescent vessels

Comparing the vessel imaging by non-antibody-based and antibody staining method, brain slices of non-perfused and perfused mice, respectively, were cleared using the FACT protocol. Then, both groups were labeled for CD31 (a marker of blood vessels epithelium) and Hoechst 33342 (marker of the cell nucleus).

In details, after clearing, the residual SDS was washed from the brains by slow shaking in PBS with 0.1% Triton X-100 (PBST) for 24 hours at 37°C. The samples were then incubated for 24 hours with anti-CD31 primary antibody (1:10, mouse species, Abcam, USA) diluted in PBST with shaking at 37°C. The samples were subsequently washed in PBST buffer for 24 hours with shaking at 37°C. Then they were incubated with the FITC-IgG secondary antibody (Goat anti-mouse, 1:100, Abcam, US) diluted in PBST for 24 hours with shaking at 37°C in a tube was covered with an aluminum sheet. To label cell nuclei, Hoechst 33342 (1:100, Bis Benzimaide H 33342, Sigma, USA) was added to the secondary antibody mixture for the final 12 hours of incubation with shaking at 37°C. Before mounting and imaging, samples were washed in PBST for 24 hours with shaking at 37°C. Samples were submerged in glycerol for 24 hours at room temperature. The antibody signals and auto-fluorescent vessels were imaged by an epifluorescence microscope (BX51 with a DP72 camera, Olympus, Japan), and CellSens imaging software (Version 1.4.1, Olympus, Japan).

To evaluate the possibility of detection of vessels in other tissues by auto-fluorescence characteristics of the red blood cell (RBC), non-perfused spinal cord and uterus along with perfused skeletal muscle and duodenum of mice were stained with Hoechst 33342.

Results

Transparent brain slices were rapidly created with the passive clearing using the FACT protocol (Figs.2, 3). As shown in Figures 2 and 3, the FACT cleared the 1-mm thick brain slices in both mice and rats within 3 days (Table 1).

To 3D reconstruct the blood vessels architecture in the brain cortex of mice, a microvasculature containing red blood cells was subsequently examined by an epifluorescent microscope (Fig.4A). In addition, using Imaris Filament algorithm, the blood vessels were segmented (Fig.4B). The 3D reconstructed blood vessels in brain cortex of mice were shown in Figure 4C.

Table 1: Comparison of clearing time (day) of whole or sectioned tissues of mouse and rat with Fast Free-of-Acrylamide Clearing Tissue (FACT), passive CLARITY, PACT, and mPACT methods

Tissue	FACT		Passive CLARITY		PACT		mPACT	
	Mouse	Rat	Mouse	Rat	Mouse	Rat	Mouse	Rat
Brain slice (1-mm thickness)	3	3	4 (21)	6 (21, 25)	4-9 (13, 15)	ND	ND	ND
Spinal cord (whole size)	7	12	14-28 (24, 26)	ND	12 (30)	12 (30)	14 (30)	21 (30)
Heart (whole size)	66	ND	ND	ND	17 (30)	16 (30)	15 (30)	16 (30)
Lung (whole size)	21	21	30 (20)	ND	18 (30)	18 (30)	14 (30)	18 (30)
Adrenal gland (whole size)	ND	33	ND	ND	ND	ND	ND	ND
Pancreas (whole size)	7	7	ND	ND	15 (30)	15 (30)	17 (30)	15 (30)
Liver (one lobe)	6	37	30 (27)	ND	22 (30)	23 (30)	ND	23 (30)
Esophagus (whole size)	7	7	ND	ND	ND	ND	ND	ND
Intestine (whole size)	7	7	12-30 (20, 28)	ND	12-14 (28)	ND	ND	ND
Bladder (whole size)	66	ND	ND	ND	ND	ND	ND	ND
Ovary (whole size)	ND	66	35 (19, 29)	ND	ND	ND	ND	ND
Uterus (whole size)	14	ND	ND	ND	ND	ND	ND	ND

ND; No data.

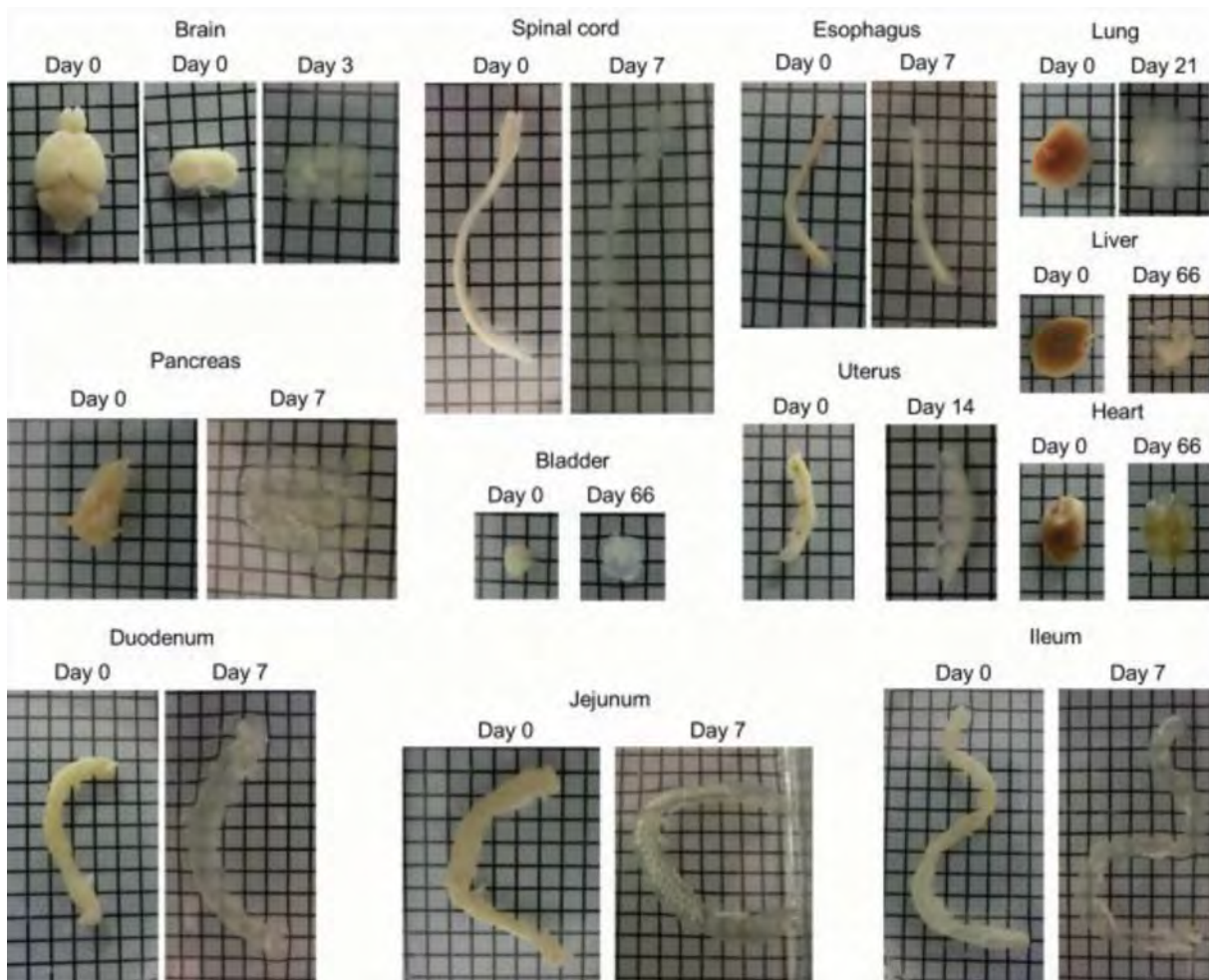


Fig.2: Clearing of mouse tissues using Fast Free-of-Acrylamide Clearing Tissue (FACT) including 1 mm brain slice, spinal cord, esophagus, lung, pancreas, bladder, uterus, heart, duodenum, jejunum, ileum (squares are 3x3 mm²). The clearing steps are before using refractive index solution (RIMs) and transparency is not more than 80%.

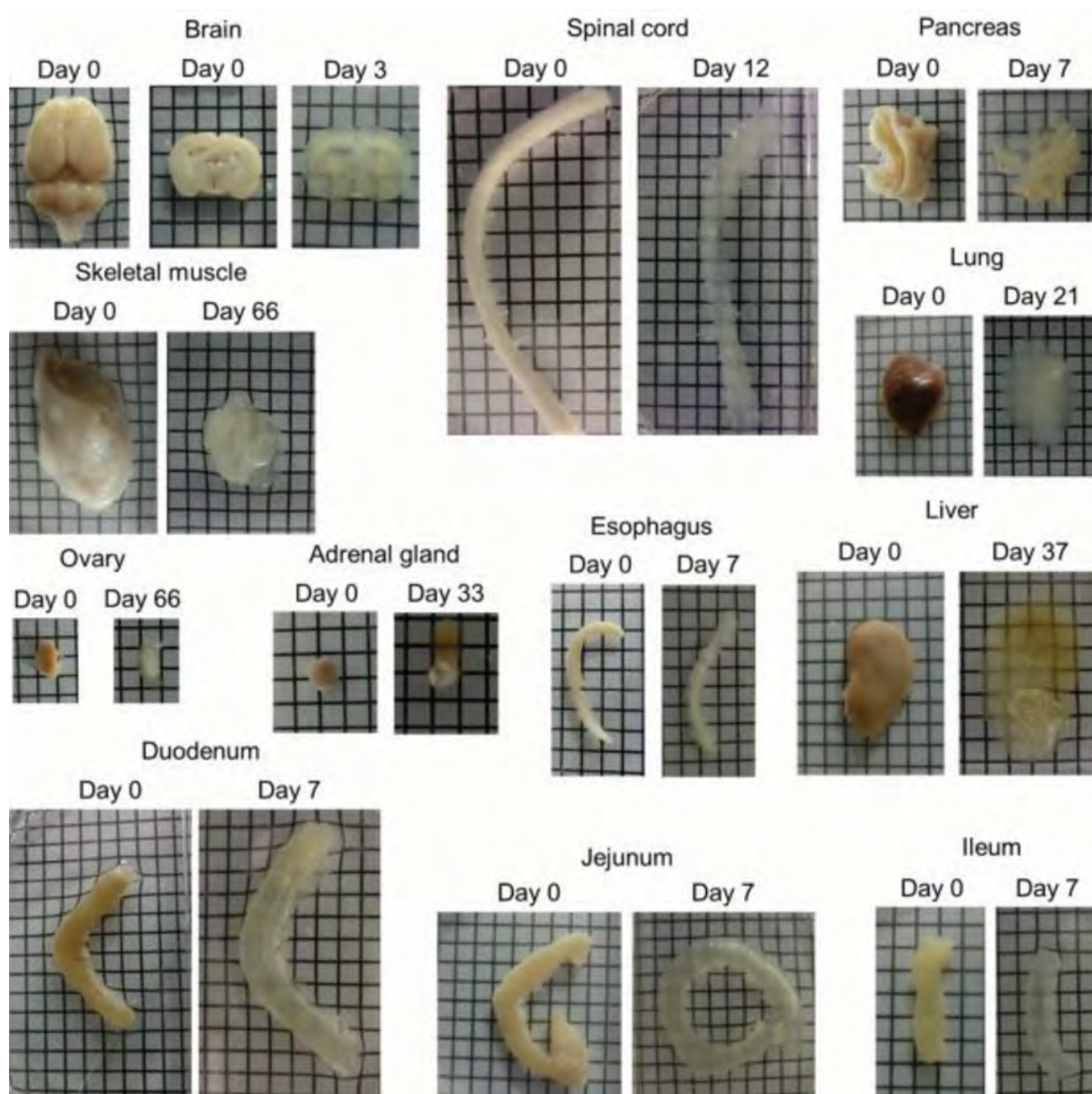


Fig.3: Clearing of rat tissues using Fast Free-of-Acrylamide Clearing Tissue (FACT) including 1 mm brain slice, spinal cord, pancreas, skeletal muscle, lung, ovary, adrenal gland, esophagus, liver, duodenum, jejunum, and ileum (squares are 3×3 mm²). The clearing steps are before using refractive index solution (RIMs) and transparency is not more than 80%.

The FACT protocol could make transparent the different types of tissues of mice (Fig.2) and rats (Fig.3). For the whole organs of adult female mice and rats, the optimal passive clearing conditions were determined for the FACT and compared with the previous studies in Table 1.

In order to show the possibility of vessels to be imaged by a non-antibody-based method based on auto-fluorescent characteristics of the RBC and to confirm detectability of the vessels in this protocol to be imaged after the FACT technique, the brain slices of non-perfused and perfused mice were stained in the same staining condition and the same tube containing CD31. Using blue (WB) and green (WG) filter boxes, the auto-fluorescent RBC signals were detected in non-perfused vessels of the brain cortex (Fig.4D). There were no vessels in the image of WB filter which

were not visible in WG filter, too. This phenomenon showed that the auto-fluorescent RBC signals and CD31-labeled vascular endothelium were completely overlapped. In contrast, in perfused mice (Fig.4E), FITC-labeled CD31 markers on vascular endothelium were only observable in WB filter. In the both non-perfused and perfused mice, vascular endothelium nuclei line-shaped structures were visible by Hoechst 33342 staining.

Using a similar method of non-antibody-based detection of vessels, we evaluated the imaging of the FACT-cleared spinal cord (Fig.5A) and uterus (Fig.5B) in non-perfused mice. Furthermore, imaging of duodenum and skeletal muscle in perfused mice after clearing by the FACT technique did not show any vascular structures (Fig.5C).

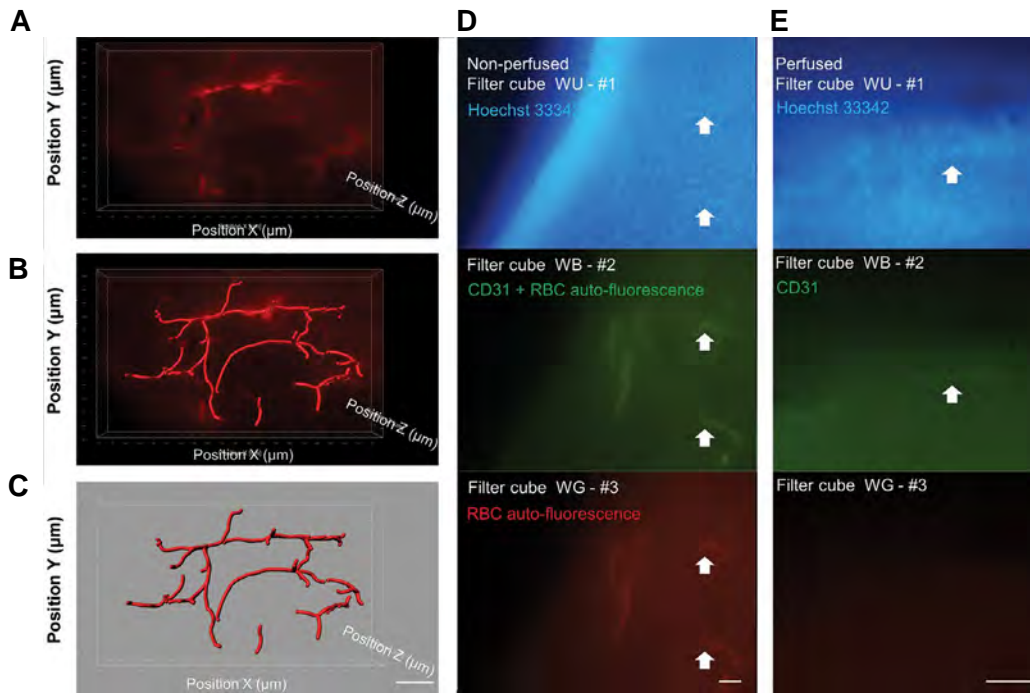


Fig.4: Fast Free-of-Acrylamide Clearing Tissue (FACT) technique for three-dimensional (3D) imaging of blood vessels in brain cortex using an epifluorescent microscope. **A.** A 3D image of the mouse blood vessels by the FACT clearing protocol. The fluorescent signal is from auto-fluorescent heme in red blood cells in the non-perfused blood vessels (tissue dimension XYZ=2000×1200×150 µm³) (scale bar: 300 µm). **B.** Using Imaris software and “Filament” algorithm of “Surpass”, vessels’ structure was reconstructed (scale bar: 300 µm). **C.** 3D segmentation of cortex blood vessels in 150 µm depth of cortex (scale bar: 300 µm), and **D, E.** Comparison of imaging of brain cortex vessels by non-antibody-based and antibody staining method, in brain slices of non-perfused and perfused mice. **D.** In non-perfused brain similarity of the architecture of vessels were imaged with WB and WG filters demonstrates that RBC signals have been completely overlapped with CD31-labeled vasculatures (scale bar: 100 µm). **E.** In perfused mice, vessels are observable with WB filter. Arrows demonstrate vessels (scale bar: 100 µm).

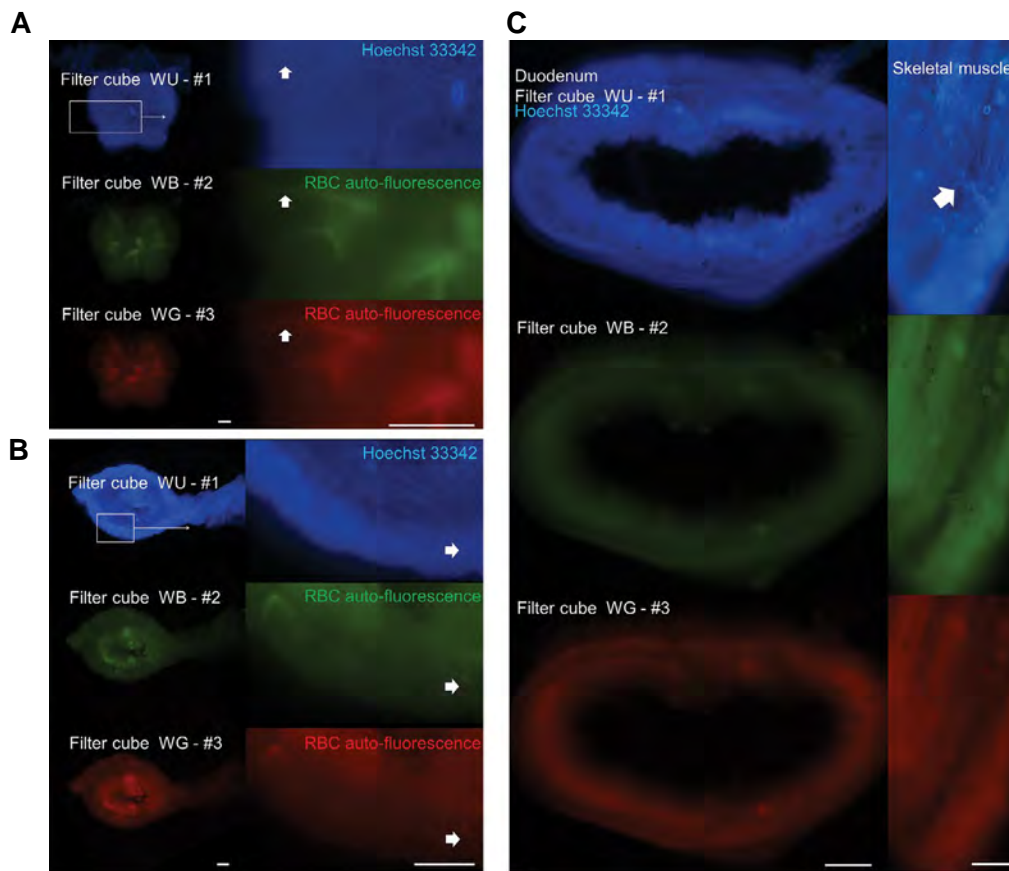


Fig.5: Vascular imaging after Fast Free-of-Acrylamide Clearing Tissue (FACT) technique. **A.** Imaging of spinal cord vessels by a non-antibody-based method in the non-perfused mice (scale bar: 200 µm). Arrows demonstrate auto-fluorescent vessels. **B.** Imaging of vessels in the uterus and attached broad ligament by a non-antibody-based method in the non-perfused mice (scale bar: 200 µm). Arrows demonstrate auto-fluorescent vessels, and **C.** Imaging of duodenum and skeletal muscle in the perfused mice after clearing by Fast Free-of-Acrylamide Clearing Tissue (FACT) technique and labeling with Hoechst 33342 (scale bar: 400 µm). Arrow alludes to vascular branches.

Discussion

For the first time, we demonstrated the clearing of the murine tissues with the FACT protocol (15) for the effective clearing of tissues and 3D imaging of brain cortex vasculatures. The FACT method, has been modified including alterations of imaging to adapt this method for non-equipped laboratories. Although the most important part of the whole tissue clearing is optical sectioning for 3D imaging and this can be optimally achieved by confocal microscopy, availability of this expensive microscope is a big challenge for adapting the whole tissue imaging for a conventional laboratory of limited resources. Therefore, in the present study of the FACT method we used an epifluorescent microscope with a motorized stage for imaging auto-fluorescent vessels in the z-plane. Bearing in mind that this approach has some limitations including a lower depth of imaging of fluorescent light in an epifluorescent microscope in comparison to a laser in a confocal microscope. This issue can be solved by cutting 1- to 2-mm piece of cleared tissue for imaging. Moreover, a lower power of the epifluorescent for collecting the enhanced signals in comparison to the laser-enhanced fluorophores in confocal caused limitation in imaging of tissue for the maximum depth of 200 to 300 μm .

The FACT cleared 1-mm of thick brain slices in both mice and rats in 3 days, while in mice and rats a passive CLARITY needs 4 and 6 days, respectively and PACT requires 9 days in mice. Regarding the clearing time, the whole brain slice (1 mm thickness) clearing in murine species with the FACT protocol as a passive method required 3 days for completion which is comparable to CUBIC (more than 1 week) (9) and ScaleA2 (5 days) (4). In addition, based on Xu et al. (15) and comparing of our data with previous studies, we can speculate that removing hydrogel decreased the clearing time in comparison to hydrogel-based methods such as CLARITY (2), PACT, PARS (13), and SWITCH (10). The CLARITY technique has been used for clearing the different murine tissues including the brain (2, 20-25), spinal cord (21, 24, 26), heart (22), lung (20, 22), liver (27), intestine (20, 28), skeletal muscle (22), and ovary (19, 29). In addition, several studies cleared different murine tissues using PACT protocol including the brain (13, 22, 30, 31), heart, lung (13, 22, 30), pancreas, liver (30), intestine (13, 28), skeletal muscle (22), adrenal gland (20), and ovary (30). In addition to above-mentioned tissues which were cleared by acrylamide-based protocols (32), using FACT protocol, the other murine tissues including bladder, uterus, and esophagus have been cleared for the first time in this study.

Brain vasculature imaging at microscopic scales and imaging deep into brain remained an open quest in neuroscience. Although, the conventional optical microscopy is still limited to surface imaging. Revolutionary approaches such as ultrasonography (33), intravital microscopy (34), and the whole tissue imaging by an optical microscope (35) have opened new windows in this aspect. The whole tissue clearing such as our

findings, can show the 3D architecture of the blood vessels and also can be used for seeking vasculature relationships in neurons (23).

Epifluorescent, confocal and light sheet microscopy provide more information for the vasculature research in the brain because of the presence of various vascular endothelial markers such as CD31, CD34, factor VIII, von Willebrand factor, and Fli-1 that can be used in these imaging methods especially, in whole tissue imaging (36). In addition to mentioned markers which can be detected by chemical or genetic labeling methods for the detection of brain vasculature (36, 37), other fluorescent materials have been also used for imaging of the brain vasculature (38). In the present study, we used the auto-fluorescent character of heme in red blood cells (39) in a non-perfused brain for the visualization of the blood vessels in the FACT-cleared mouse brain, spinal cord, and uterus.

Conclusion

The FACT method is a simple technique which might be appropriate for laboratories in developing countries lacking advanced microscopes such as confocal microscopes. Successful labeling the vessels in murine species after clearing by the FACT approach resulted in 3D imaging of brain cortex vessels for the first time. Imaging the vasculature was performed without any staining; rather accomplished by a simple auto-fluorescence imaging of the RBC.

Acknowledgments

The authors are grateful to the Research and Clinical Center for Infertility, Yazd Reproduction Sciences Institute, Shahid Sadoughi University of Medical Sciences (Yazd, Iran) for financial supporting of this research. The authors have declared that there is no conflict of interest.

Authors' Contributions

A.K., F.M., M.A., A.T.; Designed and performed the experiments and co-wrote the paper. A.K., F.M., Performed the tissue processing experiments. A.K., A.T.; Performed the microscopy and imaging. M.A., A.T.; Designed the experiments and supervised the research. All authors read and approved the final study.

References

- Steinman J, Koletar MM, Stefanovic B, Sled JG. 3D morphological analysis of the mouse cerebral vasculature: Comparison of in vivo and ex vivo methods. *PLoS One*. 2017; 12(10): e0186676.
- Tomer R, Ye L, Hsueh B, Deisseroth K. Advanced CLARITY for rapid and high-resolution imaging of intact tissues. *Nat Protoc*. 2014; 9(7): 1682-1697.
- Dotz HU, Leischner U, Schierloh A, Jährling N, Mauch CP, Deininger K, et al. Ultramicroscopy: three-dimensional visualization of neuronal networks in the whole mouse brain. *Nat Methods*. 2007; 4(4): 331-336.
- Hama H, Kurokawa H, Kawano H, Ando R, Shimogori T, Noda H, et al. Scale: a chemical approach for fluorescence imaging and reconstruction of transparent mouse brain. *Nat Neurosci*. 2011; 14(11): 1481-1488.

5. Becker K, Jährling N, Saghabi S, Weiler R, Dodt HU. Chemical clearing and dehydration of GFP expressing mouse brains. *PLoS One*. 2012; 7(3): e33916.
6. Ertürk A, Becker K, Jährling N, Mauch CP, Hojer CD, Egen JG, et al. Three-dimensional imaging of solvent-cleared organs using 3DISCO. *Nat Protoc*. 2012; 7(11): 1983-1995.
7. Ke MT, Fujimoto S, Imai T. SeeDB: a simple and morphology-preserving optical clearing agent for neuronal circuit reconstruction. *Nat Neurosci*. 2013; 16(8): 1154-1161.
8. Kuwajima T, Sitko AA, Bhansali P, Jurgens C, Guido W, Mason C. ClearT: a detergent-and solvent-free clearing method for neuronal and non-neuronal tissue. *Development*. 2013; 140(6): 1364-1368.
9. Susaki EA, Tainaka K, Perrin D, Kishino F, Tawara T, Watanabe TM, et al. Whole-brain imaging with single-cell resolution using chemical cocktails and computational analysis. *Cell*. 2014; 157(3): 726-739.
10. Murray E, Cho JH, Goodwin D, Ku T, Swaney J, Kim SY, et al. Simple, scalable proteomic imaging for high-dimensional profiling of intact systems. *Cell*. 2015; 163(6): 1500-1514.
11. Pan C, Cai R, Quacquarelli FP, Ghasemigharagoz A, Loubopoulos A, Matryba P, et al. Shrinkage-mediated imaging of entire organs and organisms using uDISCO. *Nat Methods*. 2016; 13(10): 859-867.
12. Chung K, Wallace J, Kim SY, Kalyanasundaram S, Andalman AS, Davidson TJ, et al. Structural and molecular interrogation of intact biological systems. *Nature*. 2013; 497(7449): 332-337.
13. Yang B, Treweek JB, Kulkarni RP, Deverman BE, Chen CK, Lubbeck E, et al. Single-cell phenotyping within transparent intact tissue through whole-body clearing. *Cell*. 2014; 158(4): 945-958.
14. Liu AKL, Lai HM, Chang R-C, Gentleman SM. Free of acrylamide sodium dodecyl sulphate (SDS)-based tissue clearing (FAST-Clear): a novel protocol of tissue clearing for three-dimensional visualization of human brain tissues. *Neuropathol Appl Neurobiol*. 2017; 43(4): 346-351.
15. Xu N, Tamadon A, Liu Y, Ma T, Leak RK, Chen J, et al. Fast free-of-acrylamide clearing tissue (FACT): an optimized new protocol for rapid, high-resolution imaging of three-dimensional brain tissue. *Sci Rep*. 2017; 7(1): 9895.
16. Lapi D, Colantuoni A. Remodeling of cerebral microcirculation after ischemia-reperfusion. *J Vasc Res*. 2015; 52(1): 22-31.
17. Attems J, Jellinger KA. The overlap between vascular disease and Alzheimer's disease--lessons from pathology. *BMC Med*. 2014; 12: 206.
18. Vasudev NS, Reynolds AR. Anti-angiogenic therapy for cancer: current progress, unresolved questions and future directions. *Angiogenesis*. 2014; 17(3): 471-494.
19. Hu W, Tamadon A, Hsueh AJW, Feng Y. Three-dimensional reconstruction of the vascular architecture of the passive CLARITY-cleared mouse ovary. *J Vis Exp*. 2017; (130).
20. Epp JR, Niibori Y, Liz Hsiang HL, Mercaldo V, Deisseroth K, Josselyn SA, et al. Optimization of CLARITY for clearing whole-brain and other intact organs. *eNeuro*. 2015; 2(3). pii: ENEURO.0022-15.2015.
21. Jensen KHR, Berg RW. CLARITY-compatible lipophilic dyes for electrode marking and neuronal tracing. *Sci Rep*. 2016; 6: 32674.
22. Orlich M, Kiefer F. A qualitative comparison of ten tissue clearing techniques. *Histol Histopathol*. 2018; 33(2): 181-199.
23. Phillips J, Laude A, Lightowers R, Morris CM, Turnbull DM, Lax NZ. Development of passive CLARITY and immunofluorescent labelling of multiple proteins in human cerebellum: understanding mechanisms of neurodegeneration in mitochondrial disease. *Sci Rep*. 2016; 6: 26013.
24. Roberts DG, Johnsonbaugh HB, Spence RD, MacKenzie-Graham A. Optical clearing of the mouse central nervous system using passive CLARITY. *J Vis Exp*. 2016; (112).
25. Zheng H, Rinaman L. Simplified CLARITY for visualizing immunofluorescence labeling in the developing rat brain. *Brain Struct Funct*. 2016; 221(4): 2375-2383.
26. Liang H, Schofield E, Paxinos G. Imaging serotonergic fibers in the mouse spinal cord using the CLARITY/CUBIC technique. *J Vis Exp*. 2016; (108): 53673.
27. Sindhvani S, Syed AM, Wilhelm S, Chan WC. Exploring passive clearing for 3D optical imaging of nanoparticles in intact tissues. *Bioconjug Chem*. 2017; 28(1): 253-259.
28. Neckel PH, Mattheus U, Hirt B, Just L, Mack AF. Large-scale tissue clearing (PACT): Technical evaluation and new perspectives in immunofluorescence, histology, and ultrastructure. *Sci Rep*. 2016; 6: 34331.
29. Feng Y, Cui P, Lu X, Hsueh B, Möller Billig F, Zarnescu Yanez L, et al. CLARITY reveals dynamics of ovarian follicular architecture and vasculature in three-dimensions. *Sci Rep*. 2017; 7: 44810.
30. Woo J, Lee M, Seo JM, Park HS, Cho YE. Optimization of the optical transparency of rodent tissues by modified PACT-based passive clearing. *Exp Mol Med*. 2016; 48(12): e274.
31. Shah S, Lubeck E, Schwarzkopf M, He TF, Greenbaum A, Sohn CH, et al. Single-molecule RNA detection at depth by hybridization chain reaction and tissue hydrogel embedding and clearing. *Development*. 2016; 143(15): 2862-2867.
32. Jensen KHR, Berg RW. Advances and perspectives in tissue clearing using CLARITY. *J Chem Neuroanat*. 2017; 86: 19-34.
33. Errico C, Pierre J, Pezet S, Desailly Y, Lenkei Z, Couture O, et al. Ultrafast ultrasound localization microscopy for deep super-resolution vascular imaging. *Nature*. 2015; 527(7579): 499-502.
34. Vakoc BJ, Lanning RM, Tyrrell JA, Padera TP, Bartlett LA, Stylianopoulos T, et al. Three-dimensional microscopy of the tumor microenvironment in vivo using optical frequency domain imaging. *Nat Med*. 2009; 15(10): 1219-1223.
35. Lun LK, Prystal J, Syed N, Lai HM. Visualising the vasculature of a human glioma in mouse brain using CLARITY. *Arch Cancer Res*. 2016; 4: 1.
36. Costantini I, Ghobril JP, Di Giovanna AP, Allegra Mascaro AL, Silvestri L1, Müllenbroich MC, Onofri L, et al. A versatile clearing agent for multi-modal brain imaging. *Sci Rep*. 2015; 5: 9808.
37. Zhang LY, Lin P, Pan J, Ma Y, Wei Z, Jiang L, et al. CLARITY for high-resolution imaging and quantification of vasculature in the whole mouse brain. *Aging Dis*. 2018, 9(2): 262-272.
38. Tsai PS, Kaufhold JP, Blinder P, Friedman B, Drew PJ, Karten HJ, et al. Correlations of neuronal and microvascular densities in murine cortex revealed by direct counting and colocalization of nuclei and vessels. *J Neurosci*. 2009; 29(46): 14553-14570.
39. Davis AS, Richter A, Becker S, Moyer JE, Sandouk A, Skinner J, et al. Characterizing and diminishing autofluorescence in formalin-fixed paraffin-embedded human respiratory tissue. *J Histochem Cytochem*. 2014; 62(6): 405-423.

Induction Effects of *Bacteroides fragilis* Derived Outer Membrane Vesicles on Toll Like Receptor 2, Toll Like Receptor 4 Genes Expression and Cytokines Concentration in Human Intestinal Epithelial Cells

Sara Ahmadi Badi, Ph.D.¹, Shohreh Khatami, Ph.D.², Shiva Irani, Ph.D.¹, Seyed Davar Siadat, Ph.D.^{3, 4*}

1. Department of Biology, Science and Research Branch, Islamic Azad University, Tehran, Iran

2. Department of Biochemistry, Pasteur Institute of Iran, Tehran, Iran

3. Department of Mycobacteriology and Pulmonary Research, Pasteur Institute of Iran, Tehran, Iran

4. Microbiology Research Centre, Pasteur Institute of Iran, Tehran, Iran

*Corresponding Address: P.O.Box: 1316943551, Department of Mycobacteriology and Pulmonary Research, Pasteur Institute of Iran, Tehran, Iran

Email: d.siadat@gmail.com

Received: 7/Feb/2018, Accepted: 4/May/2018

Abstract

Objective: Gastrointestinal (GI) tract, like other mucosal surface, is colonized with a microbial population known as gut microbiota. Outer membrane vesicles (OMVs) which are produced by gram negative bacteria could be sensed by Toll like receptors (TLRs). The interaction between gut microbiota and TLRs affects homeostasis and immune responses. In this study, we evaluated *TLR2*, *TLR4* genes expression and cytokines concentration in Caco-2 cell line treated with *Bacteroides fragilis* (*B. fragilis*) and its OMVs.

Materials and Methods: In this experimental study, OMVs were extracted using sequential centrifugation and their physicochemical properties were evaluated as part of quality control assessment. Caco-2 cells were treated with *B. fragilis* and its OMVs (180 and 350 µg/ml). Quantitative reverse transcriptase-polymerase chain reaction (qRT-PCR) was performed to assess *TLR2* and *TLR4* mRNA expression levels. Pro-inflammatory (IFN_γ) and anti-inflammatory (IL-4 and IL-10) cytokines were evaluated by ELISA.

Results: *B. fragilis* significantly decreased *TLR2* and slightly increased *TLR4* mRNA levels in Caco-2 cell line. The *TLR2* mRNA level was slightly increased at 180 and 350 µg/ml of OMVs. Conversely, the *TLR4* mRNA level was decreased at 180 µg/ml of OMVs, while it was significantly increased at 350 µg/ml of OMVs. Furthermore, *B. fragilis* and its OMVs significantly increased and decreased IFN_γ concentration, respectively. Anti-inflammatory cytokines were increased by *B. fragilis* and its OMVs.

Conclusion: *B. fragilis* and its OMVs have pivotal role in the cross talk between gut microbiota and the host especially in the modulation of the immune system. Based on the last studies on immunomodulatory effect of *B. fragilis* derived OMVs on immune cells and our results, we postulate that *B. fragilis* derived OMVs could be possible candidates for the reduction of immune responses.

Keywords: *Bacteroides fragilis*, Gut Microbiota, Membrane Vesicles, Toll Like Receptors

Cell Journal (Yakhteh), Vol 21, No 1, Apr-Jun (Spring) 2019, Pages: 57-61

Citation: Ahmadi Badi S, Khatami Sh, Irani Sh, Siadat SD. Induction effects of bacteroides fragilis derived outer membrane vesicles on toll like receptor 2, toll like receptor 4 genes expression and cytokines concentration in human intestinal epithelial cells. Cell J. 2019; 21(1): 57-61. doi: 10.22074/cellj.2019.5750.

Introduction

Gastrointestinal (GI) tract is colonized by a variety, complex and dynamic microbial community referring as gut microbiota. This microbial community also consists of bacteria, fungi, archaea, protozoa and viruses (1). Gut microbiota constantly interacts with the epithelium of GI tract. This putative cross talk has potential role in both host functions (locally and systemically) and establishment of gut microbiota pattern. Thus, host functions and gut microbiota pattern regulate health and diseases status (2).

Gut microbiota is considered as a reservoir for immune system stimulatory molecules due to the presence of immunogenic compounds such as lipopolysaccharides (LPS), peptidoglycans (PG) and extracellular vesicles (EVs) (3, 4). These bacterial components are encountered in the gut barrier (epithelial layer) as the first line of gut innate immunity. The gut barrier is also composed of

intestinal epithelial cells, mucus layer that is produced by goblet cells, innate and adaptive immune factors (i.e. antimicrobial peptides and immunoglobulins, mainly including IgA). Indeed, the gut barrier shapes gut microbiota and its interaction to host (5, 6). Moreover, the gut barrier functions are under the control of pattern recognition receptors (PRRs) including toll like receptors (TLRs), nucleotide binding domain leucine rich repeat containing receptors (NLRs), retinoic acid inducible gene like receptors (RLRs), C-type lectin receptors (CLRs) and absent in melanoma 2 (AIM2)-like receptors (ALRs) (7, 8). PRRs sense pathogen associated molecular patterns (PAMPs) or damage associated molecular patterns (DAMPs), trigger various signaling cascades and induce different responses (9). Various cell types including immune and intestinal epithelial cells express TLRs that are belonged to type I transmembrane receptors (10). The

expression patterns of TLRs among GI epithelial cell are different and the interaction between gut microbiota and TLRs affects local and systemic immunity (8). Disrupted homeostasis, considered as dysbiosis, results from the imbalance between gut microbiota and immune responses. It is considered as a turning point to induce many disorders including metabolic syndrome (11). This condition which is characterized by impaired permeability of gut barrier, known as leaky gut syndrome, causes a great activation of TLRs in intestinal epithelial cells (IEPCs) (12). Consequently, increased cytokines and chemokines trigger low grade inflammation. Increased inflammatory cytokines disrupt insulin signaling cascade and may cause insulin resistance (IR), ultimately promoting metabolic syndrome and obesity (13).

Bacteroides spp. such as *B. fragilis* have significant roles in gut microbiota-host interactions, especially on metabolic and immune system (14). Similarly, *Bacteroides* spp. derived outer membrane vesicles (OMVs) are key players in gut microbiota host interactions (15). OMVs are nanosized and spherical vesicles which could affect metabolic and immune system since they contain bacterial components including LPS, outer membrane proteins, phospholipids, periplasmic components, DNA, RNA, hydrolytic enzymes and signaling molecules (16).

B. fragilis also secretes capsular polysaccharide A (PSA) containing OMVs. These OMVs interact with dendritic cells (DCs) through TLR2 signaling pathway, resulting in CD4⁺ and regulatory T- cells (Tregs) induction. The latter one is crucial for host immune tolerance towards commensal intestinal bacteria. Therefore, *B. fragilis* derived OMVs contribute to maintain gut microbiota homeostasis (17, 18). In this regard, we evaluated and compared the effects of *B. fragilis* and its OMVs on *TLR2*, *TLR4* genes expression and cytokines concentration on Caco-2 cell line as a IEPCs model.

Materials and Methods

Bacterial growth conditions

In this experimental study, *B. fragilis* ATCC 23745 was grown on blood agar plates containing 5% sheep blood or brain heart infusion (BHI) broth supplemented with 5 µg/ml hemin (Sigma-Aldrich, USA) and 1 µg/ml menadione (Sigma-Aldrich, USA), while they were incubated at 37°C, in 80% N₂, 10% CO₂ and 10% H₂ atmosphere (19).

Outer membrane vesicles extraction

OMVs were isolated as described previously (20). Briefly, after an overnight cultivation, the medium was centrifuged at 6000 g, 4°C. The pellets were washed twice with phosphate buffer solution (PBS) and re-suspended in 9% sodium chloride solution. Then the suspension was centrifuged for 1 hour at 6000 g, 4°C. OMVs were extracted through sequential centrifugation for 90 minutes at 20000 g, 4°C using Tris-ethylene diamine tetra acetic acid (EDTA)-sodium deoxycholate (Sigma-Aldrich, USA) buffers. Finally, OMVs were stored at -20°C (20).

Scanning electron microscopy

The OMVs were fixed in PBS containing 2.5% glutaraldehyde and 2% paraformaldehyde. Following PBS washing, the samples were air-dried and coated with gold by sputter coater (KYKY Technology, China) (using physical vapor deposition method. The prepared samples were examined by SEM (KYKY Technology, China) (21).

Cell culture and treatment

The human epithelial cell line, IBRC C10094 Caco-2, was obtained from Iranian Biological Resource Center. The cells were grown in Dulbecco's modified eagle medium (DMEM/high glucose; Gibco™, USA), supplemented with 10% fetal bovine serum (FBS, Gibco™, USA) and 1% penicillin/streptomycin (Gibco™, USA) and incubated at 37°C in a 5% CO₂ atmosphere (22). The cells were treated with *B. fragilis* and OMVs (180 and 350 µg/ml) and incubated overnight.

RNA isolation and cDNA synthesis

Total RNA was isolated using RNX-Plus (CinnaGen, Iran). RNA quantity and quality were respectively evaluated by NanoDrop 2000 (Thermo Fisher Scientific, USA) and gel electrophoresis. cDNAs were synthesized by RevertAid first strand cDNA synthesis kit (Thermo Scientific, USA) according to manufacturers' instructions.

Quantitative reverse transcriptase polymerase chain reaction analysis

Quantitative reverse transcriptase polymerase chain reaction (qRT-PCR) was performed using LightCycler® 96 SW 1.1 instrument (Roche, Germany). Each reaction mixture was composed of SYBR Premix Ex Taq II (Takara, China), specific primers (Table 1) and DNA template. *GAPDH* was used as housekeeping gene. The amplification program was consisted of 1 cycle at 95°C for 60 seconds, followed by 40 cycles of denaturation at 95°C for 5 seconds, annealing at 55°C for 30 seconds and extension at 72°C for 30 seconds.

Table 1: List of primers for quantitative reverse transcriptase-polymerase chain reaction (qRT-PCR) analysis

Gene	Prime sequence (5'-3')
<i>GAPDH</i>	F: GGAGCGAGATCCCTCCAAAAT
	R: GGCTGTTGTCATACTTCTCATGG
<i>TLR2</i>	F: TTATCCAGCACACGAATACACAG
	R: AGGCATCTGGTAGAGTCATCAA
<i>TLR4</i>	F: AGACCTGTCCCTGAACCCTAT
	R: CGATGGACTTCTAAACCAGCCA

Cytokines concentration assay

Following overnight incubation of Caco-2 cells with *B. fragilis* and its OMVs, the supernatants were collected and stored at -20°C . The $\text{IFN}\gamma$, IL-10 and IL-4 concentrations were measured using enzyme-linked immunosorbent assay (ELISA) kit (Human cytokine ELISA^{PRO} kit, MABTECH, Swedish biotech, Sweden), according to manufacturer's instructions.

Statistical analyses

Data were analyzed by independent sample t test and one-way ANOVA using GraphPad Prism software (GraphPad Software, Inc., San Diego, CA). All results demonstrate as mean \pm standard deviation (SD). In all experiments, $P < 0.05$ was considered statistically significant.

Results

Properties of *B. fragilis* derived outer membrane vesicles

B. fragilis produced OMVs in BHI broth. The morphology and size of OMVs were examined by SEM. Diameter of spherical shaped OMVs was in the range of 30-110 nm (Fig.1). Mean dimension of OMVs was 85.7 ± 15.3 nm.

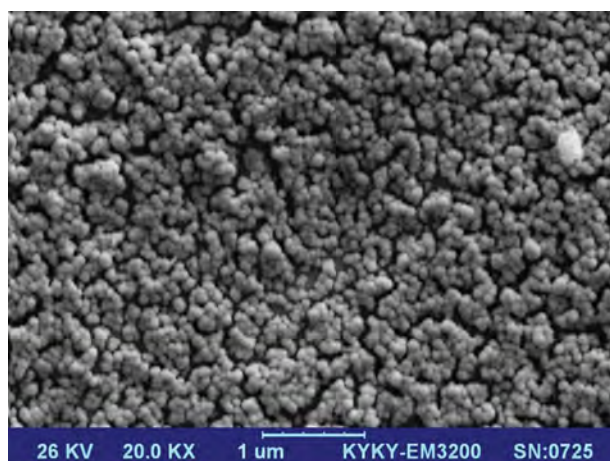


Fig.1: *B. fragilis* produces outer membrane vesicles (OMVs) with a mean dimension of 85.7 ± 15.3 nm: scanning electron microscopy of *B. fragilis* derived-OMVs (magnification: $\times 20\text{K}$).

Effect of *B. fragilis* and outer membrane vesicles on TLR gene expressions

Human intestinal epithelial cell line Caco-2 was used to study the effects of *B. fragilis* and its OMVs on *TLR2* and *TLR4* gene expressions using qRT-PCR. *B. fragilis* significantly decreased *TLR2* gene expression. *TLR4* gene expression was slightly increased by this bacterium (Fig.2A). The cells were treated with *B. fragilis* derived OMVs in two concentrations, 180 and 350 $\mu\text{g}/\text{ml}$. The mRNA levels of *TLR2* were slightly increased in both of OMVs concentrations. Interestingly, *TLR4* gene expression was decreased

and significantly increased at 180 and 350 $\mu\text{g}/\text{ml}$ of OMVs, respectively (Fig.2B).

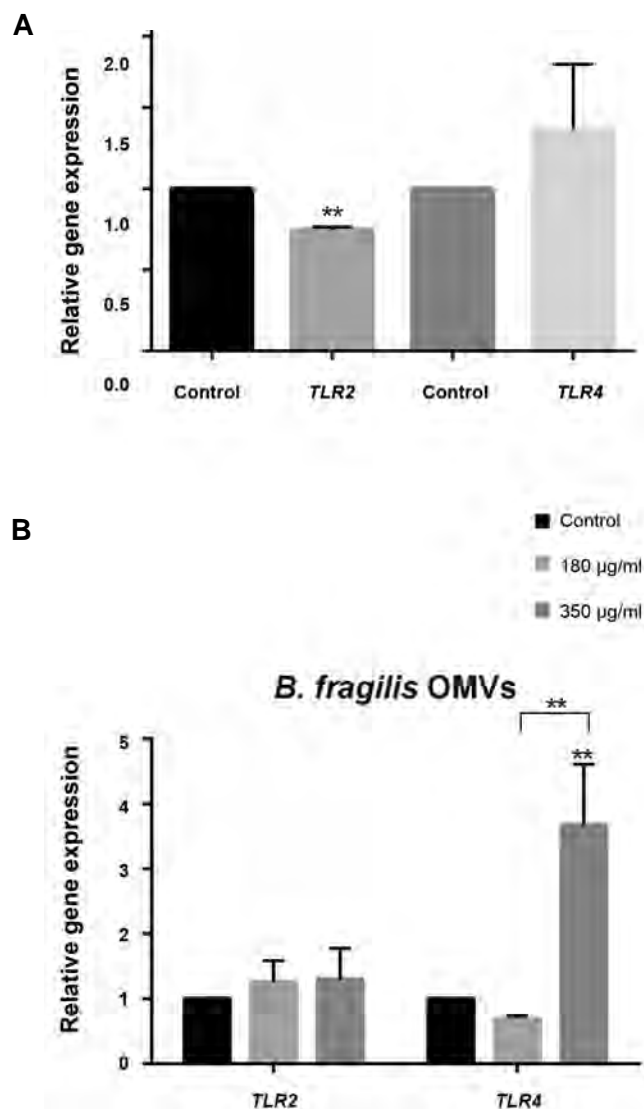


Fig.2: Quantitative reverse transcriptase-polymerase chain reaction (qRT-PCR) analyzes of *B. fragilis* and its outer membrane vesicles (OMVs) on *TLR* gene expressions. **A.** The cells were initially deprived of serum and then treated with either *B. fragilis* or phosphate buffer solution (PBS) overnight and **B.** In the same condition, the other group cells were treated with either *B. fragilis* derived OMVs (350 and 180 $\mu\text{g}/\text{ml}$) or sucrose, overnight. Values of triplicate experiments are demonstrated as mean \pm SD. Significant results are presented as ** based on $P < 0.01$.

Effect of *B. fragilis* and outer membrane vesicles on cytokines concentration

After overnight stimulation of Caco-2 cells by *B. fragilis* and its OMVs, the concentration of pro-inflammatory ($\text{IFN}\gamma$) and anti-inflammatory (IL-4 and IL-10) cytokines were measured by ELISA. *B. fragilis* significantly elevated $\text{IFN}\gamma$ concentration (Fig.3A). Interestingly, $\text{IFN}\gamma$ concentration was decreased by 180 and 350 $\mu\text{g}/\text{ml}$ of OMVs (Fig.3B). *B. fragilis* was able to increase IL-4 and IL-10 concentrations (Fig.3A). In addition, the related OMVs of this bacterium (180 and 350 $\mu\text{g}/\text{ml}$) significantly enhanced IL-4 and IL-10 concentrations (Fig.3B).

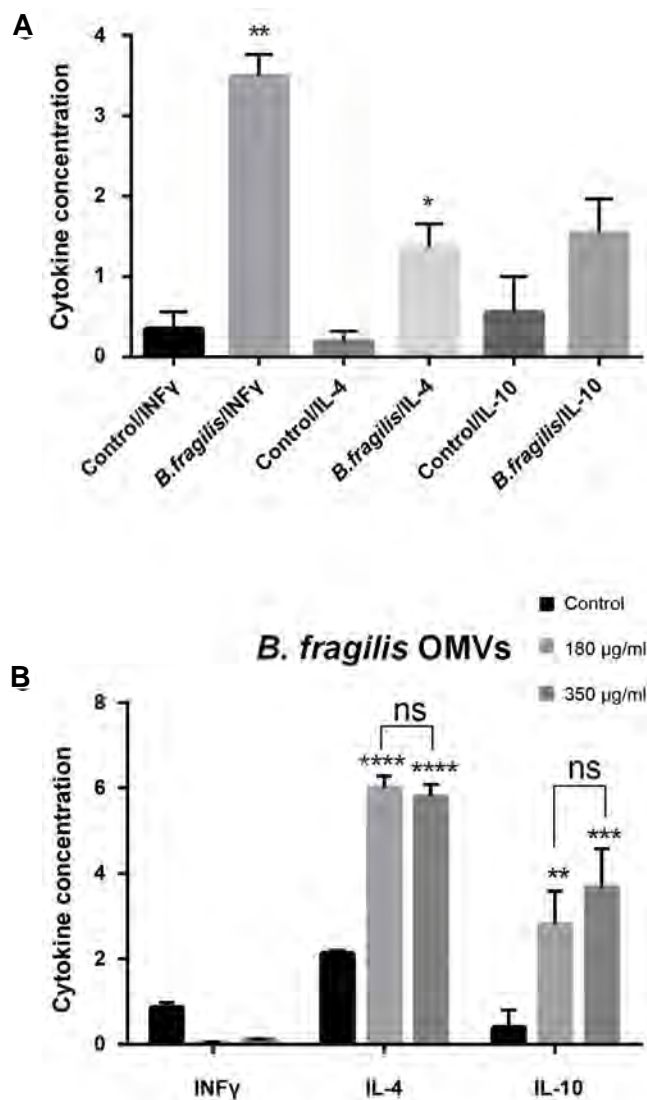


Fig. 3: ELISA analyzes of *B. fragilis* and its outer membrane vesicles (OMVs) on cytokines concentration. **A.** Cells were initially deprived of serum and then treated with either *B. fragilis* or phosphate buffer solution (PBS), overnight and **B.** In the same condition, the other group cells were treated with either *B. fragilis* derived OMVs (350 and 180 µg/ml) or sucros, for overnight. Values of triplicate experiments are demonstrated as mean \pm SD. Significant results are presented as *, **, ***, **** based on $P < 0.05$, $P < 0.01$, $P < 0.001$, and $P < 0.0001$.

Discussion

The epithelial layer of GI tract is continuously exposed to huge amount of immunogenic stimulatory molecules, derived from gut microbiota, nutrient and pathogenic microorganisms (3). IEPCs are the interface between gut microbiota and immune system via lamina propria cells. The potential of IEPCs to modulate immunity depends on PRRs gene expression (5). Additionally, the gut microbiota has immunomodulation potential in host. In this regard, *B. fragilis* and its OMVs affect gut microbiota-host interactions (15). Therefore, we aimed to study in more details the effects of *B. fragilis* and its OMVs on TLR genes expression and cytokines concentration in Caco-2 cell line as a human IEPCs model.

It has been found that TLRs play a crucial role in

immune responses and *B. fragilis* influences homeostasis and immunity (14). In other words, *B. fragilis* activate CD4⁺ T cells responses through TLR2 signaling in DCs. *B. fragilis* has anti-inflammatory effects through mediation of Th1/Th2 balanced ratio, as well as CD4⁺ T cells differentiation into Tregs and Th17 limited responses (17). Moreover, TLRs signaling in GI epithelium triggers the cross talk between gut microbiota and the host, locally and systemically (6). TLRs signaling is involved in proliferation, differentiation of IEPCs alongside with induction of pro- and anti-inflammatory cytokines responses. As IEPCs are located in frontline of gut environment, their TLRs signaling has critical role in immune tolerance to gut microbiota and defense against pathogens (8). Expression patterns and induction mode of TLRs are different throughout GI epithelium. IEPCs have relatively low expression of TLR2 and TLR4, which are the main receptors for gram positive and negative bacterial MAMPs (9). In this regard, Furrie et al. (23) reported that *B. fragilis* does not change the *TLR1-4* expression levels in Caco-2 cell line. In our study, although *B. fragilis* significantly decreased *TLR2*, but increased *TLR4* gene expression. Perhaps, differences in bacterial quantity and incubation time could justify this discrepancy.

As mentioned above, gut microbiota could intervene with cytokines secretion. For instance, *B. fragilis* has immune-modulatory effect through induction of IL-10 and reduction of IL-17 production during intestinal inflammation (17). Bahrami et al. (24) studied the influence of intestinal commensal bacteria (i.e. *B. fragilis*) on pro- and anti-inflammatory cytokine productions. Their data showed that *B. fragilis* did not affect cytokine concentration. However, we noticed that IFN γ , IL-4 and IL-10 concentrations were increased after corresponding treatment.

It has been demonstrated that *B. fragilis* releasing OMVs is an influential factor for mediation of immune responses. Since *B. fragilis* apparently does not have well established secretory system, immunogenic components (PSA) delivery is facilitated through OMVs production. Shen et al. have shown that *B. fragilis* has protective role against intestinal inflammatory disease in animal model via OMVs production. Indeed, *B. fragilis* OMVs induce Treg development and IL-10 production thorough TLR2 signaling in DCs (17, 18). We believe that this is the first study reporting the effects of *B. fragilis*-derived OMVs on *TLR2* and *TLR4* genes expression, as well as the concentration of IFN γ , IL-10 and IL-4 on Caco-2 cell line. Taken together, our results depicted that *TLR2* mRNA levels were not altered by *B. fragilis* derived OMVs. However, these vesicles significantly changed *TLR4* gene expression. Interestingly, *B. fragilis* derived OMVs had stimulatory effect on anti-inflammatory cytokines (IL-4 and IL-10) while it decreased IFN γ concentration as a pro-inflammatory cytokine.

Conclusion

Based on immunomodulatory effects of *B. fragilis*

derived OMVs on immune system and our current findings, we suggest that these OMVs may have a substantial role in the improvement of the inflammatory responses and it may have yet no recognized and understudied function in the inter-kingdom modulation of host genes.

Acknowledgements

This research was funded by Iran Biotech Fund grant 94/10243 and Pasteur Institute of Iran. The authors would like to thank Fatemeh Ettehad Marvasti for her help and our colleagues at Pasteur Institute of Iran. There is no conflict of interest in this study.

Authors' Contributions

S.A.B., S.D.S.; Contributed to conception and design. S.A.B., S.D.S., S.K., S.I.; Contributed to all experimental work, data and statistical analysis, and interpretation of data. S.D.S.; Was responsible for overall supervision. All authors read and approved the final manuscript.

References

1. Sekirov I, Russell SL, Antunes LC, Finlay BB. Gut microbiota in health and disease. *Physiol Rev.* 2010; 90(3): 859-904.
2. Ho JT, Chan GC, Li JC. Systemic effects of gut microbiota and its relationship with disease and modulation. *BMC Immunol.* 2015; 16: 21.
3. Round JL, Mazmanian SK. The gut microbiota shapes intestinal immune responses during health and disease. *Nat Rev Immunol.* 2009; 9(5): 313-323.
4. Muraca M, Putignani L, Fierabracci A, Teti A, Perilongo G. Gut microbiota-derived outer membrane vesicles: under-recognized major players in health and disease. *Discov Med.* 2015; 19(106): 343-348.
5. König J, Wells J, Cani PD, García-Ródenas CL, MacDonald T, Mercenier A, et al. Human intestinal barrier function in Health and Disease. *Clin Transl Gastroenterol.* 2016; 7(10): e196.
6. Vereecke L, Beyaert R, van Loo G. Enterocyte death and intestinal barrier maintenance in homeostasis and disease. *Trends Mol Med.* 2011; 17(10): 584-593.
7. Gourbeyre P, Berri M, Lippi Y, Meurens F, Vincent-Naulleau S, Lafitte J, Rogel-Gaillard C, Pinton P, Oswald IP. Pattern recognition receptors in the gut: analysis of their expression along the intestinal tract and the crypt/villus axis. *Physiol Rep.* 2015; 3(2). pii: e12225.
8. Fukata M, Arditi M. The role of pattern recognition receptors in intestinal inflammation. *Mucosal Immunol.* 2013; 6(3): 451-463.
9. Hooper LV, Littman DR, Macpherson AJ. Interactions between the microbiota and the immune system. *Science.* 2012; 336(6086): 1268-1273.
10. Yu S, Gao N. Compartmentalizing intestinal epithelial cell toll-like receptors for immune surveillance. *Cell Mol Life Sci.* 2015; 72(17): 3343-3353.
11. Woting A, Blaut M. The intestinal microbiota in metabolic disease. *Nutrients.* 2016; 8(4): 202.
12. Boulangé CL, Neves AL, Chilloux J, Nicholson JK, Dumas ME. Impact of the gut microbiota on inflammation, obesity, and metabolic disease. *Genome Med.* 2016; 8(1): 42.
13. Gérard P. Gut microbiota and obesity. *Cell Mol Life Sci.* 2016; 73(1): 147-162.
14. Maier E, Anderson RC, Roy NC. Understanding how commensal obligate anaerobic bacteria regulate immune functions in the large intestine. *Nutrients.* 2014; 7(1): 45-73.
15. Shen Y. Interkingdom communication of a bacterial mutualist and its mammalian host (Doctoral dissertation, California Institute of Technology). Presented for the Ph.D., California. California Institute of Technology. 2012.
16. Ahmadi Badi S, Moshiri A, Fateh A, Rahimi Jamnani F, Sarshar M, Vaziri F, et al. Microbiota-derived extracellular vesicles as new systemic regulators. *Front Microbiol.* 2017; 8: 1610.
17. Troy EB, Kasper DL. Beneficial effects of *Bacteroides fragilis* polysaccharides on the immune system. *Front Biosci (Landmark Ed).* 2010; 15: 25-34.
18. Shen Y, Giardino Torchia ML, Lawson GW, Karp CL, Ashwell JD, Mazmanian SK. Outer membrane vesicles of a human commensal mediate immune regulation and disease protection. *Cell Host Microbe.* 2012; 12(4): 509-520.
19. Elhenawy W, Debelyy MO, Feldman MF. Preferential packing of acidic glycosidases and 278 proteases into *Bacteroides* outer membrane vesicles. *MBio.* 2014; 5(2): e00909- e00914.
20. Siadat SD, Vaziri F, Eftekhary M, Karbasian M, Moshiri A, Aghasadeghi MR, et al. Preparation and evaluation of a new lipopolysaccharide-based conjugate as a vaccine candidate for brucellosis. *Osong Public Health Res Perspect.* 2015; 6(1): 9-13.
21. Nakao R, Hasegawa H, Ochiai K, Takashiba S, Ainai A, Ohnishi M, et al. Outer membrane vesicles of *Porphyromonas gingivalis* elicit a mucosal immune response. *PLoS One.* 2011; 6(10): e26163.
22. Sato K, Kumita W, Ode T, Ichinose S, Ando A, Fujiyama Y, et al. OmpA variants affecting the adherence of ulcerative colitis-derived *Bacteroides vulgatus*. *J Med Dent Sci.* 2010; 57(1): 55-64.
23. Furrir E, Macfarlane S, Thomson G, Macfarlane GT; Microbiology & Gut Biology Group; Tayside Tissue & Tumour Bank. Toll-like receptors-2,-3 and-4 expression patterns on human colon and their regulation by mucosal-associated bacteria. *Immunology.* 2005; 115(4): 565-574.
24. Bahrami B, Macfarlane S, Macfarlane GT. Induction of cytokine formation by human intestinal bacteria in gut epithelial cell lines. *J Appl Microbiol.* 2011; 110(1): 353-363.

Evaluation of Tumor Regulatory Genes and Apoptotic Pathways in The Cytotoxic Effect of Cytochalasin H on Malignant Human Glioma Cell Line (U87MG)

Samaneh Heidarzadeh, M.Sc.¹, Gholamreza Motaleb, Ph.D.^{1*}, Mohammad Jalil Zorriehzahra, Ph.D.²

1. Department of Biology, Faculty of Science, University of Zabol, Zabol, Iran

2. Department of Aquatic Animal Health and Diseases, Iranian Fisheries Science Research Institute (IFSRI), Agricultural Research, Education and Extension Organization (AREEO), Tehran, Iran

*Corresponding Address: P.O.Box: 98613-35856, Department of Biology, Faculty of Science, University of Zabol, Zabol, Iran
Email: reza.motaleb@uoz.ac.ir

Received: 3/Apr/2018, Accepted: 22/May/2018

Abstract

Objective: The aim of current study was to provide a proof-of-concept on the mechanism of *PLAU* and *PCDH10* gene expressions and caspases-3, -8, and -9 activities in the apoptotic pathway after treatment of malignant human glioma cell line (U87MG) with cytochalasin H.

Materials and Methods: In the present experimental study, we have examined cytochalasin H cytotoxic activities as a new therapeutic agent on U87MG cells *in vitro* for the first time. The cells were cultured and treated with 10^{-5} - 10^{-9} M of cytochalasin H for 24, 48 and 72 hours. The assessment of cell viability was carried out by (3-(4,5-dimethylthiazol-2-yl)-2,5-diphenyltetrazoliumbromide (MTT) assay at 578 nm. The data are the average of three independent tests. mRNA expression changes of *PLAU* and *PCDH10* were then evaluated by quantitative reverse-transcriptase polymerase chain reaction (qRT-PCR). The fluorometric of caspases-3, -8, and -9 activities were carried out. The morphology changes in the U87MG cells were observed by fluorescence microscope.

Results: MTT assay showed that cytochalasin H (10^{-5} M) inhibited the U87MG cancer cells proliferation after 48 hours. Analysis of qRT-PCR showed that the *PLAU* expression was significantly decreased in comparison with the control ($P < 0.05$). The expression of *PCDH10* also showed a significant increase when compared to the control ($P < 0.001$). Fluorescence microscope indicated morphological changes due to apoptosis in U87MG cancer cells, after treatment with cytochalasin H (10^{-5} M, 48 hours). The fluorometric evaluation of caspase-3, -8, and -9 activities showed no significant difference between the caspases and the control group.

Conclusion: This study shows the effect of caspase-independent pathways of the programmed cell death on the U87MG cancer cell line under cytochalasin H treatment. Further studies are needed to explore the exact mechanism.

Keywords: Caspases, Cytochalasin H, Glioblastoma, Plasminogen Activator Urokinase, Protocadherin-10

Cell Journal (Yakhteh), Vol 21, No 1, Apr-Jun (Spring) 2019, Pages: 62-69

Citation: Heidarzadeh S, Motaleb Gh, Zorriehzahra MJ. Evaluation of tumor regulatory genes and apoptotic pathways in the cytotoxic effect of cytochalasin H on malignant human glioma cell line (U87MG). Cell J. 2019; 21(1): 62-69. doi: 10.22074/cellj.2019.5948.

Introduction

Glioblastoma multiforme is characterized by the code 3/9440 in the International Classification of Diseases for Oncology (ICD-O) (1). This is the most common and aggressive tumor among primary brain tumors in adults (2). Recent statistics report the incidence rate of 3.20 per 100,000 individuals for this disease (3).

Applying the mesenchymal model, glioblastoma cells can propagate and spread to the adjacent cells. This has been proved as a limiting factor in the treatment of this tumor (4). Moreover, glioblastoma cells dramatically attack the brain parenchyma, resulting in a very poor prognosis (5, 6).

The origin of these tumors is glial cells, composed of about 14.9% of all primary brain tumors and 56.1% of all gliomas (3). Despite the efforts carried out to improve treatment of glioma tumor, these are not curable. The conventional methods of glioblastoma treatment are surgery, radiotherapy, and chemotherapy (7). Although chemotherapy is effective in tumor treatment, the utilized

drugs have side-effects. Sometimes, drug resistance causes limitations in the treatment of patients. Cytochalasins are alkaloids mycotoxins, as widely available compounds in fungi. These are extracted from an endophytic fungus, named *Rhizoglyphus* sp, found in a Chinese medical plant, named *Tripterygium*. Cytochalasins target the microfilaments in the cytoskeleton (8). Cytochalasins connect to their sub-units, leading to some alterations in the cytoskeleton structure and preventing polymerization. Thus, formation of microfilaments is significantly inhibited (9). These inhibitors cause cell division by connection and interaction with the microtubule-microfilament system. In addition, cellular processes are affected by cell morphology (10, 11).

Moreover, cytochalasins prevent cell transfer and create enucleated cells by penetrating the cell membrane. Additionally, cytochalasins using a variety of mechanisms affect the other biological process aspects associated with actin polymerization (12).

Many types of cytochalasins such as A, B, C, D, E,

O, and H have been identified (8), Cytochalasin H is isolated from *Paspalum scrobiculatum* Linn and affects reorganization of the cytoskeleton as an effective factor. It is a metabolite of *Phomopsis paspali*. Cytochalasin H also exerts influence on the activity of the central nervous system (13).

Apoptosis is the consequence of a planned intracellular cascade of genetically controlled stages. Caspases act an important function in the performance stage of apoptosis and they are accountable for numerous biological and morphological alterations related to the programmed cell death. Different types of caspase are identical in amino acid sequence, construction, and substrate specificity. Thusfar, 14 caspases have been recognized. Caspases have been classified based on the sequence homology, into three subclasses, including: caspase-1 subfamily (caspases-1, -4, -5, -11, -12 and -13), caspase-2 subfamily (caspases-2 and -9) as well as caspase-3 subfamily (caspases-3, -6, -7, -8 and -10). Caspases-2, -8 and -9 play initiator roles, while caspases-3, -6 and -7 are effectors (14, 15).

About 840 genes have been thus far identified to be involved in the glioblastoma, study of which can lead to design glioblastoma therapeutic strategies (16). Protocadherins are the biggest subsets of cadherins in the cell adhesion molecule groups. These are mainly expressed in the nervous system (17). There have been about 70 protocadherin genes identified in the mammalian genome (18).

PCDH10 belongs to the non-clustered protocadherins in the δ -2 protocadherin family (19). This gene is located in the chromosome 4q^{28.3} (20). *PCDH10* is considered as a tumor suppressor gene, suppressing different tumors including leukemia, lung, esophageal, colorectal and breast cancers. It is effective in cell cycle regulation and, in fact, prevents rapid growth and cell division (21).

PLAU gene is associated with cancer and located in the chromosome 10q^{22.2}. Overexpression of urokinase plasminogen activator gene (*uPA*) and its receptor (*uPAR*) has been observed in the breast, bladder, lung, pancreatic, liver and colorectal cancers (22). This gene encodes serine protease, which converts plasminogen to plasmin (23). *PLAU*, as a motivator of metastasis, encodes protein activating plasminogen urokinase, connected to the specific receptors. *PLAU* performs a key role in adjustment of the cells migration and adhesion during tissue regeneration and intracellular signaling (24). Expression of this gene in different cancers causes cell invasion and metastasis of the tumor cells to the surrounding tissues (25).

On this basis, the aim of current study was to provide a proof-of-concept on the mechanism of *PLAU* and *PCDH10* gene expressions, and caspases-3, -8, and -9 activities in the apoptotic pathway after treatment of malignant human glioma cell line (U87MG) by cytochalasin H. To our knowledge, this is the first report of cytochalasin H cytotoxic activities effect on the U87MG cells.

Materials and Methods

Cell culture and treatment with cytochalasin H

Agent treatment

Cytochalasin H was purchased from Sigma-Aldrich (USA). In all experiments, 1mg cytochalasin H was dissolved in 1ml Dimethyl Sulfoxide (DMSO, Sigma, USA) and maintained at -70°C. For cytochalasin H treatment, a relevant amount of stock solution (75 μ l cytochalasin H in 15 μ l DMEM medium) was prepared to the final concentrations of 10⁻⁵M.

Cell culture

In this experimental study, the malignant human glioma cell line U87MG (ATCC® HTB-14™) was obtained from Pasteur Institute (Iran). The cells were cultured in T25 flasks in Dulbecco's Modified Eagle's Medium (DMEM, Gibco-invitrogen, USA), comprising 10% fetal bovine serum (FBS, Gibco-invitrogen, USA), in 95% humidified environment at 37°C with 5% CO₂.

MTT assay

The 3-(4, 5-Dimethylthiazol-2-yl)-2, 5-diphenyltetrazolium (MTT) assay was employed to assess the cytotoxic impact of cytochalasin H on malignant human glioma cell line (U87MG) using Sigma-Aldrich (USA). For this, U87MG cells were placed in 96-well plates (10000 cells/well). After 24 hours, fresh DMEM medium, containing different concentrations of cytochalasin H (10⁻⁵-10⁻⁹ M), was added at 100 μ l volume per well, respectively, for 24, 48, and 72 hours. Each concentration has eight replicated wells. After incubation, the media were substituted by 100 μ l of 0.5 mg/ml MTT and then the cells were further incubated at 37°C for four hours. MTT was exchanged with isopropanol and the absorbance was measured using an absorbance micro-plate reader/Elisa DNM-9602G (Madell Technology Corp, USA) at 578 nm. Furthermore, MTT assay was repeated for normal HEK cells compared to U87MG cells.

PLAU and *PCDH10* quantitative reverse-transcriptase polymerase chain reaction evaluations

For evaluating *PLAU* and *PCDH10* gene expression levels using quantitative reverse-transcriptase polymerase chain reaction (qRT-PCR) technique, U87MG cells (5 \times 10⁵) were cultured and treated with cytochalasin H (10⁻⁵ M). After 24 hours, RNA was isolated by RNA extraction kit Transgen Biotech ER101-01 (China), from the U87MG cells and concentration was analyzed by nanodrop instrument (Nanodrop ND-1000 Technologies, USA). cDNA synthesis was performed using Transgen Biotech AE301-02 kit (China). Primers for amplification of *PCDH10* and *PLAU* were designed using Beacon Designer, Gene Runner and Primer Express Software. The primer sequences are represented in Table 1. RT-PCR program was initiated by incubating at 94°C for five minutes. This was followed by 30 cycles of 94°C,

54°C, and 72°C (30 seconds each). A last step of seven minutes (72°C) was performed. Moreover, PCR products were analyzed by agarose gel electrophoresis. qRT-PCR was carried out using ABI StepOne Real-Time PCR thermal cycler (Applied Biosystems, USA). 10 µl SYBR Green master mix, 1 µl cDNA, 1µl of forward and reverse primers (10 pmol) and 7 µl of nuclease-free water was put into each capillary tube. Each sample was performed in triplicate. The default program conditions of ABI Software were 10 minutes at 94°C (initial stage). Then, 40 cycles were carried out consisting denaturation (1 minute, 94°C), annealing and extension (70 seconds, 55°C). Melting curves were evaluated in order to confirm the specificity of PCR products.

Morphological examination by fluorescence microscope

U87MG cells (5×10^5) were treated with 10^{-5} M cytochalasin H for 48 hours, and subsequently collected and fixed in 80% Aston at 4°C for 20 minutes. The cells were then stained by Hoechst 33342 in dark for five minutes followed by thorough washing with phosphate-buffered saline (PBS). Finally, morphology changes in the U87MG cells were observed by fluorescence microscope (Nikon Eclipse Ti-S, USA).

Caspase enzymatic activity assay

The fluorometric of caspases-3, -8 and -9 activities were carried out using the NOVEX caspases kit assay (USA). This was done to quantitate the enzyme activity of caspases recognizing amino acid sequence, DEVD (for caspase-3), IETD (for caspase-8) and LEHD (for caspase-9). Briefly, U87MG cells were treated with 10^{-5} M cytochalasin H in

5% CO₂ at 37°C for 48 hours. Moreover, the cells (3×10^6 per sample) were collected and added to 50 ml lysis buffer on ice for 10 minutes. Following centrifugation at 10,000 g for one minute, the lysate was collected and stored at -20°C until use. Protein concentration was assayed according to the Bradford method cytosol extract samples containing 300 µg total protein, used for caspase activity. The samples were added to 96-well plates with substrates at 37°C for two hours. The color absorbance was measured at a wave length of 405 nm in an ELISA reader (DNM-9602G, China).

Statistical analysis

Each test was carried out in triplicate. The data are presented as mean \pm SD. Student's t test and one-way analysis of variance (ANOVA) was done to assess the significant difference through the data using IBM SPSS (IBM, USA) version 13.0. $P < 0.05$ was considered statistically significant.

Results

Effect of cytochalasin H on the proliferation inhibition and viability of U87MG Cells

Effect of cytochalasin H on the proliferation inhibition and viability of the U87MG cells were investigated using MTT assay. The results showed that cytochalasin H at concentration of 10^{-5} M inhibited the U87MG cancer cells proliferation for 48 hours ($P < 0.05$), however there was no cytochalasin H toxic effects on the U87MG cancer cells after 24 and 72 hours ($P > 0.05$, Fig. 1A). Interestingly, there was not cytochalasin H toxicity effects on the normal (HEK) cell line compared to the U87MG cancer cells ($P > 0.05$, Fig. 1B).

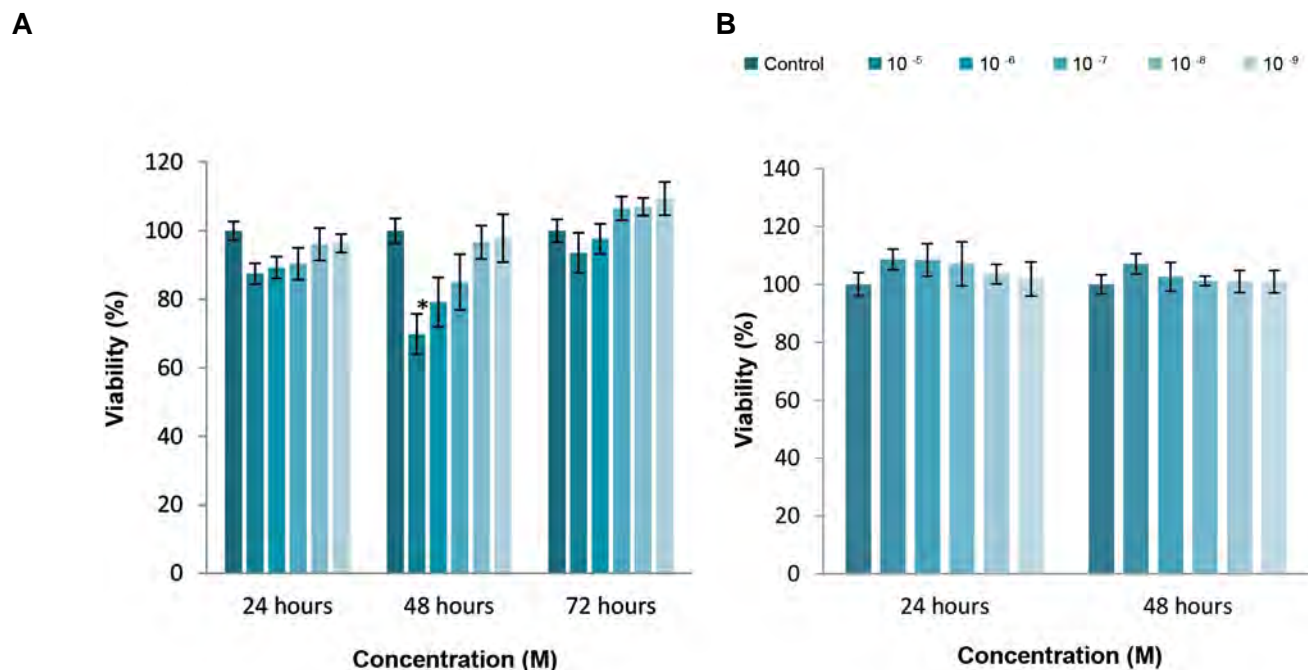


Fig.1: Effects of different cytochalasin H concentrations on cancer cells and normal cells compared to the control. The proliferation was determined using MTT assay. **A.** U87MG (cancer cells) as observed in the MTT assay during 24, 48 and 72 hours. The results are reported as means \pm SD (*; $P < 0.05$, 48 hours) and **B.** HEK cells (normal cells) as observed using the MTT assay after 24 and 48 hours exposure. No significant difference was observed compared to the control group.

Table 1: The primer sequences applied for quantitative reverse-transcriptase polymerase chain reaction

Gene	GC	Tm (°C)	Sequence primer (5'-3')	Product size (bp)
<i>PCDH10</i>	50.0	57.9	F: TCG TGG GGA ATA TCG CTG AA	81
<i>PCDH10</i>	57.9	59.3	R: TTG AGT TGG GCA CCG TCT G	
<i>PLAU</i>	57.1	60.0	F: GGT CGC TCA AGG CTT AAC TCC	123
<i>PLAU</i>	47.6	58.8	R: CTT CAG CAA GGC AAT GTC GTT	

Effect of cytochalasin H on the *PCDH10*, *PLAU* gene expressions of U87MG Cells

The results showed that *PCDH10* gene expression was 8.59 times higher in U87MG cells treated with cytochalasin H, compared to the control. *PCDH10* gene expression was significantly increased ($P < 0.001$, Fig.2A). In addition, *PLAU* gene expression was 2.5 times lower in U87MG cells treated with cytochalasin H, compared to the control. *PLAU* gene expression was significantly decreased ($P < 0.05$, Fig.2B).

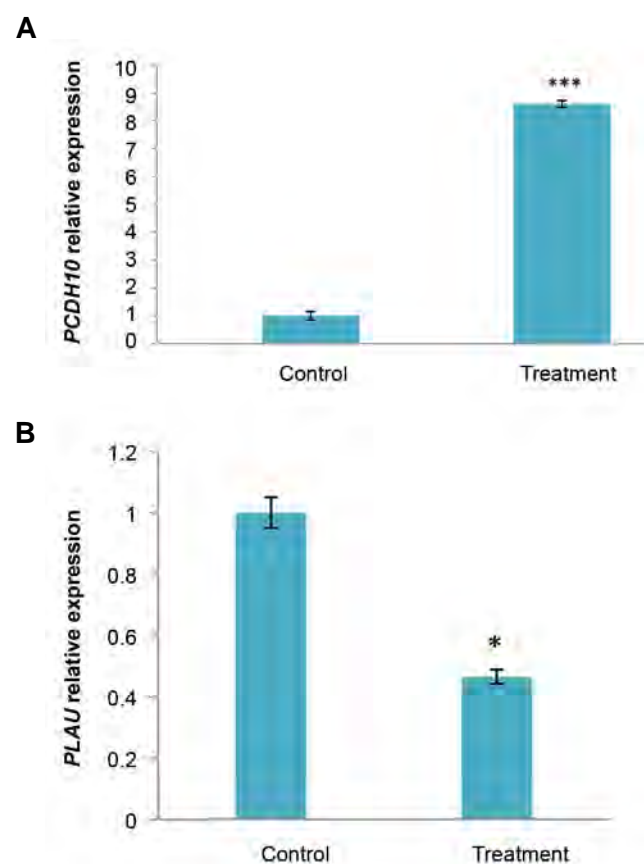


Fig.2: Expression level of some genes in U87MG cells after treatment with cytochalasin H (10^{-5} M) for 48 hours was evaluated by real-time polymerase chain reaction. **A.** *PCDH10* (tumor suppressor gene) and **B.** *PLAU* (oncogene). The data are expressed in terms of percent of control cells as the means \pm SD. ***; $P < 0.001$ and *; $P < 0.05$ compared to control.

Assessment of caspases-3, -8 and -9 assay

As shown in Figure 3A, protein concentration was assessed according to Bradford standard curve containing 300 μ g total protein in order to evaluate the caspase activity.

U87MG cells were treated with cytochalasin H (10^{-5} M) for 48 hours. As shown in Figure 3B, activity of caspase-3,

caspase-8 and caspase-9 were increased following cytochalasin H treatment (17, 12 and 7%, respectively), however no significant difference was observed ($P > 0.05$).

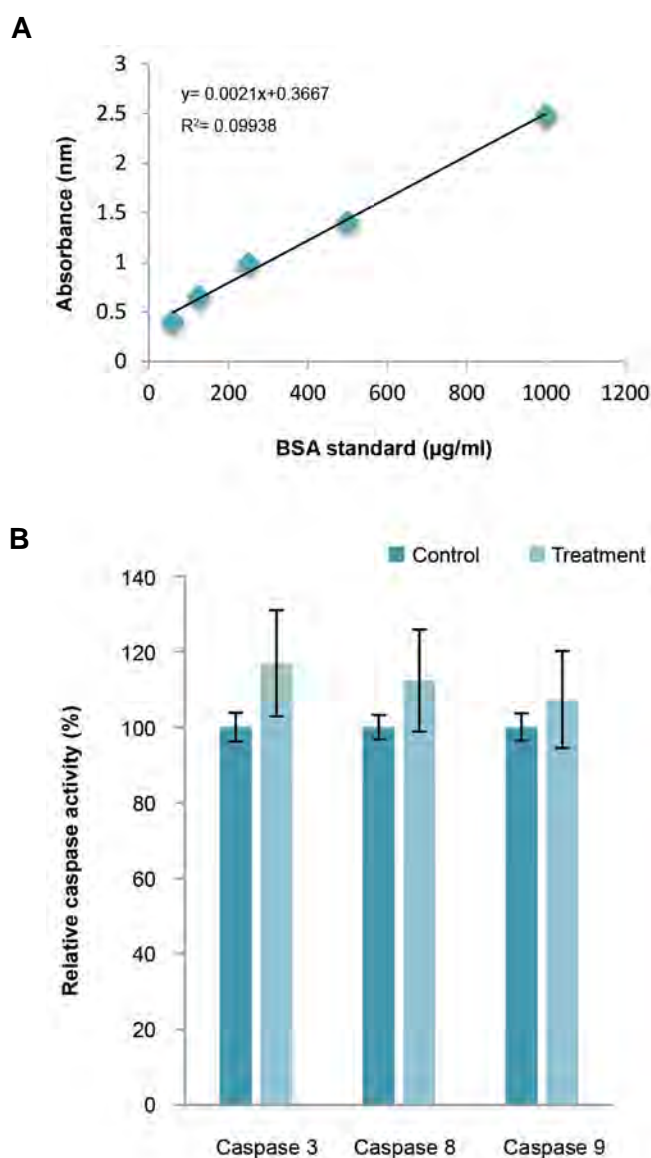


Fig.3: Stimulation of caspase-3, -8 and -9 Activity by cytochalasin H in U87MG Cells. **A.** A typical Bradford assay standard curve with samples ranging from 50 to 1000 μ g/ml BSA and **B.** Effects of cytochalasin H on caspases-3, -8, and 9 activities. U87MG cells were treated with cytochalasin H (10^{-5} M) for 48 hours. No significant difference was determined compared to the control group.

Morphological observation of human malignant glioma cell line using inverted and fluorescent microscope

After treatment for 24, 48 and 72 hours with 10^{-5} and

10^{-6} M cytochalasin H, structural changes of the cells were investigated under light microscope. Figure 4 shows the control cells with no exposure to cytochalasin H (series A), the cells exposed to cytochalasin H for 24 hours (series B), the cells exposed to cytochalasin H for 48 hours (series C) and the cells exposed to cytochalasin H for 72 hours (series D).

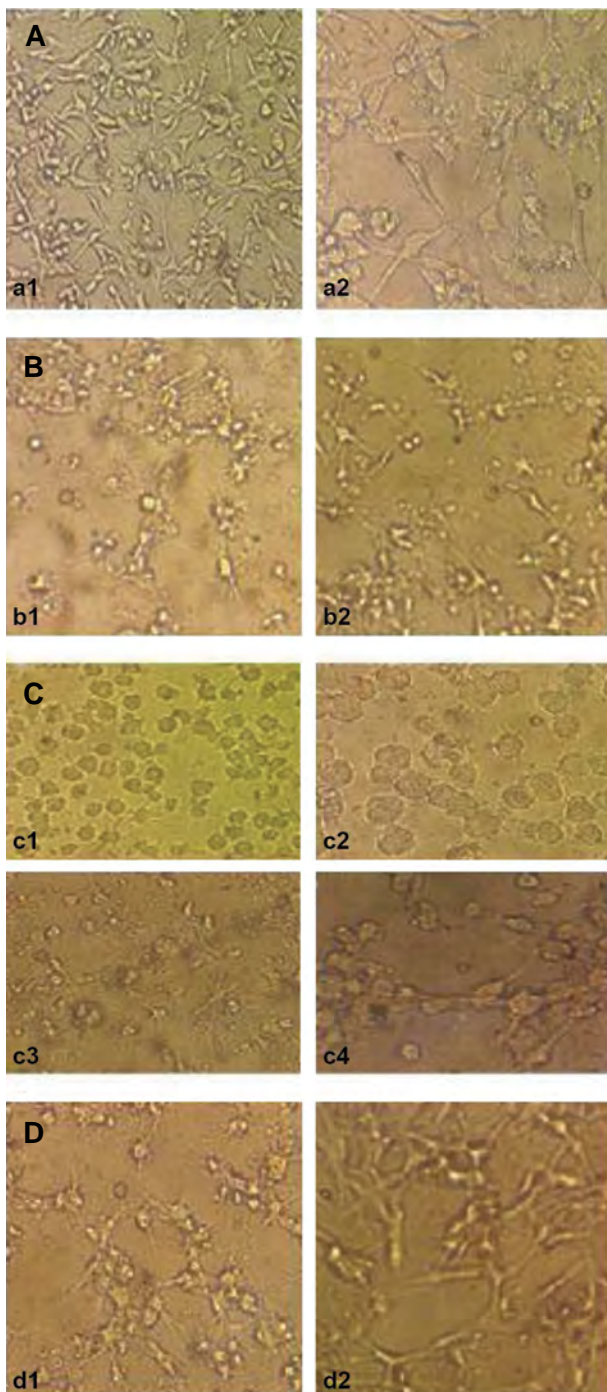


Fig.4: Light micrographs of the cancer cells exposed to cytochalasin H. **A.** Non treated U87MG cell cultures for 24, 48, 72 hours [magnifications: (a1) $\times 20$; (a2) $\times 40$], **B.** U87MG cells treated with cytochalasin H (b1) 10^{-5} M, (b2) 10^{-6} M for 24 hours [magnifications: (b1, b2) $\times 20$], **C.** U87MG cell treated with cytochalasin H (c1, c2) 10^{-5} M, (c3, c4) 10^{-6} M for 48 hours [magnifications: (c1, c3) $\times 20$, (c2, c4) $\times 40$], and **D.** U87MG cell treated with cytochalasin H (d1) 10^{-5} M, (d2) 10^{-6} M for 72 hours [magnifications: (d1, d2) $\times 20$].

After treatment for 48 hours with 10^{-5} M cytochalasin H, morphological changes were observed under fluorescence microscope. In the control group, normal nuclei were stained with a less bright blue fluorescence (Fig.5A). After cytochalasin H treatment, apoptotic cell nuclei were condensed and fragmented (Fig.5B).

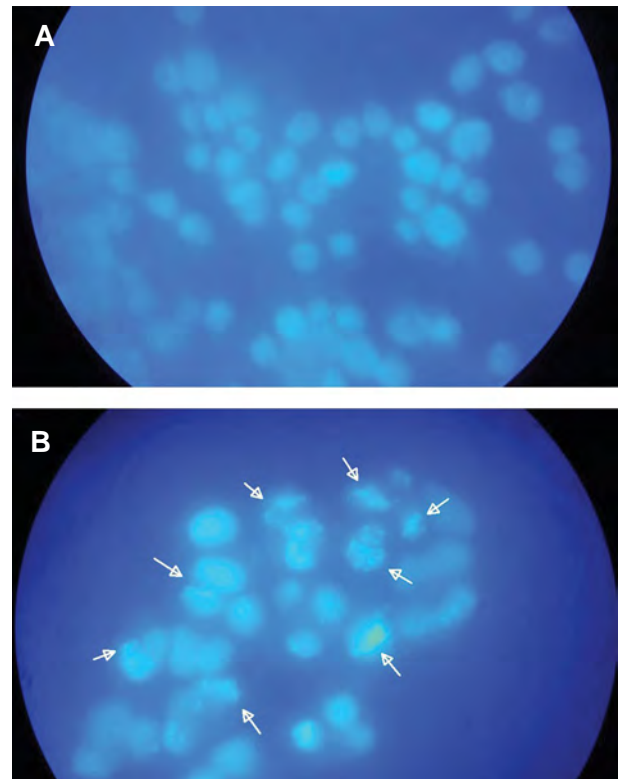


Fig.5: Morphological changes of U87MG cancer cells exposed to cytochalasin H (10^{-5} M) for 48 hours and imaged by fluorescence microscope. **A.** Illustration of the cells with normal nuclei (magnification: $\times 100$) and **B.** Illustration of the cells with apoptotic nuclei (arrowheads, magnification: $\times 100$).

Discussion

Glioblastoma is one of the most malignant central nervous system tumors located in the brain (26), with a weak prognosis. Insufficient cytotoxic factors currently exist for curing these tumors. Cytochalasins are recognized to inhibit a number of cancer types, but the effect of cytochalasin H on glioma cells is yet unidentified.

The goal of current investigation was to evaluate special effects of cytochalasin H on the U87MG cells and apoptosis. The most important outcome of this research was that cytochalasin H inhibited human glioma U87MG cells through apoptosis in a dose- and time-dependent manner. Despite development of the standard therapeutic solutions, treatment of glioblastoma has a very bad and disappointing prognosis and it is most likely to recur (27).

The mean survival of these patients is approximately 12-15 months, which is significantly decreased in older people (27). The impact of cytochalasins on the cell morphology and performances of normal and malignant

cells have been investigated *in vitro* (5, 28). Cytochalasins affect many cellular performances like cell adhesion, cell motility, secretion, drug delivery, etc. Along with chemotherapy, they induce significant clinical response in the cell systems. Cytochalasins are also considered as anti-tumor drugs for their strong feature (29).

In some studies, cytotoxic effects of cytochalasin E on the U87MG cell line (30) and impact of cytochalasin B on the U251MG, as a malignant human glioma cell line, were investigated (31). Furthermore, their impact on the inhibition of cell proliferation and growth of microfilaments were observed.

In this research, the effect of cytochalasin H (another member of cytochalasin family) on the U87MG cells was studied. Cytochalasin H significantly affects the cytoskeleton reorganization. The impact of toxicity of cytochalasin on the cancerous U87MG cell line, as well as normal HEK cells, was investigated. There was an increase of cytochalasin H toxicity in the cells treated with cytochalasin H for 48 hours. However, toxicity was statistically significant only at the concentration of 10^{-5} M. No cytochalasin H toxicity effect was observed in the cells treated with cytochalasin H for 72 hours and interestingly this important finding is in agreement with Tong et al. (31) reported that there was no difference between 72 and 96 hours after treatment of U251 cancer cell line by cytochalasin B.

It is proposed that could be due to the deactivation of the cytochalasin H components. However, lethal effect of this compound is possibly reduced *in vitro*. Therefore, U87MG cells need more time to be reproduced. Our results showed that cytochalasin H has no toxicity effect on the normal HEK cell line, which amazingly are consistent with Trendowski (32) who reported that the cytochalasins act to preferentially injury malignant cells, as revealed by their least influences on normal epithelial and immune cells.

The obvious signs of apoptotic cells include cell nucleus condensation, chromatin and cytoplasm, loss of phosphatidylserine cell membrane, DNA fragmentation, and connection of cell membrane to the apoptotic bodies (33). It was shown that the cells were appeared in a healthy and integrated form with normal nuclei, before treatment. However, cytoplasm of the cells, treated with cytochalasin H in a concentration of 10^{-5} M, was observed in a bubbled form with concentrated and fragmented nuclei. This indicated that the cells were directed towards apoptosis.

Apoptotic pathway procedure occurs in two forms: caspase-dependent and caspase-independent pathways (34). Caspases play pivotal role in the caspase-dependent apoptosis. By classifying, caspase-8 and caspase-9 were emphasized as initiator caspases (35). However, caspase-3 was classified as an effective caspase. Caspase-8 was activated through different apoptotic pathways, but the main apoptosis induction pathway was made through the extrinsic apoptosis pathway with the help of extrinsic

apoptosis induction markers of involving first apoptosis signal (FAS) (transmembrane protein) and immune cells. In the intrinsic apoptosis pathway, caspase-9 was activated by the release of cytochrome C (36). Caspase-9 led to the activation of the executive caspases (such as caspase-3), which operated on its own substrate giving rise to the apoptosis process (37).

The results obtained from this study showed that the enzyme activity of caspases was not sufficient to start the caspase-dependent apoptosis process. Moreover, statistical analysis of the caspase enzyme activity was not significant and, therefore, verified our results.

These results were inconsistent with the findings obtained from testing the cells by fluorescent microscope. The cell nuclei were observed, condensed, and fragmented under fluorescent microscope, and this is how the cells were led towards apoptosis. So, the effect of cytochalasin H on the induction of apoptosis in the U87MG cells could probably be attributed to the caspase-independent apoptosis pathway. Interestingly, our results are consistent with Trendowski (32) who reported that cytochalasins specially injure malignant cells via actin disruption.

Previous studies showed that some types of cell deaths might occur in the absence of caspase activation. Therefore, special inhibitors of caspase could stop their activity or the activity of caspase was proposed to be no sufficient for starting the caspase-dependent apoptosis process (38, 39). As of the apparent signs of caspase-independent apoptosis pathways are mitochondrial swelling, cytoplasmic vacuolation in the absence of caspase activation or nucleus alterations (33).

For the first time, our results showed that cytochalasin H could successfully increase the expression of *PCDH10* in the U87MG cells which is in agreement with Hirano and Takeichi (19); Nagase et al. (20); Wolverson and Lalande (21) and Andreasen et al. (22) reported that *PCDH10* gene plays a tumor suppressor role in most tumors and high expression of *PCDH10* in the tumor cells *in vitro* significantly inhibited the proliferation and re-invasion of tumor cells to the adjacent tissues.

On the other hand, our findings showed that the cytochalasin H could successfully decrease the expression of *PLAU* in U87MG cancer cells. This is compatible with Muñoz-Cánoves et al. (40) who reported that *uPA* levels were strongly down-regulated in C_2C1_2 myoblast cells after treating with cytochalasin B. However, they included that this phenomenon was reversible and specific. To sum it up, these results indicate the caspase-independent pathways (most probably through the cytoskeletal structure disruptions) of the programmed cell death in the U87MG cancer cell line under cytochalasin H treatment. However, the exact mechanisms should be further investigated.

Conclusion

Cytochalasin H shows cytotoxic activities on U87MG

cells in a dose- and time-dependent manner. More importantly, cytochalasin H induced apoptosis in glioma cells via the caspase-independent pathways (most probably through the cytoskeletal structure disruptions) together with decrease the expression of *PLAU* and increase the *PCDH10* respectively.

Acknowledgments

This work was funded, by University of Zabol, Islamic Republic of Iran and supported by Javid Biotechnology Company (JBC, Iran). The authors are grateful to Dr. Asgari in Javid Biotechnology Company (JBC, Iran). Authors have no conflict of interest.

Authors' Contributions

G.M.; Conducted and supervised the study design, data collection and evaluation, drafting, statistical analysis and was in charge of overall direction and planning. S.H.; Contributed to conception and design, perfumed data collection, all experimental work and drafting. M.J.Z.; Performed editing and approving the final version of this paper for submission, also participated in the finalization of the manuscript and approved the final draft and contributed to the project as co-supervisor. All authors read and approved the final manuscript.

Reference

- Xu H, Chen J, Xu H, Qin Z. Geographic variations in the incidence of glioblastoma and prognostic factors predictive of overall survival in US adults from 2004-2013. *Front Aging Neurosci.* 2017; 9: 352.
- Wang PF, Liu N, Song HW, Yao K, Jiang T, Li SW, et al. IDH-1R132H mutation status in diffuse glioma patients: implications for classification. *Oncotarget.* 2016; 7(21): 31393-31400.
- Ostrom QT, Gittleman H, Liao P, Vecchione-Koval T, Wolinsky Y, Kruchko C, et al. CBTRUS statistical report: Primary brain and other central nervous system tumors diagnosed in the United States in 2010-2014. *Neuro Oncol.* 2017; 19(Suppl 5): v1-v88.
- Nakada M, Nakada S, Demuth T, Tran NL, Hoelzinger DB, Berens ME. Molecular targets of glioma invasion. *Cell Mol Life Sci.* 2007; 64(4): 458-478.
- Murphy GJ, Johnson TW, Chamberlain MH, Rizvi SI, Wyatt M, George SJ, et al. Short- and long-term effects of cytochalasin D, paclitaxel and rapamycin on wall thickening in experimental porcine vein grafts. *Cardiovasc Res.* 2007; 73(3): 607-617.
- Goodenberger ML, Jenkins RB. Genetics of adult glioma. *Cancer Genet.* 2012; 205(12): 613-621.
- Masui K, Kato Y, Sawada T, Mischel PS, Shibata N. Molecular and genetic determinants of glioma cell invasion. *Int J Mol Sci.* 2017; 18(12): pii: E2609.
- Haidle AM, Myers AG. An enantioselective, modular, and general route to the cytochalasins: synthesis of L-696,474 and cytochalasin B. *Proc Natl Acad Sci USA.* 2004; 101(33): 12048-12053.
- Van Goietsenoven G, Mathieu V, Andolfi A, Cimmino A, Lefranc F, Kiss R, et al. In vitro growth inhibitory effects of cytochalasins and derivatives in cancer cells. *Planta Med.* 2011; 77(7): 711-717.
- Raguz S, Yagüe E. Resistance to chemotherapy: new treatments and novel insights into an old problem. *Br J Cancer.* 2008; 99(3): 387-391.
- Trendowski M. The promise of sonodynamic therapy. *Cancer Metastasis Rev.* 2014; 33(1): 143-160.
- Cooper JA. Effects of cytochalasin and phalloidin on actin. *J Cell Biol.* 1987; 105(4): 1473-1478.
- Deshmukh PG, Kanitkar UK, Pendse GS. A new fungal isolate from *Paspalum scrobiculatum*, Linn. with new biologically active metabolites. *Acta Microbiol Acad Sci Hung.* 1975; 22(3): 253-262.
- Slee EA, Harte MT, Kluck RM, Wolf BB, Casiano CA, Newmeyer DD, et al. Ordering the cytochrome c-initiated caspase cascade: hierarchical activation of caspases-2, -3, -6, -7, -8, and -10 and a caspase-9-dependent manner. *J Cell Biol.* 1999; 144(2): 281-292.
- Thornberry NA, Rano TA, Peterson EP, Rasper DM, Timkey T, Garcia-Calvo M, et al. A combinatorial approach defines specificities of members of the caspase family and granzyme B. Functional relationships established for key mediators of apoptosis. *J Biol Chem.* 1997; 272(29): 17907-17911.
- Verhaak RG, Hoadley KA, Purdom E, Wang V, Qi Y, Wilkerson MD, et al. Integrated genomic analysis identifies clinically relevant subtypes of glioblastoma characterized by abnormalities in PDGFRA, IDH1, EGFR, and NF1. *Cancer Cell.* 2010; 17(1): 98-110.
- Dilling C, Roewer N, Förster CY, Burek M. Multiple protocadherins are expressed in brain microvascular endothelial cells and might play a role in tight junction protein regulation. *J Cereb Blood Flow Metab.* 2017; 37(10): 3391-3400.
- Redies C, Vanhalst K, Roy Fv. Delta-protocadherins: unique structures and functions. *Cell Mol Life Sci.* 2005; 62(23): 2840-2852.
- Hirano S, Takeichi M. Cadherins in brain morphogenesis and wiring. *Physiol Rev.* 2012; 92(2): 597-634.
- Nagase T, Kikuno R, Ishikawa K i, Hirose M, Ohara O. Prediction of the coding sequences of unidentified human genes. XVI. The complete sequences of 150 new cDNA clones from brain which code for large proteins in vitro. *DNA Res.* 2000; 7(1): 65-73.
- Wolverton T, Lalande M. Identification and characterization of three members of a novel subclass of protocadherins. *Genomics.* 2001; 76(1-3): 66-72.
- Andreasen PA, Kjoller L, Christensen L, Duffy MJ. The urokinase-type plasminogen activator system in cancer metastasis: a review. *Int J Cancer.* 1997; 72(1): 1-22.
- Nielsen TO, Andrews HN, Cheang M, Kucab JE, Hsu FD, Ragaz J, et al. Expression of the insulin-like growth factor I receptor and urokinase plasminogen activator in breast cancer is associated with poor survival: potential for intervention with 17-allyl-amino geldanamycin. *Cancer Res.* 2004; 64(1): 286-291.
- Amos S, Redpath GT, Carpenter JE, Hussaini IM. Epidermal growth factor receptor-mediated regulation of urokinase plasminogen activator expression and glioblastoma invasion via C-SRC/MAPK/AP-1 signaling pathways. *J Neuropathol Exp Neurol.* 2010; 69(6): 582-592.
- Chaudhary A, Hilton MB, Seaman S, Haines DC, Stevenson S, Lemotte PK, et al. TEM8/ANTXR1 blockade inhibits pathological angiogenesis and potentiates tumoricidal responses against multiple cancer types. *Cancer Cell.* 2012; 21(2): 212-226.
- Louis DN, Perry A, Reifenberger G, von Deimling A, Figarella-Branger D, Cavenee WK, et al. The 2016 World Health Organization Classification of Tumors of the Central Nervous System: a summary. *Acta Neuropathol.* 2016; 131(6): 803-820.
- Hadziahmetovic M, Shirai K, Chakravarti A. Recent advancements in multimodality treatment of gliomas. *Future Oncol.* 2011; 7(10): 1169-1183.
- Bednarek ML, Speich JE, Miner AS, Ratz PH. Active tension adaptation at a shortened arterial muscle length: inhibition by cytochalasin-D. *Am J Physiol Heart Circ Physiol.* 2011; 300(4): 1166-1173.
- Małeckki JM, Bentke A, Ostrowska B, Laidler P. Cytochalasin D, LY294002 and olomoucine synergize in promoting death of melanoma cells through activation of caspase-3 and apoptosis. *Melanoma Res.* 2010; 20(1): 52-58.
- Li J, Gu B, Chen G, Ma B, Xu J, Zhang G, et al. Cytochalasin E, a potential agent for anti-glioma therapy, efficiently induces U87 human glioblastoma cell death. *Lat Am J Pharm.* 2012; 31(1): 147-151.
- Tong ZG, Liu N, Song H, Li J, Jiang J, Zhu JY, Qi JP. Cytochalasin B inhibits the proliferation of human glioma U251 cells through cell cycle arrest and apoptosis. *Genet Mol Res.* 2014; 13(4): 10811-10822.
- Trendowski M. Using cytochalasins to improve current chemotherapeutic approaches. *Anticancer Agents Med Chem.* 2015;

- 15(3): 327-335.
33. Roulston A, Marcellus RC, Branton PE. Viruses and apoptosis. *Annu Rev Microbiol.* 1999; 53: 577-628.
34. Bröker LE, Kruyt FA, Giaccone G. Cell death independent of caspases: a review. *Clin Cancer Res.* 2005; 11(9): 3155-3162.
35. Lamkanfi M, Festjens N, Declercq W, Vanden Berghe T, Vandenameele P. Caspases in cell survival, proliferation and differentiation. *Cell Death Differ.* 2007; 14(1): 44-55.
36. Stupack DG. Caspase-8 as a therapeutic target in cancer. *Cancer Lett.* 2013; 332(2): 133-140.
37. Li P, Nijhawan D, Wang X. Mitochondrial activation of apoptosis. *Cell.* 2004; 116(2 Suppl): S57-59, 2 p following S59.
38. McCarthy NJ, Whyte MK, Gilbert CS, Evan GI. Inhibition of Ced-3/ICE-related proteases does not prevent cell death induced by oncogenes, DNA damage, or the Bcl-2 homologue Bak. *J Cell Biol.* 1997; 136(1): 215-227.
39. Déas O, Dumont C, MacFarlane M, Rouleau M, Hebib C, Harper F, et al. Caspase-independent cell death induced by anti-CD2 or staurosporine in activated human peripheral T lymphocytes. *J Immunol.* 1998; 161(7): 3375-3383.
40. Muñoz-Cánoves P, Miralles F, Baiget M, Féllez J. Inhibition of urokinase-type plasminogen activator (uPA) abrogates myogenesis in vitro. *Thromb Haemost.* 1997; 77(3): 526-534.
-

A Pathogenic Homozygous Mutation in The Pleckstrin Homology Domain of *RASA1* Is Responsible for Familial Tricuspid Atresia in An Iranian Consanguineous Family

Ahoura Nozari, M.Sc.¹, Ehsan Aghaei-Moghadam, M.D.², Aliakbar Zeinaloo, M.D.², Afagh Alavi, Ph.D.¹,
Saghar Ghasemi Firouzabdi, Ph.D.¹, Shohre Minaee, B.Sc.², Marzieh Eskandari Hesari, B.Sc.²,
Farkhondeh Behjati Ph.D.^{1*}

1. Genetics Research Center, University of Social Welfare and Rehabilitation Sciences, Tehran, Iran
2. Department of Pediatrics Cardiology, Faculty of Medicine, Tehran University of Medical Sciences, Tehran, Iran

*Corresponding Address: P.O.Box: 1985713871, Genetics Research Center, University of Social Welfare and Rehabilitation Sciences, Tehran, Iran
Email: f_behjati@uswr.ac.ir

Received: 30/Jan/2018, Accepted: 21/Apr/2018

Abstract

Objective: Tricuspid atresia (TA) is a rare life-threatening form of congenital heart defect (CHD). The genetic mechanisms underlying TA are not clearly understood. According to previous studies, the endocardial cushioning event, as the primary sign of cardiac valvulogenesis, is governed by several overlapping signaling pathways including Ras/ERK pathway. *RASA1*, a regulator of cardiovascular development, is involved in this pathway and its haploinsufficiency (due to heterozygous mutations) has been identified as the underlying etiology of the autosomal dominant capillary malformation/arteriovenous malformation (CM/AVM).

Materials and Methods: In this prospective study, we used whole exome sequencing (WES) followed by serial bioinformatics filtering steps for two siblings with TA and early onset CM. Their parents were consanguineous which had a history of recurrent abortions. Patients were carefully assessed to exclude extra-cardiac anomalies.

Results: We identified a homozygous *RASA1* germline mutation, c.1583A>G (p.Tyr528Cys) in the family. This mutation lies in the pleckstrin homology (PH) domain of the gene. The parents who were heterozygous for this variant displayed CM.

Conclusion: This is the first study reporting an adverse phenotypic outcome of a *RASA1* homozygous mutation. Here, we propose that the phenotypic consequence of the homozygous *RASA1* p.Tyr528Cys mutation is more serious than the heterozygous type. This could be responsible for the TA pathogenesis in our patients. We strongly suggest that parents with CM/AVM should be investigated for *RASA1* heterozygous mutations. Prenatal diagnosis and fetal echocardiography should also be carried out in the event of pregnancy in heterozygous parents.

Keywords: Pleckstrin Homology Domain, *RASA1*, Tricuspid Atresia, Whole Exome Sequencing

Cell Journal(yakhteh), Vol 21, No 1, Apr-Jun (Spring) 2019, Pages: 70-77

Citation: Nozari A, Aghaei-Moghadam E, Zeinaloo A, Alavi A, Ghasemi Firouzabdi S, Minaee Sh, Eskandari Hesari M, Behjati F. A pathogenic homozygous mutation in the pleckstrin homology domain of *RASA1* is responsible for familial tricuspid atresia in an Iranian consanguineous family. Cell J. 2019; 21(1): 70-77. doi: 10.22074/cellj.2019.5734.

Introduction

Cardiac valvulogenesis is known as an embryogenic evolutionary conserved mechanism in all vertebrates (1). Heart valve formation is described by the primary formation of endocardial cushions (ECs) in the atrioventricular canal and outflow tract, which starts at embryonic day (E) E31-E35 in human and E9.5 in mouse (2, 3). During the complex endocardial cushioning event, endothelial-mesenchymal transition occurs in a subgroup of endothelial cells and the atrioventricular canal including the mitral and tricuspid valves will appear (4). This critical stage is governed by overlapping signaling pathways including VEGF, NFATc1, Notch, Wnt/beta-catenin, BMP/TGF-beta, ErbB, EGF and Ras/ERK (MAPK) pathways (2, 4-6). The interactions among these signaling pathways and their relative timing are proposed as a signaling network model for valvulogenesis (Fig.1) (4).

Numerous gene disruptions related to these pathways have now been revealed to influence valve phenotypes (7). Tricuspid atresia (TA, MIM#605067), with a prevalence of 1/25000 at live birth, is an infrequent form of valvular congenital heart defect (CHD) commonly associated with poor prognosis (1, 8, 9). Some studies have reported familial occurrences of TA (10-12). However, the genetic mechanisms underlying TA remain unclear. In this study, we used whole exome sequencing (WES) as a powerful method for detecting the genetic aetiology of a heterogeneous disease such as CHD (1, 13), and found a germline 'homozygous' missense mutation c.1583A>G p.(Tyr528Cys) in the pleckstrin homology (PH) domain of *RASA1* (Fig.2) in a consanguineous Iranian family.

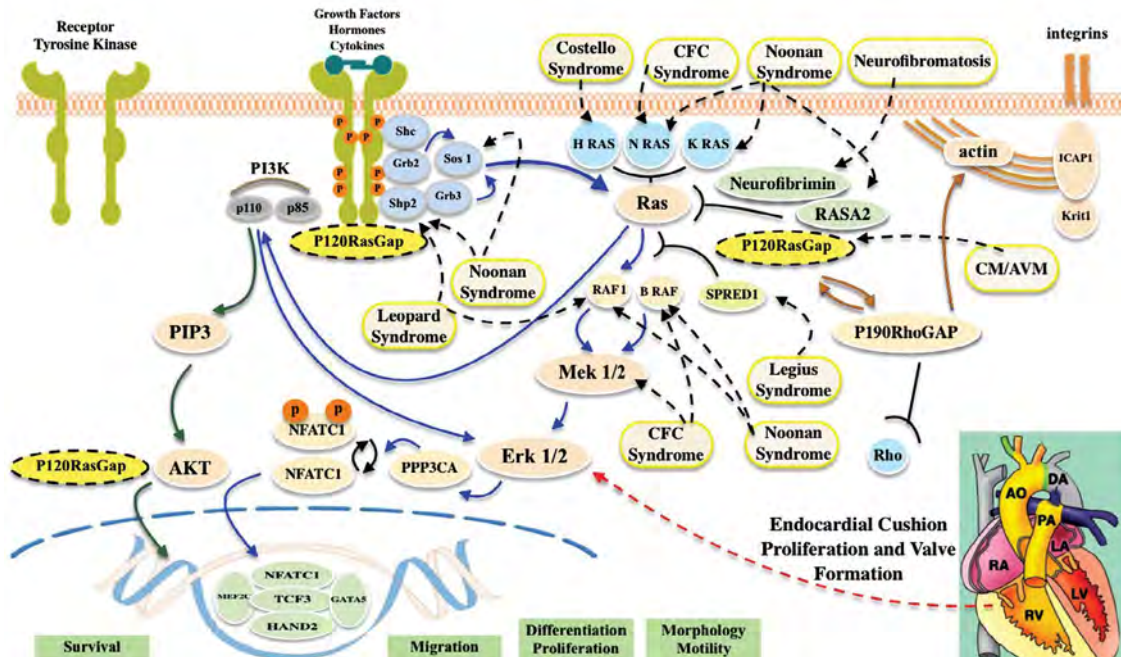


Fig.1: The Ras/ERK signal transduction pathway with emphasis on p120-RasGAP interactions. By the binding of growth factors, cytokines or hormones to tyrosine kinase receptors (TKR), cross phosphorylation of tyrosine residues occurs and following their dimerization, the Ras/ERK pathway is activated. RasGap proteins including p120-RasGAP, neurofibromin (NF1) and RAS-P21 protein activator 2 (RASA2) are able to downregulate Ras signaling by the conversion of the active form of Ras to its inactive form (GTP-bound and GDP-bound respectively) (5, 14). P120-RasGAP, in a Ras-dependent manner, binds to phosphorylated TKRs. The Ras/ERK pathway (shown by blue arrows) leads to differentiation, proliferation and migration and is involved in the development of heart valve. The inherited disorders of this pathway including NF1, Legius syndrome, Noonan, Cardiofaciocutaneous (CFC) syndrome, Costello, LEOPARD, and Capillary Malformation/Arteriovenous Malformation (CM/AVM) are indicated. Ras-independent function of RASA1 (shown by brown arrows) is promoted via the interaction between p120-RasGAP and p190 RhoGAP with the latter acting as a GAP for the Ras superfamily protein Rho (15, 16). P120-RasGAP also has the ability to bind phosphoinositides. The PI3K/ AKT pathway (shown by green arrows) leads to cell survival, which protects cells against apoptosis (1, 15).

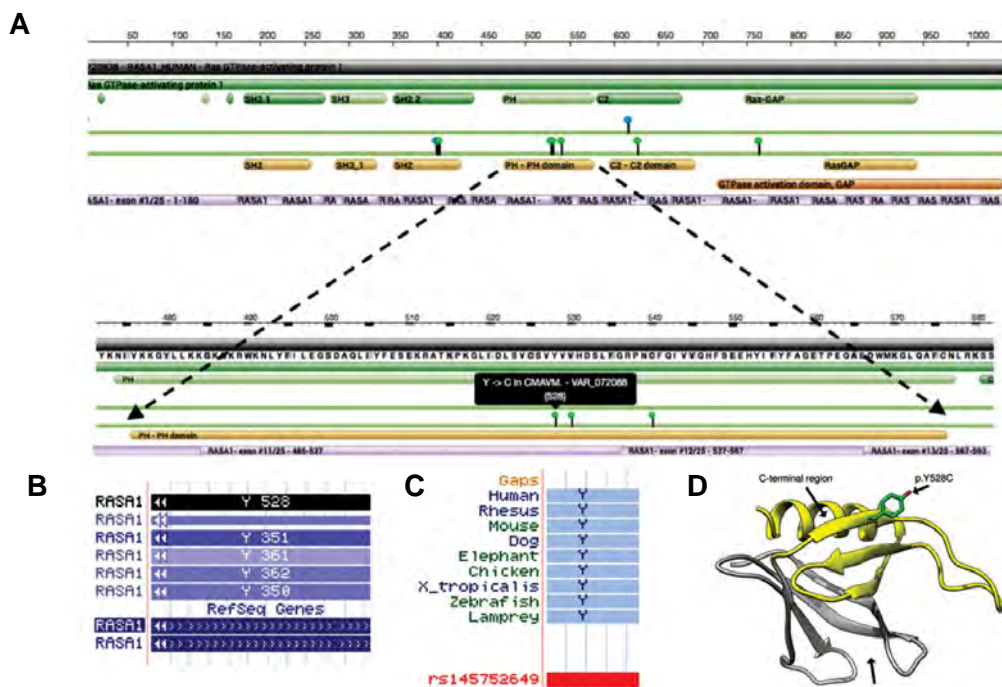


Fig.2: P120-RasGAP protein structure. **A.** P120-RasGAP is a protein with 1047 amino acid residues with the N-terminus containing SH2 and SH3 domains, and the central region containing a PH domain and a CALB/C2 domain. The C-terminus has the RasGAP domain. The position of the p.Tyr528Cys RASA1 missense mutation in the PH domain has been indicated (<https://www.rcsb.org/>), **B.** Position of the tyrosine residue in RASA1 transcripts (<http://genome.ucsc.edu>), **C.** The tyrosine residue is strongly conserved among the species (<http://genome.ucsc.edu>), and **D.** The position of the p.Tyr528Cys RASA1 missense mutation in the three-dimensional model (secondary structure) of the PH domain is shown. The p120-RasGAP PH domain comprises seven antiparallel beta-sheets, which is closed at one end by a C-terminal alpha-helix. The Tyr528 side chain is exposed in the C-terminal region, neighboring to the C-terminal alpha-helix of the PH domain (the C-terminal region of the domain and the inositol-phosphate (IP)-binding site are also shown) (12).

Material and Methods

In this prospective study, a consanguineous family, in which the parents were first cousins, were referred to the Pediatric Cardiology and Neonatal Intensive Care Unit of Tehran Children Medical Center for prenatal ultrasound screening of CHD for high risk families. The fetus' father (proband) as well as her paternal uncle were already diagnosed with TA (currently at ages 32 and 28 years respectively). The affected siblings with TA were born to healthy consanguineous parents which had a history of three pregnancy losses in 16-18 weeks of gestation. In this family, there was also one infant who had died at day 11 after birth with an unknown heart malformation (Fig.3). Although prenatal ultrasound screening of CHD for the proband's fetus appeared normal, this family was interested in determining the genetic aetiology underlying CHD in their family. A signed informed consent form was taken from all participants after being informed of the aim of the research study. This research study was approved by the Ethics Committee of the University of Social Welfare and Rehabilitation Sciences of Tehran, Iran (IR.USWR.REC.1395.132).

Cytogenetics and Fluorescent in Situ Hybridization analysis

For classical cytogenetics analysis, 5 ml venous blood samples-collected in heparinized tubes-were handled for cell culture and harvesting following standard techniques. High-resolution G-banded lymphocyte culture (520 resolution) was carefully analyzed to exclude chromosomal abnormality in patients.

Fluorescent in Situ Hybridization (FISH) analysis was carried out on a suspension of metaphase and interphase cells using Kreatech™ KBI-40103 DiGeorge HIRA

(22q11)/22q13 (SHANK3) probes, according to the manufacturer's procedure, to exclude the 22q11.2 microdeletion.

Exome sequencing

Genomic DNA was extracted from 5 ml venous blood collected in EDTA-containing tubes using the standard salting-out method. Approximately 50 ng of genomic DNA was obtained from the proband and prepared for WES with the Exome Enrichment Kit and Agilent's SureSelect Human All Exon V6 capture probes, and run on an Illumina HiSeq 4000 platform yielding an average read depth of 100x. Sequence alignment and variant calling for the targeted platform were made against the human reference genome GRCh37/hg19 build and wANNOVAR (<http://wannovar.wglab.org/>) was used for variant annotation.

Bioinformatic analysis

Several steps were taken to prioritize the entire set of high-quality variants. Briefly, variants in intergenic, down/up-stream, intronic, and UTR regions along with synonymous variants were excluded. Based on the hypothesis that the causative mutation for the disease in the siblings is rare, variants with unreported and reported minor allele frequency (MAF) ≤ 0.01 were considered in genomic variation databases including exac, (<http://exac.broadinstitute.org/>), the 1000 Genomes project (www.1000genomes.org), genomAD browser (<http://gnomad.broadinstitute.org>) and NHLBI Exome Sequencing Project (ESP) (<http://evs.gs.washington.edu/EVS/>). Moreover, variants observed in the exomes of 100 unrelated healthy Iranians or Iranians affected with non-cardiovascular diseases were further excluded.

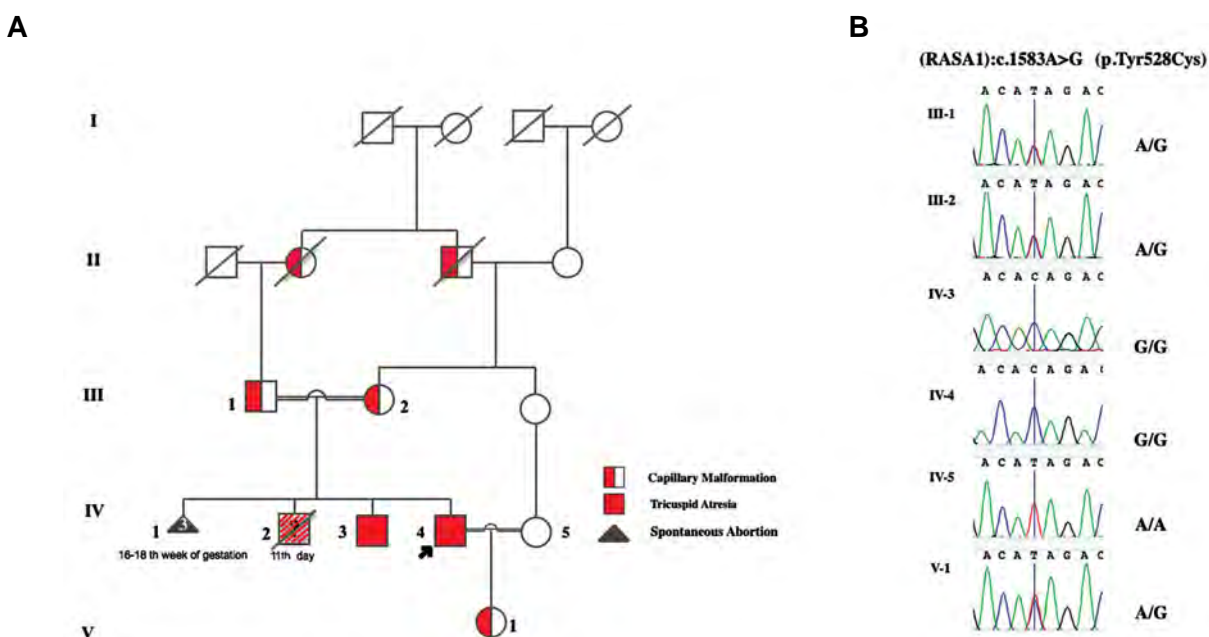


Fig.3: The family pedigree and chromatogram results of *RASA1*:c.1583A>G p.(Tyr528Cys). **A.** The pedigree displays an autosomal dominant pattern of inheritance and **B.** The Sanger sequencing validation for all the family members. Individual IV-2 died due to cardiac anomalies, TA was not investigated.

In the next step, we classified the rare variants according to their in silico prediction scores in Polyphen2 (<http://genetics.bwh.harvard.edu/pph2/>), SIFT (<http://sift.bii.aster.edu.sg/>), MutationTaster (www.mutationtaster.org), CADD_phred (cadd.gs.washington.edu/) and GERP++ (UCSC Genome Browser). Taking into account variants that were present in homozygous, X-linked or compound heterozygous states, we achieved gene-based arrangements by incorporating conservation scores of the variants based on the SiPhy_29way_logOdds score.

Validation of candidate mutations

We finally focused on variants in genes that are involved in biological pathways related to the cardiovascular system and/or in the pathogenesis of cardiac defects in animal models (<http://www.informatics.jax.org/>). The candidate variants were validated by Sanger sequencing (as the gold standard for screening and verifying variants of interest) for all family members to identify causative variants shared by two patients but not in the unaffected individuals. Moreover, to predict the impact of the candidate variant on protein structure and function, we also undertook protein structural modeling based on the homologous structures present in PDB using SPDBV 4.10 (<http://spdbv.vital-it.ch/>).

Results

Cytogenetics and Fluorescent in Situ Hybridization

None of the patients showed chromosome abnormalities in either the karyotype analysis or the FISH-based 22q11.2 microdeletion detection analysis.

Exome sequencing and bioinformatics analyses

Five candidate variants were identified by WES (Table 1). Sanger sequencing validated the c.1583A>G (p.Tyr528Cys) variant (rs145752649) in *RASA1* in homozygous state as the only candidate variant shared by the two patients. Other family members including parents and proband's offspring were heterozygote as expected (Fig.3). However, the mutation in *RASA1* gene has already been recorded (<http://www.hgmd.cf.ac.uk/ac/index.php>) in heterozygous form as the cause of autosomal dominant capillary malformation/arteriovenous malformation (CM/AVM) (17). Moreover, as several truncating heterozygous mutations in this gene have previously been reported with vascular anomalies in association with multiple forms of CHD (18) (Table 2), we propose that the p.Tyr528Cys *homozygous* mutation could be responsible for non-syndromic TA in our family.

Characteristics of family members

Having evaluated the heterozygous parents more precisely, we noted a unilateral purple-red lesion (2.5×3 cm) on the father's hand and bilateral varicose veins on mother's legs, indicative of CM. Moreover, the father had a history of spontaneous subarachnoid hemorrhage. After the birth of the proband's offspring, a pale-pink lesion also appeared in her forehead. None of the parents or proband's offspring showed cardiovascular abnormality by echocardiography. The cardiologists and clinical geneticists thoroughly evaluated both patients to rule out extra-cardiac malformations. Cardiac phenotypic characterization of the patients was undertaken with echocardiography (Table 3).

Table 1: Candidate variants used for cosegregation analysis

Gene	Position	Zygoty	Variant	db SNP ID	MAF in genomAD (exome_all)	CADD	GERP++	SiPhy
<i>RASA1</i>	Chr5: 86659294	Hom	NM_002890: c.1583A>G. p.Tyr528Cys	rs145752649	0.0015	28.3	5.58	15.75
<i>BBS12</i>	Chr 4: 123664906	Hom	NM_152618: c.1859 A>G: p.Gln620Arg	rs368861241	0.0005	23.7	5.81	10.955
<i>HUWE1</i>	Chr X: 53602150	Hemi	NM_031407: c. 6062C>T:p.Thr2021Ile	Novel	ND	22.6	4.37	12.15
<i>MYOIE</i>	Chr 15: 59430501	Het	NM_004998: c. 3146 C>A: p.Pro1049His	rs147579391	0.0023	31	5.79	20.044
<i>MYOIE</i>	Chr 15: 59519746	Het	NM_004998: c.554 G>A p.Asp185Gly	rs141565214	0.0022	25	6.02	16.545

Mutations were named according to <http://varnomen.hgvs.org/>.

SNP; Single nucleotide polymorphisms, MAF; Minor allele frequency, CADD; Combined annotation dependent depletion, GERP++; Genomic evolutionary rate profiling, Chr; Chromosome, Hom; Homozygous, Hemi; Hemizygous, Het; Heterozygous, and ND; No data.

Table 2: Congenital Heart defects associated with CM/AVM due to heterozygous *RASA1* truncating mutations

<i>RASA1</i> gene nucleotide change*	Putative effect at amino acid level	Cardiac feature
c.1572_1575dup	p.Ser526MetfsX8	CO, TOF
c.1682_1683dup	Pro562LeufsX9	CF, ASDII/PFO
c.1698+3_1698+4insT	Splicing affected	PS
c.2125C>T	p.Arg709X	CF
c.21841+1delG	Splicing affected	PDA, ASD, PS, prolapsed TV
c.806_810delTTTAC	p.Leu269ProfsX11	CO
c.957G>A	p.Trp319X	CO

*This table is adapted from Revenu et al. (18). Nucleotide numbering was based on cDNA sequence NM_002890.1. Mutations were named according to <http://www.hgvs.org/mutnomen/>. CM/AVM; Capillary malformation/arteriovenous malformation, CO; Cardiac overload, TOF; Tetralogy of fallot, CF; Cardiac failure, ASD; Atrial septal defect, PFO; Patent foramen ovale, PS; Pulmonary stenosis, PDA; Patent ductus arteriosus, and TV; Tricuspid valve.

Table 3: Cardiac phenotypic characterization of the patients

Patient no.	Cardiac phenotype	Capillary malformation symptoms
III-1	Normal values for echocardiographic measurements	A unilateral purple-red lesion (2.5×3 cm) on hand. Subarachnoid Hemorrhage
III-2	Normal values for echocardiographic measurements	Bilateral varicose veins on legs
IV-3	TA Functionally single ventricle with LV morphology LV is normal with LVEF:45% RV is rudimentary ASD (2 cm) PS Small VSD Mild MVP Mild MR	Early onset bilateral varicose veins on legs
IV-4	TA Functionally single ventricle with LV morphology LV is normal with LVEF:45% RV is rudimentary ASD (2 cm) PS Mild MR	Early onset mild bilateral varicose veins on legs
V-1	Normal values for echocardiographic measurements	A pale pink lesion (2×2 cm) in forehead

TA; Tricuspid atresia, LV; Left ventricle, RV; Right ventricle, ASD; Atrial septal defect, PS; Pulmonary valve stenosis, VSD; Ventricular septal, MVP; Mitral valve prolapse, MR; Mitral regurgitation, and LVEF; Left ventricular ejection fraction.

Discussion

Here, we report a co-segregating homozygous p.Tyr528Cys germline mutation in *RASA1* in two patients with isolated TA. *RASA1* (also known as Ras p21 protein activator 1) is a GTPase activator for normal RAS p21 but not its oncogenic counterpart. It is the first described member of Ras GTPase-activating protein (RasGAP) family that encodes a p120-RasGAP protein (16, 19). The involvement of Ras-related signaling pathways in the development of embryonic heart has been emphasized by the significant contribution of the components of these pathways in the pathogenesis of RASopathy disorders (17, 20-22). These molecular components include either RasGAP family members or other downstream molecules in the Ras/Raf/Mek/ERK cascade. Compound heterozygous missense mutations in the gene encoding NFATC1, which acts downstream of the Ras/ERK pathway, was also recently identified in a non-syndromic case of TA in a Lebanese family (1).

In spite of the syndromic nature of Rasopathy disorders, heterozygous germline mutations in *RASA1* cause vascular development disorders without any developmental defects (23). *RASA1* haploinsufficiency due to heterozygous mutations has been identified in a subset of individuals with CM/AVM (16). CM/AVM is mainly characterized by small multifocal and randomly distributed CM as pink-red to purple lesions, varicosities vein with or without deep venous anomalies, and fast flow lesions including arteriovenous malformation (AVM) or arteriovenous fistula (AVF). Vascular anomalies typically arise in several parts of body including skin, bone, muscle, spine and even brain causing life-threatening complications including bleeding and congestive heart failure (14, 15, 18, 21, 24). In our study, the daughter and parents of the proband who were heterozygous for the p.Tyr528Cys mutation displayed multiple forms of CM/AVM. The two siblings also displayed early onset bilateral varicose veins. Furthermore, these patients are at increased risk of fast blood flow lesions as their father.

Until now, more than 100 highly penetrant mutations have been identified across *RASA1* (14, 18, 25), however, no genotype-phenotype correlation has been established (25). It is noteworthy that in a study by Revencu et al. (18) several heterozygous *RASA1* mutations (mostly nonsense, frameshift and splice defect) were identified in familial cases of CM/AVM in association with multiple forms of CHD. Although They focused on various forms of vascular anomalies due to *RASA1* mutation, they did not consider the cardiac phenotypes of their patients in detail. This kind of association indicates that while there is no data suggesting that *RASA1* homozygous mutation cause more serious phenotypes, we speculate that the high mortality rate in this family along with two children affected by severe cardiac defects may be a consequence of the complete loss of the PH domain of *RASA1*.

The p120-RasGAP protein is a monomeric cytoplasmic

protein with several domains (16). Each protein domain is involved in several cellular and developmental processes in a Ras-dependent or Ras-independent manner (26). In a functional study performed on homozygote mice with a point mutation in the GAP domain (Rasa1 R780Q/R780Q), the severity of blood vascular abnormalities was identical to Rasa1-null mice and their cardiovascular manifestations were also mostly restricted to ECs. This finding suggested that cardiovascular anomalies are caused by the inability of *RASA1* to control Ras activation in a Ras-dependent manner (24). In accordance with this finding, we focused on the functional importance of the PH domain responsible for Ras-dependent function of p120-RasGAP, which seems to contribute to the pathogenesis of the cardiovascular phenotype observed in the family reported here. The missense substitution p.Tyr528Cys found in our patients alters tyrosine to cysteine in the PH domain. Since this residue is extremely conserved among human PH domain-containing proteins (<http://grch37.ensembl.org/index.html>) and among other species, it is likely to be essential for *RASA1* function.

Generally, PH domains have structurally conserved motifs and contain about 100 amino acid residues. They are present in several proteins and contribute to signal transduction pathways. The PH domain of p120-RasGAP is consists of aminoacids 474-577 and is in the noncatalytic region of the protein. However, it binds to the catalytic domain (GAP domain) within the same protein and interferes with Ras/GAP interaction (27). According to Hernandez et al. (28) the PH domain of p120-RasGAP has the ability to bind to phospholipid subgroups as well as being involved in numerous protein-protein interactions. The C-terminal region of the PH domain (residues 523-591) interacts with Ras and competes with it for binding to the GAP domain. The Tyr528 side chain, which is substituted by the cysteine residue in our patients, is exposed on the C-terminal region of the PH domain (27, 29). This substitution leads to the removal of the aromatic side chain and creation of a slightly negatively charged residue (28). The surface exposed position of tyrosine suggests that this substitution may alter binding of the PH domain to protein partners or the GAP domain within the same protein (29). Therefore, it seems that complete loss of function of the PH domain in a Ras-dependent manner would lead to the inability of *RASA1* to regulate the Ras molecule, and thereby may have an effect on TA pathogenesis in our patients.

Finally, we considered previous functional studies on murine models deficient for *Rasa1*. These data suggest the essential role of *Rasa1* in the regulation of cardiovascular development. Although heterozygous mice, due to the loss of one germline *Rasa1* allele, had no observable phenotype, homozygous loss caused embryonic death at E9.5 to E10.5 which is correlated with the primary formation of EC in the atrioventricular canal and outflow tract (2, 3, 19, 30, 31). Interestingly, adult mice with induced homozygous loss of *Rasa1* in all tissues have no detectable spontaneous cardiovascular defect.

Therefore, *Rasa1* seems to be necessary for embryonic cardiovascular development, however, it is not necessary for cardiovascular maintenance (31). These studies also indicated that, while *Rasa1* is ubiquitously expressed, embryonic mortality of mice deficient for *Rasa1* is mostly restricted to ECs (16).

Conclusion

On the basis of the contribution of the Ras/ERK pathway in embryonic development of heart valves, bioinformatics-based evaluation of the p.Tyr528Cys mutation, and evidence from functional studies in mice models deficient for *Rasa1*, we suggest that the identified p.Tyr528Cys homozygous mutation in *RASA1* is likely to be responsible for the TA phenotype observed in the pedigree analysed here. However, this hypothesis needs to be supported by generating an animal model carrying the p.Tyr528Cys point mutation. We also recommend that parents with CM/AVM should be screened for *RASA1* heterozygous mutations and if both parents are carriers, fetal echocardiography should be undertaken as a precaution in the event of pregnancy.

Acknowledgments

We would like to thank the patients and their families for contributing to this study. We appreciate the help of the laboratory staff of the Genetics Research Center of the University of Social Welfare and Rehabilitation Sciences. We thank the staff of the Pediatric Cardiology and Neonatal Intensive Care Unit of Children Medical Center of Tehran University of Medical Sciences for their excellent assistance in recruiting and providing clinical data of the patients. This project was funded (Grant Number: 801/95/5/1249) by the Research Division of the University of Social Welfare and Rehabilitation Sciences, for which we are very much indebted. The authors declare that they have no conflict of interest.

Authors' Contributions

F.B.; Participated in study design, grant application, drafting and was responsible for overall supervision. M.E.H., A.A.Z., Sh.M., E.A.-M.; Clinical investigation and sample collection. A.N.; Contributed to all experimental work, preparation of samples, data collection, evaluation, and drafting. A.N., A.A., S.G.F.; Exome data analysis and interpretation. All authors performed editing and approving the final version of this paper for submission, also participated in the finalization of the manuscript and approved the final manuscript.

References

1. Abdul-Sater Z, Yehya A, Beresian J, Salem E, Kamar A, Baydoun S, et al. Two heterozygous mutations in NFATC1 in a patient with Tricuspid Atresia. *PLoS One*. 2012; 7(11): e49532.
2. Chakraborty S, Combs MD, Yutzey KE. Transcriptional regulation of heart valve progenitor cells. *Pediatr Cardiol*. 2010; 31(3): 414-421.
3. Moorman A, Webb S, Brown NA, Lamers W, Anderson RH. Development of the heart:(1) formation of the cardiac chambers and arterial trunks. *Heart*. 2003; 89(7): 806-814.
4. Armstrong EJ, Bischoff J. Heart valve development: endothelial cell signaling and differentiation. *Circ Res*. 2004; 95(5): 459-740.
5. Butcher JT, Markwald RR. Valvulogenesis: the moving target. *Philos Trans R Soc Lond B Biol Sci*. 2007; 362(1484): 1489-1503.
6. Digilio MC, Marino B, Sarkozy A, Versacci P, Dallapiccola B. The heart in Ras-MAPK pathway disorders. In: Zanker M, editor. Noonan syndrome and related disorders-A matter of deregulated ras signaling. Basel: Karger; 2009; 109-118.
7. Schroeder JA, Jackson LF, Lee DC, Camenisch TD. Form and function of developing heart valves: coordination by extracellular matrix and growth factor signaling. *J Mol Med (Berl)*. 2003; 81(7): 392-403.
8. Flores Arizmendi A, Fernández Pineda L, Quero Jiménez C, Mañire Azcárate MJ, Herráiz Sarachaga I, Urroz E, et al. The clinical profile of Ebstein's malformation as seen from the fetus to the adult in 52 patients. *Cardiol Young*. 2004; 14(1): 55-63.
9. Berg C, Georgiadis M, Geipel A, Gembruch U. The area behind the heart in the four-chamber view and the quest for congenital heart defects. *Ultrasound Obstet Gynecol*. 2007; 30(5): 721-727.
10. Bonnet D, Fermont L, Kachaner J, Sidi D, Amiel J, Lyonnet S, et al. Tricuspid atresia and conotruncal malformations in five families. *J Med Genet*. 1999; 36(4): 349-350.
11. Kumar A, Victorica BE, Gessner IH, Alexander JA. Tricuspid atresia and annular hypoplasia: report of a familial occurrence. *Pediatr Cardiol*. 1994; 15(4): 201-203.
12. Lin AE, Rosti L. Tricuspid atresia in sibs. *J Med Genet*. 1998; 35(12): 1055-1056.
13. Gelb BD, Chung WK. Complex genetics and the etiology of human congenital heart disease. *Cold Spring Harb Perspect Med*. 2014; 4(7): a013953.
14. Whitaker S, Leech S, Taylor A, Splitt M, Natarajan S, Rajan N. Multifocal capillary malformations in an older, asymptomatic child with a novel *RASA1* mutation. *Clin Exp Dermatol*. 2016; 41(2): 156-158.
15. Erickson RP, Wynshaw-Boris AJ. Epstein's inborn errors of development: the molecular basis of clinical disorders of morphogenesis. 3rd ed. Oxford: Oxford University Press; 2016.
16. King PD, Lubeck BA, Lapinski PE. Nonredundant functions for Ras GTPase-activating proteins in tissue homeostasis. *Sci Signal*. 2013; 6(264): re1.
17. Revencu N, Boon LM, Mendola A, Cordisco MR, Dubois J, Clapuyt P, et al. *RASA1* mutations and associated phenotypes in 68 Families with capillary malformation-arteriovenous malformation. *Hum Mutat*. 2013; 34(12): 1632-1641.
18. Revencu N, Boon LM, Mulliken JB, Enjolras O, Cordisco MR, Burrows PE, et al. Parkes Weber syndrome, vein of Galen aneurysmal malformation, and other fast-flow vascular anomalies are caused by *RASA1* mutations. *Hum Mutat*. 2008; 29(7): 959-965.
19. Boon LM, Mulliken JB, Vikkula M. *RASA1*: variable phenotype with capillary and arteriovenous malformations. *Curr Opin Genet Dev*. 2005; 15(3): 265-269.
20. Aoki Y, Niihori T, Inoue S, Matsubara Y. Recent advances in RASopathies. *J Hum Genet*. 2016; 61(1): 33-39.
21. Rauen KA. The RASopathies. *Annu Rev Genomics Hum Genet*. 2013; 14: 355-369.
22. Yutzey KE, Colbert M, Robbins J. Ras-related signaling pathways in valve development: ebb and flow. *Physiology (Bethesda)*. 2005; 20: 390-397.
23. Denayer E, de Ravel T, Legius E. Clinical and molecular aspects of RAS related disorders. *J Med Genet*. 2008; 45(11): 695-703.
24. Lubeck BA. The Ras GTPase activating protein p120 RasGAP as a regulator of cardiovascular system development, lymphatic system maintenance, and a T cell lineage tumor suppressor. Presented for the Ph.D., Michigan. University of Michigan. 2015.
25. Weitz NA, Lauren CT, Behr GG, Wu JK, Kandel JJ, Meyers PM, et al. Clinical spectrum of capillary malformation-arteriovenous malformation syndrome presenting to a pediatric dermatology practice: a retrospective study. *Pediatr Dermatol*. 2015; 32(1): 76-84.
26. Agazie YM, Hayman MJ. Molecular mechanism for a role of

- SHP2 in epidermal growth factor receptor signaling. *Mol Cell Biol.* 2003; 23(21): 7875-7886.
27. Drugan JK, Rogers-Graham K, Gilmer T, Campbell S, Clark GJ. The Ras/p120 GTPase-activating protein (GAP) interaction is regulated by the p120 GAP pleckstrin homology domain. *J Biol Chem.* 2000; 275(45): 35021-35027.
 28. Hernandez F, Huether R, Carter L, Johnston T, Thompson J, Gossage JR, et al. Mutations in RASA1 and GDF2 identified in patients with clinical features of hereditary hemorrhagic telangiectasia. *Hum Genome Var.* 2015; 2: 15040.
 29. Scheffzek K, Welte S. Pleckstrin homology (PH) like domains- versatile modules in protein-protein interaction platforms. *FEBS Lett.* 2012; 586(17): 2662-2673.
 30. Rauen KA, Huson SM, Burkitt-Wright E, Evans DG, Farschtschi S, Ferner RE, et al. Recent developments in neurofibromatosis and RASopathies: management, diagnosis and current and future therapeutic avenues. *Am J Med Genet A.* 2015; 167A(1): 1-10.
 31. Lubeck BA, Lapinski PE, Bauler TJ, Oliver JA, Hughes ED, Saunders TL, et al. Blood vascular abnormalities in *Rasa1*(R780Q) knockin mice: implications for the pathogenesis of capillary malformation-arteriovenous malformation. *Am J Pathol.* 2014; 184(12): 3163-3169.
-

Comparison of miRNA Profiles of Cord Blood Stem Cells in Identical and Fraternal Twins

Monireh Ajami, M.Sc.¹, Mohammad Hadi Sadeghian, M.D.^{1,2*}, Masoud Soleimani, Ph.D.^{3*}, Mohammad Reza Keramati, M.D.^{1,2}, Mansoureh Ajami, M.Sc.³, Azadeh Anbarlou, M.Sc.⁴, Amir Atashi, Ph.D.⁵

1. Faculty of Medicine, Mashhad University of Medical Sciences, Mashhad, Iran
2. Cancer Molecular Pathology Research Center, Mashhad University of Medical Sciences, Mashhad, Iran
3. Department of Hematology, Faculty of Medical Sciences, Tarbiat Modares University, Tehran, Iran
4. Department of Tissue Engineering, School of Advanced Technologies in Medicine, Shahid Beheshti University of Medical Sciences, Tehran, Iran
5. Stem Cell and Tissue Engineering Research Center, Shahrood University of Medical Sciences, Shahrood, Iran

*Corresponding Addresses: P.O.Box: 9176759416, Faculty of Medicine, Mashhad University of Medical Sciences, Mashhad, Iran
P.O.Box: 14115-331, Department of Hematology, Faculty of Medical Sciences, Tarbiat Modares University, Tehran, Iran
Emails: sadeghianmh@mums.ac.ir, soleim_m@modares.ac.ir

Received: 29/Dec/2017, Accepted: 12/May/2018

Abstract

Objective: The role of epigenetic in regulating of the gene expression profile the embryo has been documented. MicroRNAs (miRNAs) are one of these epigenetic mechanisms. Twins are valuable models in determining the relative contributions of genetics and the environment. In this study, we compared differences in the expression levels of 44 miRNAs in hematopoietic stem cells (HSCs) of identical twins to that of fraternal twins as a controls.

Materials and Methods: In this experimental study, CD133⁺ HSCs were isolated from cord blood of identical and fraternal twins via magnetic-activated cell sorting (MACS). Variation in of gene expression levels of 44 miRNAs were evaluated using quantitative reverse transcription-polymerase chain reaction (qRT-PCR).

Results: Significant differences in expression were observed in both fraternal and identical twins to varying degrees, but variations alteration in expression of the miRNAs were higher in fraternal twins.

Conclusion: Identical twins had a positive correlation in miRNA expression, while the correlation was not statistically significant in fraternal twins. Altogether, more differences in miRNA expression level in fraternal twins can be attributed to the both genetics and the intrauterine environment. The contribution of the intrauterine environment and genetics to miRNAs expression in HSCs was estimated 8 and 92%, respectively. By comparing of miRNA expression in identical and fraternal twins and identification of their target genes and biological pathways, it could be possible to estimate the effects of genetics and the environment on a number of biological pathways.

Keywords: Cord Blood, Epigenetic, Hematopoietic Stem Cells, miRNA, Twins

Cell Journal (Yakhteh), Vol 21, No 1, Apr-Jun (Spring) 2019, Pages: 78-85

Citation: Ajami M, Sadeghian MH, Soleimani M, Keramati MR, Ajami M, Anbarlou A, Atashi A. Comparison of miRNA profiles of cord blood stem cells in identical and fraternal twins. Cell J. 2019; 21(1): 78-85. doi: 10.22074/cellj.2019.5683.

Introduction

MicroRNAs (miRNAs) are small (~22-nucleotide) noncoding RNA molecules that can negatively regulate gene expression at the post-transcriptional level (1, 2). miRNAs bind to their target mRNAs and cause instability and target mRNA fragmentation when this pairing is complete. In the case of a partial binding which often occurs in the 3'UTR, the mRNA is prevented from being translated into a protein. It is expected that each miRNA can regulate many mRNAs and each mRNA may be regulated by several miRNAs (3, 4). miRNA expression profiling is important because of key role of miRNA in regulating gene expression networks and their effects on many biological processes, as well as their role as disease markers (5, 6).

Epigenetics refers to temporary modifications to DNA that can turn genes "on" or "off" (7). These modifications do not change the DNA sequence. Recent findings have shown the role of epigenetic mechanisms such as DNA methylation and histone modifications in

miRNAs expression (8). A lot of research has shown that CpG islands upstream of miRNAs act as a promoters and are regulated through DNA methylation (9, 10). Enzymes which are involved in miRNA processing pathways also participate in epigenetic mechanisms (11). Some miRNAs participate in DNA methylation, for instance miR-165 and miR-166 are essential for PHABULOSA (PHB) methylation in Arabidopsis, also the key enzyme DNMT1, 3a and 3b are all potential targets for miRNAs (12, 13). In general, miRNAs can be considered an important factor in epigenetics and the control of gene expression (14).

Twins studies can provide information on the relative contribution of genetics and the environment on phenotypic characteristic and discover the etiology of the diseases. Recently, a study on twins has been done to assess the regulatory effects of epigenetic factors on gene expression (15). Differences in the epigenome can determine disease susceptibility in a pair of twins (16). Twins are considered a valuable model in determining the relative contribution of genetic and environmental factors regarding the

relationship between epigenetics and miRNAs (17). Collection of umbilical cord blood (UCB) cells is considered a noninvasive method, and primitive CD133⁺ hematopoietic stem cells (HSCs) isolated from UCB would be appropriate for investigating of difference in the miRNA expression profiles of newborn twins. In this study, we compared and analyzed miRNA expression profiles of identical and fraternal twins.

Materials and Methods

Subjects and samples

This experimental study was approved by Ethical Committee of Mashad University of Medical Sciences (IR.MUMS.REC.1392.12). The study was performed using cord blood from two pairs of identical (monozygotic) and two pairs of fraternal (dizygotic) twins. Cord bloods were collected from 36-37 week full term twins with the informed consent of the mothers. Mothers were aged in the range of 30-35 years and the gender of both fraternal and identical twins was male.

Zygoty

Same sex twins that shared a placenta with one or two amniotic sacs (monochorionic-diamniotic or monochorionic-monoamniotic) were considered as identical twins and same sex that come with two placentas and two amniotic sacs (dichorionic-diamniotic) were considered as fraternal twins.

CD133⁺ cells isolation

UCB samples were obtained immediately after birth, diluted with hydroxyethyl starch in the ratio of 1:4 to deplete red blood cells. The diluted cell suspensions were gently layered over Ficoll-Paque (Pharmacia-Amersham, Piscataway, USA) and centrifuged for 20-30 minutes at 400×g at room temperature to the separate mononuclear cell fraction.

The samples were enriched for CD133⁺ cells with magnetic activated cell sorting (MACS) using CD133⁺ cell isolation Kit (MiltenyiBiotec, Gladbach, Germany) according to the manufacturer's instructions. Purity of isolated CD133⁺ cells and the homogeneity of the population were assessed with flow cytometry.

Flow cytometry analysis

Purity of isolated CD133⁺ cells from UCB using MACS and the homogeneity of the population were assessed by flow cytometry. CD133⁺ cells were stained with PE-conjugated anti-human CD133 antibody (Miltenyi Biotec, Germany) and mouse IgG1 antibody (IQ-Products, Netherlands) was used as an isotype control according to the manufacturer's instructions.

RNA extraction and quantitative reverse transcription-polymerase chain reaction for miRNA

About 800.000 CD133⁺ cells were isolated from each bag

of cord blood and 700.000 of them used for RNA extraction with TRIzol (Invitrogen, Carlsbad, CA, USA) according to the manufacturer's instructions. cDNA synthesis was performed using miRNA EasyScript cDNA Synthesis Kit (G269 ABM, USA) following the manufacturer's protocol. Synthesized cDNA was mixed with primers and EvaGreen miRNA qPCR MasterMix-ROX (MasterMix-mR ABM, USA) following the manufacturer's instructions. Quantitative reverse transcription-polymerase chain reaction (qRT-PCR) analysis was performed on ABI 7000 system (Applied Biosystems, USA). Two reliable endogenous controls (U6-2, SNORD 48) were used to normalize and calculate the relative expression levels. Calculations were based on the comparative $\Delta\Delta CT$ method. All of 46 primer pairs were custom-ordered from ABM Inc (Table S1) (See Supplementary Online Information at www.celljournal.org). All samples were run in triplicates.

Bioinformatic analysis

DIANA-miRPath (<http://diana.imis.athena-innovation.gr/DianaTools/index.php?r=mirpath>) was used to show which biological pathways are related to the miRNAs. DIANA-mirExTra software (<http://diana.cslab.ece.ntua.gr/hexamers/>) was used to determine microRNA target genes.

Estimating heritability

Studies on identical and fraternal twins provide an opportunity to estimate the contribution of the environment and genetics with the use of the heritability formula:

$$H^2=2(r_{mz}-r_{dz})$$

H^2 : heritability/r: regression/mz: monozygotic/dz: dizygotic

Statistical analysis

Statistical analyses were performed using Microsoft Excel. Data means were compared using Student's t test and one-way ANOVA. Statistical significance was defined as $P<0.05$.

Results

Purity of CD133⁺ cells isolated from cord blood

Cord blood samples were obtained from identical and fraternal twins. The purity of separated cells from the cord blood samples was measured for all of the twins. One flow cytometry histogram for fraternal twins (Fig. 1A) and one for identical twins (Fig. 1B) is presented here. Purity of CD133⁺ cells isolated from cord blood was about 90% in all samples.

miRNA expression profiling of CD133⁺ cells

Based to previous studies(18-24), 44 miRNAs that play key roles in self renewal/differentiation and have high expression in CD133⁺ HSCs from various origins (peripheral blood, bone marrow, and umbilical cord blood) were selected and evaluated (Table S1) (See Supplementary Online Information at www.celljournal.org). The lists of MicroRNAs with the highest expression in fraternal twins and identical twins are reported in Table 1. MiR-10b was not expressed in any of the samples.

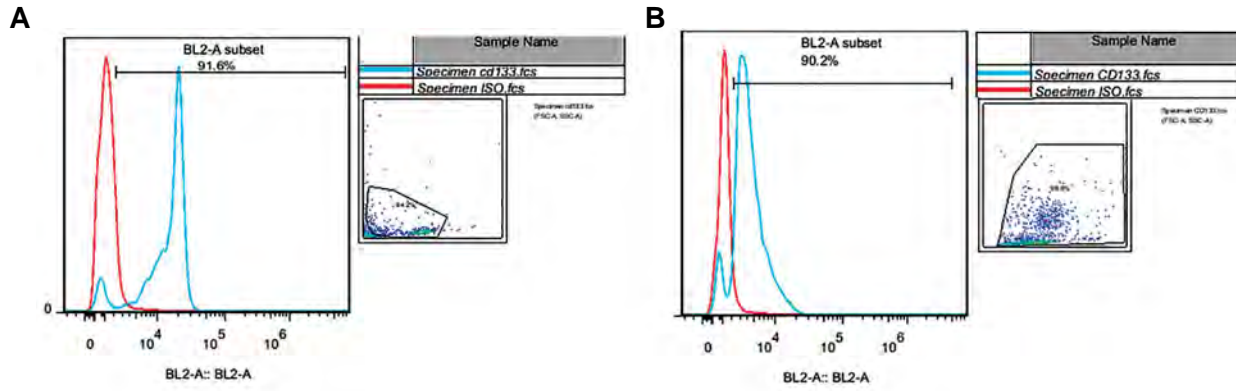


Fig.1: Flow cytometry result of CD133⁺ cells separated from cord blood of twins. **A.** Flow cytometry histogram for fraternal twins and **B.** Flow cytometry histogram for identical twins.

Table 1: MicroRNAs with the highest expression levels in fraternal twins and in identical twins (Δ CT)

Fraternal twins			
Pair 1		Pair 2	
miRNA	Level of expression	miRNA	Level of expression
<i>miR-107</i>	10.07	<i>miR-129-3P</i>	17.04
<i>miR-10a</i>	10.07	<i>miR-34c-3p</i>	17.01
<i>miR-20a</i>	9.77	<i>miR-181d</i>	16.08
<i>miR-411</i>	9.57	<i>miR-29a</i>	14.88
<i>miR-125d</i>	9.07	<i>miR-34b</i>	14.11
<i>miR-181d</i>	9.07	<i>miR-125d</i>	14.06
<i>miR-19b</i>	9.07	<i>miR-20a</i>	14.05
<i>miR-29a</i>	9.07	<i>miR-181b</i>	14.02
<i>miR-520h</i>	8.22	<i>miR-10a</i>	13.03
<i>miR-128</i>	8.22	<i>miR-181c</i>	13.03
<i>miR-144</i>	8.12	<i>miR-125a-3p</i>	13.02
<i>miR-34b</i>	8.12	<i>miR-34a</i>	13.00
<i>miR-142-5p</i>	8.10		
Identical twins			
<i>miR-181d</i>	10.82	<i>miR-181c</i>	12.20
<i>miR-20a</i>	10.82	<i>miR-144</i>	11.39
<i>miR-20b</i>	10.82	<i>miR-125a-3p</i>	11.36
<i>miR-29a</i>	10.82	<i>miR-181d</i>	10.40
<i>miR-107</i>	8.82	<i>miR-20a</i>	10.34
<i>miR-10a</i>	8.82	<i>miR-10a</i>	10.29
<i>miR-125d</i>	8.82	<i>miR-130a</i>	10.27
<i>miR-9</i>	7.32	<i>miR-29a</i>	10.05
<i>miR-106b</i>	6.12	<i>miR-19a</i>	9.80
<i>miR-19a</i>	5.82	<i>miR-181b</i>	9.45

There was not significant correlation between miRNA expression of pair 1 and pair 2 in fraternal twins ($r=0.15$, $P=0.3433$). There was a significant positive correlation between miRNA expression of pair 1 and pair 2 in identical twins ($r=0.61$, $P<0.0001$) (Fig.2).

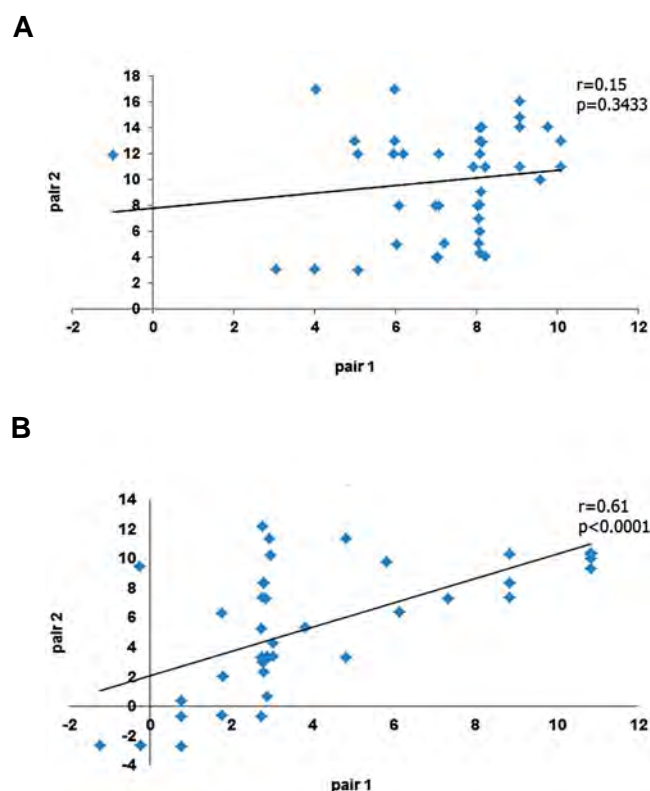


Fig.2: The Correlation between miRNAs expression. **A.** Fraternal twins and **B.** Identical twins.

The discordance of miRNA expression levels in identical and fraternal twins was calculated using the comparative Ct ($\Delta\Delta Ct$) method of calculation. The mismatch variances in the levels of miRNA expression is shown in Table 2. Altogether 44 miRNAs were categorized into three groups: high (more than 10-fold), low (less than 2-fold) and moderate (between 2-10 fold) difference in expression. In fraternal twins, 20 miRNAs had high, 10 miRNAs had low and 13 miRNAs had moderate difference in expression. In identical twins, 13 miRNAs had high, 18 miRNAs had low and 12 miRNAs had moderate difference in expression. MiR-10b was not expressed in any of the samples. The levels of differential expression in studied of the miRNAs in identical and fraternal twins are shown in Figure 3. These miRNAs can be divided into four groups (A, B, C, and D) according to how their expression is affected by genetics and the environment (Table S2) (See Supplementary Online Information at www.celljournal.org) target genes and biological pathways related to these miRNAs are

shown in Table 3 (heat maps are presented in Figure S1) (See Supplementary Online Information at www.celljournal.org).

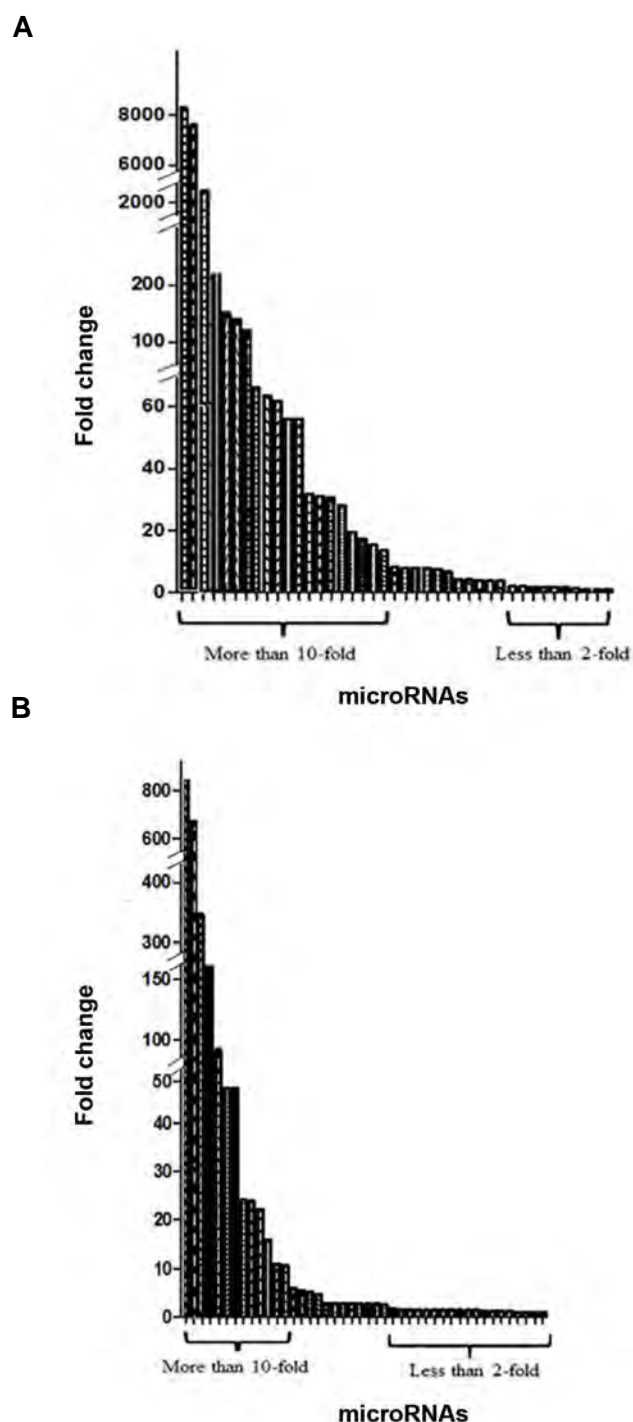


Fig.3: Bar graphs showing the difference in expression in studied of 44 miRNAs. **A.** The levels of differential expression in fraternal twins and **B.** The levels of differential expression in identical twins.

Calculation of heritability

The role of genetic contribution in microRNAs expression levels was estimated at 92% [$H^2=2(0.61-0.15)=0.92$]. The role of environment on the differences in microRNA expression levels was estimated at 8% ($1-0.92=0.08$).

Table 2: The discordance of miRNA expression in identical and fraternal twins. High difference and low difference between miRNA expression

High difference miRNAs expression				
Fraternal twins		Identical twins		
Expression discordance (fold change)		Expression discordance (fold change)		
<i>miR-129-3p</i>	8248.98	<i>miR-181b</i>	837.53	
<i>miR-106b</i>	7858.29	<i>miR-181c</i>	689.78	
<i>miR-34c-3p</i>	2105.57	<i>miR-144</i>	352.13	
<i>miR-34a</i>	261.37	<i>miR-130a</i>	158.68	
<i>miR-125a-3p</i>	131.59	<i>miR-125a-3p</i>	93.05	
<i>miR-181d</i>	128.89	<i>miR-519d</i>	47.17	
<i>miR-17</i>	123.63	<i>miR-520h</i>	47.17	
<i>miR-519d</i>	66.25	<i>miR-181a</i>	24.08	
<i>miR-34b</i>	63.55	<i>miR-19b</i>	23.75	
<i>miR-181b</i>	61.81	<i>miR-17</i>	22.16	
<i>miR-181a</i>	56.10	<i>miR-19a</i>	15.77	
<i>miR-29a</i>	56.10	<i>miR-92a</i>	10.92	
<i>miR-125b</i>	31.77	<i>miR-24</i>	10.63	
<i>miR-181c</i>	31.12			
<i>miR-19a</i>	30.69			
<i>miR-144</i>	28.24			
<i>miR-20a</i>	19.42			
<i>miR-520h</i>	17.38			
<i>miR-130a</i>	15.45			
<i>miR-34c-5p</i>	13.64			
		Low difference miRNAs expression		
<i>miR-223</i>	1.97	<i>miR-29a</i>	1.70	
<i>miR-155</i>	1.94	<i>miR-221</i>	1.47	
<i>miR-107</i>	1.93	<i>miR-20a</i>	1.39	
<i>miR-142-5p</i>	1.91	<i>miR-155</i>	1.38	
<i>miR-411</i>	1.35	<i>miR-22</i>	1.38	
<i>miR-221</i>	1.00	<i>miR-411</i>	1.37	
<i>miR-92a</i>	1.00	<i>miR-181d</i>	1.33	
<i>miR-10b</i>	1.00	<i>miR-16</i>	1.31	
<i>miR-20b</i>	1.00	<i>miR-34c-3p</i>	1.31	
<i>miR-93</i>	1.00	<i>miR-106b</i>	1.21	
		<i>miR-34a</i>	1.20	
		<i>miR-34b</i>	1.20	
		<i>miR-34c-5p</i>	1.16	
		<i>miR-9</i>	1.01	
		<i>miR-129-3p</i>	1.00	
		<i>miR-125b</i>	1.00	
		<i>miR-10b</i>	1.00	
		<i>miR-125a-5p</i>	1.00	
		<i>miR-128</i>	1.00	

Table 3: Target genes and biological pathways related to the miRNAs (group A: more affected by genetic, group B: more effect of environment, group C: the environment and genetics have the same kind of effect, and group D: the environment and genetics have opposite effect)

Group	miRNA	Target genes	KEGG pathway
A	<i>miR-129-3P</i>		Cell cycle
	<i>miR-106b</i>	ZNF419, RTN4, B2M, KLHL28	Chronic myeloid leukemia
	<i>miR-34c-3p</i>		Pathways in cancer
	<i>miR-34a</i>	ARHGAP1, KDRF(hsa), CDC46(hsa), ALR(hsa)	P53 signaling pathway
	<i>miR-34b</i>	MET, CREB, CDK4	HIF-1 signaling pathway
	<i>miR-29a</i>	E2F7, ACTB	PI3K-Akt signaling pathway
	<i>miR-125b</i>	CALU, EFNB2, RPA1	
	<i>miR-34c-5p</i>	MET, MYB, CDK4	
B	<i>miR-181b</i>	TCL1, CDX2, BCL2	TGF-beta signaling pathway
	<i>miR-181c</i>	POLR2B, TWF1, CCNG1	
	<i>miR-144</i>	FGG, FGB	
	<i>miR-520h</i>	SMAD6, ABCG2	
	<i>miR-130a</i>	POLR2B, RTN4, TWF1	
C	<i>miR-181d</i>	BCL2	Pathways in cancer
	<i>miR-17</i>	RBM14, PTK4, SOX4, B2M, KLHL28, POU2F1	P53 signaling pathway
	<i>miR-519d</i>	PPARA, CDKN1A	PI3K-Akt signaling pathway
	<i>miR-181a</i>	FAM47B, POLR2B, TWF1	
	<i>miR-19a</i>	POLR2B, 2DHHC18, ESR1, TWF1	
	<i>miR-125a-3p</i>		
D	<i>miR-24</i>	SLITRK1, NOTUN, COPS7A, ABCB10, CCL2	Cell cycle
	<i>miR-19b</i>	POLR2B, ZDHHC18, ESR1	Chronic myeloid leukemia
	<i>miR-92a</i>	ANP32E, SAP18, ALKBH3, SOX4	P53 signaling pathway RNA transport TGF-beta signaling pathway

Discussion

Studies on twins have provided the possibility of determining the contribution of genes and environment to phenotypic characteristics and etiology of diseases (15). Recently, studies on twins were performed to introduce epigenetic as a factor effecting gene expression (25). Differences in the epigenome can show the susceptibility to disease, variability in age of onset and severity of diseases in twins (16, 26).

Differences in the expression of some genes particularly in twins represent a group of genes whose expression levels are more sensitive to the effects of the environment. The lowest difference in the intrauterine environment can affect gene expression profile (27). The fetal programming is independent of genomic DNA sequences and may be associated with epigenetic mechanisms (28).

Identical twins are a good model for studying epigenetic

differences. To date, conflicting evidence of epigenetic differences in identical twins from childhood to adulthood have been reported (29). In general, phenotypic discordance between identical twins is attributed to non-shared environments that identical twins in encounter during their lives (15, 29). The epigenome is dynamic and affected by environmental changes. Many studies have been shown that epigenetics is a key factor in the discordance between identical twins (30-32).

Recent studies have proposed some reasons for differences between identical twins. One of them is miRNAs which are able to control epigenetic mechanisms (33). On the other hand, epigenetic mechanisms are also capable of regulating miRNA expression (32).

In this study, we compared miRNA expression levels in HSCs derived from cord blood of identical and fraternal twins at birth. The evaluation of miRNAs in both identical

and fraternal twins showed different expression levels of miRNAs, to a greater extent in (fraternal twins than identical twins). So far, no similar study has investigated the differences in miRNA expression in cord blood HSCs. However, there have only been a few studies on the differences in methylation and genomic imprinting in identical twins (34).

Ollikainen et al. (35) evaluated the level of methylation in different tissues in identical and fraternal twins. They found differences in the methylation of specific loci in newborn twins. They attributed the epigenetic differences in identical twins to environmental factors and random events which occur in the uterus. But in fraternal twins, genetic diversity plays a major role. The difference in methylation in identical twins was different even between same tissues in twin pairs.

Gordon et al. (27) compared gene expression in mononuclear and endothelial cells of UCB in identical twins. They observed significant differences in gene expression and concluded that these differences may be attributed to the intrauterine environment. Gordon et al. (36) also studied the methylation profile of CpG regions as a phenotype in different tissues (mononuclear and endothelial cells of UCB and endothelial cells of placenta) in twins. Identical twins had many differences at birth but differences were greater between fraternal twins.

In this study, the difference in the expression of 44 miRNAs which have high expression in cord blood stem cells were evaluated in two pairs of identical and fraternal twins. As previously mentioned these miRNAs divided in to four groups according to how their expression is affected by genetics and the environment. Group A contains miRNAs which showed high differences in expression in fraternal twins, but little difference in identical twins. This group is impacted to higher degree by genetics than the environment at the level of mRNA expression. Group B contains miRNAs which had high differences in both types of twins. The expression of miRNAs is likely more influenced by the environment. Group C is similar to group B, but the differences between fraternal twins were higher than between identical twins. Group D contains miRNAs which had high differences in expression in identical twins, but not in fraternal twins. In order to demonstrate the importance of these four groups, target genes and biological pathways were predicted. More than 80% of miRNAs in each group are involved in the mentioned biological pathways.

miRNAs in group A are involved in some pathways like hypoxia-inducible factor 1 (HIF-1) signaling. There for miRNAs related to the HIF-1 pathway are more affected by genetics, and the intrauterine environment has not been a major contributor in determining the expression levels of these miRNAs. Group B which is involved in the transforming growth factor-beta (TGF-beta) signaling pathway also showed a significant effect from the intrauterine environment in the regulation of their expression.

In groups C and D, both factors, environment and genetic, are involved in determining the level and discordant expression of miRNAs. Group C consists of miRNAs which had high differences in both identical and fraternal twins, but the differences in fraternal twins were higher than in identical twins. In fact, the combined effects of genetic variation and the environment plays an important role in increasing the variance in this group. miRNAs placed in group D showed high expression differences in identical twins, but had low discordance in fraternal twins despite them having genetic heterogeneity, meaning the effect of environment and the expression of these miRNAs is a little.

In summary, our study showed that observed discordance in miRNAs expression in identical twins can be attributed to the intrauterine environment (its contribution was estimated at 8%). In other words, miRNA expression levels can be affected by the smallest difference in intrauterine environment such as different position of the twins in the uterus. Expression discordance of the studied miRNAs was higher in fraternal twins than identical twins. In fraternal twins in addition to the environment, heterogeneous genetics has an important role (its contribution was estimated at 92%).

Conclusion

The differences in the expression of 44 miRNAs which have high expression levels in cord blood stem cells were evaluated in two pairs of identical and fraternal twins. The identical twins had a positive correlation in miRNA expression, while the correlation was not statistically significant in fraternal twins. Altogether, more discordance in miRNA expression of fraternal twins can be attributed to both genetics and the intrauterine environment. The Contribution of the intrauterine environment and genetics on miRNA expression in HSCs was estimated at 8 and 92%, respectively. By comparing miRNAs expression levels in identical and fraternal twins and identifying their target genes and biological pathways, estimating the contribution of genetics and the environment to a number of biological pathways is possible.

Acknowledgments

We thank Tarbiat Modares University for their support and technical assistance. Financial support was provided by Mashhad University of Medical Sciences which is greatly appreciated. All authors declare no conflict of interest.

Authors' Contributions

M.S., M.H.S.; Participated in study design and the conclusion. Mo.A., Am.A., M.R.K.; Bioinformatic analysis and interpretation of the data. Am.A.; Were responsible for overall supervision. Mo.A., Ma.A.; Contributed to all experimental work, conducted molecular experiments, RT-qPCR analysis. Mo.A., M.R.K.; Drafted the manuscript, which was revised by Az.A.; All authors

performed editing and approving the final version of this manuscript for submission, also participated in the finalization of the manuscript and approved the final draft.

References

- Lin S, Gregory RI. MicroRNA biogenesis pathways in cancer. *Nat Rev Cancer*. 2015; 15(6): 321-333.
- Ha M, Kim VN. Regulation of microRNA biogenesis. *Nat Rev Mol Cell Biol*. 2014; 15(8): 509-524.
- Meltzer PS. Cancer genomics: small RNAs with big impacts. *Nature*. 2005; 435(7043): 745-746.
- Esquela-Kerscher A, Slack FJ. OncomiRs-microRNAs with a role in cancer. *Nat Rev Cancer*. 2006; 6(4): 259-269.
- Pritchard CC, Cheng HH, Tewari M. MicroRNA profiling: approaches and considerations. *Nat Rev Genet*. 2012; 13(5): 358-369.
- Catalanotto C, Cogoni C, Zardo G. MicroRNA in control of gene expression: an overview of nuclear functions. *Int J Mol Sci*. 2016; 17(10). pii: E1712.
- Perri F, Longo F, Giuliano M, Sabbatino F, Favia G, Ionna F, et al. Epigenetic control of gene expression: potential implications for cancer treatment. *Crit Rev Oncol Hematol*. 2017; 111: 166-172.
- Gagnidze K, Pfaff DW. Epigenetic mechanisms: DNA methylation and histone protein modification. *Neuroscience in the 21st Century*: Springer; 2013; 1939-1978.
- Toyota M, Suzuki H, Sasaki Y, Maruyama R, Imai K, Shinomura Y, et al. Epigenetic silencing of microRNA-34b/c and B-cell translocation gene 4 is associated with CpG island methylation in colorectal cancer. *Cancer Res*. 2008; 68(11): 4123-4132.
- Han L, Witmer PD, Casey E, Valle D, Sukumar S. DNA methylation regulates MicroRNA expression. *Cancer Biol Ther*. 2007; 6(8): 1284-1288.
- He L, Hannon GJ. MicroRNAs: small RNAs with a big role in gene regulation. *Nat Rev Genet*. 2004; 5(7): 522-531.
- Rajewsky N. microRNA target predictions in animals. *Nat Genet*. 2006; 38 Suppl: S8-S13.
- Bao N, Lye K-W, Barton MK. MicroRNA binding sites in Arabidopsis class III HD-ZIP mRNAs are required for methylation of the template chromosome. *Dev Cell*. 2004; 7(5): 653-662.
- Chuang JC, Jones PA. Epigenetics and microRNAs. *Pediatr Res*. 2007; 61(5 Pt 2): 24R-29R.
- Liu C, Molenaar PCM, Neiderhiser JM. The impact of variation in twin relatedness on estimates of heritability and environmental influences. *Behav Genet*. 2018; 48(1): 44-54.
- Machin G. Non-identical monozygotic twins, intermediate twin types, zygosity testing, and the non-random nature of monozygotic twinning: a review. *Am J Med Genet C Semin Med Genet*. 2009; 151C(2): 110-127.
- Schwab TL, Hogenson TL. Effect of epigenetic differences in identical twins. In: Patel V, Preedy VR, editors. *Handbook of nutrition, diet, and epigenetics*. Springer International Publishing; 2017; 1-18.
- Liao R, Sun J, Zhang L, Lou G, Chen M, Zhou D, et al. MicroRNAs play a role in the development of human hematopoietic stem cells. *J Cell Biochem*. 2008; 104(3): 805-817.
- Merkerova M, Vasikova A, Belickova M, Bruchova H. MicroRNA expression profiles in umbilical cord blood cell lineages. *Stem Cells Dev*. 2010; 19(1): 17-26.
- Bissels U, Bosio A, Wagner W. MicroRNAs are shaping the hematopoietic landscape. *Haematologica*. 2012; 97(2): 160-167.
- Laine SK, Hentunen T, Laitala-Leinonen T. Do microRNAs regulate bone marrow stem cell niche physiology? *Gene*. 2012; 497(1): 1-9.
- Lin CP, Choi YJ, Hicks GG, He L. The emerging functions of the p53-miRNA network in stem cell biology. *Cell Cycle*. 2012; 11(11): 2063-2072.
- Calloni R, Cordero EA, Henriques JA, Bonatto D. Reviewing and updating the major molecular markers for stem cells. *Stem Cells Dev*. 2013; 22(9): 1455-1476.
- Báez A, Martín-Antonio B, Piruat JI, Barbado MV, Prats C, Álvarez-Laderas I, et al. Gene and miRNA expression profiles of hematopoietic progenitor cells vary depending on their origin. *Biol Blood Marrow Transplant*. 2014; 20(5): 630-639.
- Gervin K, Vigeland MD, Mattingsdal M, Hammerø M, Nygård H, Olsen AO, et al. DNA methylation and gene expression changes in monozygotic twins discordant for psoriasis: identification of epigenetically dysregulated genes. *PLoS Genet*. 2012; 8(1): e1002454.
- Joshita S, Umemura T, Tanaka E, Ota M. Genetics and epigenetics in the pathogenesis of primary biliary cholangitis. *Clin J Gastroenterol*. 2018; 11(1): 11-18.
- Gordon L, Joo JH, Andronikos R, Ollikainen M, Wallace EM, Umstad MP, et al. Expression discordance of monozygotic twins at birth: effect of intrauterine environment and a possible mechanism for fetal programming. *Epigenetics*. 2011; 6(5): 579-592.
- Gluckman PD, Hanson MA, Cooper C, Thornburg KL. Effect of in utero and early-life conditions on adult health and disease. *N Engl J Med*. 2008; 359(1): 61-73.
- Xiang Z, Yang Y, Chang C, Lu Q. The epigenetic mechanism for discordance of autoimmunity in monozygotic twins. *J Autoimmun*. 2017; 83: 43-50.
- Czyz W, Morahan JM, Ebers GC, Ramagopalan SV. Genetic, environmental and stochastic factors in monozygotic twin discordance with a focus on epigenetic differences. *BMC Med*. 2012; 10: 93.
- Talens RP, Christensen K, Putter H, Willemsen G, Christiansen L, Kremer D, et al. Epigenetic variation during the adult lifespan: cross-sectional and longitudinal data on monozygotic twin pairs. *Aging Cell*. 2012; 11(4): 694-703.
- Kaut O, Schmitt I, Tost J, Busato F, Liu Y, Hofmann P, et al. Epigenome-wide DNA methylation analysis in siblings and monozygotic twins discordant for sporadic Parkinson's disease revealed different epigenetic patterns in peripheral blood mononuclear cells. *Neurogenetics*. 2017; 18(1): 7-22.
- Denis H, Van Grembergen O, Delatte B, Dedeurwaerder S, Putmans P, Calonne E, et al. MicroRNAs regulate KDM5 histone demethylases in breast cancer cells. *Mol Biosyst*. 2016; 12(2): 404-413.
- Yet I, Tsai PC, Castillo-Fernandez JE, Carnero-Montoro E, Bell JT. Genetic and environmental impacts on DNA methylation levels in twins. *Epigenomics*. 2016; 8(1): 105-117.
- Ollikainen M, Smith KR, Joo EJ, Ng HK, Andronikos R, Novakovic B, et al. DNA methylation analysis of multiple tissues from newborn twins reveals both genetic and intrauterine components to variation in the human neonatal epigenome. *Hum Mol Genet*. 2010; 19(21): 4176-4188.
- Gordon L, Joo JE, Powell JE, Ollikainen M, Novakovic B, Li X, et al. Neonatal DNA methylation profile in human twins is specified by a complex interplay between intrauterine environmental and genetic factors, subject to tissue-specific influence. *Genome Res*. 2012; 22(8): 1395-1406.

The Study of rs693 and rs515135 in *APOB* in People with Familial Hypercholesterolemia

Fatemeh Karami, M.Sc.¹, Iman Salahshourifar, Ph.D.¹, Massoud Houshmand, Ph.D.^{2*}

1. Department of Biology, Science Faculty, Science and Research Branch, Islamic Azad University, Tehran, Iran
2. Department of Medical Genetics, National Institute for Genetic Engineering and Biotechnology, Tehran, Iran

*Corresponding Address: P.O.Box: 14965/161, Department of Medical Genetics, National Institute for Genetic Engineering and Biotechnology, Tehran, Iran
Email: massoudh@nigeb.ac.ir

Received: 4/Jan/2018, Accepted: 3/Jun/2018

Abstract

Objective: *APOB*-related familial hypercholesterolemia (FH) is the most common hereditary hypercholesterolemia with an autosomal dominant pattern. A number of *APOB* variants are the most important risk factors for hypercholesterolemia. *APOB* is a large glycoprotein that plays an important role in the metabolism of lipoproteins in the human body. Small changes in the structure and function of *APOB* can cause major problems in lipid metabolism. Two forms of *APOB* are produced by an editing process of gene replication. *APOB48* is required for the production of chylomicrons in the small intestine and *APOB100* is essential in liver for the production of very low density lipoprotein (VLDL) and is also a ligand for LDL receptor (LDLR) that mediates LDL endocytosis.

Materials and Methods: In this case-control study, rs693 (in exon 26 of *APOB*) and rs515135 (5' end of *APOB*) single nucleotide polymorphisms (SNPs) were analyzed in 120 cases of familial hypercholesterolemia and 120 controls. Both SNPs were genotyped by polymerase chain reaction-restriction fragment length polymorphism (PCR-RFLP) where PCR products were digested with specific restriction enzymes recognising each single nucleotide polymorphism.

Results: This study was analyzed by odds-ratio (OR) and its 95% confidence interval (CI) to examine the association of the two SNPs with familial hypercholesterolemia susceptibility. Statistical analysis showed that both SNPs were in Hardy-Weinberg equilibrium.

Conclusion: We found no significant relationship between rs515135 and familial hypercholesterolemia. However, there was a significant association between the C allele of rs693 and high familial cholesterol levels. Furthermore, it seems the dominant model of T allele occurrence has a protective role in emergence of disease.

Keywords: *APOB*, Familial Hypercholesterolemia, Single Nucleotide Polymorphism

Cell Journal (Yakhteh), Vol 21, No 1, Apr-Jun (Spring) 2019, Pages: 86-91

Citation: Karami F, Salahshourifar I, Houshmand M. The study of rs693 and rs515135 in *APOB* in people with familial hypercholesterolemia. Cell J. 2019; 21(1): 86-91. doi: 10.22074/cellj.2019.5692.

Introduction

Familial hypercholesterolemia (FH) is a monogenic inherited disorder. The FH heterozygote type has a two- to three-fold increase in low-density lipoprotein (LDL) cholesterol in serum and has a prevalence of 0.2% (at least 1 in 500) in most countries (1-3). The frequency of homozygous FH is 1 in a million and has a six- to eight-fold increase in plasma LDL-cholesterol (LDL-c) with signs appearing in childhood (1, 4). To reduce the risk of atherosclerosis and premature cardiovascular complications, clinical management focuses on early diagnosis of FH (5). The available evidence demonstrates that FH results from a combination of genetic variants and environmental (diet risk factors and tobacco smoking) factors in different populations (3, 6, 7). Genetic predisposition is assumed to be the cumulative result of mutations and/or polymorphisms of genes that may even have a small-effect, leading to a slight increase in LDL-C (8). Detection of heterozygote and homozygote FH in affected family members is an important step for success rate in accurate diagnosis and subsequent family screening (2).

Given that FH is one of the sole risk factors of coronary heart disease (CHD), identifying FH causing variants and

classifying patients into possible FH is important (9). The majority of cases with FH could be explained by genetic mutations in *LDLR*, *APOB*, *PCSK9* and *LDLRAP1* (10). *APOB* is the well-known gene that encodes the protein involved in LDL. The defect in apo B-100 receptor binding domain (Arg3500→Gln) is the most prevalent cause of ligand-defective LDL and cause of FH. Mutations or polymorphisms in *APOB* have been described as causal risk factors of FH (2, 3, 8, 11).

The *APOB* gene is approximately 43kb in size, and consists of 29 exon and is located on the short arm of chromosome 2 (2 p24.1) (12). Susceptible single nucleotide polymorphisms (SNPs), the most common type of genetic variation, are known to be markers of different chromosomal loci in heritable disease (13). Genome-wide association study (GWAS) focuses on cognizance of SNPs as biomarkers of a disease which have been used in numerous biomedical studies (14, 15). As mentioned above, genotyping SNPs helps in the early detection of some patients with genetic susceptibility (6, 13).

The results of the SNP studies must be expounded circumspectly, as these results may be applied exclusively or multiple SNPs can work cooperatively and create a

functional difference. Interplay among multiple SNPs may commonly affect the risk of a disease. Evaluation of SNPs may be problematic with respect to SNP-SNP interactions, because taking the individual SNPs without considering SNP-SNP interactions hinders the discovery of weak achievements (16-19). The frequency of the clinical phenotype of FH has been estimated at almost 0.002 in the general population, but in some isolated populations, like French Canadians, Finns, Afrikaners, Druze and Lebanese, occurrence of FH can be in a higher-than-normal frequency because of founder effects and de novo mutations in a population (20, 21). Data on allele and genotype frequencies for *APOB* have been reported for European (22, 23) and Asian (24-26) populations. For example, allele frequencies of *APOB* and the relationship of its genotypes with plasma lipid and lipoprotein levels in the Mongolian Buryat population resembled the Indians but their frequency distribution differed significantly from the Chinese, Malaysians, and Caucasians (25).

At present, the molecular basis of FH has been shown in detail in many populations, but there is still very limited molecular data relating to FH in Iran (20). To investigate associations between the *ApoB* genotype and levels of LDL-C, two SNPs of *APOB*, referred to in more than one study (3, 18, 19), were examined to determine the role of these SNPs in developing FH in Iran. There has been no independent study on the genetic association of rs693 and rs515135 with FH in the Iranian population. Here, we examined the association of these two selected SNPs with increased serum cholesterol and FH.

Materials and Methods

One hundred and twenty patients with FH, recruited from Karaj hospital, and 120 healthy persons, as the control group, were included in this study. The clinical characteristics of patients including age, gender, familial heart and brain disease, and familial high cholesterol were collected. Mean age of patients was 48.65 ± 14.02 years. All the participants were informed about the study and signed a written consent form. This study was approved by the Ethical Committee in Karaj Hospital.

Blood sample and DNA isolation

Blood samples were collected in tubes containing EDTA (Golden Vac., China). Genomic DNA was extracted with a DNA extraction kit (MBST, Iran) according to the manufacturer's instructions. The extracted DNA samples were stored in a freezer at -20°C until further use.

Genotyping of *APOB* rs693, rs515135 polymorphism

The case and control samples were genotyped for rs515135 and rs693 SNP using polymerase chain reaction-restriction fragment length polymorphism (PCR-RFLP).

Oligonucleotide primers for rs693 C>T were:

F: 5'AGA GGA AAC CAA GGC CAC AGT TGC3'
R: 5'TAC ATT CGG TCT CGT GTA TCT TCT3'

and the oligonucleotide primers for rs515135 A>G were:

F: 5'CCT AGT TAA TCC TCA GAA TGA CAC TG3'
R: 5' ATT GGG GTG GCA ATA GGC GCA AAT TG3'.
PCR amplification was carried out in a total volume of 25 μl consisting of 12.5 μl Master Mix (Tris-HCl, pH=8.5, 1.5 mM MgCl_2 , 0.2% Tween-20, 0.4 mM dNTP, 2 U/ μl Amplicon Taq DNA polymerase, stabilizer and inert red (Amplicon Co., Denmark), 0.5 μM of each primer and 100 ng DNA template and ddH₂O. PCR cycles were an initial denaturation step at 95°C for 4 minutes followed by 35 cycles of denaturation at 95°C for 30 seconds, annealing temperature of 58°C for 30 seconds, extension at 72°C for 1 minute, and a final extension step at 72°C for 10 minutes.

PCR products were digested with 0.5 μL (10 U) of BglIII (Fermentase, Canada) for rs515135 A>G and XbaI (Fermentase, Canada) for rs693C>T at 37°C for 16 hours. The digested fragments were separated on a 2% agarose gel (containing 0.5 $\mu\text{g/ml}$ DNA Staining) and observed under UV light.

The BglIII recognition site is represented by the presence of A allele which produces two fragments of 108bp and 261 bp, while the presence of G allele is represented by the remaining uncut fragment of 369 bp. The XbaI recognition site is represented by the presence of T allele which produces two fragments of 26 bp and 110 bp, while the presence of C allele is represented by the remaining uncut fragment of 136 bp. The fragments were separated by 2% agarose gel electrophoresis and then visualized under UV light.

Sequencing analysis

The PCR products were examined for specificity using 2% agarose gel electrophoresis. Double-stranded DNA automated sequencing was performed by using an ABI capillary sequencing machine (Applied Biosystems, gene Fanavar Company, Iran). All fragments were sequenced with the forward primers. Sequence variants were analyzed using FinchTV (<http://www.geospiza.com/finchtv/>) (Fig.1).

Statistical analysis

Statistical analysis was conducted using Graphpad (<https://www.graphpad.com/>) and Medcalc to perform the chi-square and 95% confidence interval (CI) tests based on *APOB* rs693 and rs515135 frequencies in FH cases in Iran. A $P < 0.01$ was considered as statistically significant.

Results

The clinical characteristics of the case and control groups were first compared (Table 1).

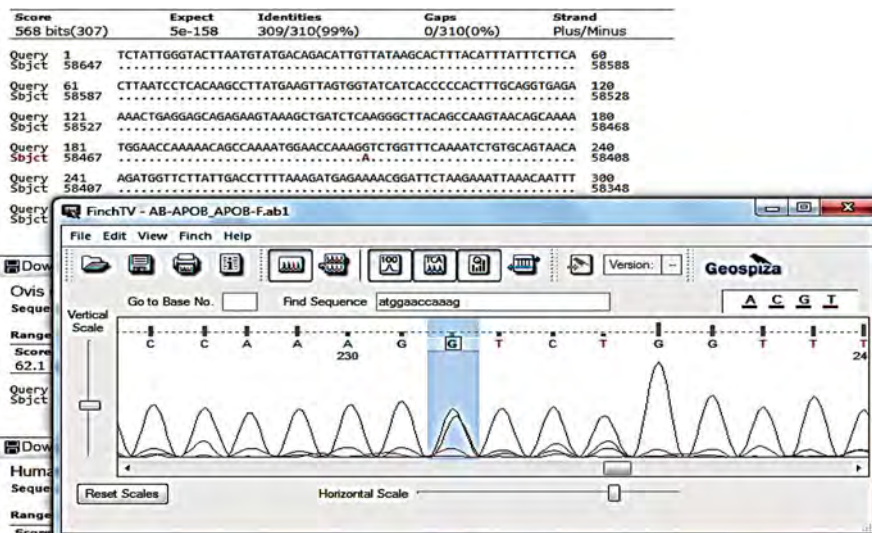


Fig.1: GA genotype of the APOB rs515135 single nucleotide polymorphisms (SNP).

Table 1: Demographic characteristics of the FH case group and the healthy control group

Variable	Case n=120	Control n=120	Total n=240	P value
Age (Y, mean ± SD)	48.65 ± 14.02	41.35 ± 11.15	-	
Age of disease onset (Y, mean ± SD)	40.46 ± 9.61	NA	-	
Age (Y), n (%)				
<45	53 (44.16)	79 (65.83)	132 (55)	0.0001
45-60	41 (34.17)	35 (29.17)	76 (31.67)	
>60	26 (21.67)	6 (5)	32 (13.33)	
Gender				
Female	60 (50)	35 (29.17)	95 (39.58)	0.0015
Male	60 (50)	85 (70.83)	145 (60.42)	
Cholesterol (mg/dl)				
<200	27 (22.5)	120 (100)	147 (61.25)	
200-220	66 (55)	0 (0)	66 (27.5)	>0.0001
>220	27 (22.5)	0 (0)	27 (11.25)	
Familiar heart and brain disease				
Yes	56 (46.67)	18 (15)	74 (30.83)	>0.0001
No	64 (53.33)	102 (85)	166 (69.17)	
Familiar high cholesterol				
Yes	12 (100)	-	-	
No		NA	-	

NA; Not available and FH; Familial hypercholesterolemia.

To confirm the results of RFLP, 10 samples were sent for sequencing from both SNPs. According to Table 2, in 120 patients group, 84 patients had CC genotype and 36 patients had TT or CT genotypes. In 120 control groups, 103 patients with CC genotype and 17 with TT and CT genotypes were observed. There was a significant correlation between the CC genotype in the patient group and high familial cholesterol ($P=0.0037$). Table 3 shows the frequency of GG, AA and GA genotypes in patients with high familial cholesterol and the control group.

Statistical analysis of rs515135 and rs693 in APOB in the Iranian population

Results of logistic regression analysis showed no significant correlation between genotype and familial high cholesterol disease (Table 4). Regarding the results of logistic regression modeling, there was no significant relationship between genotype and high familial cholesterol patients ($P=0.67$). Regarding allelic frequencies of rs693 in both groups, the C allele is the prevalent allele in both groups. There was a significant correlation between the C allele and familial high cholesterol.

Table 2: Frequency of the genotype of rs515135 and rs693 in the control group and case group

Genotype	Case n (%)	Control n (%)	Total	P value	OR	95% CI	df
rs515135							
AA	3 (2.5)	2 (1.67)	5	-	Ref (1)	-	2
GG	82 (68.33)	85 (70.83)	167	0.6336	1.5549	0.2533-9.5464	
GA	35 (29.17)	33 (27.5)	73	0.7136	1.4141	0.2221-9.0068	
Total	120	120	240	-	-	-	
rs693							
TT	4 (3.33)	1 (0.83)	5	-	Ref (1)	-	2
CC	84 (70)	103 (85.84)	100	0.1585	4.9048	0.5377-44.74	
CT	32 (26.67)	16 (13.33)	125	0.5499	2.0000	0.2062-19.3983	
Total	120	120	240	-	-	-	

OR; Odd ratio, CI; Confidence interval, and df; Degrees of freedom.

Table 3: Frequency of genotype GG+GA and AA in rs515135

Genotype	Patients	Controls	Total	P value	95% CI	df
GG+GA	117 (97.5)	118 (98.33)	135	0.6535	0.2482-9.2201	1
AA	3 (2.5)	2 (1.67)	5			
Total	120	120	240			

CI; Confidence interval and df; Degrees of freedom.

Table 4: Frequency of genotype TT+CT and CC rs693

Genotype	Patients	Controls	Total	P value	95% CI	df
CT+TT	36 (30)	17 (141.17)	53			1
CC	84 (70)	103 (85.83)	187	0.0037	1.362-4.949	
Total	120	120	240			

CI; Confidence interval and df; Degrees of freedom.

Table 5: Frequency of genotype GA+AA and AA rs515135

Genotype	Case	Control	Total	P value	OR	95% CI	df
GA+AA	38 (31.67)	35 (29.17)	73		Ref (1)		1
GG	82 (68.33)	85 (70.83)	167	0.6739	1.125	0.6491-1.9514	
Total	120	120	240				

OR; Odd ratio, CI; Confidence interval, and df; Degrees of freedom.

Comparison of variables such as age, sex, cholesterol and history of cardiovascular disease in both control and patient groups showed significant differences. With regard to the incidence and history of cardiovascular disease, the results indicate that in patients with high cholesterol, incidence of cardiovascular disease is higher than healthy people, thus indicating a potential genetic link between hypercholesterolemic family and heart disease. The significance of HWE testing in population-based genetic association studies is immense especially when analyzing the control group. This is because an important assumption underlying these studies is that the control group is a representative sample of the population under investigation. Another assumption in such studies is that individuals of both case and control groups belong to the same single large random-mating population.

In this study Hardy-Weinberg equilibrium for the alleles studied in rs515135 and rs693 polymorphisms in the *APOB* gene and the unbalance of G and T was established ($P > 0.05$).

Discussion

Of the theoretical estimated prevalence of 1/500 for heterozygous FH, <1% are diagnosed in most countries. Recently, direct screening in a Northern European general population diagnosed approximately 1/200 with heterozygous FH. All reported studies document the failure to achieve the recommended LDL cholesterol targets in a large proportion of individuals with FH, which may have up to 13-fold increased risk of CHD. Based on prevalences between 1/500 and 1/200, between 14 and 34 million individuals worldwide have FH (22).

Early detection and treatment probably would reduce premature morbidity and mortality of this disease. Cascade screening of family members of known index cases is the most cost-effective approach for identification of new FH cases (23). Once diagnosed, individuals with FH can be treated with lifestyle measures, lipid-lowering therapies, and possibly novel therapies including PCSK9 monoclonal antibodies, anti-sense oligonucleotides targeting *APOB* and microsomal triglyceride transfer protein inhibitors to change the clinical course of the disease (22).

This is the first study investigating the association of *APOB* polymorphisms with FH. This study provides

an analysis of two *APOB* polymorphisms and their correlation with variation in serum lipid levels in the Iranian population. Significant findings were observed for the genetic association between *APOB* (rs515135) and (rs693) polymorphisms with variation in TC genotype levels among the Iranian samples analyzed. Heterozygous samples at the *APOB* rs693 locus were significantly associated with lower TC serum levels. This may suggest an interaction between the two alleles to influence serum TC levels and thus genetically predispose individuals to dyslipidemia.

Univariate analysis of the *APOB* rs693 polymorphism revealed a significant association between carriers of the allele with lower mean serum TC. These abnormalities in lipid profile associated with the *APOB* rs693 polymorphism may be the result of a change in the degree of hydrophobicity and efficacy of *APOB* processing (24-26). Moreover, there was no statistically significant difference in plasma levels of the total cholesterol with respect to the *APOB* rs515135 SNP.

Among our studied population, the rare T allele was observed may be have a "protective" role exhibiting decrease in the risk of high TC levels in individuals homozygous for the rare T allele. Some of the subjects in the present study with positive family history of hypercholesterolemia ($n=120$) also showed a significant association with the rare T allele where there was a higher frequency of heterozygotes (26.67%). Logistic regression analysis also showed a significantly lower TC levels in individuals with the homozygous TT genotype.

Conclusion

In this study no significant relationship was found between rs515135 and familiar hypercholesterolemia. However, there was a significant association between the C allele of rs693 and high familial cholesterol levels.

Acknowledgements

The authors of this study would like to appreciate all patients with FH disorder from Karaj city, Iran, for blood donation. The authors would like to express their utmost gratitude to Masoume Dehghan and Parvin Pishva from Medical Genetic Department, Metabolic Center of TUMS for providing practical support to conduct this study. The

authors declare there is no conflict of interest. The authors would like to express their utmost gratitude to NIGEB for providing financial support to conduct this study.

Authors' Contributions

F.K.; Performed the experiments and contributed to reagents, materials, analysis tools, wrote the manuscript, contributed to the discussion, and reviewed the manuscript. I.S.; Conceived and designed the experiments. M.H.; Analyzed the data. All the authors read and approved the final manuscript and contributed toward data analysis, drafting and revising the paper and agree to be accountable for all aspects of the work.

Reference

- Ekrami M, Torabi M, Ghafouri-Fard S, Mowla J, Mohammad Soltani B, Hashemi-Gorji F, et al. Genetic analysis of iranian patients with familial hypercholesterolemia. *Iran Biomed J.* 2018; 22(2): 117-122.
- Faiz F, Nguyen LT, van Bockxmeer FM, Hooper AJ. Genetic screening to improve the diagnosis of familial hypercholesterolemia. *Clin Lipidol.* 2014; 9(5): 523-532.
- Tragante V, Asselbergs FW, Swerdlow DI, Palmer TM, Moore JH, de Bakker PI, et al. Harnessing publicly available genetic data to prioritize lipid modifying therapeutic targets for prevention of coronary heart disease based on dysglycemic risk. *Hum Genet.* 2016; 135(5): 453-467.
- Soutar AK, Naoumova RP. Mechanisms of disease: genetic causes of familial hypercholesterolemia. *Nat Clin Pract Cardiovasc Med.* 2007; 4(4): 214-225.
- Lye SH, Chahil JK, Bagali P, Alex L, Vadivelu J, Ahmad WA, et al. Genetic polymorphisms in LDLR, APOB, PCSK9 and other lipid related genes associated with familial hypercholesterolemia in Malaysia. *PLoS One.* 2013; 8(4): e60729.
- Willer CJ, Sanna S, Jackson AU, Scuteri A, Bonnycastle LL, Clarke R, et al. Newly identified loci that influence lipid concentrations and risk of coronary artery disease. *Nat Genet.* 2008; 40(2): 161-169.
- Ahmadi F, Mortazavi Y, Fouladsaz K, Mazloomzadeh S. Association of the 12669G> A apolipoprotein B gene polymorphism with apo-B serum level and lipid profile in patients with coronary artery disease comparing with individuals without coronary artery disease in Zanjan population of iran. *Indian J Clin Biochem.* 2016; 31(3): 315-320.
- Paththinige CS, Sirisena ND, Dissanayake V. Genetic determinants of inherited susceptibility to hypercholesterolemia-a comprehensive literature review. *Lipids Health Dis.* 2017; 16(1): 103.
- Futema M, Plagnol V, Li K, Whittall RA, Neil HA, Seed M, et al. Whole exome sequencing of familial hypercholesterolaemia patients negative for LDLR/APOB/PCSK9 mutations. *J Med Genet.* 2014; 51(8): 537-544.
- Paththinige CS, Sirisena ND, Dissanayake VHW. Genetic determinants of inherited susceptibility to hypercholesterolemia-a comprehensive literature review. *Lipids Health Dis.* 2017; 16: 103.
- Fisher E, Scharnagl H, Hoffmann MM, Kusterer K, Wittmann D, Wieland H, et al. Mutations in the apolipoprotein (apo) B-100 receptor-binding region: detection of apo B-100 (Arg3500→ Trp) associated with two new haplotypes and evidence that apo B-100 (Glu3405→ Gln) diminishes receptor-mediated uptake of LDL. *Clin Chem.* 1999; 45(7): 1026-1038.
- Ludwig EH, Blackhart BD, Pierotti VR, Caiati L, Fortier C, Knott T, et al. DNA sequence of the human apolipoprotein B gene. *DNA.* 1987; 6(4): 363-372.
- Hubacek JA, Adamkova V, Lanska V, Dlouha D. Polygenic hypercholesterolemia: examples of GWAS results and their replication in the Czech-Slavonic population. *Physiol Res.* 2017; 66 Suppl 1: S101-S111.
- Festen EA, Goyette P, Green T, Boucher G, Beauchamp C, Trynka G, et al. A meta-analysis of genome-wide association scans identifies IL18RAP, PTPN2, TAGAP, and PUS10 as shared risk loci for Crohn's disease and celiac disease. *PLoS Genet.* 2011; 7(1): e1001283.
- Egan KM, Thompson RC, Nabors LB, Olson JJ, Brat DJ, LaRocca RV, et al. Cancer susceptibility variants and the risk of adult glioma in a US case-control study. *J Neurooncol.* 2011; 104(2): 535-542.
- Dinu I, Mahasirimongkol S, Liu Q, Yanai H, Sharaf Eldin N, Kreiter E, et al. SNP-SNP interactions discovered by logic regression explain Crohn's disease genetics. *PLoS One.* 2012; 7(10): e43035.
- Onay VU, Briollais L, Knight JA, Shi E, Wang Y, Wells S, et al. SNP-SNP interactions in breast cancer susceptibility. *BMC Cancer.* 2006; 6: 114.
- Liu X, Wang Y, Qu H, Hou M, Cao W, Ma Z, Wang H. Associations of polymorphisms of rs693 and rs1042031 in apolipoprotein B gene with risk of breast cancer in Chinese. *Jpn J Clin Oncol.* 2013; 43(4): 362-368.
- Gao M, Tang H, Zheng X, Zhou F, Lu W. Association analysis of GWAS and candidate gene loci in a Chinese population with coronary heart disease. *Int J Clin Exp Med.* 2015; 8(5): 7497-7506.
- Asadi E, Farashahi Yazd E, Sheikhha MH, Ghasemi N, Zarifian Yeganeh R. Familial Hypercholesterolemia: From Diagnosis to Treatment. *Iranian journal of diabetes and obesity.* 2014; 6(4): 186-196.
- Marais AD. Familial hypercholesterolaemia. *Clin Biochem Rev.* 2004; 25(1): 49-68.
- Nordestgaard BG, Chapman MJ, Humphries SE, Ginsberg HN, Masana L, Descamps OS, et al. Familial hypercholesterolaemia is underdiagnosed and undertreated in the general population: guidance for clinicians to prevent coronary heart disease: consensus statement of the European Atherosclerosis Society. *Eur Heart J.* 2013; 34(45): 3478-3490a.
- Marks D, Wonderling D, Thorogood M, Lambert H, Humphries SE, Neil HA. Screening for hypercholesterolaemia versus case finding for familial hypercholesterolaemia: a systematic review and cost-effectiveness analysis. *Health Technol Assess.* 2000; 4(29): 1-123.
- Visvikis S, Chan L, Siest G, Drouin P, Boerwinkle E. An insertion deletion polymorphism in the signal peptide of the human apolipoprotein B gene. *Hum Genet.* 1990; 84(4): 373-375.
- Xu CF, Tikkanen MJ, Huttunen JK, Pietinen P, Bütler R, Humphries S, et al. Apolipoprotein B signal peptide insertion/deletion polymorphism is associated with Ag epitopes and involved in the determination of serum triglyceride levels. *J Lipid Res.* 1990; 31(7): 1255-1261.
- Talmud P, Lins L, Brasseur R. Prediction of signal peptide functional properties: a study of the orientation and angle of insertion of yeast invertase mutants and human apolipoprotein B signal peptide variants. *Protein Eng.* 1996; 9(4): 317-321.

Comparison of The Therapeutic Effect of Syngeneic, Allogeneic, and Xenogeneic Adipose Tissue-Derived Mesenchymal Stem Cells on Abortion Rates in A Mouse Model

Fatemeh Rezaei Kahmini, M.Sc., Seyed Mohammad Moazzeni, Ph.D.*

Department of Immunology, Faculty of Medical Sciences, Tarbiat Modares University, Tehran, Iran

*Corresponding Address: P.O.BOX: 14115-331, Department of Immunology, Faculty of Medical Sciences, Tarbiat Modares University, Tehran, Iran
Email: moazzeni@modares.ac.ir

Received: 8/Apr/2018, Accepted : 3/Jun/2018

Abstract

Objective: Mesenchymal stem cells (MSCs), due to their immunomodulatory functions, are an ideal candidate for the treatment of immune-related diseases. Recurrent spontaneous abortion (RSA) is one of the most common complications of pregnancy which in many cases is related to the immune system disorders. Our previous study has shown that the abortion rate was decreased following the syngeneic MSCs therapy in abortion-prone mice. In this study, the therapeutic effect of syngeneic, allogeneic, and xenogeneic MSCs was compared in a mouse model of RSA.

Materials and Methods: In this experimental study, MSCs were isolated from adipose tissue (ASCs) of CBA/J and BALB/c mice and human. After characterization, ASCs were injected (IP) at day 4 of gestation to female CBA/J mice following their mating with DBA/2 male mice. In the control group, phosphate-buffered saline (PBS) was injected and CBA/JxBALB/c mating was also used as the normal pregnancy control. On day 14.5 of pregnancy, embryo resorption rate was determined.

Results: The abortion rate significantly decreased following the ASCs therapy from syngeneic (6.31%), allogeneic (6.54%), and xenogeneic group (12.36%) compared to ASCs non-treated group (34.4%). There was no statistical difference between ASCs treated groups, however syngeneic and allogeneic ASCs reduced the abortion rate more efficiently than xenogeneic ASC.

Conclusion: The abortion rate was significantly decreased following the intraperitoneal administration of ASCs from various donated sources in abortion-prone mice. These results indicated that the immunogenicity of allogeneic and xenogeneic ASCs is not a contradictory problem for their therapeutic effects on RSA.

Keywords: Cell Therapy, Mesenchymal Stem Cells, Spontaneous Abortion

Cell Journal (Yakhteh), Vol 21, No 1, Apr-Jun (Spring) 2019, Pages: 92-98

Citation: Rezaei Kahmini F, Moazzeni SM. Comparison of the therapeutic effect of syngeneic, allogeneic, and xenogeneic adipose tissue-derived mesenchymal stem cells on abortion rates in a mouse model. Cell J. 2019; 21(1): 92-98. doi: 10.22074/cellj.2019.5954.

Introduction

Mesenchymal stem cells (MSCs), due to their ability to secrete various immunomodulatory factors, including prostaglandin E₂ (PGE₂), transforming growth factor- β (TGF- β), interleukin 10 (IL-10), human leukocyte antigen G (HLA-G), inducible nitric oxide synthase (iNOS) and their differentiation potential are an appropriate option for cell-based therapy (1, 2). MSCs have been isolated from different organs including bone marrow, adipose tissue, umbilical cord blood, placenta, muscle, liver, and synovial fluid (3-5). However, adipose tissue could be an ideal source of MSCs, because of its availability and simplicity of established techniques to extract abundant MSCs from this tissue. In addition, various studies have shown that adipose-derived MSCs (ASCs) have strong immunomodulatory properties with no side effects (6-8). ASCs' immunomodulatory effects are due to the secretion of various growth factors and cytokines, as well as direct cell to cell contact (7).

Recurrent spontaneous abortion (RSA) is one of the most common complications of the pregnancy, with a prevalence of 2-5 percentage among pregnant women. A major fraction of RSA is closely related to the maternal immune system disorders, especially the local immune responses at the fetomaternal interface (9-11). Female CBA/J mice mating

to male DBA/2 mice are susceptible to abortion because of numerous immunological disorders and are commonly used as a mouse model of immunologic RSA. The rate of embryo resorption by these mice has been reported to be about 20-40%, while in normal mice it is 4-5% (12, 13). Our previous study has shown that autologous ASCs therapy could reduce the abortion rate in abortion-prone mice (14). Since ultimately, animal studies have to be generalized to humans and most studies are based on allogeneic cell therapy because the separation of the autologous MSCs is time-consuming, in this study, we compared the effect of human (xenogeneic), allogeneic and syngeneic ASCs on the reduction of abortion rate in an RSA model.

Materials and Methods

Mice and experimental design

In this experimental study, CBA/J female mice (6-8 weeks), BALB/c, and DBA/2 male mice (9-11 weeks) were purchased from Pasteur Institute of Iran (Tehran, Iran). All animals were kept under controlled conditions of temperature, humidity, and light (cycles of 12 hours dark/light). All experimental procedures on animals were followed according to the rules of the Ethical Committee

of the Faculty of Medical Science, Tarbiat Modares University IR.TMU.REC.1394.255). CBA/J female mice were mated to either DBA/2 or BALB/c males overnight. Detection of the vaginal plug was considered the day 0.5 of gestation. It is accepted that CBA/J female mating to DBA/2 males mice show immunological abortion and are defined as abortion-prone pregnant mice. The mating of CBA/J mice to BALB/c results in normal pregnancy and is considered as normal pregnant mice in this experiments (15).

Some pregnant mice in the abortion-prone group (CBA/J×DBA/2) received 10^6 syngeneic, allogeneic or xenogeneic ASCs in phosphate-buffered saline (PBS) intraperitoneally on the day 4.5 of gestation (implantation window) (ASCs treated group, n=5 for each kind of ASC). Some mice in the same mating pairs received an i.p. injection of PBS as a control group (n=5). CBA/J×BALB/c mating as the normal pregnancy control also received PBS (n=5). Animals were sacrificed by cervical dislocation on the day 14.5 of gestation. Afterward, uteri horns were isolated from pregnant mice and the total number of embryo resorption was counted. The percentage of resorption in experimental groups was calculated according to the formula: resorption rate % = (number of resorbed fetus/number of the total fetus)×100 (16).

Isolation of mesenchymal stem cells from the adipose tissue

MSCs were isolated from the abdominal fat of CBA/J and BALB/c mice (3-5 week), adipose tissue was cut into small pieces and digested with 1 mg/mL collagenase type I (Sigma-Alderich, USA) for 30 minutes at 37°C with every 10 minutes shaking to get a single cell suspension. After neutralization of collagenase with Dulbecco's Modified Eagle Medium (DMEM, Gibco, UK) containing fetal calf serum (FCS), the separated cells were centrifuged (1500 g for 15 minutes) and the cell pellet was cultured in DMEM containing 10% FCS and kept in 5% CO₂ at 37°C. After 24 hours, the medium was changed to remove the non-adherent cells. When approximately 70-80% confluence was achieved, the adherent cells were trypsinized and harvested. Passage 2 cells were used for injection.

Human ASCs were isolated from Lipoaspirate samples as described by Zhu et al. (17). In brief, adipose tissue was obtained after liposuction with informed consent and digested by collagenase type I (1 mg/mL, Sigma-Alderich, USA). For this purpose, adipose samples were mixed with collagenase solution and placed at 37°C for 30 minutes. DMEM with 10% FCS was used to neutralize collagenase (5 minutes at room temperature). Then the cell pellets were collected by centrifugation (1200 g for 10 minutes) and cultured in DMEM containing 10% FCS and kept in 5% CO₂ at 37°C. After removal of non-adherent cells and getting a confluent culture, the cells from the second passage were used for experiments. It has been shown that MSCs lost their stem cells properties and enter the senescence during *in vitro* cultures (18). So we chose the second passage for the cell therapy.

Immunophenotyping of adipose tissue-derived mesenchymal stem cells

The expression of surface markers on MSCs was

investigated using the following antibodies. Anti-mouse CD34 (PE, eBioscience, USA), anti-mouse CD44 (APC, BD, USA), anti-mouse CD45 (APC-cy7, Biolegend, USA), anti-mouse CD73 (PE, BD, USA), anti-mouse CD90 (APC, BD, USA), anti-mouse CD105 (PE, eBioscience, USA), anti-mouse Sca1 (FITC, Biolegend, USA), anti-mouse CD3 (PE, BD, USA), anti-human CD90 (APC, Biolegend, USA), anti-human CD105 (APC, Biolegend, USA), anti-human CD29 (PE, eBioscience, USA), anti-human CD45 (FITC, Biolegend, USA) and anti-human CD34 (PE, eBioscience, USA). Passage 2 cells were used for the analysis of cell surface markers by flow cytometry (FACS calibur, Becton Dickinson, USA). For flow cytometry analysis, 10,000 events were counted and data were analyzed using the flowJo software.

Multi-lineage differentiation of adipose tissue-derived mesenchymal stem cells

Isolated MSCs from the adipose tissue were cultured in DMEM containing 10% FCS, dexamethasone (0.5 mM, Sigma-Alderich, USA), indomethacin (50 mM, Sigma-Alderich, USA), insulin (5 μM, Sigma-Alderich, USA), and isobuthylmethylxanthine (0.5 mM, Sigma-Alderich, USA) for 3 weeks to induce adipose differentiation. Differentiated cells were assessed using oil red O for adipocyte detection.

To induce the differentiation toward osteocytes, MSCs were incubated in condition medium (DMEM+10% fetal bovine serum) supplemented with ascorbic acid (50 mg/ml), β-glycerolphosphate (10 mM), and dexamethasone (0.1 μM). After 3 weeks incubation at 37°C the cells were fixed by formalin 10%, then the cells were stained with Alizarin red (Sigma-Alderich, USA) to detect mineralized matrix of the bone (17, 19).

Statistical analysis

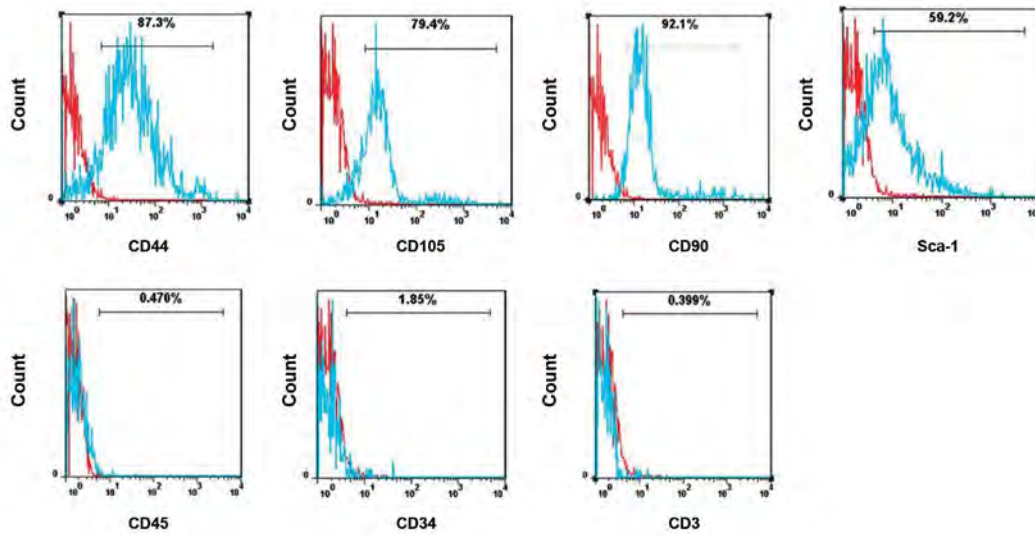
Statistical analysis of the data was performed using the SPSS version 23 software (IBM company, USA). The differences in resorption rate between experimental groups were analyzed by chi-square (χ^2) and Fisher's exact test where appropriate. Data are presented as mean ± SD. The P<0.05 were considered statistically significant.

Results

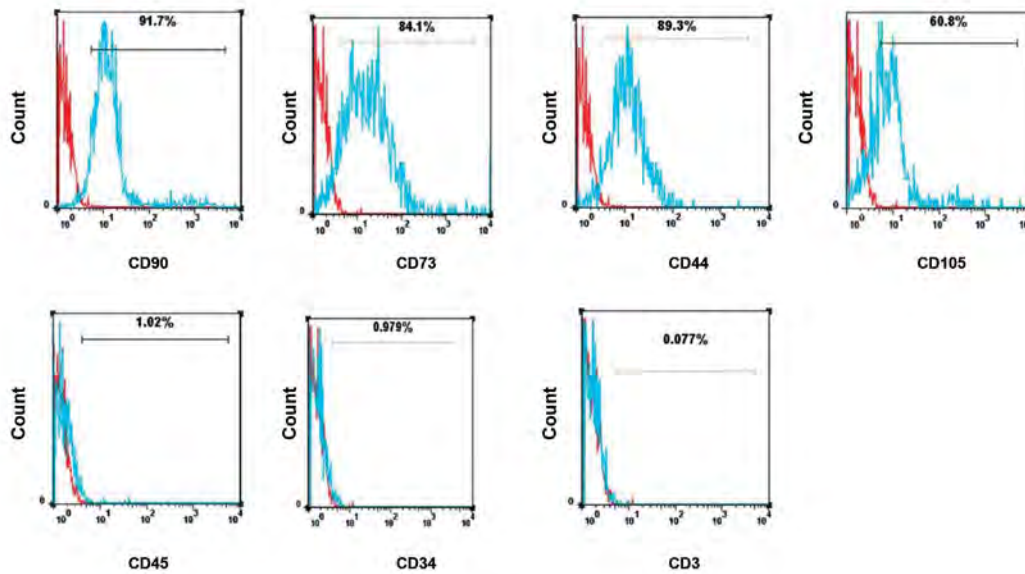
Isolation of mesenchymal stem cells from adipose tissue and their characterization

MSCs were isolated from different sources including abdominal fat of CBA/J and BALB/c mice, and human lipoaspirate. Cultured ASCs were fibroblast-like, plastic adherent, and spindle-shaped which were consistent with MSC morphology. Immunophenotyping analysis demonstrated that MSCs cultures from passage 2 in mice were positive for CD105, CD44, Sca-1, CD73, and CD90 and negative for CD45, CD3, and CD34 (Fig.1A, B). Immunophenotyping analysis also demonstrated that isolated MSCs from human liposuction were positive for CD90, CD105, and CD29 and negative for CD45 and CD34 (Fig.1C).

A



B



C

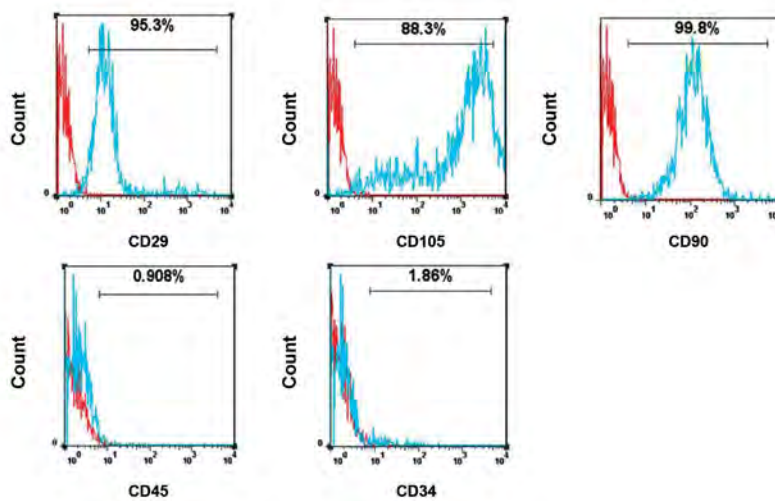


Fig.1: Cell surface phenotype analysis of adipose tissue-derived mesenchymal stem cells (ASCs). **A.** The syngeneic (obtained from CBA/J), **B.** Allogeneic (obtained from BALB/c), and **C.** Xenogeneic ASCs (obtained from human) were analyzed for the expression of cell surface markers at the second passage of cultured cells by flow cytometry. The cells were positive for stem cell markers and negative for the hematopoietic markers in all kinds of ASCs. Histograms show the expression of surface markers (blue) which were plotted against the unstained control (red).

Differentiation of adipose tissue-derived mesenchymal stem cells into osteogenic and adipogenic lineages

To evaluate the multi-lineage differentiation ability of the isolated ASCs, the cells were induced to osteoblast and adipocyte under appropriate culture conditions. In the osteogenic medium, both human and mice ASCs formed the calcium mineralization confirmed by Alizarin red staining (Fig.2A). The ASCs were also cultured in adipogenic medium and revealed that ASCs of all sources formed lipid droplet confirmed by oil red O staining (Fig.2B)

Adipose tissue-derived mesenchymal stem cells reduced the abortion rate in the abortion-prone mice

We observed that the administration of ASCs from all sources at the day 4.5 of pregnancy to CBA/J pregnant

mice in CBA/J×DBA/2 matting, significantly reduced the abortion rate compared to the untreated control group which received PBS ($P < 0.05$). The difference in abortion rate down-regulation between syngeneic, allogeneic, and xenogeneic ASCs was not statistically significant, however syngeneic and allogeneic ASCs reduced the abortion rate more efficiently ($P = 0.0007$) than xenogeneic ASC ($P = 0.014$). The percentage of abortion rate on the day 14.5 of gestation in non-treated control group was 34.4% (16 out of 46 implanted fetuses; $n = 5$) in syngeneic ASCs-treated group was 6.31% (3 out of 48 implanted fetuses, $n = 5$), in allogeneic ASCs-treated group was 6.54% (3 of 47 implanted fetuses, $n = 5$) in xenogeneic ASCs-treated group was 12.36% (6 of 48 implanted fetuses, $n = 5$). The resorption rate in normal pregnancy group was 6.04% (3 of 49 implanted fetuses, $n = 5$) (Fig.3).

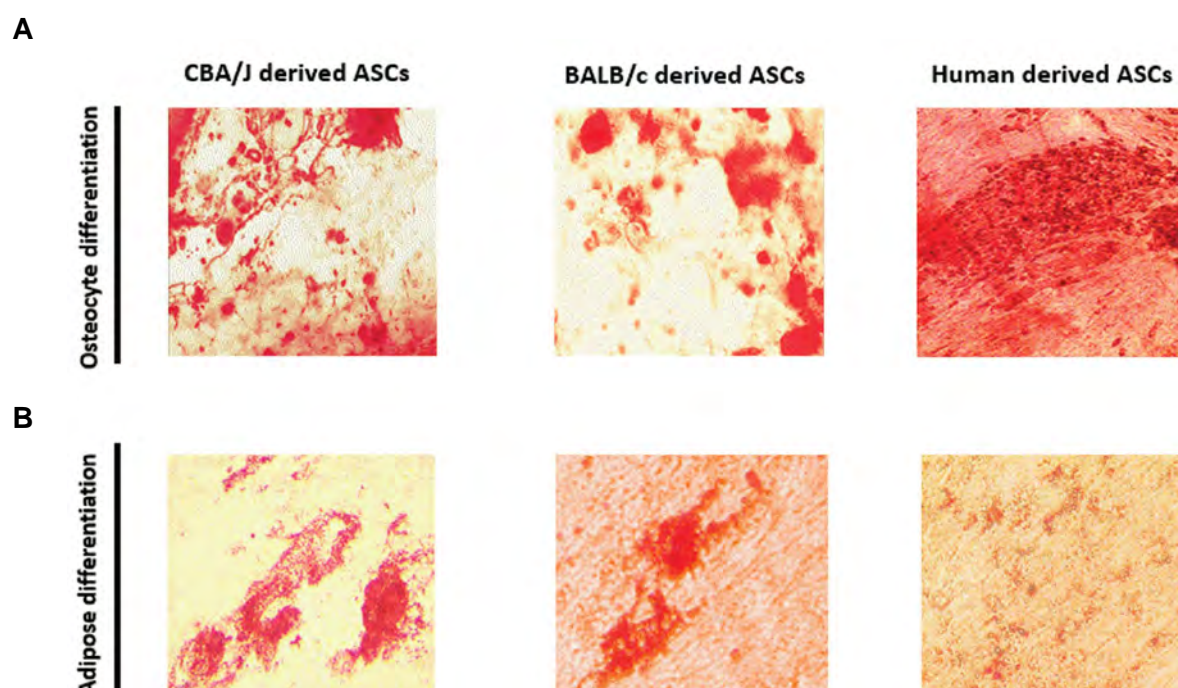
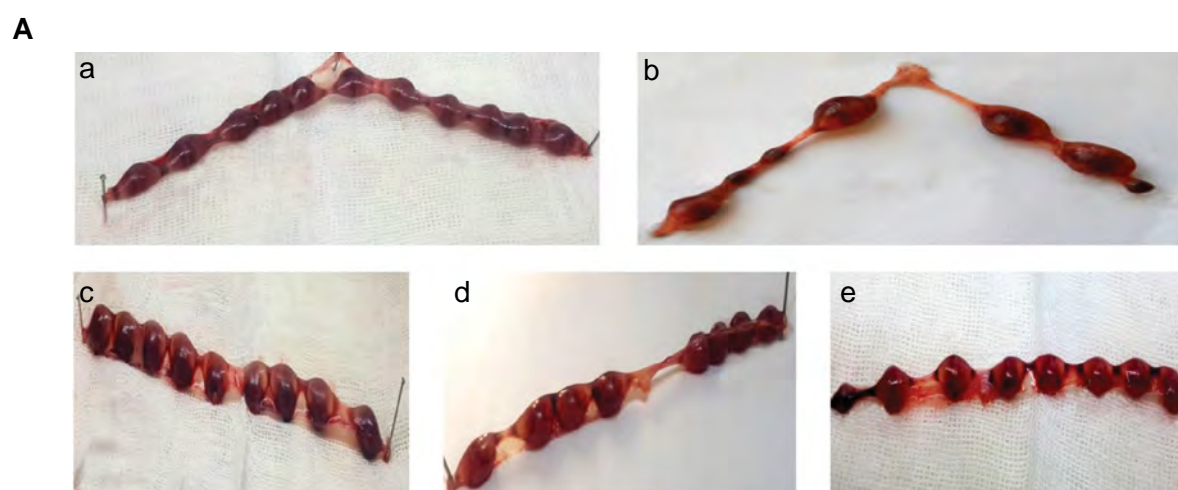


Fig.2: Differentiation potential of adipose tissue-derived mesenchymal stem cells (ASCs). **A.** Osteogenic capability of cells was determined by Alizarin Red staining after 21 days of induction in osteogenic medium and **B.** The ability of ASCs to differentiate into adipocyte was characterized by oil red O staining after being cultured in the adipogenic medium.



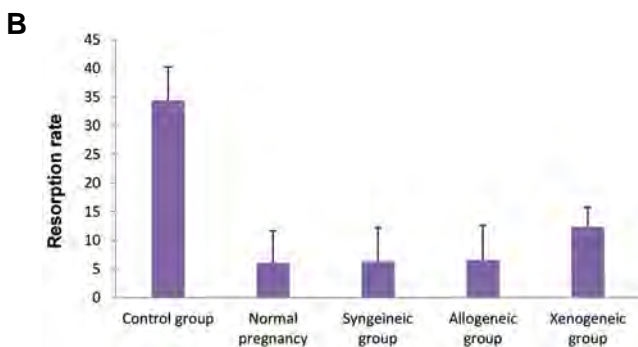


Fig. 3: Effect of cell therapy on the embryo resorption rate. Mice were injected i.p with syngeneic, allogeneic, and xenogeneic adipose tissue-derived mesenchymal stem cells (ASCs) or PBS on day 4.5 of gestation. On day 14.5 of gestation uteri were removed and investigated for resorption rate. **A.** Representative photographs indicating the implantation sites in normal pregnancy (a), control group (b), syngeneic group (c), allogeneic group (d), and xenogeneic group (e) and **B.** Resorption rate in studied groups. In the ASCs treated groups, the percentage of embryo loss was significantly lower than the control group. The data are presented as mean \pm SD.

Discussion

Our previous studies showed that syngeneic ASCs therapy could reduce the abortion rate in abortion-prone mice and might be considered a promising treatment route for immune-mediated pregnancy loss (14, 20). Here, we showed that allogeneic and xenogeneic ASCs therapy could also reduce the abortion rate in this model.

Several studies demonstrated that disorders of immune responses play a crucial role in the pathophysiology of RSA (12, 21), so immunomodulatory therapy could be an attractive and hopeful treatment for this disorder. Various sources of MSCs including allogeneic, syngeneic, and xenogeneic have been used in the treatment of different regenerative and auto-immune disorders (22-24). We have used autologous ASCs in our previously mentioned studies to reduce the abortion rate. Because autologous ASCs are not always simply available, in this study, we compared the therapeutic effects of syngeneic, allogeneic, and xenogeneic ASCs in the cell therapy of recurrent pregnancy loss using an appropriate RSA animal model.

Our results showed that the abortion rate was decreased following ASCs therapy in all studied groups. ASCs therapy could significantly reduce the abortion rate from 34.4% in non-treated abortion-prone mice to 6.3%, 6.54%, and 12.36% in syngeneic, allogeneic and xenogeneic ASCs-treated groups, respectively. As seen, all kinds of ASCs remarkably reduced the abortion rate in comparison to the untreated control group.

It has been shown that adverse immune response plays a crucial role in most cases of spontaneous abortion. Dysregulated activities of natural killer cells, T cells, and macrophages, as well as the decreased density of regulatory T cells and altered activities of dendritic cells, are reported to be involved in the etiology of RSA by many investigators (12, 13, 21, 25). Regarding to the aberrant immune response as the main player in most cases of

spontaneous abortion and accepted immunomodulatory properties of MSCs (26-28), it could be concluded that downregulation of abortion rate could be mainly due to the immunomodulatory effects of MSCs, which could abrogate or regulate the undesirable immune reactions. Besides, the immunoregulation through a direct cell to cell contact, the most important immunomodulatory factors of MSCs are PGE2, hepatocyte growth factors (HGF), Indoleamine 2, 3-dioxygenase (IDO), nitric oxide (NO), IL-10, and TGF- β 1 which lead to the suppression of B, T, and NK-cell proliferation and DC maturation. MSCs are also reported as strong inducers of regulatory T cells and M2 macrophages (2, 28-33). Several studies also indicated the protection of fetus from abortion through immunosuppressive molecules such as TGF- β and IL-10 (34, 35). These results suggest that MSCs may improve the pregnancy outcome through the modulation of the adverse immune responses at the fetomaternal interface.

In this study, we observed no statistical difference among therapeutic effect of the different sources of ASCs, however xenogeneic ASCs had less efficiency compared to syngeneic and allogeneic ASCs. It is likely that the cross-talk between mouse-derived MSCs and mouse immune cells in this model is more effective than xenogeneic (human-derived) MSCs. However, some molecules that induce immunomodulatory function of MSCs are common among species such as PGE2, IL-10, hemoxygenase-1 (HO-1), and IL-6, but there are some structural differences between these MSCs-derived secretory components between mouse and human which cause a lower response of target cells from the mouse immune system to human-derived cytokines. Direct cell-cell interaction is another mechanism for immunomodulating by MSCs. This interaction is exerted through the cell surface ligands and ligates such as programmed cell death 1 ligand 1 (PD-L1), PD1, intercellular adhesion molecule-1 (ICAM-1), vascular cell adhesion molecule-1 (VCAM-1), integrin alpha-4 (ITGA4), and galectin (36, 37). In this case, the structural differences in surface molecules among species do not let an effective cross-talk between the human and mouse cells. MSCs from various species also exert their effects through different mechanisms. Some studies showed that murine MSCs use inducible nitric oxide synthase, while the human MSCs use IDO as a tool for their immunomodulatory properties (30, 38). This could be another possible explanation for the difference in their therapeutic effects in our model.

Although most *in vitro* studies have indicated the immunosuppressive effect of MSCs, several studies have also shown the immunogenicity of these cells for non-syngeneic species. After systemic injection of allogeneic and xenogeneic MSCs, their presence in recipient tissues is probably limited because of the immunological process (29, 31, 38). The effects of syngeneic versus allogeneic MSCs were investigated in EAE and have shown that allogeneic MSCs stimulate the immune responses compared to syngeneic MSCs.

However, both treatments had similar curative effects (38). We also observed the same results and there was no difference between therapeutic effects of syngeneic and allogeneic groups. This finding may be related to weak immunogenicity of allogeneic MSCs compared to other cell types from allogeneic source, which causes their slow rejection and longer presence in recipient animals (29). For xenogeneic MSCs the immunogenicity could be stronger and more limitary. So the structural differences in implicated molecules in immunomodulation and weak immunogenicity of xenogeneic MSCs could be considered the main reasons for the lower efficiency of these cells in the reduction of the abortion rate.

Conclusion

The results of the present study demonstrated that, in spite of the weak immunogenicity of allogeneic MSCs, it can be used instead of autologous MSCs. The separation of autologous MSCs is time-consuming and not suitable for the acute conditions. Additionally, MSCs from various donors are somewhat different in their therapeutic effects but allogeneic MSCs can be harvested from the healthy donors and their therapeutic and immunomodulatory efficacy could be investigated for the banking purposes.

Acknowledgments

The authors would like to acknowledge the financial support of Tarbiat Modares University and National Institute for Medical Research Development (NIMAD), Tehran, Iran. The authors declare no conflict of interest.

Authors' Contributions

F.R.K.; Contributed to all experimental work, data collection and statistical analysis. S.M.M.; Was responsible for overall supervision, and interpretation of data. Both authors performed editing and approving the final version of this paper.

References

- Ferris RA, Frisbie DD, McCue PM. Use of mesenchymal stem cells or autologous conditioned serum to modulate the inflammatory response to spermatozoa in mares. *Theriogenology*. 2014; 82(1): 36-42.
- Lavoie JR, Rosu-Myles M. Uncovering the secrets of mesenchymal stem cells. *Biochimie*. 2013; 95(12): 2212-2221.
- Park D, Yang G, Bae DK, Lee SH, Yang YH, Kyung J, et al. Human adipose tissue-derived mesenchymal stem cells improve cognitive function and physical activity in ageing mice. *J Neurosci Res*. 2013; 91(5): 660-670.
- Rosignoli F, Caselli A, Grisendi G, Piccinno S, Burns JS, Murgia A, et al. Isolation, characterization, and transduction of endometrial decidual tissue multipotent mesenchymal stromal/stem cells from menstrual blood. *Biomed Res Int*. 2013; 2013: 901821.
- Jacobs SA, Roobrouck VD, Verfaillie CM, Van Gool SW. Immunological characteristics of human mesenchymal stem cells and multipotent adult progenitor cells. *Immunol Cell Biol*. 2013; 91(1): 32-39.
- Zhang S, Danchuk SD, Imhof KM, Semon JA, Scruggs BA, Bonvilain RW, et al. Comparison of the therapeutic effects of human and mouse adipose-derived stem cells in a murine model of lipopolysaccharide-induced acute lung injury. *Stem Cell Res Ther*. 2013; 4(1): 13.
- Marconi S, Bonaconsa M, Scambi I, Squintani GM, Rui W, Turano E, et al. Systemic treatment with adipose-derived mesenchymal stem cells ameliorates clinical and pathological features in the amyotrophic lateral sclerosis murine model. *Neuroscience*. 2013; 248: 333-343.
- Minonzio G, Corazza M, Mariotta L, Gola M, Zanzi M, Gandolfi E, et al. Frozen adipose-derived mesenchymal stem cells maintain high capability to grow and differentiate. *Cryobiology*. 2014; 69(2): 211-216.
- Yin G, Li C, Shan B, Wang W, Chen H, Zhong Y, et al. Insufficient peroxiredoxin-2 expression in uterine NK cells obtained from a murine model of abortion. *J Cell Biochem*. 2011; 112(3): 773-781.
- Kuśnierczyk P. Killer cell immunoglobulin-like receptor gene associations with autoimmune and allergic diseases, recurrent spontaneous abortion, and neoplasms. *Front Immunol*. 2013; 4: 8.
- Baek KH, Lee EJ, Kim YS. Recurrent pregnancy loss: the key potential mechanisms. *Trends Mol Med*. 2007; 13(7): 310-317.
- Kwak-Kim J, Bao S, Lee SK, Kim JW, Gilman-Sachs A. Immunological modes of pregnancy loss: inflammation, immune effectors, and stress. *Am J Reprod Immunol*. 2014; 72(2): 129-140.
- Ahmadabad HN, Salehnia M, Saito S, Moazzeni SM. Decidual soluble factors, through modulation of dendritic cells functions, determine the immune response patterns at the fetomaternal interface. *J Reprod Immunol*. 2016; 114: 10-17.
- Sadighi-Moghaddam B, Salek Farrokhi A, Namdar Ahmadabad H, Barati M, Moazzeni SM. Mesenchymal stem cell therapy prevents abortion in CBA/Jx DBA/2 mating. *Reprod Sci*. 2017; 25(8): 1261-1269.
- Zenclussen AC, Gerlof K, Zenclussen ML, Sollwedel A, Bertoja AZ, Ritter T, et al. Abnormal T-cell reactivity against paternal antigens in spontaneous abortion: adoptive transfer of pregnancy-induced CD4+ CD25+ T regulatory cells prevents fetal rejection in a murine abortion model. *Am J Pathol*. 2005; 166(3): 811-822.
- Lin Y, Zhong Y, Saito S, Chen Y, Shen W, Di J, et al. Characterization of natural killer cells in nonobese diabetic/severely compromised immunodeficient mice during pregnancy. *Fertil Steril*. 2009; 91(6): 2676-2686.
- Zhu M, Heydarkhan-Hagvall S, Hedrick M, Benhaim P, Zuk P. Manual isolation of adipose-derived stem cells from human lipos aspirates. *J Vis Exp*. 2013; (79): e50585.
- Bonab MM, Alimoghaddam K, Talebian F, Ghaffari SH, Ghavamzadeh A, Nikbin B. Aging of mesenchymal stem cell in vitro. *BMC Cell Biol*. 2006; 7: 14.
- Yousefi F, Ebtekar M, Soleimani M, Soudi S, Hashemi SM. Comparison of in vivo immunomodulatory effects of intravenous and intraperitoneal administration of adipose-tissue mesenchymal stem cells in experimental autoimmune encephalomyelitis (EAE). *Int Immunopharmacol*. 2013; 17(3): 608-616.
- Salek Farrokhi A, Zarnani AH, Moazzeni SM. Mesenchymal stem cells therapy protects fetuses from resorption and induces Th2 type cytokines profile in abortion prone mouse model. *Transpl Immunol*. 2018; 47: 26-31.
- Zhang J, Dunk C, Croy AB, Lye SJ. To serve and to protect: the role of decidual innate immune cells on human pregnancy. *Cell Tissue Res*. 2016; 363(1): 249-265.
- Kartiko BH, Siswanto FM, Purwata TE. Mesenchymal stem cell (MSC) as a potential cell therapy for immune related disease. *Bali Med J*. 2017; 6(1): 38-43.
- Álvarez-Gracia JM, Jover JA, García-Vicuña R, Carreño L, Alonso A, Marsal S, et al. Intravenous administration of expanded allogeneic adipose-derived mesenchymal stem cells in refractory rheumatoid arthritis (Cx611): results of a multicentre, dose escalation, randomised, single-blind, placebo-controlled phase Ib/IIa clinical trial. *Ann Rheum Dis*. 2017; 76(1): 196-202.
- Ibraheem H, Giacomini C, Kassam Z, Dazzi F, Powell N. Advances in mesenchymal stromal cell therapy in the management of Crohn's disease. *Expert Rev Gastroenterol Hepatol*. 2018; 12(2): 141-153.
- Zhou J, Xiao XM, Wu YH. Expression of interferon- γ in decidual natural killer cells from women with hypertensive disorder complicating pregnancy. *J Obstet Gynaecol Res*. 2014; 40(3): 670-676.
- Gao F, Chiu SM, Motan DA, Zhang Z, Chen L, Ji HL, et al. Mesenchymal stem cells and immunomodulation: current status and future prospects. *Cell Death Dis*. 2017; 7(1): e2062.
- Leijs MJ, Villafuertes E, Haeck JC, Koevoet WJ, Fernandez-Gutierrez B, Hoogduijn MJ, et al. Encapsulation of allogeneic mesenchymal stem cells in alginate extends local presence and therapeutic function. *Eur Cell Mater*. 2017; 33: 43-58.
- Kiernan CH, Wolvius EB, Brama PAJ, Farrell E. The immune response to allogeneic differentiated mesenchymal stem cells in the

- context of bone tissue engineering. *Tissue Eng Part B Rev.* 2018; 24(1): 75-83.
29. Ankrum JA, Ong JF, Karp JM. Mesenchymal stem cells: immune evasive, not immune privileged. *Nat Biotechnol.* 2014; 32(3): 252-260.
 30. Wang Y, Chen X, Cao W, Shi Y. Plasticity of mesenchymal stem cells in immunomodulation: pathological and therapeutic implications. *Nat Immunol.* 2014; 15(11): 1009-1016.
 31. Murphy MB, Moncivais K, Caplan AI. Mesenchymal stem cells: environmentally responsive therapeutics for regenerative medicine. *Exp Mol Med.* 2013; 45: e54.
 32. Zhuang Y, Li D, Fu J, Shi Q, Lu Y, Ju X. Comparison of biological properties of umbilical cord-derived mesenchymal stem cells from early and late passages: Immunomodulatory ability is enhanced in aged cells. *Mol Med Rep.* 2015; 11(1): 166-174.
 33. Zhao Q, Ren H, Han Z. Mesenchymal stem cells: immunomodulatory capability and clinical potential in immune diseases. *J Cell Immunother.* 2016; 2(1): 3-20.
 34. Clark DA, Flanders KC, Banwatt D, Millar-Book W, Manuel J, Stedronska-Clark J, et al. Murine pregnancy decidua produces a unique immunosuppressive molecule related to transforming growth factor beta-2. *J Immunol.* 1990; 144(8): 3008-3014.
 35. Chaouat G, Assal Meliani A, Martal J, Raghupathy R, Elliott JF, Mosmann T, et al. IL-10 prevents naturally occurring fetal loss in the CBA x DBA/2 mating combination, and local defect in IL-10 production in this abortion-prone combination is corrected by in vivo injection of IFN-tau. *J Immunol.* 1995; 154(9): 4261-4268.
 36. Pedemonte E, Benvenuto F, Casazza S, Mancardi G, Oksenberg JR, Uccelli A, et al. The molecular signature of therapeutic mesenchymal stem cells exposes the architecture of the hematopoietic stem cell niche synapse. *BMC Genomics.* 2007; 8: 65.
 37. Shi Y, Su J, Roberts AI, Shou P, Rabson AB, Ren G. How mesenchymal stem cells interact with tissue immune responses. *Trends Immunol.* 2012; 33(3): 136-143.
 38. Ma S, Xie N, Li W, Yuan B, Shi Y, Wang Y. Immunobiology of mesenchymal stem cells. *Cell Death Differ.* 2014; 21(2): 216-225.
-

Hypothesis: A Challenge of Overexpression *Zfp521* in Neural Tendency of Derived Dental Pulp Stem Cells

Fatemeh Behrouznejad, M.Sc.¹, Fatemeh Ejeian, M.Sc.², Modjtaba Emadi-Baygi, Ph.D.^{1*},
Parvaneh Nikpour, Ph.D.³, Mohammad Hossein Nasr-Esfahani, Ph.D.^{2*}

1. Department of Genetics, Faculty of Basic Sciences, Shahrekord University, Shahrekord, Iran
2. Department of Cellular Biotechnology, Cell Science Research Center, Royan Institute for Biotechnology, ACECR, Isfahan, Iran
3. Department of Genetics and Molecular Biology, Faculty of Medicine, Isfahan University of Medical Sciences, Isfahan, Iran

*Corresponding Addresses: P.O.Box: 8818634141, Department of Genetics, Faculty of Basic Sciences, Shahrekord University, Shahrekord, Iran

P.O.Box: 8165131378, Department of Cellular Biotechnology, Cell Science Research Center, Royan Institute for Biotechnology, ACECR, Isfahan, Iran

Emails: Emadi-m@sci.sku.ac.ir, mh_nasr@med.mui.ac.ir

Received: 25/Oct/2017, Accepted: 21/Apr/2018

Abstract

Neurodegenerative diseases have now become a major challenge, especially in aged societies. Most of the traditional strategies used for treatment of these diseases are untargeted and have little efficiency. Developments in stem cell investigations have given much attention to cell therapy as an alternative concept in the regeneration of neural tissues. Dental pulp stem cells (DPSCs) can be readily obtained by noninvasive procedures and have been shown to possess properties similar to well-known mesenchymal stem cells. Furthermore, based on their neural crest origin, DPSCs are considered to have a good potential to differentiate into neural cells. *Zfp521* is a transcription factor that regulates expression of many genes, including ones involved in the neural differentiation process. Therefor based on neural crest origin of the cell and high expression of neural progenitor markers, we speculate that sole overexpression of *Zfp521* protein can facilitate differentiation of dental stem cells to neural cells and researchers may find these cells suitable for therapeutic treatment of neurodegenerative diseases.

Keywords: Mesenchymal Stem Cell, Neurodegenerative Diseases, Neuronal Differentiation, Zinc Finger Protein 521

Cell Journal (Yakhteh), Vol 21, No 1, Apr-Jun (Spring) 2019, Pages: 99-102

Citation: Behrouznejad F, Ejeian F, Emadi-Baygi M, Nikpour P, Nasr-Esfahani MH. Hypothesis: a challenge of overexpression *Zfp521* in neural tendency of derived dental pulp stem cells. Cell J. 2019; 21(1): 99-102. doi: 10.22074/cellj.2019. 5600.

Neurodegenerative diseases have the profound impacts on modern human life, which common treatment in the medical field often fail. This event is mainly attributed to the limited ability of the adult central nervous system (CNS) for regeneration of neurons and glial cells (1, 2). Therefore, this dearth has lead researchers in the nascent field of regenerative medicine to assess the ability of different types of stem cells, including adult stem cells (ASCs) and embryonic stem cells (ESCs) to differentiate into neurons (2-4). Despite the high ability of ESCs to self-renewal and also to differentiate into various types of cells, the risk of teratogenicity, rejection, and ethical issues narrow their medical application. In contrast to ESCs, these risks are less associated with ASCs that show lower degree of plasticity. In this regard, different approaches are used to improve the transdifferentiation potential of ASCs to applying in regenerative medicine (2, 4).

Dental stem cells (DSCs) originated from the cranial neural crest and reside in different parts of the oral cavity. These cells are easily obtained by relatively noninvasive methods and can differentiate into neurons, chondrocytes, cardiomyocytes and osteoblasts cells (5). During the last decade, many studies have revealed that these cells also express key neurotropic factors including neurotrophin 3 (NT3), brain-derived neurotrophic factor (BDNF)

and neurotrophin 4 (NT4) as well as some of the main neural markers such as Nestin, Sox2 and Glial Fibrillary Acidic Protein (GFAP) (6-11). Previously, an exciting experiment revealed a relatively high similarity in DNA methylation pattern in dental pulp stem cells (DPSCs) and some neural stem cell lines, which confirmed their neural regeneration plasticity and their common origin. So, it is believed that these cells have an innate tendency to differentiate into neurons, which can be augmented by exogenous transcription factors (1, 12).

Zinc finger protein 521 (*Zfp521*, also known *ZNF521* in human) is a highly conserved nuclear factor that contains 30 Kruppel-like zinc finger motifs and different co-regulatory domains. As a result, *Zfp521* is capable of interacting with many transcriptional co-factors (13, 14) in diverse developmental processes and is involved with nucleosome remodeling in various tissues and organs (15-17).

Furthermore, it has been proven that *Zfp521* shares a common 12 amino acid motif with many transcriptional repressors, like nucleosome remodeling and deacetylase (NuRD). A significant amount of *Zfp521* protein in osteo/chondro progenitor cells recruits NuRD and some other histone deacetylases (HDCA) that consequently attenuates *RUNX2*, as a specification gene (18-20).

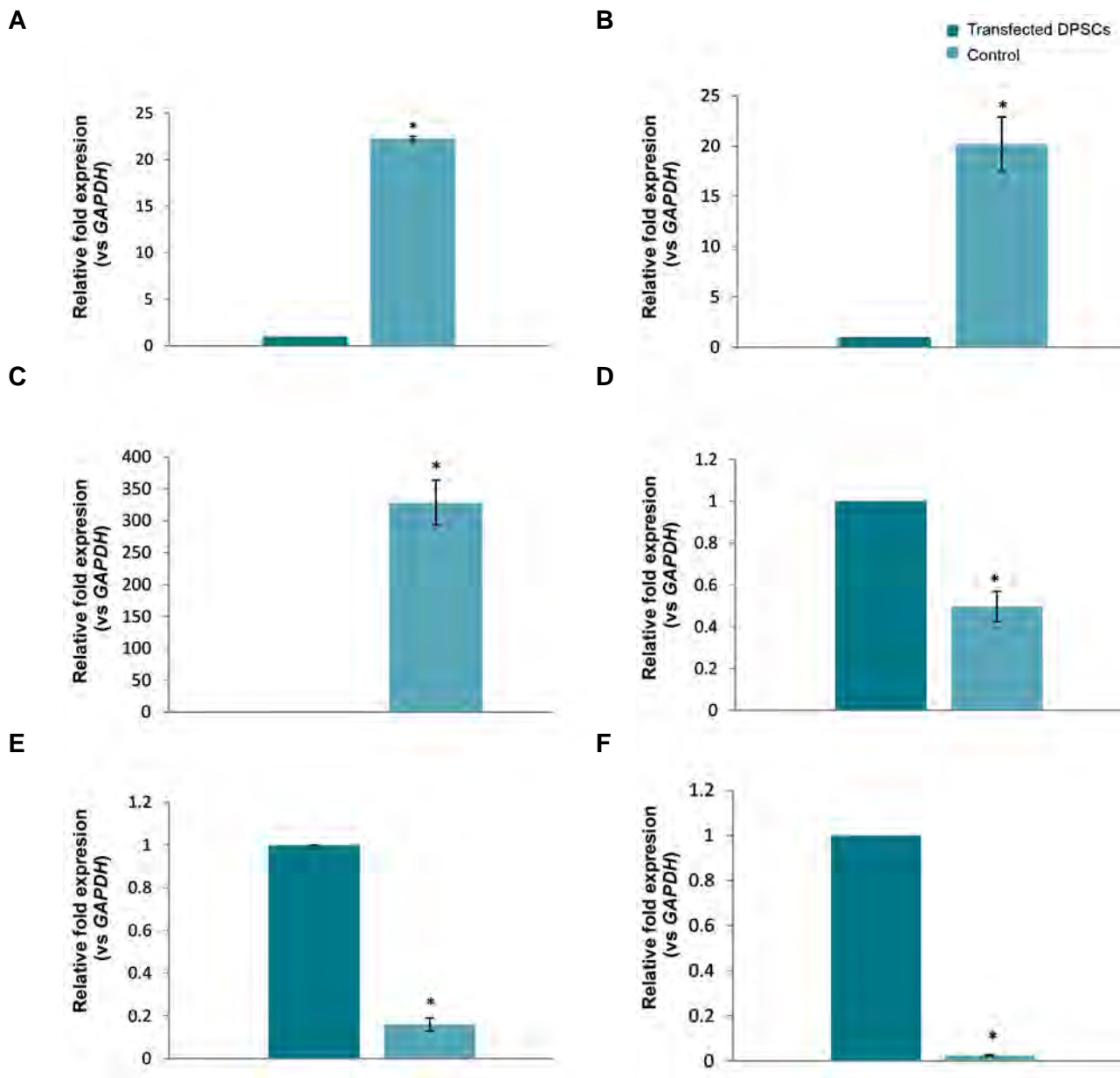


Fig.1: Expression of some genes related to *Zfp521*. **A.** The higher level of *Zfp521* expression detected in transfected cells in comparison with untransfected dental pulp stem cells (DPSCs). **B.** *Zfp521* overexpression resulted to the significantly up-regulation of *SOX3*, *PAX6* as neural progenitor markers, while induced down-regulation in **D.** *CDK1* expression as a key player in cell cycle progression and non-neural determination genes such as **E.** *PPAR- γ* , and **F.** *BMP2* that reflected adipogenesis and osteogenesis respectively ($P \leq 0.05$). Data are presented as mean \pm SE.

Several studies demonstrated that *Zfp521* is highly expressed in the cerebellum, striatonigral neurons and neural stem cells. In this regard, Kamiya et al. (4) showed a pronounced expression of *Zfp521* in the neuroectoderm of the rostral neural tube during neurulation, which play a key role in the conversion of ES cells into the neural progenitors. They also found that during neural differentiation *Zfp521* acts in cooperation with the P300 activator via its N-terminal zinc-finger motifs and induces expression of many early neural genes, such as *SOX1*, *SOX3*, and *PAX6*. In this regard, *Shahbazi* et al. (21). verified that *Zfp521* has the potential to directly convert human fibroblasts into neural progenitor cells. These cells are capable of surviving, migrating, and achieving neural phenotypes upon transplantation into the neonatal mouse and adult rat brains

without tumor formation. Generally, there is considerable evidence that *Zfp521* acts in association with its close paralog *Zfp423*, at least in part, for various explained functions (22, 23).

Recently, more attention has been paid to dental stem cells as a promising source of cells for the regeneration of various tissues due to availability, ectomesenchymal origin, and a relatively high level of neural progenitor markers. Despite many reports on the effective neural induction in DSCs, little success were achieved to produce clinically applicable neurons (24, 25).

Considering all the aforementioned promising features of the DSCs, to pave the way for the application of DSCs to challenging neurodegenerative disorders through neural

regeneration in future, we will propose that temporal overexpression of *Zfp521* may efficiently leads DSCs to differentiate into functional neurons under specific culture conditions.

Previous studies have been revealed that epigenetic modifications have high impacts on the regulation of gene expression during neurogenesis (26). We believe that *Zfp521* can mediate remodeling of nucleosome through recruitment of P300 in neural progenitor cells, which in turn promotes activation of neuron specification genes, like *SOX3* (4). The intrinsic histone acetyltransferase (HAT) activity of P300 co-activator on neural genes (27) and co-repression of histone deacetylase (NuRD) complex on some sets of non-neural determination genes, such as *RUNX2* or *SOX9*, via interaction with *Zfp521*, are suggested as the main mechanism involved in the neural induction effect of *Zfp521*.

Furthermore, *Zfp521* can promote cell cycle transition from precursor to post-mitotic state via down regulating cyclin dependent kinase 1 (*CDK1*) (28). Some recent studies provided evidences for the sequential switch of chromodomain-helicase-DNA-binding (CHDs) in NuRD complex during neural progenitor proliferation and cortical layer specification, which can be further considered as a promoter of *Zfp521* action (29).

Based on this speculation, we expect to observe higher efficacy of trans-differentiation of DPSCs after single transduction of *Zfp521* in comparison to previously reported fibroblast induction by Shahbazi et al. (21). In this regard, to provide an evaluation for this hypothesis we assessed the impact of *Zfp521* on some important genes such as *SOX3*, *PAX6*, *CDK1*, *PPAR-γ* and *BMP2*,

which supported the neural induction potential of *Zfp521* in mesenchymal stem cells.

Gene expression analysis was performed by real time polymerase chain reaction (PCR) after transduction of characterized DPSCs with a doxycycline inducible lentiviral vector and induction of *Zfp521* overexpression for 2 days. We found a significant increase in *Zfp521* expression in comparison to untransfected cells, which was accompanied by significantly acceleration in expression level of two main neural markers, *SOX3* and *PAX6* (Fig.1). In contrast, it seems that the overexpression of *Zfp521* not only resulted to the considerable reduction in *CDK1* but also inhibited the expression of *PPAR-γ* and *BMP2* which related to adipogenesis and osteogenesis, respectively. These data provide primary evidence in support of neural inductive potential of *Zfp521*, especially for dental stem cells.

Due to remarkable potency and their neural crest origin, DPSCs are considered to have a potential to differentiate into neural cells. Although numerous studies in the last decade focused on the neural differentiation of DPSCs, the extension to functional nerve cells remains a challenge. In conclusion, we speculate that the temporal overexpression of *Zfp521* in dental pulp stem cells may prime cells for neural differentiation through chromatin modification that can lead to the expression of neural specification genes. Suggested mechanism of this effect is schematically presented in Figure 2. This proposed hypothesis should be evaluated in the neural differentiation progress to assess the neurogenesis efficiency in *Zfp521* overexpressed in these cells. Further studies of involved cellular mechanisms and proteins interaction with *Zfp521* are also valuable.

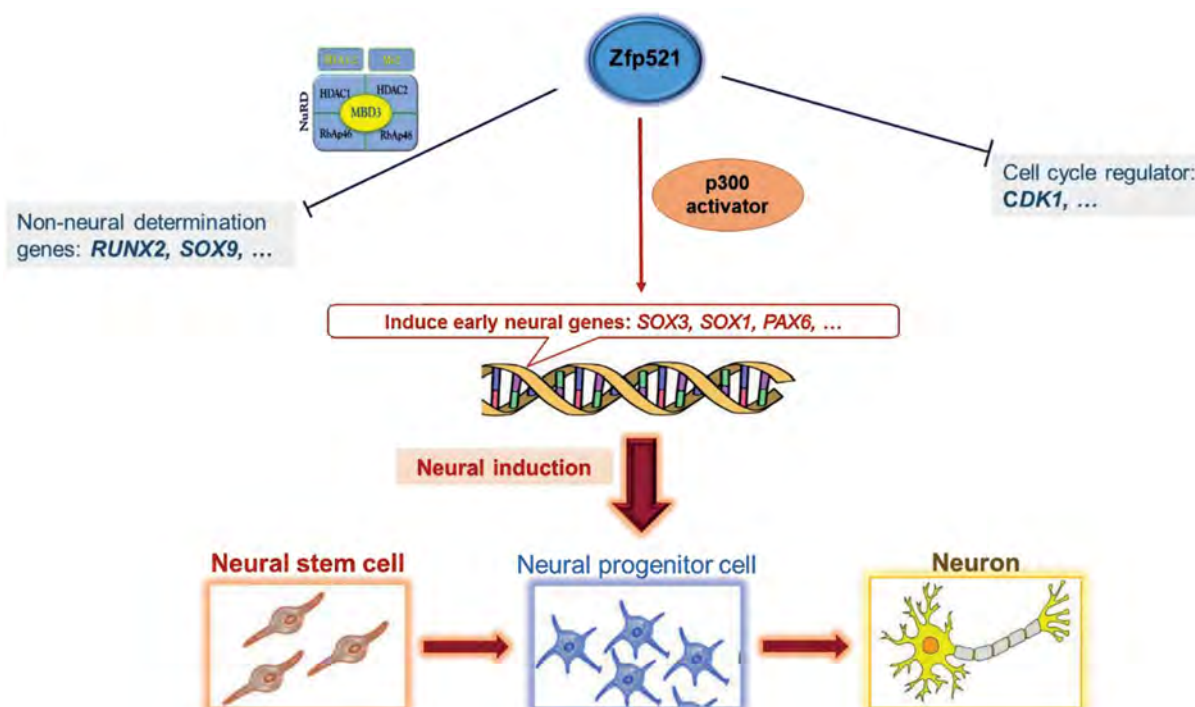


Fig.2: Proposed role of *Zfp521* in induction of neural differentiation through mesenchymal stem cells.

Acknowledgements

We like to express our thanks to our colleagues at Stem Cell Department of Royan Institute who encouraged us for preparation of this manuscript. This hypothesis is based on our present study on neural differentiation of dental-originated stem cells, which was funded by Department of Cellular Biotechnology Cell Science Research Center, Royan Institute for Biotechnology and was supported in part by Shahrekord University. None of the authors have any conflict of interest to declare.

Authors' Contributions

F.E., M.E.-B., M.H.N.-E.; Conceived of the presented idea and participated in drafting the manuscript. F.B.; Compiled the literature sources and developed the theory. P.N., M.E.-B.; Helped to evaluate and edit the manuscript. All authors give final approval of the submitted version of manumit.

References

- Bakopoulou A, About I. Stem cells of dental origin: current research trends and key milestones towards clinical application. *Stem Cells Int.* 2016; 2016: 4209891.
- Hemmat S, Lieberman DM, Most SP. An introduction to stem cell biology. *Facial Plast Surg.* 2010; 26(5): 343-349.
- Sakai K, Yamamoto A, Matsubara K, Nakamura S, Naruse M, Yamagata M, et al. Human dental pulp-derived stem cells promote locomotor recovery after complete transection of the rat spinal cord by multiple neuro-regenerative mechanisms. *J Clin Invest.* 2012; 122(1): 80-90.
- Kamiya D, Banno S, Sasai N, Ohgushi M, Inomata H, Watanabe K, et al. Intrinsic transition of embryonic stem-cell differentiation into neural progenitors. *Nature.* 2011; 470(7335): 503-509.
- Gronthos S, Brahim J, Li W, Fisher LW, Cherman N, Boyde A, et al. Stem cell properties of human dental pulp stem cells. *J Dent Res.* 2002; 81(8): 531-535.
- Gato A, Moro JA, Alonso MI, Bueno D, De La Mano A, Martín C. Embryonic cerebrospinal fluid regulates neuroepithelial survival, proliferation, and neurogenesis in chick embryos. *Anat Rec A Discov Mol Cell Evol Biol.* 2005; 284(1): 475-484.
- Gronthos S, Mankani M, Brahim J, Robey PG, Shi S. Postnatal human dental pulp stem cells (DPSCs) in vitro and in vivo. *Proc Natl Acad Sci USA.* 2000; 97(25): 13625-13630.
- Huang AH, Snyder BR, Cheng PH, Chan AW. Putative dental pulp-derived stem/stromal cells promote proliferation and differentiation of endogenous neural cells in the hippocampus of mice. *Stem Cells.* 2008; 26(10): 2654-2663.
- Karaöz E, Demircan PC, Sağlam O, Aksoy A, Kaymaz F, Duruksu G. Human dental pulp stem cells demonstrate better neural and epithelial stem cell properties than bone marrow-derived mesenchymal stem cells. *Histochem Cell Biol.* 2011; 136(4): 455-473.
- Lehtinen MK, Zappaterra MV, Chen X, Yang YJ, Hill AD, Lun M, et al. The cerebrospinal fluid provides a proliferative niche for neural progenitor cells. *Neuron.* 2011; 69(5): 893-905.
- Laino G, d'Aquino R, Graziano A, Lanza V, Carinci F, Naro F, et al. A new population of human adult dental pulp stem cells: a useful source of living autologous fibrous bone tissue (LAB). *J Bone Miner Res.* 2005; 20(8): 1394-1402.
- Arthur A, Rychkov G, Shi S, Koblar SA, Gronthos S. Adult human dental pulp stem cells differentiate toward functionally active neurons under appropriate environmental cues. *Stem cells.* 2008; 26(7): 1787-1795.
- Bond HM, Mesuraca M, Carbone E, Bonelli P, Agosti V, Amodio N, et al. Early hematopoietic zinc finger protein (EHZF), the human homolog to mouse Evi3, is highly expressed in primitive human hematopoietic cells. *Blood.* 2004; 103(6): 2062-2670.
- Lin AC, Roche AE, Wilk J, Svensson EC. The N termini of Friend of GATA (FOG) proteins define a novel transcriptional repression motif and a superfamily of transcriptional repressors. *J Biol Chem.* 2004; 279(53): 55017-55023.
- Hong W, Nakazawa M, Chen YY, Kori R, Vakoc CR, Rakowski C, et al. FOG-1 recruits the NuRD repressor complex to mediate transcriptional repression by GATA-1. *EMBO J.* 2005; 24(13): 2367-2378.
- Hashemi M-S, Esfahani AK, Peymani M, Nejati AS, Ghaedi K, Nasr-Esfahani MH, et al. Zinc finger protein 521 overexpression increased transcript levels of *Fndc5* in mouse embryonic stem cells. *J Biosci.* 2016; 41(1): 69-76.
- Shen S, Pu J, Lang B, McCaig CD. A zinc finger protein Zfp521 directs neural differentiation and beyond. *Stem Cell Res Ther.* 2011; 2(2): 20.
- Correa D, Hesse E, Seriwatanachai D, Kiviranta R, Saito H, Yamana K, et al. Zfp521 is a target gene and key effector of parathyroid hormone-related peptide signaling in growth plate chondrocytes. *Dev Cell.* 2010; 19(4): 533-546.
- Hesse E, Saito H, Kiviranta R, Correa D, Yamana K, Neff L, et al. Zfp521 controls bone mass by HDAC3-dependent attenuation of Runx2 activity. *J Cell Biol.* 2010; 191(7): 1271-1283.
- Wu M, Hesse E, Morvan F, Zhang J-P, Correa D, Rowe GC, et al. Zfp521 antagonizes Runx2, delays osteoblast differentiation in vitro, and promotes bone formation in vivo. *Bone.* 2009; 44(4): 528-536.
- Shahbazi E, Moradi S, Nemati S, Satarian L, Basiri M, Gourabi H, et al. Conversion of human fibroblasts to stably self-renewing neural stem cells with a single zinc-finger transcription factor. *Stem Cell Reports.* 2016; 6(4): 539-551.
- Kang S, Akerblad P, Kiviranta R, Gupta RK, Kajimura S, Griffin MJ, et al. Regulation of early adipose commitment by Zfp521. *PLoS Biol.* 2012; 10(11): e1001433.
- Warming S, Rachel RA, Jenkins NA, Copeland NG. Zfp423 is required for normal cerebellar development. *Mol Cell Biol.* 2006; 26(18): 6913-6922.
- Victor AK, Reiter LT. Dental pulp stem cells for the study of neurogenetic disorders. *Hum Mol Genet.* 2017; 26(R2): R166-R171.
- Ghasemi Hamidabadi H, Rezvani Z, Nazm Bojnordi M, Shirinza-deh H, Seifalian AM, Joghataei MT, et al. Chitosan-intercalated montmorillonite/poly (vinyl alcohol) nanofibers as a platform to guide neuronlike differentiation of human dental pulp stem cells. *ACS Appl Mater Interfaces.* 2017; 9(13): 11392-11404.
- Denslow SA, Wade PA. The human Mi-2/NuRD complex and gene regulation. *Oncogene.* 2007; 26(37): 5433-5438.
- Goodman RH, Smolik S. CBP/p300 in cell growth, transformation, and development. *Genes Dev.* 2000; 14(13): 1553-1557.
- Matsushime H, Ewen ME, Strom DK, Kato J-Y, Hanks SK, Rous-sel MF, et al. Identification and properties of an atypical catalytic subunit (p34PSK-J3/cdk4) for mammalian D type G1 cyclins. *Cell.* 1992; 71(2): 323-334.
- Nitarska J, Smith JG, Sherlock WT, Hillege MM, Nott A, Barshop WD, et al. A functional switch of NuRD chromatin remodeling complex subunits regulates mouse cortical development. *Cell Rep.* 2016; 17(6): 1683-1698.